Characterising the Interactions Between HSV and HIV During Coinfection of the Anogenital Mucosa

Blake Johnson

A thesis submitted in fulfilment of the requirements for the degree of Master of Philosophy

June 2025

Lead Supervisor: Associate Professor Najla Nasr
Auxiliary Supervisors: Professor Anthony Cunningham & Dr Naomi Truong

Centre for Virus Research
The Westmead Institute for Medical Research

School of Medical Sciences, Faculty of Medicine and Health,
The University of Sydney

i. Student Declarations

I, Blake Johnson, declare that the contents of this thesis are presented solely for the fulfilment of the requirements of the degree of Master of Philosophy, and have not been used for the award of any other degree at any other institution. I further certify that all works hereby presented are the result of my own work unless otherwise acknowledged herein.

I declare that this thesis did not utilise generative AI for the production of written material, figures, or any other content contained within this thesis.

The research produced within this thesis was supported by an Australian Government Research Training Program (RTP) and the RTP Stipend Scholarship.

Main Body Word Count: 40 720

Name: Blake Raymond Johnson

ii. Abstract

Both the epidermis and dermis of type II anogenital mucosa are host to a variety of mononuclear phagocytes (MNPs; Langerin$^+$ cells, CD11c$^+$ Dendritic Cells (DCs)) and T lymphocytes (CD3+), which play a significant role in the sexual transmission of HIV infection. While it is well known that prior infection with HSV increases the risk of acquiring HIV, likely by inducing a proinflammatory state and ulcerating the mucosal barrier, the precise mechanisms through which this happens during early mucosal infection have not yet been well defined.

As such, we first took a well-optimised HSV1 *ex vivo* inner foreskin tissue explant model and quantified the impact of HSV1 infection on the migration and densities of epidermal Langerin$^+$ cells, epidermal CD11c$^+$ DCs, subsets of dermal CD3$^+$ T cells, dermal Langerin$^+$ MNPs and dermal CD11c$^+$ DCs. We showed that at sites of HSV1 infection, there is potentially migration of epidermal MNPs into the dermis, while dermal MNPs and T lymphocytes are concentrated directly under sites of HSV infection. We also found that several key inflammatory cytokines and chemokines are upregulated in HSV1 infected tissue. The formation of a cell relay to carry virus into a dermis enriched with HIV target cells and a proinflammatory environment could be significant mechanisms by which HSV increases HIV acquisition.

Secondly, we also attempted to develop a novel HSV2-HIV coinfection explant. Despite facing significant experimental challenges, we made substantial progress towards the completion of this valuable model. We first demonstrated HSV2 infection in vaginal tissue which showed similar T lymphocyte redistributions as observed in the HSV1 foreskin explant. We identified that using a cloning cylinder to deliver HIV 18 hours after HSV2 infection at a TCID50 70 000, and leaving HIV in culture for 24 hours, resulted in optimal HIV infection. Ultimately, although we were not able to achieve true overlapping HSV2-HIV coinfection, we were able to produce an explant that contained both HSV2 and HIV infection, and where we reported HSV2 uptake by a langerin$^+$ cell lining the basement membrane and HIV uptake by an epidermal CD4$^+$ T cell infected with HIV, lending credence to our conclusions in chapter 3.

Overall, this thesis has provided further clarity into the mechanisms by which HSV may increase the risk of HIV acquisition while also making significant progress on optimising a HSV2-HIV coinfection explant model, which will be utilised by the host lab to directly visualise and provide further clarity into the relationship between these two viruses.

iii. Acknowledgements

Although submitted as my thesis, it would be inappropriate not to acknowledge all the support and hard work others put in to allow me to submit. First and most importantly, I need to thank Najla, who has been the best supervisor and mentor any HDR student can ask for. Your support since my first day at WIMR, and the beginning of my research journey has been very appreciated. Your blend of being there when I needed help to overcome challenges, but also stepping back at the right time to give me independence, allowed me to develop skills as a researcher in a safe environment, which was exactly what I needed to get the most out of my time at WIMR. I'm very grateful for the opportunity to complete this project as your student!

My other supervisors, firstly Tony, also deserve a huge thank you. Your ability to contextualise my work within the greater literature has proven invaluable when determining what direction the project needed to move in next, and helped me with all components of the writing. Secondly, Naomi, who despite joining the team more recently, put her incredible scientific rigour and attention to detail to work, greatly increase the quality of this thesis. Of special note, Naomis extensive understanding of statistics and cyclic immunofluorescent microscopy proved indispensable to the completion of the appropriate statistics and representative images.

I also thank Hafsa, whose work on optimising the original foreskin explant model, and for training me in the lab, which set the foundations of all the work completed within this thesis. Similarly, Tom, whose incredible understanding of all things data related, deserves a significant acknowledgement for leading the charge in creating an analytics pipeline that could be utilised in this project. I also acknowledge the hard work put in by the honours students Samantha, Sherry, and Dona, who all contributed to this thesis in unique and important ways. I also thank all those at WIMR who have supported me and this project including: Kirstie, Kerrie, Jason, Heeva, Jacinta, and no doubt others I'm forgetting!

I'd also like to thank my family for their support in all my endeavours from (quite literally) day one, and the friends I've made along the way – your support is what keeps me sane during the stressful times. Finally, I thank and acknowledge all those who donate their tissue to projects such as this – it is only through their generosity that projects like mine take place.

iv. Table of Contents

i. Student Declarations ii
ii. Abstract iii
iii. Acknowledgements iv
iv. Table of Contents v
v. List of Figures ix
vi. List of Tables x
vii. List of Abbreviations xi
Chapter 1: Literature Review 1
1.1. Human Immunodeficiency Virus 1 2
1.1.1. HIV Origins and Current Status 2
1.1.2. The Structure and Genomic Organisation of HIV Virions 3
1.1.3. Lifecycle of HIV 5
1.1.3.1. Cell Entry 5
1.1.3.2. Replication and Inhibition by Antiretroviral Therapy 6
1.1.4. Clinical Course of HIV Infection 8
1.1.4.1. Sexual Acquisition of HIV 8
1.1.4.2. Later stages of HIV Infection 9
1.2. Herpes Simplex Virus 1 & 2 11
1.2.1. Epidemiology and History of HSV1 and 2 11
1.2.2. Virion Structure and Genomic Organisation of HSV 12
1.2.3. Sexual Transmission of HSV 14
1.2.4. HSV Lifecycle 16
1.2.4.1. Entry into Target Cells 16
1.2.4.2. Lytic Replication of HSV and Therapeutic Targets 17
1.2.5. Significant Stages of HSV Infection 20
1.2.5.1. Immune Response to Primary Infection 20
1.2.5.2. Establishment and Maintenance of Latency 21
1.2.5.3. Reactivation and HSV Secondary Infection 23
1.3. Structure of Anogenital Tissue 25
1.3.1. Skin 25
1.3.2. Type II Mucosa 27
1.3.2.1. The Foreskin 27
1.3.2.2. The Vagina 29
1.3.3. Type I Mucosa 30

1.4. $CD4^+$ T Cells 31
1.4.1. The Role of $CD4^+$ T Cell Subsets in HIV and HSV Infection 33
1.4.2. $CD4^+$ T_h Cells Subsets 33
1.4.2.1. $CD4^+$ T_h1 Cells 33
1.4.2.2. $CD4^+$ T_h2 and T_h9 Cells 34
1.4.2.3. $CD4^+$ T_h17 Cells 34
1.4.2.4. $CD4^+$ T_h22 Cells 35
1.4.2.5. $CD4^+$ T_{REG} cells 35
1.4.2.6. $CD4^+$ T_{FH} Cells 36
1.4.3. $CD4^+$ T Memory Cells 37
1.4.4. $CD4^+$ T Memory Cells Subsets and Their Contribution to the Latent Reservoir 38
1.4.4.1. $CD4^+$ TSCM 38
1.4.4.2. $CD4^+$ TCM Cells 40
1.4.4.3. $CD4^+$ TTM Cells 40
1.4.4.4. $CD4^+$ TEM Cells 41
1.4.4.5. $CD4^+$ TRM Cells 41
1.4.5. Maintenance and Establishment of HIV Latency 42
1.5. $CD8^+$ T Cells 43
1.5.1. Introduction to $CD8^+$ T Cells 43
1.5.2. $CD8^+$ Tissue Resident Memory Cells 45
1.5.3. $CD8^+$ T Cells and HSV Infection 45
1.5.4. $CD8^+$ T Cells and HIV Infection 46
1.6. Subsets of Mononuclear Phagocytes in Human Tissue 47
1.6.1. Langerhans Cells 49
1.6.2. Tissue Residing Conventional Dendritic Cells 1 50
1.6.3. Tissue Residing Conventional Dendritic Cells 2 51
1.6.3.1. Epidermal $Langerin^+$ $CD11c^+$ cDC2s 51
1.6.4. Tissue Residing Conventional Dendritic Cells 3 52
1.7. HIV and HSV Coinfection in the Context of MNPs and T Lymphocytes 53
1.7.1. Mechanisms of Increased HIV Acquisition During HSV-HIV Coinfection 54
1.8. Aims and Hypothesis 55
Chapter 2: Materials and Methods 58
2.1. General Solutions and Comments 59
2.1.1. Human Antibody Serum 59
2.1.2. Foetal Bovine Serum 59
2.1.3. Blocking Solution 59
2.1.4. Cyclic Immunofluorescence Photobleaching Solution 59
2.1.5. High-Density Microarray Patch Coating Solution 59

2.1.6. Cell/Tissue Culture Media 60
2.1.7. Cell Lines 60
2.2. Experimental Rationale 61
2.3. Preparation of Viral Stocks 61
2.3.1. Growth of HIV Stock 61
2.3.2. Growth of HSV1-GFP and HSV2 Stocks 62
2.4. Preparation of Anogenital Tissue Explants and Microscopy Slides 63
2.4.1. Preparation of Tissue Explants and Infection by HSV 63
2.4.2. Infection of Explants by HIV 64
2.4.3. Microscopy Slide Preparation and Selection 66
2.5. Immunofluorescence Microscopy Staining 66
2.6. HSV1/2 and HIV RNAscope 69
2.6.1. Visualisation of Either HSV1/2 or HIV 69
2.6.2. Visualisation of HSV2 and HIV Coinfected Tissue 70
2.7. Analysis of Microscopy Images 71
2.7.1. Determining $CD3^+$ Lymphocyte and MNP Distribution and Density 71
2.7.2. Spatial Analysis of $CD11c^+$ MNPs and $CD3^+CD4^+$ Lymphocytes 72
2.8. LEGENDplex 75
2.9. Data Representation and Statistical Analysis 76
Chapter 3: Identifying HSV Induced Changes in Anogenital Tissues that Enhance HIV Acquisition and Infection 77
3.1. Introduction 78
3.2. Summary of Key Methodology 79
3.2.1. Selection of Inner Foreskin Donors 82
3.3. Validation of the Cyclic Immunofluorescence Bleaching Solution 83
3.4. Analysis of Epidermal LC and Epi-DC Density and Distribution 85
3.4.1. Epi-DCs were Sparsely Distributed and Closer to the Basement Membrane at Sites of HSV1 Infection 87
3.4.2. Epidermal LCs were Less Dense at Sites of HSV1 Infection 88
3.5. T Lymphocyte and MNP Distribution in the Dermis 89
3.5.1. Distribution and Density of LCs and DCs in the Dermis 92
3.5.1.1. Dermal $CD11c^+$ DCs were Denser at Sites of HSV1 Infection and Closer to the Basement Membrane 92
3.5.1.2. Dermal LCs were Denser at Sites of HSV1 Infection and Closer to the Basement Membrane 95
3.5.2. Distributions and Densities of T Lymphocyte Populations in the Dermis 96
3.5.2.1. Dermal T Lymphocytes Were Uniformly Denser at Sites of HSV1 Infection 97
3.5.2.2. Dermal $CD4^+$ T cells Were Uniformly Denser at Sites of HSV1 Infection 99
3.5.2.3. Dermal $CD3^+CD4^-$ T cells Were Uniformly Denser at Sites of HSV1 Infection 100
3.5.2.4. Summary of the T Cell Distributions in the HSV1 Inner Foreskin Explant Model 102

3.5.3. HSV1 Infection Reduced the Lymphocyte-MNP Cross Distance in the Dermis 103
3.6. HSV1 Infection Altered the Chemokine/Cytokine Environment of Inner Foreskin Explants 106
3.7. Chapter Three Discussion 109
Chapter 4: Optimisation and Implementation of an HSV2 and HIV Coinfection Explant Model 118
4.1. Introduction 119
4.2. Summary of Key Methodology 120
4.2.1. Selection of Tissue Donors 122
4.3. Assessment of HSV2 Infection in Vaginal Tissue 123
4.4. Changes in Cell Distributions in HSV2 Infected Vaginal Tissue 124
4.5. Application of Two HD-MAPs to the Same Explant 128
4.6. Optimisation of HIV Infection of Vaginal Tissue 130
4.6.1. Titration and Selection of a Route of Delivery for HIV 130
4.6.2. Defining the Optimal Time Post HIV Treatment to Visualise Infection 134
4.7. Updates to the Cyclic Immunofluorescent Microscopy Panel and the HD-MAP for the Coinfection Explant 136
4.7.1. Optimisation of a New Immunofluorescent Microscopy Panel 137
4.7.2. Polymer HD-MAP Punctures Were More Frequent and Deeper Than Silicon 139
4.8. Trialling the HSV2 and HIV Coinfection Foreskin Explant Model 141
4.9. Chapter Four Discussion 146
4.9.1. Conclusions 153
Chapter 5: Overall Discussion 155
References 162
Appendices 190
A. Fiji script for alignment of two rounds of image based on registration 191

v. List of Figures

Figure 1.1. HIV Virion Structure and Organisation of Genome 4
Figure 1.2. HIV cell entry and lifecycle 8
Figure 1.3. Clinical Course HIV Infection 10
Figure 1.4. Key structural features of HSV1 and HSV2 14
Figure 1.5. HSV1 and HSV2 entry into target cells and inhibition of replication by antiviral therapeutics 19
Figure 1.6. The establishment of latent infection within ganglia 24
Figure 1.7. Comparison of Type I and II mucosa 31
Figure 1.8. Summary of $CD4^+$ T helper cell subsets 37
Figure 1.9. Differentiation and phenotype of subsets of $CD4^+$ T memory cells 39
Figure 2.1. Key equipment used during explant preparation 65
Figure 2.2. ImageJ analysis pipeline for cell distributions and densities in the dermis 75
Figure 3.1. Inner foreskin infection explant model workflow 81
Figure 3.2. Assessment of the efficacy of the Cyclic IF photobleaching process 84
Figure 3.3. Representative images of foreskin explants stained for epidermal counting 86
Figure 3.4. The density and average distance from the basement membrane of Epi-DCs 87
Figure 3.5. Density and the average distance from the basement membrane of LCs residing in the epidermis 88
Figure 3.6. Representative images of foreskin explants stained for dermal manual counting 92
Figure 3.7. Distribution and density of DCs in the most superficial 120 µm of the dermis 94
Figure 3.8. Distribution and density of LCs in the first 120 µm of the dermis 96
Figure 3.9. Distribution and density of $CD3^+$ T cells in the first 120 µm of the dermis 98
Figure 3.10. Distribution and density of $CD4^+$ T cells in the first 120 µm of the dermis 100
Figure 3.11. Distribution and density of $CD4^-$ T cells in the first 120 µm of the dermis 102
Figure 3.12. The average cross distance between T Cell and MNP populations 105
Figure 3.13. Quantification of inflammatory cytokines and chemokines in foreskin explant supernatants 109
Figure 4.1. Optimisation of HSV2-HIV coinfection explant model 121
Figure 4.2. Visualisation of HSV2 infection in vaginal tissue explants 124
Figure 4.3. Density and distribution of lymphocytes in the epidermis and dermis 127
Figure 4.4. The structural integrity of tissue following HD-MAP application 129
Figure 4.5. Optimisation of method of infection and TCID50 133
Figure 4.6. Selection of the best time point after HIV infection 136
Figure 4.7. Titration of antibodies for FFPE preserved foreskin tissue 138
Figure 4.8. Comparison of the frequency and depth of punctures generated by different HD-MAP material 140
Figure 4.9. HSV2 and HIV coinfection and visualisation attempt 145

vi. List of Tables

Table 1.1. Summary of significant tissue residing MNPs 53
Table 2.1. Antibodies used for IF microscopy before Section 4.8.1 re-optimisation 68
Table 2.2. Antibodies used for IF microscopy after Section 4.8.1. re-optimisation 68
Table 2.3. Summary of employed cyclic IF panel 68
Table 2.4. Optimised Probe Amplification by RNAscope 2.5 HD Assay - Red 70
Table 2.5. Optimised Probe Amplification by RNAscope 2.5 HD Duplex Assay 71
Table 3.1. Summary of donors selected for the inner foreskin explant infection model. 82
Table 4.1. Summary of donors used for the optimisation of a coinfection explant model 122
Table 4.2. Range of Densities and average cell distances from the basement membrane reported in Chapter 3 127
Table 4.3. Summary of re-optimised cyclic IF panel for FFPE explant infections 137

vii. List of Abbreviations

3-OS HS	3-O-sulfated HS
AIDS	Acquired Immunodeficiency Syndrome
Akt	protein kinase B
APC	Antigen presenting cell
ART	Antiretroviral Therapy
bcl	B cell lymphoma
BSA	Bovine serum albumin
CADM	Cell adhesion molecule
cAMP	Cyclic adenosine monophosphate
CCL	Chemokine C-C ligand
CCR	C chemokine receptor
CD	Cluster of Differentiation
CD4bs	CD4 binding site
cDC3	Conventional dendritic cell 3
CDK	Cyclin-dependent kinases
Clec9A	C-Type Lectin Domain Containing
CXCL	C-X-C ligand
CXCR	C-X-C chemokine receptor
DCM	DC culture medium
DC-SIGN	Dendritic Cell-Specific Intercellular adhesion molecule 3 Grabbing Non integrin
DISC	death-induced signalling complex
DMEM	Dulbecco's Modified Eagle Medium
DNA	Deoxyribonucleic acid
Epi-cDC2	Epidermal Langerin^{+} CD11c^{+} cDC2s
epz	Human Immunodeficiency Virus
FADD	Fas-associated death domain
FasL	Fas ligand
FBS	Foetal bovine serum
FFPE	PFA fixed paraffin embedded
gB	Glycoprotein B
gC	Glycoprotein C
gD	Glycoprotein D
GFP	Green fluorescent protein
gG	Glycoprotein G
gH:L	GlycoproteinH:L
GITRL	Glucocorticoid-induced tumour necrosis factor receptor family-related protein ligand
GM-CSF	Granulocyte macrophage colony stimulating factor
gp	glycoprotein
GUD	Genital ulcer disease
hpi	Hours post infection
hpp	Hours post patch
hAb	Human antibody
HBS	HEPES Buffered Saline
HCF	Host cell factor
HD-MAP	High Density Microarray Patch
HIV	Human Immunodeficieny Virus
HLA-DR	human leukocyte antigen DR isotype
HREC	Human Research Ethics Committee

HSPG	HS proteoglycan
HSV	Herpes simplex virus
HVEM	Herpes virus entry mediator
ICP	Infected cell protein
ICP	Infected cell protein
IDEC	Inflammatory dendritic epidermal cell
IF	Immunofluorescence
IFN	Interferon
Ig	Immunoglobulin
IL	Interleukin
ILC	Innate lymphocyte cell
IMC	Imaging Mass Cytometry
LAT	Latency associated transcript
LB	Luria-Bertani
LC	Langerhans cell
LTR	Long terminal repeat
M1	Classical macrophage
M2	Alternative macrophage
MALT	Mucosa associated lymphoid tissue
mDC	Myeloid dendritic cell
MDDC	Monocyte derived DC
MDM	Monocyte derived macrophage
MFI	Mean fluorescent intensity
MHC	Major histocompatibility complex
MNP	Mononuclear phagocyte
MOI	Multiplicity of infection
NC	Nucleocapsid Proteins
NEB	New England Biolabs
Nef	Negative effector factor
NFAT	Nuclear factor of activated T cells
NF-κB	Nuclear factor kappa light chain enhancer of activated B cells
NGF	Nerve growth factor
NIH	National Institutes of Health
NK	Natural killer
NLR	Nod-like receptor
Oct	Octamer transcription factor
OCT	Optimal cutting temperature compound
ORF	Open reading frame
p6	Late Assembly Proteins
pBal	Bal plasmid
PD	Programmed death
pDC	Plasmacytoid dendritic cell
pDC	Plasmacytoid dendritic cell
pDCs	Plasmacytoid dendritic cell
PDK	Phosphoinositide dependent kinase
PFA	paraformaldehyde
PFU	Plaque forming units
PI3K	Phosphoinositide 3-kinases
PKA	Protein kinase A
PKR	protein kinase RNA-activated
PrEP	Pre-exposure prophylaxis
RARγ	RAR-related orphan receptor gamma
RLR	RIG-I-like receptor

RNA	Ribonucleic acid
rpm	Rotations per minute
RPMI	Roswell Park Memorial Institute
S1P	Sphingosine 1-phosphate
SAMHD	sterile alpha and motif aspartic acid domain containing protein
SD	Standard Deviation
SIRP	Signal Regulatory Protein
SIV	Simian Immunodeficiency Virus
SLO	Secondary lymphoid organs
STI	Sexually transmitted infection
Tat	Trans-activator of transcription
TBS	Tris buffered saline
TCID50	50% tissue culture infective dose
TCM	Central memory
TCR	T cell receptor
TEM	Effector memory
TGF	Transforming growth factor
TGN	trans Golgi network
T_h	T helper
TIM	T-cell immunoglobulin and mucin-domain containing
TLR	Toll-like receptor
TRM	Tissue resident memory
TSCM	Stem cell like memory
TTM	Transitional memory
U_L	Unique long region
U_L30	Viral DNA polymerase
U_s	Unique short region
VCM	Virus containing media
Vif	Virion infectivity factor
Vpr	Viral protein R
Vpu	Viral protein U
VS	Virtual Slide
WHO	World Health Organisation
WRH	Westmead Research Hub
WSLHD	Western Sydney Local Health District
α	Immediate early
β	Early
γ	Late

Chapter 1: Literature Review

1.1. Human Immunodeficiency Virus 1

1.1.1. HIV Origins and Current Status

During the early half of the 20th century, changing hunting practices within Africa permitted Simian Immunodeficiency Virus (SIV) to enter human populations by zoonotic transfer from primates, resulting in the evolution of Human Immunodeficiency Virus (HIV)1 (Crawford, 2013). As there are four highly divergent strains of HIV1: M, N, O and P, it is believed four separate primate to human transfers occurred; the most common and oldest HIV1 strain, M, is believed to have originated from chimpanzees due to similarities between chimpanzee isolated SIV (SIVcpz) and HIV1 M isolates (Sharp and Hahn, 2011). Current evidence suggests that this jump occurred in the Kinshasa region of the Democratic Republic of Congo, where a large group of migrants following the construction of a railway network for work extending from Kinshasa, and a high population of sex workers facilitated the spread of the virus throughout Africa (Nuno *et al.*, 2014). As a result of the poor healthcare system in Africa, and a long-lasting asymptomatic period in infected individuals, HIV wasn't officially reported until June 1981 in Los Angeles, where a cluster of individuals presented with opportunistic infections not associated with their age and apparent health (CDC, 1981, Hymes *et al.*, 1981).

In 1983 a viral agent, HIV, had been reported as being responsible for the Acquired Immunodeficiency Syndrome (AIDS) rapidly becoming globally prevalent, resulting in a period of mass hysteria and the eventual declaration of a 'global epidemic' by the World Health Organisation (WHO) as AIDS became the fourth most common cause of mortality globally (Barré-Sinoussi *et al.*, 1983, Quinn, 1996). Today, approximately 40 years onwards since the discovery of HIV/AIDS, it remains a significant burden to global health, with an estimate of 38 million cases worldwide and only 26 million accessing treatment; in 2023 alone, there were 1.3 million new cases and 600 000 AIDS related deaths (HIVGov, 2025). In the absence of a

HIV vaccine, understanding factors that influence the infection of HIV target cells is essential to reduce the number of cases per year, and to design more successful preventative therapies.

1.1.2. The Structure and Genomic Organisation of HIV Virions

HIV is a lipid bilayer enveloped Baltimore Class VI member of the *Retroviridae* family and *Lentivirus* genus; each virion is spherical, pleomorphic, and has a diameter of approximately 60 nm (**Figure 1.1a**) (Cheslock *et al.*, 2003). HIV virions contain two copies of non-covalently linked positive-sense single-stranded RNA attached to late assembly proteins (p6) and nucleocapsid proteins (NC), functioning as the viral genome; the viral genome is surrounded by a conical capsid composed of p24 (Lu *et al.*, 2011). External to the p24 capsid is the virion matrix, composed of p17, which maintains virion structural integrity and plays a critical role in carrying proteins essential for interactions with target cells and is in turn surrounded by an envelope produced from the host cell (Dorfman *et al.*, 1994). The capsid also contains the core proteins: protease, integrase, and reverse transcriptase, while accessory proteins are packaged in the space between the matrix and the capsid and include: viral protein R (Vpr), viral protein U (Vpu), virion infectivity factor (Vif), and negative effector factor (Nef) (Hill *et al.*, 2005). Extending from the matrix and envelope are glycosylated spikes referred to as glycoprotein (gp)160; these protrusions are organised in trimers and are composed of gp120 and gp41 which mediate cell entry (Magaret *et al.*, 2019).

The HIV genome is approximately 9.7 kb long and contains nine genes across three different open reading frames (ORF) encoding a total of 15 proteins (**Figure 1.1b)**. The first reading frame consists of a 5'-long terminal repeat (LTR), the *gag* gene, which encodes for a polyprotein cleaved into the structural genes: p17, p24, NC and p6 (Bell and Lever, 2013). Both Vif and Nef are also encoded in ORF one, separately as *vif* and *nef* respectively (Frankel and Young, 1998). The second ORF contains the *vpu* gene, which encodes Vpu and the 3'-

LTR, while the third ORF encodes *pol*, a polyprotein cleaved to form protease, reverse transcriptase, and integrase (Cohen *et al.*, 1988, Wayengera, 2011). The gene *vpr,* which encodes Vpr, and *env*, which encodes a polyprotein consisting of gp120 and gp41, are also located in the third reading frame (Le Rouzic and Benichou, 2005, Bell and Lever, 2013). Finally, the gene *tat*, encoding trans-activator of transcription (Tat), has exons in both the first and second ORF, while the gene *rev*, encoding regulator of expression of viral proteins (Rev), has exons in the second and third ORF (Likhoshvai *et al.*, 2014).

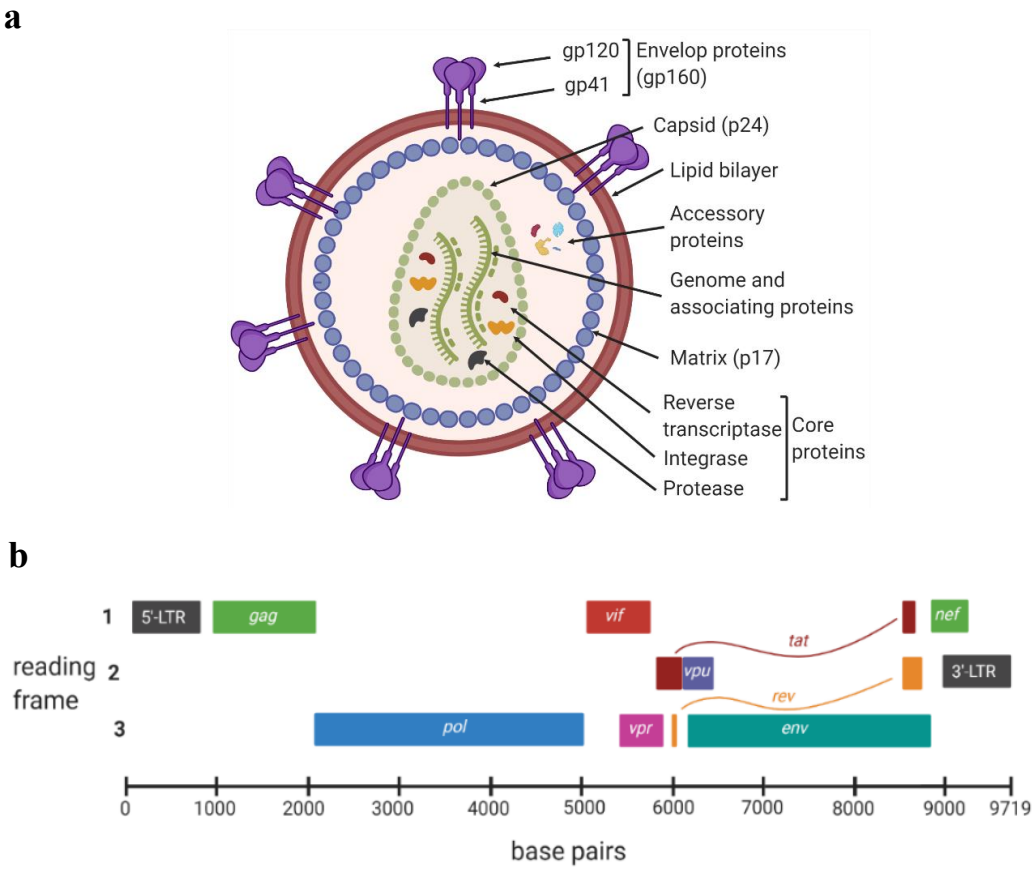

Figure 1.1. HIV Virion Structure and Organisation of Genome. (a) The structure of the HIV virion. Each virion contains two copies of the virus's genome associated with NC and p6 in a capsid composed of p24 containing the core proteins: reverse transcriptase, integrase and protease. The capsid is surrounded by the virion matrix composed of p17 which also contains small amounts of various accessory proteins. The virion is enveloped with gp160 envelop proteins protruding. **(b)** The structure of the HIV genome. The HIV genome is 9.7 kb in length and arranged in three ORFs, composed of 9 genes and encodes for 15 proteins.

1.1.3. Lifecycle of HIV

1.1.3.1. Cell Entry

As alluded to previously, the glycosylated protein spikes extending from the spherical virion are responsible for mediating entry into the target cells. Both gp120 and gp41 form trimers with N-linked glycosylation; gp120 is one of the most heavily glycosylated proteins discovered with over half its mass a result of attached glycans (Zhu *et al.*, 2000). Glycosylation ensures correct folding of trimers, reduces the detection of HIV by the host immune system, and limits the enzymatic activity of proteases, however, it has been demonstrated that glycosylation is not essential for folding or infection (Rathore *et al.*, 2017, Ping *et al.*, 2008). gp120 has five constant and five variable regions known as C1-C5 and V1-V5 respectively (Julien *et al.*, 2013). The variable regions **(Figure 1.2a)** mediate conformational changes responsible for HIV cell entry while constant regions act as anchors to gp41 (Hamoudi *et al.*, 2013). gp41 is attached to the lipid bilayer and interacts with structural proteins beneath the envelope; gp41 is responsible for mediating the fusion between the virion and Cluster of Differentiation (CD)4^+ T cells, the site of explosive viral replication (Garg and Blumenthal, 2008), and other CD4-expressing target cells (macrophages and dendritic cells).

When HIV virions interact with $CD4^+$ T cells, the gp120 CD4 binding site (CD4bs), located near the V1/V2 variable sites, induces a conformational change that exposes the V3 site, pulling the virion close to the target cell (Lijun *et al.*, 1996, Cicala *et al.*, 2011). The V3 site binds to the HIV infection coreceptors, either C chemokine receptor (CCR)5 or C-X-C chemokine receptor (CXCR)4 depending on the strain; this results in further conformational changes in gp120 which brings gp41 into contact with the cell membrane and induces virion-cell mediated fusion, resulting in virion entry (**Figure 1.2b)** (Rizzuto *et al.*, 1998). Various mononuclear phagocytes (MNP) also take up and/or are infected by HIV virions. Macrophages, $CD16^+$ monocytes, myeloid dendritic cells (mDC), plasmacytoid dendritic cells (pDC), and

Langerhans cells (LC) express CD4 and the HIV infection co-receptors CCR5 (or CXCR4) at varying levels making them susceptible to infection (Zaitseva *et al.*, 1997). Furthermore, many MNPs also express a unique repertoire of surface receptors which facilitate other mechanisms of HIV cell entry (Bertram *et al.*, 2019).

1.1.3.2. Replication and Inhibition by Antiretroviral Therapy

Following cell entry and uncoating, virion reverse transcriptase will use host nucleotides to synthesis proviral cDNA; due to the absence of any ability to proofread and self-correct this process is highly error-prone and is responsible for at least half of the mutations that form in the HIV genome (Goto *et al.*, 1998, Abram *et al.*, 2014). The *de novo* synthesised cDNA is then integrated into the host cells genome by a three-step process involving the viral protein integrase: 1) processing, 2) joining, and 3) post-integration repair (Gonçalves *et al.*, 2016). It is theorised that unlike many retroviruses, HIV integration is not strongly tropic for specific loci, rather integration occurs at a range of sites where chromatin is loosely packed and transcription of proximal host genes occurs at a high rate (Gonçalves *et al.*, 2016). The vast majority of integrated HIV provirus is defective, however, the intact provirus acts as a template for transcription by RNA polymerase II to produce both spliced and unspliced viral messenger RNA; full-length unspliced messenger RNA acts as the genome for the HIV virion (Einkauf *et al.*, 2019). Both spliced and unspliced messenger RNA can be translated at ribosomes to produce the viral proteins essential for the assembly of new virions (Liu *et al.*, 2014b).

Protein assembly and productive infection occur in cells that are actively transcribing resulting in cell death and cytopathicity (Wang and Pang, 2008). During virion assembly, Gag polyproteins will form a spherical shell around the genome; immature virions pass through the host cell membrane through a process called budding and virus protease cleaves the polyprotein

gag to generate a set of structural proteins that will assemble to form the layers of a mature virion (Ganser-Pornillos *et al.*, 2008).

Antiretroviral therapy (ART) prevents HIV infection from resulting in AIDS by targeting the various stages of the HIV lifecycle discussed above (**Figure 1.2c)**; while this has resulted in reduced HIV related mortality, many HIV patients are unable to access ART drugs at the frequency required for treatment, and others do not comply with the treatment regime (Reniers *et al.*, 2017). Furthermore, it has been demonstrated ART has limited capacity to penetrate tissues that harbour significant HIV reservoirs, such as the brain (Marban *et al.*, 2016). Typically, multiple ART drugs are administered at the same time (combined ART) targeting different stages of the lifecycle to prevent the development of resistance (Davey *et al.*, 1999). ART does not clear infection in latent reservoirs, rather it suppresses productive viral replication, and upon cessation of treatment viral rebound will occur from these reservoirs.

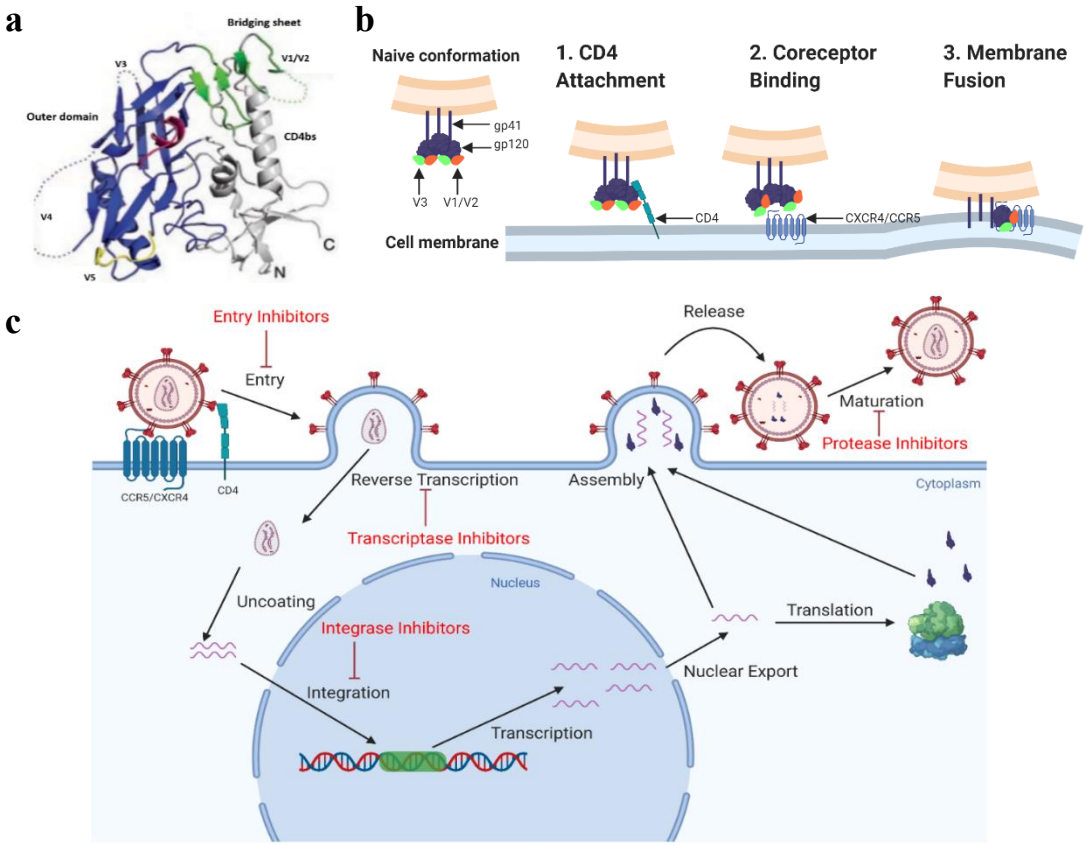

Figure 1.2. HIV cell entry and lifecycle. (a) The structure of gp120 showing the distribution of the variable regions and location of the CD4bs. Adapted from Didgu and Doms, 2012. **(b)** The mechanism employed by HIV to bind and fuse with the cell membrane. Initially trimeric gp120 is in a closed configuration, however, following CD4bs-CD4 binding gp120 shifts to an open configuration, exposing V3. V3 binds to CCR5 or CXCR4, the HIV infection coreceptors, which allows gp41 to fuse with the cell membrane resulting in viral entry. **(c)** The lifecycle of HIV in target cells and the inhibition targets of ART medications (red text).

1.1.4. Clinical Course of HIV Infection

1.1.4.1. Sexual Acquisition of HIV

Generally it is estimated that 90% of HIV transmission occurs at anogenital sites through sexual activity (HIVGov, 2025). However, a wide range of factors influence the likelihood of virus acquisition resulting in a great deal of variability in the observations of HIV infectivity. Following entry at mucosal sites, HIV initially interacts with its target cells: DCs, macrophages, LCs and the newly discovered $CD11c^{+}$ epidermal DCs which then pass the

infection to activated $CD4^+$ T cells. These antigen-presenting cells (APC) DCs transfer HIV virions to $CD4^+$ T cells in two phases: after uptake into virus-containing compartments, or after productive infection (Rhodes *et al.*, 2021). HIV crosses a viral synapse, which is a modified immunological synapse, between APCs and the $CD4^+$ T cell, where it is protected from anti-HIV antibodies, and results in explosive replication (McDonald *et al.*, 2003, Turville *et al.*, 2002). Alternatively, productively infected $CD4^+$ T cells and MNPs expressing the gp160 trimer, may form a variant of the viral synapse with uninfected bystander $CD4^+$ T cells, passing on virions **(Figure 1.3a)**. CD4 T cells can be infected in lymph nodes, or in anogenital tissue in which resident memory $CD4^+$ T cells form the primary cells of infection (Baharlou *et al.*, 2022, Cantero-Pérez *et al.*, 2019). The probability of HIV acquisition upon exposure is relatively low compared to other sexually transmitted infections (STI), however, this can be increased by certain factors. The integrity of the epithelial surface determines if virions can directly enter submucosal compartments of anogenital tissue, and regions that are richer in HIV target cells due to inflammation increase the likelihood of acquisition (Abu-Raddad *et al.*, 2008). Diseases that may ulcerate or disrupt the epithelium and cause inflammation such as bacterial vaginosis and the STIs Herpes Simplex Virus (HSV)1 and 2 greatly increase the risk of HIV acquisition (Looker *et al.*, 2017).

1.1.4.2. Later stages of HIV Infection

Following the acquisition of HIV, primary infection ensues and the number of $CD4^+$ T cells in the blood is markedly reduced **(Figure 1.3b)**; infected individuals may experience flu-like symptoms, however this typically resolves after 6 weeks when the $CD4^+$ T cell population begins to rebound (Mellors *et al.*, 1996). After approximately 12 weeks $CD4^+$ T cell rebound ceases, and the number of $CD4^+$ T cells circulating in the blood will gradually decline as the host immune system fails to recognise and destroy infected cells (McCune, 2001). During the early stages of HIV infection, $CD8^+$ T cells recognise and kill infected cells by secreting

perforin and granzyme B, limiting HIV viremia (Borrow *et al.*, 1994). However, as the infection progresses, $CD8^+$ T cells experience exhaustion, expressing markers of exhaustion including T-cell immunoglobulin and mucin-domain containing (TIM)-3 and programmed death (PD)-1 which prevents their activation and reduces proliferation of $CD8^+$ T cells by interfering with the T cell receptor (TCR) (Roberts *et al.*, 2016, Kuchroo *et al.*, 2014). Once the number of circulating $CD4^+$ T cells reduces to <350 cells/μL the risk of severe bacterial infections, notably tuberculosis, increases; at <200 cells/μL oesophageal candidiasis and pneumocystis pneumonia become common, and at <100 cells/μL HIV-associated wasting syndrome and severe cryptococcosis, cryptosporidiosis, and encephalopathy occur (Deeks *et al.*, 2015). Progression to AIDS is slow, taking approximately 10 years for most patients, although HIV progresses much quicker in some individuals, and other individuals, termed 'elite controllers', possess immune systems capable of slowing or even preventing disease progression (Deeks and Walker, 2007).

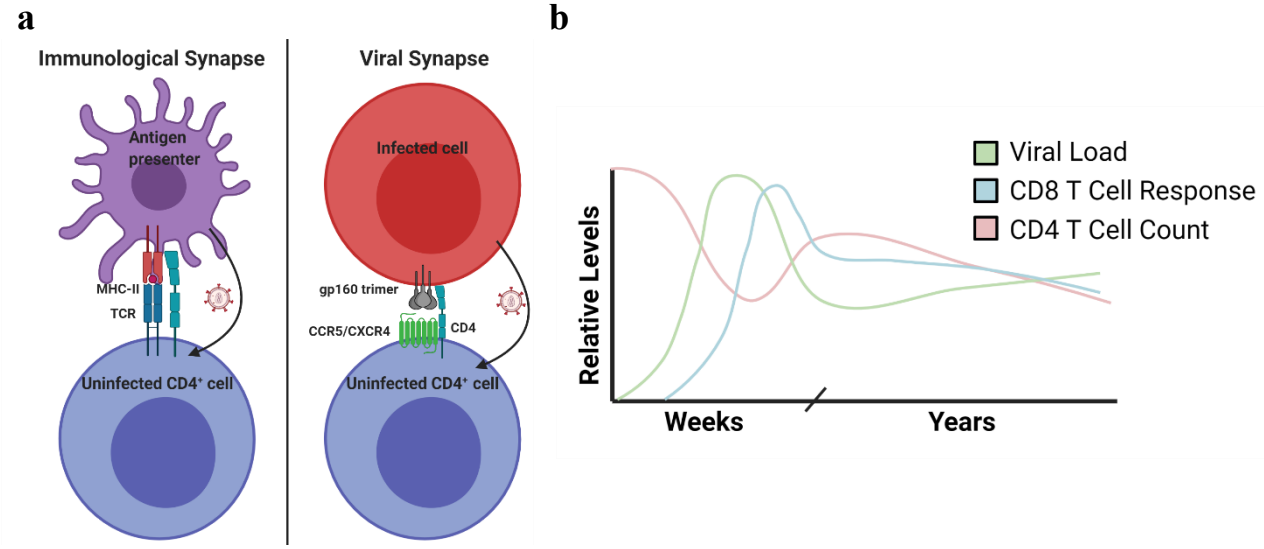

Figure 1.3. Clinical Course HIV Infection. (a) Once HIV virions are acquired in the anogenital mucosa, APCs may pass the virus uninfected $CD4^+$ T cells in lymph nodes or at the site of infection by an interaction closely resembling the immunological synapse incorporating MHCII and the TCR; alternatively, HIV infected cells may express gp160 allowing for the formation of a viral synapse with uninfected $CD4^+$ T cells and transmission of the virus. **(b)** Relative levels of HIV, CD4 T cells numbers, and the CD8 T cell response following HIV infection.

1.2. Herpes Simplex Virus 1 & 2

1.2.1. Epidemiology and History of HSV1 and 2

It is believed that herpes simplex viruses have infected members of the order of primates for hundreds of millions of years (Luebcke *et al.*, 2006). HSVs have undergone zoonotic jumps multiple times in history with viral codivergence, the parallel divergence of a lineage in two distinct phylogenies, being a common occurrence (Kitchen *et al.*, 2011). Studies employing phylogenetic modelling suggest that HSV1 resulted as a product of codivergence and HSV2 evolved from a cross-species transmission event (Wertheim *et al.*, 2014). It is theorised that HSV2 originated from chimpanzees as it is closely related to the chimpanzee HSV (Severini *et al.*, 2013). HSV1 is classified into 6 clades with the majority being present in East Africa, suggesting this region was the origin of the virus; HSV2 can be subdivided into two clades, one limited to Sub-Saharan Africa and the other globally distributed (Kolb *et al.*, 2013, Burrel *et al.*, 2017). Symptoms of herpes simplex, the disease caused by the two HSV serotypes, have been reported for 2,000 years and there is evidence that rulers of the ancient Roman empire took measures to limit the spread of disease in the population (Whitley *et al.*, 1998).

Herpes simplex disease was linked to HSV1 and 2 during the mid-20th century (Roizman and Whitley, 2001). It is estimated that on average globally 67% of individuals are infected with HSV1 and that 16% of the population is infected with HSV2, however this varies significantly globally (Chayavichitsilp *et al.*, 2009). The seroprevalence of HSV2 is highest in Africa, where approximately half of the female population between the ages of 25 and 34 are infected with HSV2 and over 90% of males and females are seropositive for HSV1 (James *et al.*, 2020). In Australia, 84% of the population is seropositive for HSV1 (AlMukdad *et al.*, 2023) and 12% is seropositive for HSV2 (AlMukdad *et al.*, 2022). HSV1 is responsible for orolabial herpes which usually results in an asymptomatic primary infection followed by reactivation and development of recurrent orolabial lesions during which are accompanied by burning, itching

and tingling (Bader *et al.*, 1978). HSV-2 is the causal agent for the majority of cases of genital herpes, although a growing number of genital herpes cases are associated with HSV1 (Ayoub *et al.*, 2019). Genital HSV1 or HSV2 infection results in epidermal lesions most commonly located on the vagina or labia, and both the inner and outer foreskin (Looker *et al.*, 2008). Although the vast majority of HSV infections only causes minor discomfort or are asymptomatic, in immunocompromised patients HSV may be disseminated through the body and infect the central nervous system which results in life-threatening encephalitis with a mortality rate that exceeds 70%, or severe neonatal disease, or keratitis which may lead to loss of vision (Jereb *et al.*, 2005). HSV2 significantly increases the risk of acquiring other STIs such as HIV which is particularly problematic given the high incidence of both HIV and HSV in Sub-Saharan Africa (Reniers *et al.*, 2017). Transmission of HSV1 most commonly occurs orolabially during childhood from the mother, or orogenitally during adolescence and young adulthood, while HSV2 is almost exclusively transmitted by sexual contact between a seropositive and seronegative individual symptomatically (20%), or asymptomatically (80%) (Fatahzadeh and Schwartz, 2007). In the absence of an effective vaccine for the two HSV serotypes, the infection can be treated and controlled by anti-viral therapy either prophylactically or as prodromal symptoms emerge (Kimberlin and Rouse, 2004).

1.2.2. Virion Structure and Genomic Organisation of HSV

HSV1 and HSV2 are members of the *Herpesviridae* family, which is a taxonomic group divided into three subfamilies: *alphaherpesviridae, betaherpesviridae,* and *gammaherpesviridae* (Nahmias *et al.*, 1981). Both HSV1 and HSV2 are members of the *alphaherpesviridae* group*,* which is also occupied by Varicella-Zoster virus (Purohit *et al.*, 2021). All animal herpesviruses possess a large double-stranded DNA genome enclosed in an icosahedral capsid that is tightly coiled, similar to the genome of bacteriophages (Howley *et al.*, 2021). The capsid is enclosed by a lipid bilayer envelope expressing 600-750 glycoprotein

spikes and by an intermediate proteinaceous layer termed the tegument (Mettenleiter *et al.*, 2006). Like all members of *alphaherpesviridae*, HSV1 and HSV2 virions express 16 surface glycoproteins, most important are: glycoproteins B (gB), D (gD), G (gG), and H:L (gH:L) which is frequently cross-linked and present as a heterodimer (Heldwein and Krummenacher, 2008, Howley *et al.*, 2021). The virion is pleiomorphic in size, ranging from 170-200 nm with the extending glycoprotein spikes making the full diameter 225 nm on average (**Figure 1.4.**) (Grünewald *et al.*, 2003).

Both HSV1 and HSV2 have a colinear and near identical genome approximately 150 kbp in length that is believed to have at least 84 unique protein-coding genes, although through splicing and gene overcrowding there could be more than this number (Boldogkői *et al.*, 2018). The majority of genes are separated into two covalently linked regions called the short unique region (U_S) and the long unique region (U_L), and are classified as immediate-early (α), early (β), and late (γ) genes (Howley *et al.*, 2021). The key difference between the genomes of HSV1 and HSV2 is the length of U_S4 which encodes for gG (Howley *et al.*, 2021). The viral capsid consists of the capsid portal, and 150 hexameric and 11 pentameric blocks primarily made up of 6 U_L encoded proteins: U_L17, U_L18, U_L25, U_L35, U_L38, and the most significant component, U_L19 (McElwee *et al.*, 2018). The tegument, initially believed to be a disordered and poorly structured layer, consists of over 24 unique proteins from genes encoded in both the U_L and the U_S interacting in complex ways not yet fully understood (Vittone *et al.*, 2005). Of the proteins that make up the tegument, there are four considered to be most important and are the most defined: 1) U_L36, which is the largest and is required for virion assembly and cellular entry, 2) pUL25, which binds with 3) U_L37 to facilitate intracellular transport of the capsid on microtubules, and 4) U_L48, which is believed to be the central organiser of the tegument and also play a role in the transcription of immediate-early viral genes (Bohannon *et al.*, 2013, Schipke *et al.*, 2012, El Bilali *et al.*, 2017).

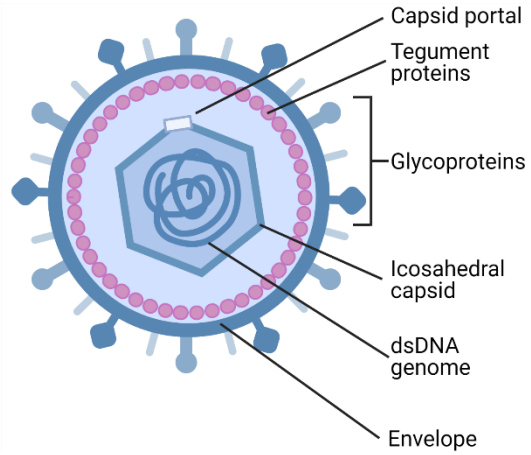

Figure 1.4. Key structural features of HSV1 and HSV2. Both HSV1 and HSV2 have virtually identical virion structures. The genome consists of dsDNA encased in an icosahedral capsid which is attached to the tegument. The tegument is a complex protein layer that connects the capsid to a bilayer envelope which carries a wide range of protruding glycoproteins, many of which play an important role in mediating cell entry.

1.2.3. Sexual Transmission of HSV

Approximately 4.4% of HSV seropositive individuals aged 15-49 present with obvious vesicles, fissures, genital ulceration, and other lesion types within the genital epithelium and the anal canal, however it is estimated that upon careful examination less obvious lesions are present in approximately 20-30% of seropositive individuals (Bernstein *et al.*, 2012). Collectively these presentations are referred to as genital ulcer disease (GUD) (Looker *et al.*, 2020). HSV associated GUD leads to an increase in viral production compared to asymptomatic shedding periods and typically lasts for 2-3 weeks following initial infection; GUD reoccurs far more frequently as a result of HSV2 compared to HSV1 which often only occurs once, however both present similarly and disrupt the epithelial layer of anogenital tissue (Schiffer *et al.*, 2010). GUD is twice as likely to occur in women compared to men and is highest in Africa with female to male sexual transmission being the primary source of new infections (Looker *et al.*, 2020). Studies on serodiscordant couples have demonstrated that the use of condoms reduce the likelihood of male to female HSV transmission significantly, however, the use of condoms during sexual acts between long term partners is infrequent

(Magaret *et al.*, 2016, Wald *et al.*, 2001). Furthermore, the frequency of sexual intercourse in discordant couples plays an important role in transmission: a clinical study has demonstrated that HSV2 transmission is more likely to occur when sexual acts are performed over a longer period at a lower frequency compared to the same number of sexual acts performed in a shorter period of time resulting in a higher frequency (Wald *et al.*, 2001). This is attributed to an increase in the risk of performing sexual acts during a period of increased viral shedding.

It has been demonstrated that HSV2 transmission requires a viral load in excess of 10^4 copies of the virus genome, and that larger ulcers result in a greater degree of viral shedding (Schiffer *et al.*, 2014). Infection primarily occurs from viral shedding by infected keratinocytes that make up 98% of epithelium of the mucosa or skin, however HSV DNA has also been isolated from seminal plasma and can contribute to transmission (Wald *et al.*, 1999). While the risk of virus acquisition from one sexual encounter is low, repeated sexual acts in a short period results in a reduction of the integrity of tissue and degradation of the typically impermeable mucosal barrier, this results in an increased risk of infection (Vitali *et al.*, 2020). Similarly, the injuries that are frequently sustained by anogenital tissue during coercive sexual intercourse also greatly increase the risk of HSV acquisition (Ghebremichael *et al.*, 2009). Furthermore, as shown in patients with psoriasis and atopic dermatitis, HSV1 infiltrates diseased skin with greater ease compared to healthy skin, and may result in the development of a life-threatening secondary viral infection known as Eczema Herpeticum (Liaw *et al.*, 2012). Collectively, these studies highlight the significant role played by microtrauma during sexual encounters in the acquisition and sexual transmission of HSV.

1.2.4. HSV Lifecycle

1.2.4.1. Entry into Target Cells

Both serotypes of HSV can enter a wide range of target cells by mechanisms that are some of the most complex observed in mammalian viruses **(Figure 1.5a)** (Heldwein and Krummenacher, 2008). Cells commonly infected by HSV1 include epithelial cells of the oral-perioral mucosa, while HSV2 infects epithelial cells in the anogenital mucosa; this includes resident MNPs (2%), and keratocytes (98%) (Carmichael *et al.*, 2018). The HSV envelope protein glycoprotein C (gC) binds to glycosaminoglycans, most commonly heparan sulphate (HS) proteoglycans (HSPG) on host cells to initiate viral attachment, however gC deficient virions have been observed to employ gB for attachment to HSPG on host cells at a reduced binding affinity suggesting that gC is not essential to the process (Cagno *et al.*, 2019). In many cases, virion attachment occurs on filopodial surfaces and the virus will migrate to the cell body through an interaction between gB, HSPGs, and actin organisers referred to as viral 'surfing'. (Oh *et al.*, 2010).

Upon arrival at the cell body, interactions between gB, gD, and gH:L and host cell receptors nectin-1/2, herpes virus entry mediator (HVEM), and 3-O-sulfated HS (3-OS HS) result in membrane fusion (Nicola and Straus, 2004). The precise details of how HSV cell entry occurs has not yet been precisely elucidated, however it is well established that gD on the surface of the virion will bind to one or more of the aforementioned host cell surface receptors bringing the virion into close proximity (Akhtar and Shukla, 2009). This induces a conformational change in gD allowing it to interact with gH:L heterodimers; gB that did not bind to HSPGs will then interact with the newly formed gD-gH:L complex causing the gB to extend from a Christmas tree like morphology to an extended form exposing the fusion loops, which puncture the cell membrane and allowing for the viral envelope to fuse with the cell membrane (Vollmer and Grünewald, 2020). gB is the 'conserved fusogen', as its absence completely inhibits fusion

between the viral and host membranes (Cooper and Heldwein, 2015). Once inside the cytoplasm, residual tegument proteins, notably U_L37, facilitate intracellular movement of the capsid to the nucleus, where the capsid portal attaches to a nuclear entry pore and virus DNA is ejected from the capsid into the nucleus (Cardone *et al.*, 2007). Although surface membrane fusion is the most frequent method of cell entry, in epidermal keratinocytes, and both retinal pigment and conjunctival epithelial cells, HSV can be endocytosed in a non-clathrin mediated manner requiring activation of Rho GTPases to trigger significant cytoskeletal rearrangements (Clement *et al.*, 2006) then fuses through the endosomal membrane (Vollmer and Grünewald, 2020). It has also recently been demonstrated that HSV1 may be taken up by epidermal MNPs in subset specific pathways described in **Sections 1.6.1.** and **1.6.3.1.** (Bertram *et al.*, 2021).

1.2.4.2. Lytic Replication of HSV and Therapeutic Targets

The life cycle of HSV1 and HSV2 takes approximately 18-20 hours to complete and is divided into the following major stages: 1) entry into the host cell (discussed above), 2) viral gene expression, 3) replication, 4) assembly of the virion, and 5) egress of the *de novo* synthesised virion particles **(Figure 1.5b)** (Kukhanova *et al.*, 2014). Upon HSV entry into the nucleus, the nucleolus is disrupted, and chromatin condensation is halted while host RNA polymerase II with the assistance of viral factors from the tegument initiate transcription of the viral genome (Neumann *et al.*, 1997, Callé *et al.*, 2008). α genes transcription is facilitated by VP16, these genes produce proteins that significantly reorganise cellular pathways to benefit the virus such as infected cell protein (ICP)0, a protein that degrades proteins involved in defence against viral infection (Rodríguez *et al.*, 2020). Immediate early proteins also initiate the transcription of β genes; these genes initiate viral genome replication such as the gene that encodes a viral DNA polymerase (U_L30) which plays a pivotal role in duplicating the genome (Zarrouk *et al.*, 2017). Once genome replication is initiated, the double helix will unwind and a rolling circle

mechanism will produce concatemeric molecules of viral DNA in a process involving U_L30, other proteins encoded by β genes, and cellular proteins (Howley *et al.*, 2021).

Once genome replication initiates, expression of γ genes is triggered; these genes are essential to the construction of *de novo* capsids and the packaging of the genome into new virions which occurs in the nucleus (Burch and Weller, 2005). HSV is enveloped and de-enveloped at the inner and outer nuclear membrane respectively; once in the cytoplasm, the newly forming virion passes through the trans-Golgi network (TGN) where it undergoes secondary envelopment and acquires envelope proteins (Mettenleiter *et al.*, 2009). After passing through the TGN, the virus is transported in exocytic vesicles by actin fibrils to the cell membrane where it undergoes exocytosis, releasing the virus into the extracellular environment (Miranda-Saksena *et al.*, 2018). HSV infected cells also produce non-infectious virus particles known as L-particles, which consist only of tegument and glycoproteins coated in host cell clathrin that can enter bystander target cells delivering proteins capable of suppressing host cell immune functions increasing infection by infectious HSV virions (Ibiricu *et al.*, 2013). Although there is currently no cure or vaccine for HSV1 or HSV2, there exists a wide range of antiviral medications for HSV that prevent viral genome replication (McCormack *et al.*, 2019).

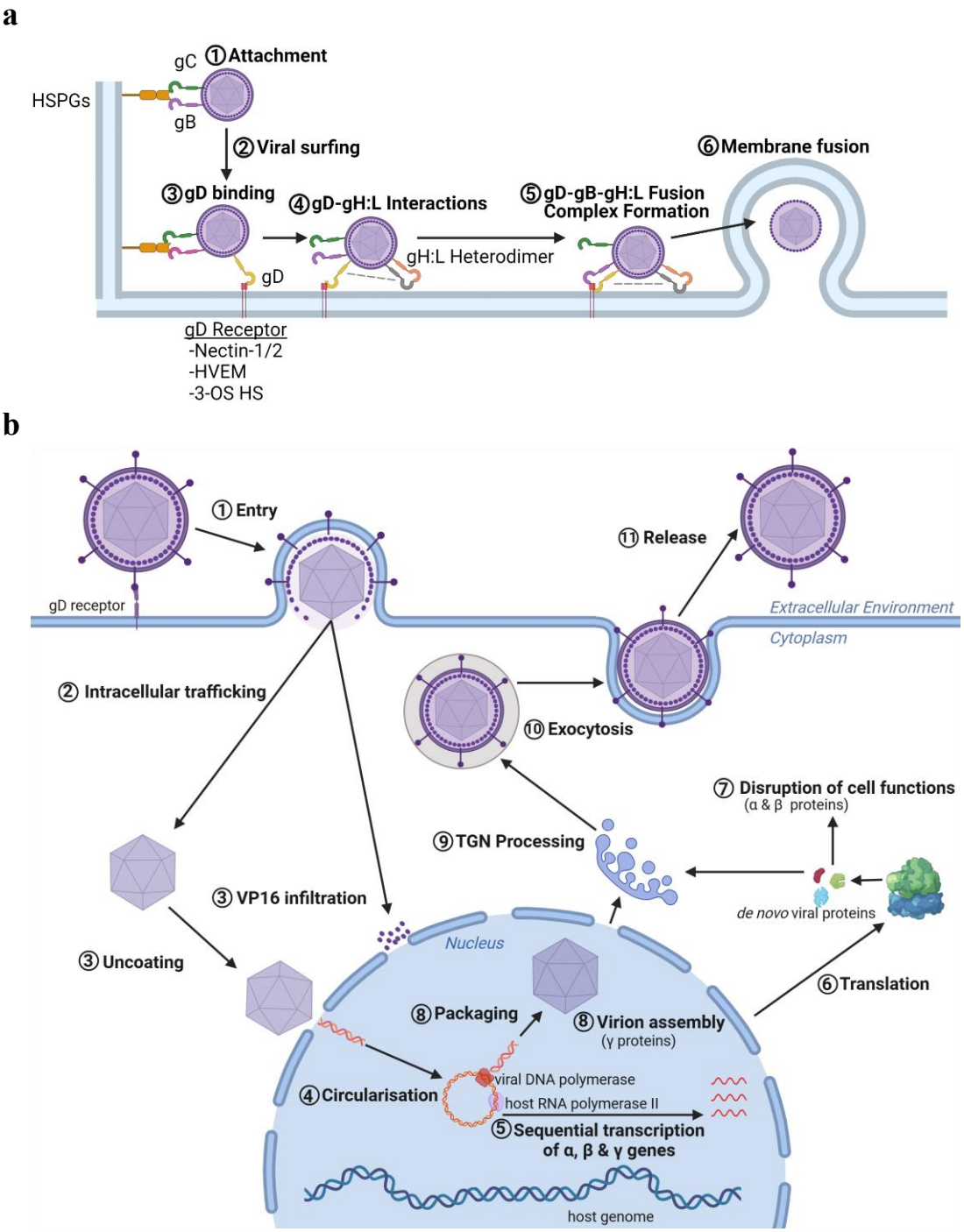

Figure 1.5. HSV1 and HSV2 entry into target cells and inhibition of replication by antiviral therapeutics. (a) HSV entry into host cells is facilitated by envelope glycoproteins. gB or gC binds to HSPGs on the membrane or filopodial surfaces pulling the virion close to the cell surface. gD interacts with gD receptors on the cell surface inducing a conformational change allowing for it to interact with the heterodimer gH:L, and then gB, eventually resulting in membrane fusion. **(b)** The replication cycle of HSV1 and HSV2. Following entry into the cell, tegument proteins traffic the capsid to nuclear pores where the genome is released via the capsid portal for circularisation of the genome, and sequential transcription and translation of

α (facilitated by VP16 infiltrating the nucleus), β, and γ genes. While α and β proteins disrupt the functions of the cell, γ proteins allow for *de novo* replication of the host genome and assembly of viral capsids which are coated in a tegument, enveloped in the TGN, and exocytosed from the cell.

1.2.5. Significant Stages of HSV Infection

1.2.5.1. Immune Response to Primary Infection

Initial or primary HSV1 or HSV2 infection occurs upon first exposure to the virus. Keratinocytes act as the first line of defence against HSV infection by both forming a barrier to pathogen entry and acting as a key component of innate immunity (Heath and Carbone, 2013). Keratinocytes employ pattern recognition receptors such as Toll-like receptors (TLR), RIG-I-like receptors (RLR), and Nod-like receptors (NLR) to detect HSV infection, resulting in the secretion of a vast array of cytokines and chemokines, notably interferon (IFN)β and chemokine C-C ligand (CCL)3-5, triggering the activation of local $CD8^+$ and T helper 1 $CD4^+$ T cells (Sandgren *et al.*, 2020). Early during HSV infection pDCs migrate to infection sites to secrete type I interferons, primarily IFNα, further stimulating T cell proliferation (Schuster *et al.*, 2015). Natural killer (NK) cells play an important role in controlling the severity of infection: it has been demonstrated that mice with defective NK cell populations experience more severe infection than observed in mice with intact NK cell populations (Ashkar and Rosenthal, 2003). Innate lymphocyte cells (ILC), have been demonstrated to infiltrate to inflamed skin in many inflammatory skin conditions and infections and ILCs may also play a role that is currently undefined in HSV infection (Brüggen *et al.*, 2016).

LCs are typically the first APC to encounter HSV. Infected LCs carry HSV to the dermis where they apoptose; $BDCA3^+$ dermal DCs form clusters near infected LC fragments, phagocytose debris, and migrate to nearby lymph nodes for antigen presentation to T and B cells to activate the adaptive immune response (Kim *et al.*, 2015). Following the infiltration of inflammatory cells to infected tissue, components of the adaptive immune system will activate in an attempt

to control infection. B cells residing in lymph nodes will begin to produce IgG a few days and IgA 2 weeks post-infection, these antibodies bind to glycoproteins preventing virions from entering cells (Agostini *et al.*, 2017). T cells play the most critical role in managing HSV infection: $CD4^+$ T helper 1 cells secrete IFNγ, which induces antiviral genes in infected cells (Cunningham *et al.*, 1985). One such gene, protein kinase RNA-activated (PKR), prevents translation from occurring within HSV infected cells (Egan *et al.*, 2013). Interferon gamma also restores major histocompatibility complex (MHC)I expression on infected keratinocytes after downregulation by HSV1 and allows their recognition by specific $CD8^+$ T cells (Cunningham and Noble, 1989). In recurrent lesions, resident memory $CD8^+$ T cells secrete IFNγ to control HSV infection and terminate shedding (Roychoudhury *et al.*, 2020). $CD4^+$ T regulatory cells have also been reported to be present later on in HSV lesions; their role is controversial as they could suppress the immune response resulting in increased infection, but also prevent the inflammatory environment associated with herpetic lesions from excessively damaging surrounding tissue (Fernandez *et al.*, 2008).

1.2.5.2. Establishment and Maintenance of Latency

Although the majority of HSV infected keratinocytes are killed by $CD8^+$ T cells and other components of the immune system, latency is established within sensory neurons resulting in lifelong infection **(Figure 1.6.)** (Cohen, 2020, Truong *et al.*, 2019). Virions enter the neurons via the axon terminal where the capsid travels a long-distance relative to the infection of epithelial cells to reach the cell body in the ganglion and enter the nucleus (Wilson and Mohr, 2012). HSV1 infection of the orolabial region typically establishes latency in the sensory neurons proximal to the trigeminal ganglia, while HSV2 latency is more commonly observed in the sacral ganglia (Whitley *et al.*, 2007). The molecular mechanisms that result in latency in neurons are not yet well defined. For three decades the theory it has been suggested that rapid microtubule-mediated axonal transport of the capsid over long distances within the dorsal root

ganglia compared to the slower transport of VP16 contributes to latency establishment in some neurones by preventing productive gene expression (Roizman and Sears, 1987). Once inside the nucleus, the genome is circularised and loaded with histones by the host cell's DNA repair machinery, allowing for long-term episomal persistence without integration (Howley *et al.*, 2021). During latency, the HSV genes required for productive replication are not transcribed, rather a latency-associated transcript (LAT) is transcribed and several microRNAs units are rapidly developed; these microRNAs stabilise latency by influencing viral and cellular gene expression, preventing antiviral immune responses and host cell apoptosis, and regulate the production of viral proteins (Cohen, 2020).

Infected neurons play a major role in maintaining latency by preventing the virus from reactivating and leading to secondary infection (Howley *et al.*, 2021). Several seminal studies have demonstrated that preventing nerve growth factor (NGF) from binding to its receptor increases viral shedding, suggesting NGF plays a role in latency maintenance (Wilcox and Johnson Jr, 1987, Hill *et al.*, 1997, Camarena *et al.*, 2010). NGF binds to Tropomyosin receptor kinase A (TrkA) to activate several signalling pathways to suppress reactivation: 1) phosphoinositide-dependent kinase (PDK)1, 2) phosphoinositide 3-kinases (PI3K), and 3) protein kinase B (Akt) (Camarena *et al.*, 2010). H3K9me3, an epigenetic modification to histone H3 resulting in gene silencing, is present at an increased frequency in HSV chromatin during latency, likely contributing to the suppression of gene expression (Cohen, 2020). HSV latency is not a uniform process; viral DNA is not evenly distributed among latently infected neurons although the majority of latently infected neurons harbour between 10 to 100 copies of the viral genome, however up to 1000 copies in one neuron has been observed (Cabrera Jorge *et al.*, 2018). Although the significance of this heterogeneity is not clear, it is postulated that ganglia with higher viral copy numbers are more likely to reactivate and cause secondary infections (Nicoll *et al.*, 2012).

1.2.5.3. Reactivation and HSV Secondary Infection

Upon exposure to a triggering factor, latent HSV within ganglia may resume productive infection and release infectious virions **(Figure 1.6)**; triggering factors include UV exposure, stress, trauma to the area surrounding the infected neuron, changes in hormone secretion, and a weakened immune system (Stoeger and Adler, 2019). Reactivation requires HSV episomes to reorganise the chromatin in such a way that α gene expression overcomes the effects of microRNA and other suppressive mechanisms of productive infection; this typically occurs when VP16 levels steadily accumulate in the nucleus (Wysocka and Herr, 2003). During latency reversal, VP16 forms a complex with octamer transcription factor (Oct)-1 and host cell factor (HCF)-1 which replaces the histone modifications suppressing replication such as H3K27me3 with those that assist in the activation of transcription, such as H3K4me3 (Wilson and Mohr, 2012). Gene knockout experiments in HSV1 infected mice have also revealed that ICP0 plays an important role in latency, likely initiating or sustaining cellular gene expression following the activities of VP16 (Halford and Schaffer, 2001). Cyclin-dependent kinases (CDK)2, 4, and 7 are all elevated in neurons during reactivation and replication of HSV; it is believed they play a role in ensuring ICP0 functions nominally (Arthur *et al.*, 2001).

In vitro studies with HSV infected primary rat neurons demonstrated that withdrawal of NGF resulted in virus replication suggesting that when NGF supply *in vivo* is disrupted HSV reactivation may occur (Roizman and Whitley, 2013). Following reactivation of HSV within ganglia, productive infection resumes resulting in the characteristic symptoms of herpes simplex or subclinical shedding of infectious virions; this is termed a secondary or recurrent infection (Groves, 2016). recurrent HSV infection typically resolves much more rapidly than primary infection due to a near-immediate response from the adaptive immune response and are less likely to become systemic (Truong *et al.*, 2019). For unknown reasons there is strong selective pressure on HSV to maintain the fidelity of its genome sequence during reactivation

from the latent state; this genetic conservation will likely prove to be beneficial to vaccine attempts (Minaya *et al.*, 2017). The median frequency of reactivation is 1 and 5 per year for HSV1 and HSV2 respectively in the first two years following primary infection; however, the frequency of reactivation from latency often reduces as time since primary infection increases (Benedetti *et al.*, 1999).

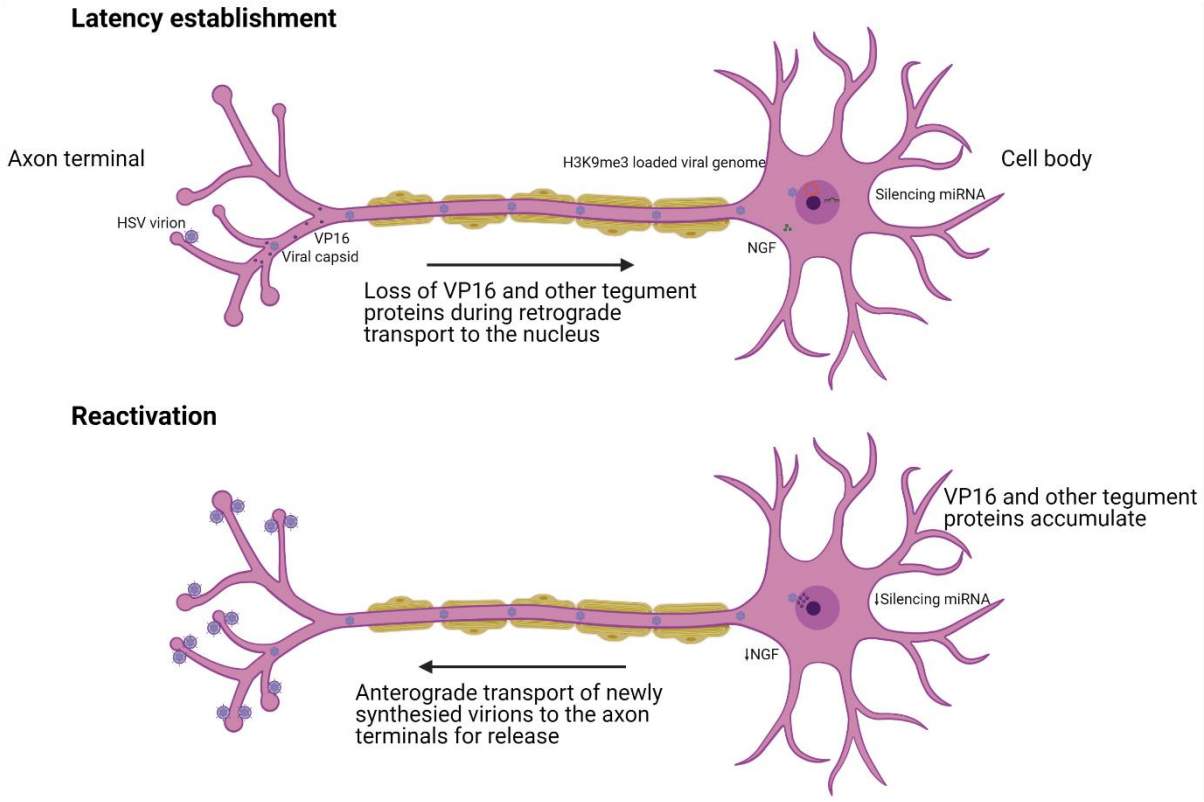

Figure 1.6. The establishment of latent infection within ganglia. During initial HSV infection, virions enter sensory neurons at the axon terminal and travel to the cell body where they enter the nucleus. Due to the intracellular distance virions travel, VP16 and other tegument proteins are lost, preventing transcription of α genes in the nucleus. Host silencing miRNA and chemical cascades initiated by NGF maintain suppression of the virus which is circularised and loaded with the H3K9me3 histone. Over time through accidental transcription by the host of VP16 and other tegument proteins necessary for productive infection allows them to accumulate, resulting in reactivation which can be aided by a reduction in silencing mIRNA or NGF production. Newly synthesised virions will travel from the cell body to the axon terminal where they will release and infect surrounding cells, leading to recurrent or secondary infection.

1.3. Structure of Anogenital Tissue

The physical barrier of various tissues that make up the anogenital tract is the first line of defence against sexually transmitted infections such as HIV, and HSV1 and HSV2. Knowledge of the differences in their anatomy, chemistry, biology, and immunology is important as it provides a better understanding of differences in their susceptibility to infection. The anogenital tract is composed of three tissue types: 1) skin, 2) type II mucosa, and 3) type I mucosa (Hladik and Hope, 2009).

1.3.1. Skin

Skin provides the most robust challenge to STIs as it is the thickest tissue type that comprises the human anogenital tract, ranging from 1 to 5 mm; It is composed of an underlying dermis and the superficial epidermis, linked by the basement membrane (Porth, 2011, Marieb and Hoehn, 2007). The epidermis is composed of 4 or 5 keratinised layers of stratified squamous epithelium, from most superficial to basal, these are: 1) the stratum corneum, 2) the stratum lucidum (only found on hands and feet), 3) the stratum granulosum, the stratum spinosum, and the stratum basale (Marieb and Hoehn, 2007). The stratum corneum is composed of flattened, dead, keratin filled cells that protect against penetration and abrasion; this layer is approximately 25 cells thick and glycolipids are present to protect against water loss (Strayer, 2015). The stratum granulosum is composed of several layers of keratocytes; these cells migrate up towards the stratum corneum while increasing accumulation of keratin and glycolipid granules (Feingold, 2012). The stratum spinosum is of similar thickness to the stratum granulosum and is the most frequent site of LCs; it consists of several layers of keratinocytes containing intermediate filament bundles (Marieb and Hoehn, 2007). The deepest layer of the epidermis is the stratum basale, which consists of a single layer of highly mitotic keratinocytes that are in a state of near-constant division, renewing the keratocyte populations in the superficial layers of the epidermis. Melanocytes in this layer produce melanin granules,

and Merkel cells are sparsely distributed, functioning as mechanoreceptors associated with type A sensory nerve endings in the dermis (Fradette *et al.*, 2003).

The basement membrane plays an important role in adhering the epidermis to the dermis, it also maintains epithelial cell polarity (Strayer, 2015). The dermis is the most significant component of the skin. It hosts nerves, both blood and lymphatic vessels, and skin appendages; it is broadly divided into two layers: the papillary and the reticular layer (Marieb and Hoehn, 2007). The papillary layer is the most superficial and vascularised layer; it is composed of a thin layer of collagen and elastin with projections termed the dermal papillae (Eroschenko and Di Fiore, 2013). The dermal papilla plays a role in keeping the epidermis associated with the dermis and houses both sensory receptors and nerve endings. The reticular layer typically makes up 80% of the dermis; this layer contains much more densely packed collagen and elastin, providing much of the skin's elasticity, strength, and water retention capacities (Eroschenko and Di Fiore, 2013, Marieb and Hoehn, 2007). The dermis is home to most of the immune cells in the skin; these cells and their distributions will be discussed in later sections of this thesis. The dermis also contains several appendages, including hair follicles, sebaceous glands and sweat glands (Marieb and Hoehn, 2007). Hair follicles, located in the dermis, act as a pathway for pathogens to traffic between the dermis and the epidermis (Gilliam *et al.*, 1998). Sebaceous glands associate closely with hair follicles and secrete bactericidal oils which also prevent water loss, while sweat glands secrete either a predominantly water-based substance or a mixture of protein and fatty oils, depending on their type and location (Grice and Segre, 2011).

1.3.2. Type II Mucosa

Type II mucosal surfaces closely resemble skin except for a few key differences that increase their susceptibility to infection (**Figure 1.7**). Type II mucosa consists of a superficial stratified squamous epithelium resembling closely resembling the epidermis, however. it is not as keratinised and is typically covered in mucous (Iwasaki, 2010). Type II mucosal surfaces do not secrete immunoglobulin A due to the lack of polymeric immunoglobulin expression, rather IgG is released by diffusion (Iwasaki, 2010). The underlying sub-epithelium closely resembles the dermis of the skin, except it often lacks the appendages that are found in the skin and contain a higher density of immune cells relative to skin (Hladik and McElrath, 2008). Due to the similarities between the epidermis and dermis of skin, and the squamous epithelium and underlying submucosa of type II mucosa, the terms epidermis and dermis are often used when referring to type II mucosa. Type II anogenital mucosal sites include the vagina, ectocervix, fossa navicularis, and inner foreskin. Due to the extensive use of the inner foreskin and vagina in this thesis, the structure and environment of these tissues will be elaborated on in **Section 1.3.2.1.** & **1.3.2.2.** respectively. Previous work by the host lab has demonstrated that type II mucosa harbours more tissue-resident and non-tissue resident $CD4^+$ T cells than abdominal skin, and this likely holds true for skin from the majority of the body (O'Neil, 2023). This is hypothesised to be an evolutionary response to STIs and as a result of a thinner epidermis, allowing infected hosts to respond to invading pathogens quicker.

1.3.2.1. The Foreskin

The foreskin is a region of tissue that covers the glans of the penis and is composed of an inner and outer component; the inner foreskin makes contact with the glans while the outer foreskin is exposed to the external environment (Dinh *et al.*, 2012). Classification of the inner and outer foreskin as type II mucosa rather than skin is controversial as there is much more keratinisation than what is typically seen in type II mucosa, although observations vary greatly from between

individuals, which may be due to race (Ganor and Bomsel, 2011). Furthermore, some studies have reported that the inner foreskin is less keratinised than the outer foreskin (Ganor and Bomsel, 2011, Lemos *et al.*, 2014), while other studies have not observed any difference (Dinh *et al.*, 2012, Dinh *et al.*, 2010). For the purposes of this thesis, inner foreskin will be considered a form of type II mucosa, which possesses a thin keratinised layer, while the outer foreskin will be considered a form of skin. There are also mixed reports about the abundance and types of immune cells in the inner and outer foreskin.

It is well established that LCs reside in the epidermis (Dinh *et al.*, 2015) and that various subsets of DCs and macrophages can be found in the dermis (Donoval *et al.*, 2006). Some studies have reported no difference in the amount of LCs between the inner and outer foreskin, while others have shown that the inner foreskin is home to more LCs than the outer foreskin (Donoval *et al.*, 2006, Ganor *et al.*, 2010). It has been demonstrated that LC dendrites in the inner foreskin extend more superficially compared to the outer foreskin; this is often attributed to differences in the level of keratinisation (McCoombe and Short, 2006). Both $CD4^+$ and $CD8^+$ T cells are present in the dermis of the inner and outer foreskin, the majority of $CD8^+$ T cells are tissue resident (Donoval *et al.*, 2006, Ganor *et al.*, 2010). Previous work by the host lab has also demonstrated a small population of $CD4^+$ tissue-resident memory T cells in the epidermis of the inner foreskin (O'Neil, 2023), it has also been demonstrated that the inner foreskin contains more $CD4^+$ T cells than the outer foreskin (Dinh *et al.*, 2015). These differences in the number of immune cells in the inner and outer foreskin likely contribute to the differences in susceptibility to HIV infection at each site that has been observed (Liu *et al.*, 2014a). The thinner cornified layers of inner foreskin also acts as an easier entry site for HSV and is a clinically common site of recurrent lesions (Rana *et al.*, 2024).

1.3.2.2. The Vagina

The vagina is an 8-10 cm tube of fibromuscular tissue between the hymen and the cervix; it acts as the connection between the internal and external female genital tract (Lloyd *et al.*, 2005). The vagina consists of type II mucosa of a thickness that is approximately 200 μm with multiple ridges which allow for extension during sexual intercourse and childbirth (Marieb and Hoehn, 2007). Mucous is secreted by the cervical glands and then acidified by the microflora of the vagina, providing an extra defence against pathogens (Klebanoff and Coombs, 1991). The tough stratified squamous epithelial epidermis plays an important role in protecting the dermis from friction at this site (Shen *et al.*, 2011). As seen with most type II mucosa, the surface of the vagina is characterised by limited keratinisation. The diverse microflora present in the vagina, especially *Lactobacilli*, limits the establishment of pathogens through competition and the production of hydrogen peroxide and lactic acid (Quayle, 2002). It has been demonstrated that the likelihood of HSV and HIV infection is reduced in the presence of vaginal lactobacilli both *in vivo* and *in vitro* (Zabihollahi *et al.*, 2012), and there is currently great interest into the role of vaginal dysbiosis in HIV acquisition. The underlying dermis has deeper papillae than seen in type II mucosal surfaces; these extend deep into the epidermis and are supplied with nutrients by a significant network of small blood vessels (Pudney *et al.*, 2005).

Similar to the inner and outer foreskin epidermis, the vagina houses LCs, both $CD8^+$ and $CD4^+$ T cells as well as low numbers of macrophages (Edwards and Morris, 1985, Duluc *et al.*, 2013, Pudney *et al.*, 2005). The dermis contains significant numbers and types of DC subsets as well as both $CD8^+$ and $CD4^+$ T cells (Mselle *et al.*, 2007). Previous work from the host lab has demonstrated that there is a larger $CD4^+$ tissue-resident memory cell population in the epidermis of the vagina than the inner and outer foreskin, although these cells are more frequent in the dermis (O'Neil, 2023). It has also been shown that $CD8^+$ T cells are more prevalent in the dermis of the vagina than the epidermis; $CD103^+$, a marker for mucosal tissue residency, is

also expressed at higher levels than observed in other sites of the body (Hladik *et al.*, 2007, Pudney *et al.*, 2005). The majority of T cells in non-inflamed vaginal tissue, like all type II and I mucosa, and the skin as a whole, are memory cells, although some circulating naïve cells are also present (Ildgruben *et al.*, 2003, Pudney *et al.*, 2005). The number of immune cells in the dermis is highest proximal to the basement membrane (Pudney *et al.*, 2005); this is also true for other type II mucosa such as the inner and outer foreskin (Marieb and Hoehn, 2007).

1.3.3. Type I Mucosa

Type I mucosa has significant structural differences compared to skin and type II anogenital mucosa **(Figure 1.7.)**. The epithelium of type I mucosa is a single layer of columnar epithelium that is maintained by paracrine and autocrine secretion of interleukin (IL)-3; this allows for more efficient transport of molecules and nutrients (Oh *et al.*, 2019). Such a thin epithelium results in an increased susceptibility to ulcers and micro-abrasions that can be used as portals for HIV entry (Miller *et al.*, 2005). The epithelial layer also contains goblet cells, which are responsible for maintaining the mucous membrane through the secretion of mucins, which are large glycoproteins that store large amounts of water, giving them gel like properties (Johansson *et al.*, 2013). The underlying sub-epithelium of type I mucosa is termed the lamina propria and contains lymphoid aggregates known as mucosa-associated lymphoid tissue (MALT), which act as local lymph nodes housing lymphocytes and plasma cells; it is believed that this contributes to an even higher density of immune cells than that observed in type II mucosa (Iwasaki, 2010). The innermost sites of the body are lined with type I mucosa, including the endocervix, rectum, bronchi, lungs, colon, and penile urethra.

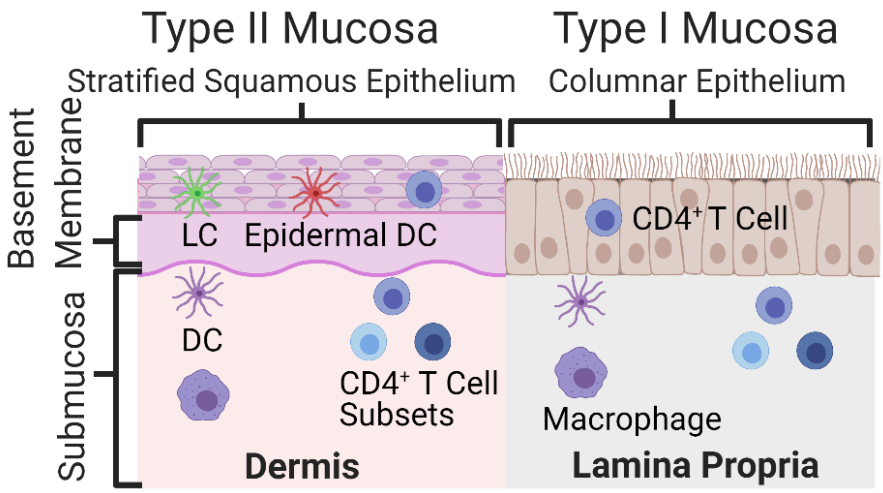

Figure 1.7. Comparison of Type I and II mucosa. Type I and II mucosa make up the majority of the anogenital mucosa. Type II mucosa consists of an outer layer of stratified squamous epithelium resembling a thinner version of the epidermis seen in the skin; it harbours LCs, epidermal DCs and $CD4^+$ T cells. Type II mucosal surfaces less keratinised than skin. The stratified squamous epithelium is attached to an underlying submucosa referred to as the dermis by a layer of connective tissue known as the basement membrane. The dermis harbours significantly more immune cells than the above layers, including macrophages, DCs, and $CD4^+$ T cells. Type I mucosa consists of an outer single row of columnar epithelial cells that harbour $CD4^+$ T cells and is attached to an underlying submucosa termed the lamina propria. The lamina propria harbours similar immune cells to those observed in type I mucosal dermis, albeit at increased densities.

1.4. $CD4^+$ T Cells

$CD4^+$ T cells are the major site of HIV infection, where it undergoes explosive replication, and also the latent reservoir, as well as an important cell in the HSV1 and HSV2 immune response. This section will explore the different subsets of both naïve and memory $CD4^+$ T cells. $CD4^+$ T cells originate from the bone marrow as haematopoietic stem cells, they migrate to the thymus where they specialise and progressively differentiate into T cells (Koch and Radtke, 2011). The developing 'thymocytes' undergo beta-selection, a process that selects for cells that develop pre-TCR chains; cells that successfully pass beta-selection will develop TCR-CD3

complexes, promoting cell survival and proliferation, while those that do not develop pre-TCR will be apoptosed (Kang *et al.*, 2001). The surviving CD3 expressing cells go on to express both CD4 and CD8 and are assessed by positive selection for low affinity for self-peptides bound to MHC expressed on epithelial cells; successful low affinity binding results in survival signals for the cell (O'Neil *et al.*, 2021). Following successful positive selection, negative selection takes place where high or excessive affinity for self-peptides bound to MHC expressed by thymic DCs results in cells receiving apoptotic signals (Vanhecke *et al.*, 1995b). The surviving cells differentiate into CD8 or CD4 single-positive cells and downregulate the tissue retention marker CD69, allowing their emigration from the thymus as mature T cells (Vanhecke *et al.*, 1995a).

Following their development in the thymus, $CD4^+$ T cells are termed 'naïve' due to their lack of exposure to antigen; naïve $CD4^+$ T cells express CD45A, CD62L, CCR7 and sphingosine 1-phosphate (S1P)1, which allows for migration to lymph nodes, the spleen, Peyer's patches and tonsils (Gunn *et al.*, 1998, Caccamo *et al.*, 2018). Upon exposure to their cognate antigen, $CD4^+$ T cells differentiate into a T helper subset, which if exposed to stimulating memory signals, may progress to a memory cell. $CD4^+$ T helper (T_h) cells play a critical role in the immune system by secreting cytokines that combat infection, and activate other immune cells and components of innate and adaptive immunity (Deepak *et al.*, 2017). Memory T cells play important roles in limiting reinfection; upon re-exposure to an antigen, they rapidly proliferate from a repertoire of antigen-specific, long-lived, resting cells to develop a $CD4^+$ T cell population that is specific to the foreign antigen (Murray *et al.*, 2016).

1.4.1. The Role of CD4$^+$ T Cell Subsets in HIV and HSV Infection

Upon antigen presentation by DCs and LCs, the majority of naïve CD4$^+$ T cells activate and differentiate into the specialised subsets of CD4$^+$ T_h effector cells: follicular (T_{FH}), regulatory (T_{REG}) and T_h 1, 2, 9, 17, and 22; they then downregulate markers associated with naivity and upregulate a variety of chemokine receptors **(Figure 1.8)**, notably CCL3, CCL4, and CCR5, allowing for migration to sites of inflammation such as the source antigen to clear infection (Castellino *et al.*, 2006). As the respective mediators of antiviral immunity and mucosal immunity, CD4$^+$ T_h1 and T_h17/T_h22 cells play an essential role in the immune response against HIV and both HSV serotypes (d'Ettorre *et al.*, 2014, Baiyegunhi *et al.*, 2018). All subsets of T_h cells interact with HIV in unique ways, however CD4$^+$ T cells are more important in the control of HSV infection (Cunningham *et al.*, 1985), and instead act as target cells for HIV.

1.4.2. CD4$^+$ T_h Cells Subsets

1.4.2.1. CD4$^+$ T_h1 Cells

A key effector function of CD4$^+$ T_h1 cells is IFNγ secretion, which promotes adaptive immune responses against intracellular pathogens such as HIV and HSV (Cope *et al.*, 2011). T_h1 differentiation is induced by IL-12 and they are regulated by the transcription factor T-bet; T_h1 cells also produce IL-22, IL-2 and TNF-α (Löhning *et al.*, 2008). A recent *in vitro* study demonstrated that T_h1 cells express elevated levels of CCR5, resulting in increased susceptibility to infection by CCR5 tropic HIV strains (Orlova-Fink *et al.*, 2017). It has also been demonstrated that CD4$^+$ T_h1 cells are not only productively infected with HIV, but contain genetically intact HIV provirus DNA and undergo significant clonal expansion during HIV infection; this implicates T_h1 cells as a significant source of both productive and latent infected CD4$^+$ memory cells (Lee *et al.*, 2017).

1.4.2.2. $CD4^+$ T_h2 and T_h9 Cells

$CD4^+$ T_h2 cells play an important role in helminth immunity and the regulation of the humoral response through the facilitation of B cell proliferation; they are regulated by the transcription factor GATA-3 and secrete IL-13, IL-5 and IL-4 (Walker and McKenzie, 2018). $CD4^+$ T_h9 cells play roles in tumour suppression, allergic inflammation, and autoimmune diseases; they are regulated by the transcription factor PU.1 and primarily produce IL-9 (Kara *et al.*, 2013, Chang *et al.*, 2010). There is limited information on the role of T_h2 and T_h9 cells in the context of HIV infection, however studies have demonstrated that these T_h subsets express high levels of CXCR4 making them more susceptible to CXCR4 tropic HIV strains rather than CCR5 strains (Gosselin *et al.*, 2010, Orlova-Fink *et al.*, 2017).

1.4.2.3. $CD4^+$ T_h17 Cells

$CD4^+$ T_h17 cells are regulated by the transcription factor RAR-related orphan receptor gamma (RORγ)T and primarily secrete IL-17, initiating the production of antimicrobial molecules by epithelial cells that protect against mucosal pathogens (Xu and Cao, 2010). T_h17 cells produce 6 types of IL-17 proteins (A-F) as well as IL-22, IL-26, and IL-26 (Dambacher *et al.*, 2009, Xu and Cao, 2010). T_h17 express high levels of both HIV co-receptors, lack HIV inhibitory RNAses, and do not secrete CCR5 ligands, making them highly susceptible to HIV infection (Christensen-Quick *et al.*, 2016, Alvarez *et al.*, 2013). In studies focusing on HIV patients and SIV infected macaques it has been observed that T_h17 cells deplete at a more rapid rate than other T_h subsets in both the intestinal mucosa and peripheral blood; this results in chronic inflammation and increased microbial translocation from the intestinal lumen (Chege *et al.*, 2011, Ryan *et al.*, 2016). Importantly, T_h17 cells are also enriched in the inner foreskin of uninfected men, although the dynamics of these cells during HIV infection remain to be determined (Galiwango *et al.*, 2019). While suppression of viral load by ART restores T_h17

cell populations in the blood, for the majority of HIV infected individuals, there remains a decreased number of T_h17 cells in mucosal tissue (Sandler and Douek, 2012).

1.4.2.4. CD4$^+$ T_h22 Cells

Similar to T_h17 cells, CD4$^+$ T_h22 cells play an important function in gut homeostasis; T_h22 cells express levels of IL-22 similar to T_h17, which stimulates enterocytes to produce antimicrobials and preserves the structural integrity of the gut epithelial barrier (Xu *et al.*, 2014). T_h22 cells are regulated by Aryl hydrocarbon receptors and can be phenotypically differentiated from T_h17 cells by CCR10 expression (Duhen *et al.*, 2009). Similar to T_h17 cells, studies in SIV infected macaques and HIV infected individuals have demonstrated that T_h22 cells are depleted in peripheral blood, colon and the rectum, resulting in mucosal barrier damage and increased microbial translocation (Kök *et al.*, 2015, Ryan *et al.*, 2016). Unlike T_h17 cells, viral suppression by ART restores T_h22 populations in tissue, however despite their similar function to T_h17 they are unable to compensate for the loss of T_h17 cells at mucosal surfaces that is observed in ART virologically suppressed patients (Sandler and Douek, 2012). The presence of T_h22 cells in the gut despite the absence of T_h17 cells is attributed to the use of a CCR10-CCL28 chemotactic gradient that continues to occur in virologically suppressed HIV patients; the CCR6-CCL10 gradient typically employed by immune cells for gut migration, including T_h17 cells, is impaired during ART treatment (Nayrac *et al.*, 2021). Finally, a recent study focusing on uninfected men has demonstrated that T_h22 cells are enriched in the outer foreskin compared to the inner foreskin (Galiwango *et al.*, 2019).

1.4.2.5. CD4$^+$ T_{REG} cells

CD4$^+$ T_{REG} cells play an essential role in regulating inflammation during an immune response through the secretion of immunosuppressive cytokines, notably IL-10 and transforming growth factor (TGF)-β; they also sequester IL-2, resulting in the apoptosis of T cell populations (Smith,

2012). Rather than deplete, studies focusing on the rectal mucosa and cervix demonstrate that T_{REG} cell frequencies become elevated during HIV infection (Rueda *et al.*, 2013, Shaw *et al.*, 2011). It has been demonstrated that HIV elite controllers, patients with the ability to limit $CD4^+$ T cell depletion and thus potentially not progress to AIDS, have lower frequencies of T_{REG} cells compared to normal progressors in rectal mucosa (Shaw *et al.*, 2011). However, in both cohorts, T_{REG} cells limit the proliferation of other T cell populations to similar extents, suggesting they maintain their functions during chronic infection and play a role in diminishing the T cell response to HIV (Jiao *et al.*, 2015, Shaw *et al.*, 2011). While sustained ART reduces the T_{REG} cell frequency, it does not return to the levels observed prior to HIV infection (Caruso *et al.*, 2019, Rueda *et al.*, 2013). T_{REG} cells have also been implicated in the formation of the latent reservoir: A recent study showed HIV replication was inhibited by T_{REG} cells in resting $CD4^+$ cells by a cyclic adenosine monophosphate (cAMP) dependent protein kinase A (PKA) pathway, potentially contributing to virus latency (Li *et al.*, 2017). T_{REG} cells themselves are also an important HIV reservoir: Significant amounts of proviral DNA has been found in these cells in ART-treated HIV infected individuals and SIV infected macaques(McGary *et al.*, 2017).

1.4.2.6. $CD4^+$ T_{FH} Cells

$CD4^+$ T_{FH} cells are located in the germinal centres of lymphoid tissue. They are responsible for class-switching and promote somatic hypermutation of antibodies; T_{FH} cells are regulated by B cell lymphoma (bcl)-6 (Crotty, 2014). T_{FH} cells express high levels of CXCR4 and low levels of CCR5, making them susceptible to CXCR4 tropic strains, however CCR5 tropic strain provirus is still the primary DNA detected in T_{FH} cells (Xu *et al.*, 2017). It is hypothesised that T_{FH} precursor populations that express CCR5 are preferentially infected with CCR5 strains of HIV, and upon TCR stimulation, these populations differentiate into HIV infected T_{FH} cells (Xu *et al.*, 2017). $CD8^+$ T cells are unable to enter the follicular regions of lymph nodes to

target infected cells, and ART is unable to effectively penetrate lymphoid tissue; this implicates T_{FH} cells residing in follicles as a potentially significant site for persistent HIV replication (Martinez-Picado and Deeks, 2016, Connick *et al.*, 2007).

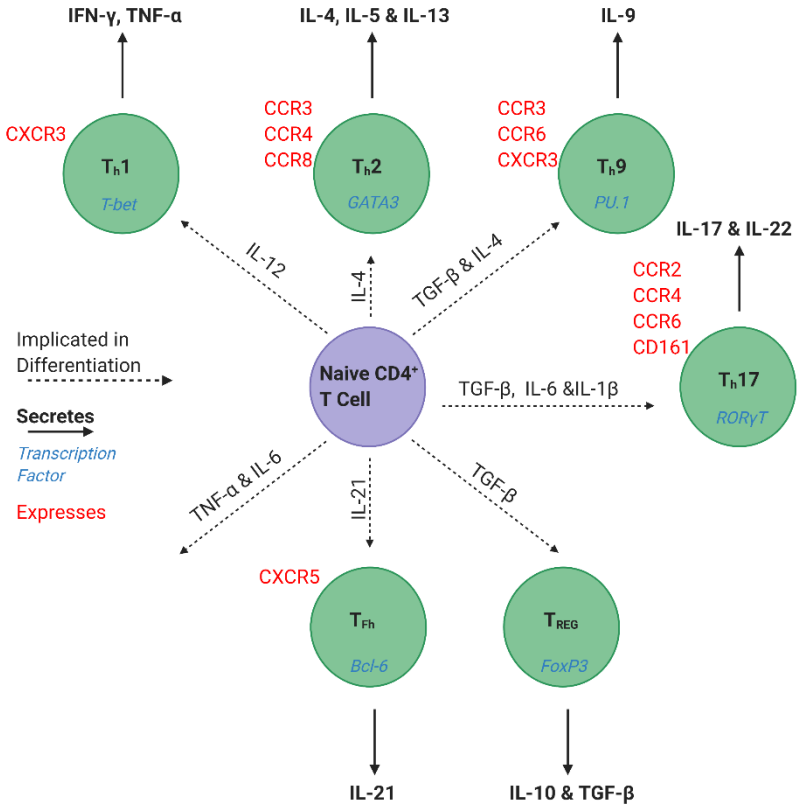

Figure 1.8. Summary of CD4$^+$ T helper cell subsets. Each subset of CD4$^+$ T_h cells is characterised by a combination of the cytokines they secrete (bolded), and the transcription factors that regulate them (italicised, blue). Each CD4$^+$ T helper cell subset also expresses a combination of surface markers (red) that is unique and specific to the function they perform and where they localise.

1.4.3. CD4$^+$ T Memory Cells

After CD4$^+$ T cells help clear foreign pathogens, a small number differentiate to form CD4$^+$ T memory cells (Fritsch *et al.*, 2005). It has not yet been established whether specific subsets of CD4$^+$ T_h cells progress to form memory cells for each, or if the process is generalised; however, the host lab is undergoing studies to address this gap in the literature. Despite their

heterogeneity, $CD4^+$ T memory cells typically express CD45RO, contrasting with naïve $CD4^+$ T cells which express CD45RA (Beynon *et al.*, 2012). Unlike naïve $CD4^+$ T_h cells, T memory cells progressively differentiate in a particular order through four major circulating subsets: stem cell-like memory (TSCM), central memory (TCM), transitional memory (TTM) and effector memory (TEM) (**Figure 1.9.)** (Youngblood *et al.*, 2013). There also exists a more recently discovered and highly differentiated subset of $CD4^+$ T memory known as tissue-resident memory (TRM) cells: These cells are retained in the tissue and therefore do not circulate (Wakim *et al.*, 2010). Following exposure to a cognate antigen, naïve $CD4^+$ T cells progressively differentiate from $CD4^+$ TSCM to TRM cells, how far they progress depends on the persistence and strength of the signals that initiated memory differentiation (Gattinoni *et al.*, 2017). The capacity for $CD4^+$ T memory cells to perform their T effector cell functions increases as they become more differentiated, this is accompanied by increased antigen dependence for cell survival and reduced proliferation and self-renewal (Dagenais-Lussier *et al.*, 2016). Each $CD4^+$ T memory cell subset expresses different surface markers, these can play a role in survival (CD27), lymph node homing (CCR7) and mediation of apoptosis (CD95; **Figure 1.9)** (Okada *et al.*, 2008).

1.4.4. $CD4^+$ T Memory Cells Subsets and Their Contribution to the Latent Reservoir

1.4.4.1. $CD4^+$ TSCM

It was hypothesised, and now generally accepted, that before the development of canonical memory cell subsets (TCM-TEM), a population of memory $CD4^+$ T cells with stem cell-like properties, termed $CD4^+$ TSCM cells exists (Gattinoni *et al.*, 2011). TSCM cells have a phenotype largely resembling $CD4^+$ naïve T cells, however overexpress CD95 (Lugli *et al.*, 2013). Although most activated and resting memory T cell populations diminish in the absence of cognate antigen, TSCM cells have a tenfold increase in survival when compared to TCM cells in the absence of antigen; this, along with their multipotency has implicated them as being

essential in the maintenance and regeneration of other CD4$^+$ memory T cell subsets (Gattinoni *et al.*, 2011). It has also been demonstrated that TSCM cells contain the highest proportion of integrated HIV provirus (Buzon *et al.*, 2014). Despite the high amount of integrated HIV provirus and the long-lived nature of TSCM cells, the scarcity of the cell population means that they only make up an average of 8% of cells that contribute to the latent HIV reservoir (Buzon *et al.*, 2014, Gattinoni *et al.*, 2011).

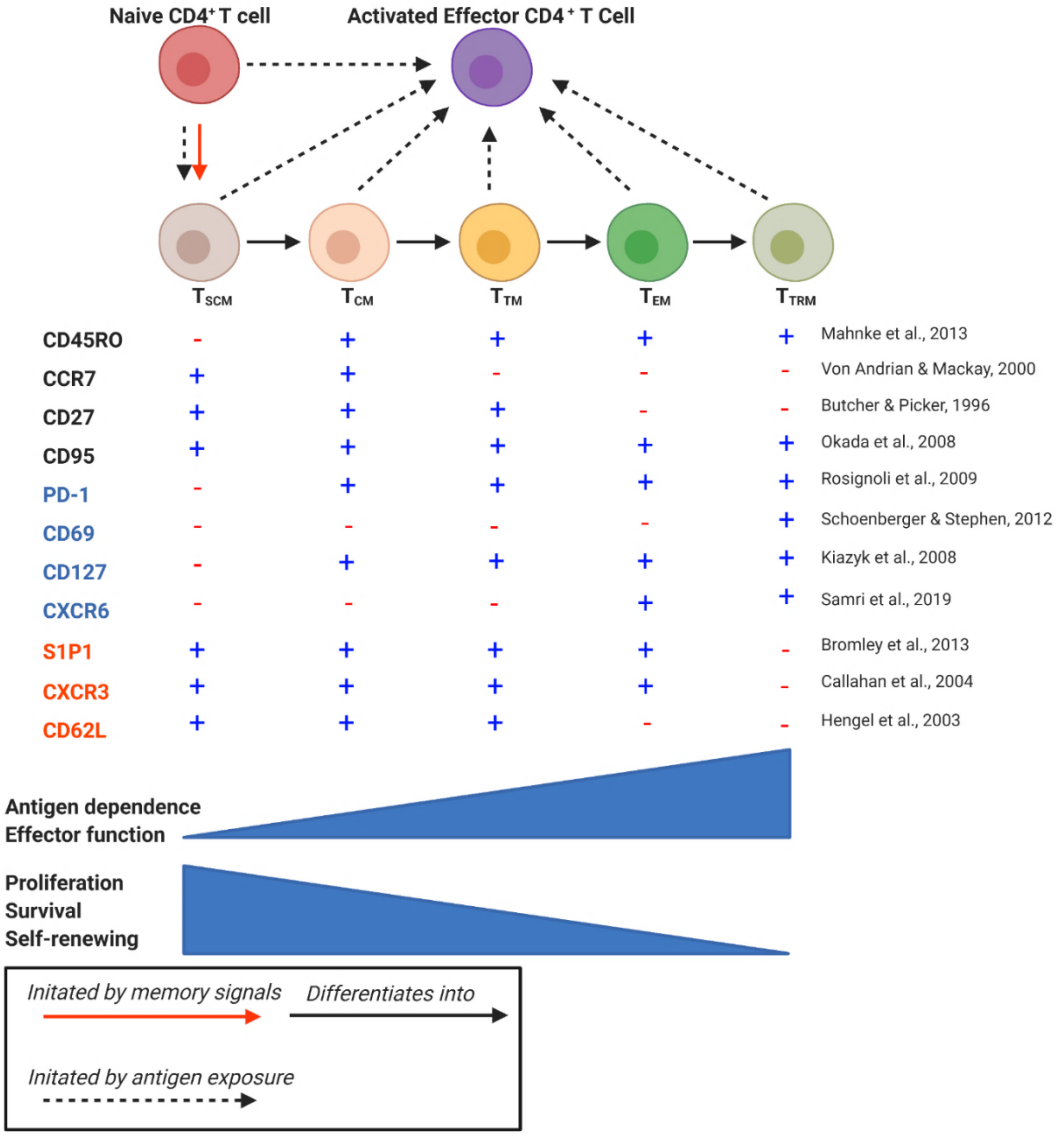

Figure 1.9. Differentiation and phenotype of subsets of CD4$^+$ T memory cells. There are 4 circulating subsets of CD4$^+$ T memory cells: TSCM, TCM, TTM, and TEM while TRM cells reside in tissues around the body. Surface markers that are in red are downregulated in CD4$^+$ TRM while those that are red are upregulated; this phenotype plays a significant role in tissue retention.

1.4.4.2. $CD4^+$ TCM Cells

$CD4^+$ TCM cells are a long-lived memory subset with some capacity for self-renewal; they have limited effector function however upon recognition of antigen, rapidly differentiate into subsets capable of responding to reinfecting pathogens (Sallusto *et al.*, 2004). TCM cells express CCR7 and CD62L, which allows for migration between secondary lymphoid organs (SLO); this has implied that the limited effector functions TCM cells perform are localised to SLOs (Cyster, 2005). While significant amounts of HIV DNA can be found in TCM cell genomes, it is typically defective and doesn't lead to productive infection (Horsburgh *et al.*, 2020). Interestingly, it has been demonstrated that in viremic non-progressors, individuals with high viremia but normal $CD4^+$ T cell numbers, $CD4^+$ TCM cells have a decreased susceptibility to infection, implicating these cells in the preservation of T cell homeostasis (Klatt *et al.*, 2014). Furthermore, a recent study showed that CXCR4 dependent HIV strains are more commonly found integrated in TCM and naïve T cells than CCR5 dependent HIV strains (Samri *et al.*, 2019).

1.4.4.3. $CD4^+$ TTM Cells

$CD4^+$ TTM cells have a capacity for proliferation similar to $CD4^+$ TCM cells, however, are more differentiated and responsive to IL-15, a cytokine associated with the inducement of proliferation; they represent a transitional state between TCM and TEM cells (Soriano-Sarabia *et al.*, 2014). TTM cells express CD27, however downregulate the lymphoid homing marker CCR7, allowing them to circulate in the blood without homing to lymph nodes (Mo *et al.*, 2020). While TTM cells harbour more replication-competent virus than TCM memory cells, they have significantly less than TEM cells (Soriano-Sarabia *et al.*, 2014). During HIV infection, it has also been demonstrated that longer durations of ART in HIV patients are linked to a decreased frequency of infected TTM cells in peripheral blood; this suggests that while

TTM cells may contribute to the HIV reservoir, over time their contribution wanes (Soriano-Sarabia *et al.*, 2014).

1.4.4.4. $CD4^+$ TEM Cells

$CD4^+$ TEM cells are a memory subset that is differentiated by a lack of CCR7 and CD27 expression, preventing lymph node homing and survival without antigen presence (Lintermans *et al.*, 2017). TEM cells are short-lived, however are able to respond to reinfection rapidly and have a significant capacity for effector function (Caccamo *et al.*, 2018). TEM cells contain a higher proportion of replication-competent integrated HIV provirus than TTM and TCM cells, but make up a very small proportion of memory cells, limiting their contribution to the latent reservoir (Hiener *et al.*, 2017). It has been demonstrated that IFNα secretion by plasmacytoid dendritic cells reactivates latent reservoirs within resting TEM cells, however, this happens in the absence of infection of bystander cells suggesting the cell employs mechanisms to prevent viral release (Tong *et al.*, 2021).

1.4.4.5. $CD4^+$ TRM Cells

$CD4^+$ TRM cells are a more recently discovered memory subset that resides in peripheral tissue without recirculation, this allows for near-immediate responses in tissue to invading pathogens (Kumar *et al.*, 2017). What triggers TRM cell differentiation from TEM cells remains unclear, however, their phenotypic similarity to TEM cells and interactions with IFNα secreting pDCs has suggested that when TEM cells enter tissue, exposure to pDCs and other local factors induces their differentiation into TRM cells (Tong *et al.*, 2021). $CD4^+$ TRM cells express the tissue retention markers CD103 and, most frequently, CD69; they also upregulate survival the survival marker CD127 and decrease egression markers such as CCR7, CD62L, and S1PR1 (Mackay *et al.*, 2015a, Rajasuriar *et al.*, 2010). PD-1, which is known to inhibit T cell activation is upregulated on $CD69^+$ TRM cells and TRM demonstrate phenotypic differences that are

specific to the tissue from which they are isolated from; some of these differences include CCR9 and cutaneous lymphocyte antigen which play a role in determining tissue homing (Sharpe and Pauken, 2018, Nguyen *et al.*, 2019).

Interestingly, it has been demonstrated that TRM cells harbour more than 200 times more HIV DNA and protein than any other subset of memory T cells in cervix (Cantero-Pérez *et al.*, 2019). It has also been postulated that the $CD4^+$ T cells that localise to the neuronal ganglia, suppressing HSV reactivation alongside $CD8^+$ T cells, are $CD4^+$ TRM cells, however this has not yet been conclusively proven (van Velzen *et al.*, 2013, O'Neil *et al.*, 2021). In murine models, it has been shown that $CD4^+$ T cells responding to HSV1 infection form memory cells at the site of infection. Nevertheless these cells have only be observed returning to circulation and not being retained in tissue as TRM cells, however this has not yet been excluded (Gattinoni *et al.*, 2011, Mackay *et al.*, 2015a). Furthermore, it has been demonstrated in the vagina of parabiotic mice infected with attenuated HSV-2 then reinfected at a later point that mice with $CD4^+$ TRM cells cleared infection quicker, suggesting that $CD4^+$ TRM cells are an important immunological component in the defence against HSV1 and 2 (Iijima and Iwasaki, 2014). In humans, Zhu *et al.* (2007) have observed the persistence of memory $CD4^+$ and $CD8^+$ T cells between recurrent herpes lesions which are almost certainly TRM cells (Zhu *et al.*, 2007).

1.4.5. Maintenance and Establishment of HIV Latency

$CD4^+$ T memory cells are characterised as resting or in an activated state. Activated cells express the activation markers CD69, CD38, CD25 and human leukocyte antigen DR isotype (HLA-DR) (Mahnke *et al.*, 2013). While infection of activated $CD4^+$ T memory cells result in explosive viral replication, infection of resting memory cells results in latent infection. Virus is integrated into the host genome and is transcriptionally silent in the various memory cell lineages (Mahnke *et al.*, 2013, Kumar *et al.*, 2017). Two pathways lead to latent infection: 1)

directly due to depletion of deoxyribonucleotide triphosphates employed by HIV for reverse transcription through the actions of cell factors such as sterile alpha and motif aspartic acid domain-containing protein (SAMHD)-1; or 2) indirectly when an activated $CD4^+$ T memory cell is infected and returns to a quiescent state before apoptotic pathways responsible for the cessation of provirus production are initiated (Lahouassa *et al.*, 2012, Choudhary *et al.*, 2012). HIV latency is maintained by reduced expression of cell factors that are essential for transcription; notably this includes nuclear factor of activated T cells (NFAT) and nuclear factor kappa light chain enhancer of activated B cells (NF-κB) (Acchioni *et al.*, 2019). A recent *in vitro* study performed with $CD4^+$ T memory cells isolated from peripheral blood also demonstrated that PD-1 is important in latency maintenance and that blocking PD-1 reduced the number of latently infected memory cells (Evans *et al.*, 2018). Integrated HIV can survive and remain dormant in $CD4^+$ T memory cells for many years during ART suppression due to their long-lived nature, however, upon ART interruption, virus replication is induced (Burnett *et al.*, 2010).

1.5. $CD8^+$ T Cells

1.5.1. Introduction to $CD8^+$ T Cells

$CD8^+$ T cells, commonly referred to as cytotoxic or killer T cells, are a type of T lymphocyte adept at recognising intracellular pathogens including HSV1/2 and HIV, as well as neoplastic cells (Al-Shura, 2020). Similar to $CD4^+$ T cells, $CD8^+$ T cells express CD3 and possess antigen-specific TCRs that mature in the thymus through positive and negative selection resulting in the production of naïve $CD8^+$ T cell populations (Koch and Radtke, 2011). Activation of naïve $CD8^+$ T cells is initiated by exposure to MHC-I molecules carrying antigens that interact with the TCR and CD8 coreceptor (Lanzavecchia, 1998). Unlike MHC-II, MHC-I is expressed on the surface of the majority of cells to allow for the recognition of infected or dysfunctional cells. $CD8^+$ T cells also require a second signal to activate, the CD28 surface receptor must

bind to costimulating molecules such as CD80 or CD86 on DCs; costimulatory molecules are also secreted by $CD4^+$ T cells (Shedlock *et al.*, 2003). Once a naïve $CD8^+$ T cell is activated, CD40 signalling will trigger differentiation from a naïve $CD8^+$ T cell to an activated T cell and paracrine secretion of IL-2 by $CD4^+$ T cells will result in clonal expansion of antigen recognising $CD8^+$ T cell lineages, resulting in a large population of $CD8^+$ T cells specific to the offending antigen (Bennett *et al.*, 1998). The transcription factor implicated in $CD8^+$ T cell regulation is Eomesodermin: A study using murine models demonstrated that reduced Eomesodermin prevented $CD8^+$ T cells from producing proteins essential to their effector function (Pearce *et al.*, 2003).

When an activated $CD8^+$ T cell binds to a dysfunctional/infected cell, it releases cytotoxins such as granzymes, perforin, and granulysin (Bennett *et al.*, 1998). Perforin creates pores in the membrane of cells allowing granzymes to gain access to the cell; once inside the cell granzymes, which act as serine proteases, initiating the caspase cascade which results in apoptosis (Ahmadzadeh and Rosenberg, 2005). It has also been demonstrated that an essential part of this process is the restructuring of the cell membrane of $CD8^+$ T cells to prevent accidental autologous cell death through the actions of perforin and granzymes (Ahmadzadeh and Rosenberg, 2005). Granulysin is a pore-forming protein that only affects microbial cells, this gives $CD8^+$ T cells some effector function against bacterial pathogens and other microorganisms (Dotiwala and Lieberman, 2019). $CD8^+$ T cells may also induce apoptosis by an interaction between the surface protein Fas ligand (FasL) which is expressed on activated $CD8^+$ T cells and Fas, which is expressed on most cells (Li *et al.*, 2002). When FasL binds with Fas, the death-induced signalling complex (DISC) is recruited and the Fas-associated death domain (FADD) associates with DISC leading to the recruitment of procaspases 10 and 8; the newly formed complex activates caspases 7, 6 and 3 resulting in cleavage of DNA and

activation of protein kinases, poly-adenosine diphosphate ribose polymerase, and other death substrates, resulting in target cell apoptosis (Lee *et al.*, 2003).

1.5.2. $CD8^+$ Tissue Resident Memory Cells

Similar to $CD4^+$ T cells, $CD8^+$ T cells form several types of distinct memory subsets: TCM, TEM and TRM; however, as $CD8^+$ T memory cells are not susceptible to latent HIV infection, and $CD8^+$ TRM cells play a much more significant role in HSV1 and HSV2 infections than other memory subsets (O'Neil *et al.*, 2021), this literature review will focus primarily on $CD8^+$ TRM cells. $CD8^+$ T memory cells develop by repetitive interactions with APCs, notably DCs, in the presence of $CD4^+$ T_h cells which licence DCs to provide memory forming signals to the $CD8^+$ T cell (Yang *et al.*, 2011). IL-21 secreting virus-specific $CD4^+$ TRM cells have also been implicated in the development of $CD8^+$ TRM cells (Ren *et al.*, 2020). Murine models have shown that $CD8^+$ TRM memory is established by downregulating of S1PR1 and Krüppel-like Factor (KLF)2 with simultaneous upregulation of CD69 expression (Skon *et al.*, 2013). Studies on $CD8^+$ TRM cells isolated from the gastrointestinal tract and mouse skin implicate IL-7 and IL-15 in their maintenance (Mackay *et al.*, 2015b, Thome *et al.*, 2014); and a study examining the role of TGF-β, which is secreted by keratocytes in the mucosa, demonstrated that CD103 is regulated by TGF-β on $CD8^+$ TRM cells, inducing a long-lived, immobilised phenotype (Fonseca *et al.*, 2020).

1.5.3. $CD8^+$ T Cells and HSV Infection

$CD8^+$ T cells play an essential role during both HSV1 and HSV2 infections at the site of initial infection, genital mucosa/skin, the neuronal ganglia, and recurrent lesions (Knickelbein *et al.*, 2008, Zhu *et al.*, 2007, Cunningham *et al.*, 1985). IFNγ causes epithelial cells to secrete CXC ligand (CXCL)9 and 10 as well as TGF-β which recruits $CD8^+$ T cells to infected mucosa (Nakanishi *et al.*, 2009). HSV specific $CD8^+$ T cells use their TCR to recognise cells expressing

HSV antigen on MHC-I molecules, these cells are targeted for killing through the use of perforin and granzyme B (Knickelbein *et al.*, 2008). $CD8^+$ T cells have been demonstrated to be essential for the clearance of herpetic lesions and their activation and infiltration to infection sites typically results in the eradication of activated virus during primary infection (Knickelbein *et al.*, 2008). Following lesion clearance in the female genital tract, $CD8^+$ TRM cells with specificity for HSV2 have been identified residing in the epidermal-dermal junction near former lesion sites and also surveying local peripheral neuronal endings (Posavad *et al.*, 2017). It has been demonstrated that HSV2 specific $CD8^+$ T cells accumulate near the sensory nerve endings of neurons in the anogenital mucosa allowing for a rapid response during HSV-2 reactivation (Zhu *et al.*, 2007), The frequency of reactivation at these nerve endings is dependent on the number of $CD8^+$ T cells present via their secretion of IFNγ not direct cytotoxicity (Cunningham *et al.*, 1985, Roychoudhury *et al.*, 2020). Finally, both TRM and $CD8^+$ T cells have been demonstrated to persist between lesions (Zhu *et al.*, 2007).

1.5.4. $CD8^+$ T Cells and HIV Infection

As briefly discussed previously, $CD8^+$ T cells play an important role in the control of HIV spread through their effector function. However chronic HIV infection is characterised by the loss of their efficacy due to the expression of exhaustion markers such as PD-1 and TIM-3 (Borrow *et al.*, 1994, Roberts *et al.*, 2016). A recent study showed that during HIV infection a novel $CD8^+$ T cell phenotype emerged: $CD27^-$ $CD38^+$ $CD8^{low}$ T cells that express CD8 at very low frequencies reducing their efficacy against viruses; the majority of $CD8^+$ T cells that demonstrate specificity to HIV match this novel phenotype while the minority of HIV specific $CD8^+$ T cells were characterised as having CD8 expression at traditional levels (Eller *et al.*, 2016). Furthermore, an increased proportion of $CD27^-$ $CD38^+$ $CD8^{low}$ T cells correlated with a more severe and earlier loss of $CD4^+$ T cells, suggesting that variable proportions of this ineffective $CD8^+$ T cell population contribute to the differences in AIDS onset between those

infected with HIV (Eller *et al.*, 2016). In elite controllers, $CD8^+$ T cells have been shown to have greater proliferative capabilities and can develop their cytolytic potential by *in vitro* stimulation alone (Migueles *et al.*, 2008). However, $CD8^+$ T cells isolated from normal progressors fail to respond to *in vitro* stimulation (Migueles *et al.*, 2002).

1.6. Subsets of Mononuclear Phagocytes in Human Tissue

Mononuclear phagocytes are a group of leukocytes that have significant phagocytic activity and are specialised for antigen presentation; MNPs include LCs, DCs, macrophages and monocytes (Guilliams *et al.*, 2014). Traditionally, only macrophages and monocytes were considered MNPs, however, the grouping was extended to include dendrite possessing antigen presenters: LCs and DCs (Harman *et al.*, 2013b). It was originally believed that both macrophages and DCs were all derived from monocytes. However, studies examining the transcriptome and ontogeny of these cells demonstrated that they may form independent clusters and develop independently of monocytes (Miller *et al.*, 2012, Haniffa *et al.*, 2012). DCs are a subset of cells derived from bone marrow that possess extending dendrites, they can be found in blood, and both non-lymphoid and lymphoid tissues including, lymph nodes, skin, liver, intestines, tonsils, lungs and the anogenital mucosae (Steinman and Cohn, 1973). LCs were the first subset of dendritic cell identified and were initially believed to be a type of nerve cell (Langerhans, 1868). In healthy tissue, LCs typically patrol the epidermis and can home to the lymph node upon detection and uptake of antigen to activate the immune response (Kaplan *et al.*, 2005). There is a wide range of DC subsets each with a unique cytokine secretion and surface protein expression profile contributing to the specificity and magnitude of their function (McGovern *et al.*, 2014).

Monocytes are a $CD14^+$, highly plastic MNP subset with the capacity to differentiate into a wide range of cells depending on their stimulation; blood monocytes may differentiate into a

distinct macrophage population, monocyte-derived macrophages (MDM), and a DC population, monocyte-derived DCs (MDDC) (Randolph *et al.*, 1999, Randolph *et al.*, 1998, Becker *et al.*, 1987). There are tissue-resident macrophages derived from the yolk sac across most tissues of the body, although they have unique names and functions at different sites (i.e. Kupffer cells located in the liver and microglia cells of the brain). Macrophages do not migrate out of tissue and are relatively poor antigen presenters despite their high phagocytic potential (Sica and Mantovani, 2012, Mantovani *et al.*, 2013). Macrophage populations are broadly classified functionally as either: IFNγ and TNF-α secreting pro-inflammatory classical macrophages (M1); or IL-10 and IL-4 secreting anti-inflammatory alternative macrophages (M2) (Martinez and Gordon, 2014, Varol *et al.*, 2015). pDCs are a type of circulating MNP that secrete significant amounts of type 1 IFNs, playing an important role in responding to viral infections; pDCs are also found in lymph nodes and inflamed tissues (Musumeci *et al.*, 2019). As described previously, when sexually transmitted pathogens such as HSV and HIV breach the physical barriers of human anogenital tissue the first immune cells they interact with are MNPs (Joeris *et al.*, 2017). MNPs express the HIV entry receptor CD4 and the co-receptors CXCR4 and CCR5 allowing them to become infected by HIV (Arakelyan *et al.*, 2019). Furthermore, many MNP subsets express binding C-type lectin receptors, this allows these cells to take up virions into intracellular compartments (Turville *et al.*, 2003) through the mechanisms described in **Section 1.1.4.1.** Many MNPs act as 'trojan horses' and pass HIV virions to nearby $CD4^+$ T cells or carry the virus to naïve $CD4^+$ T cells in lymph nodes for viral transfer, thus making MNPs of critical importance in HIV cell to cell transmission (Rhodes *et al.*, 2019). The literature traditionally classified macrophages, monocytes, DCs and LCs based on their function, location and phenotype (Guilliams *et al.*, 2014). However, the increasing availability of transcriptomic analysis has resulted in the controversial reclassification of some subsets and updated nomenclature, resulting in multiple names for the same MNP; this is

further complicated by subsets that possess features associated with multiple cell types (Rhodes *et al.*, 2019). A summary of the major MNP subsets previously defined by the host lab and others is provided in **Table 1.1.** and those of importance to this thesis are reviewed in **Section 1.6.1-1.6.3.**

1.6.1. Langerhans Cells

Langerhans cells are a population of cells with the capacity for self-renewal that reside in the epidermis of type II mucosal surfaces and the skin (Kanitakis *et al.*, 2011). LCs are primarily characterised by the expression of Langerin and CD1a as well as the presence of unique 'tennis racket' shaped granules termed Birbeck granules (Bigley *et al.*, 2015). LCs express TLR-1 through to 6 and 10; LCs also produce higher amounts of CXCL10 and IL-8 than DCs, however produce low levels of IL-10, IL-6 and IL-1β (Haniffa *et al.*, 2012, Flacher *et al.*, 2006). LCs are traditionally considered to be a highly immunogenic APC, with the capacity to stimulate $CD4^+$ T_h1 and T_h2 cells (Furio *et al.*, 2010), as well as T_H subsets involved in mucosal immunity: T_h22 (Fujita *et al.*, 2009) and T_h17 (Mathers *et al.*, 2009). However, they also display some tolerogenic properties, notably the ability to stimulate $CD4^+$ T_{REG} cells (Seneschal *et al.*, 2012).

The classification of LCs is controversial: The function of LCs closely resembles DCs as they uptake antigen, migrate from the epidermis of peripheral tissue to lymph nodes, and present the antigen to naïve T cells. However, LCs ontogeny resembles macrophages more so than DCs as they share a common precursor and both LCs and macrophages are self-renewing (Guilliams *et al.*, 2016, Mass *et al.*, 2016). Furthermore, early *in vitro* studies demonstrated that monocytes stimulated with granulocyte-macrophage colony-stimulating factor (GM-CSF) and TGF-β could develop into cells that partly resemble LCs through the expression of langerin (Geissmann *et al.*, 1998), However, by transcriptomics, they resemble monocyte-derived DCs

more closely than LCs (Bertram *et al.*, 2019). It was later shown that the same was true for certain subsets of DCs (Milne *et al.*, 2015, Martínez-Cingolani *et al.*, 2014). While residing within the epidermis, LC dendrites can extend between the tight junctions formed by keratinocytes, allowing them to process and sample antigens without disrupting the integrity of the barrier formed by the keratinocytes (Ouchi *et al.*, 2011). It has also been demonstrated that epidermal LCs express the HSV entry receptors HVEM and nectin-1, allowing for uptake and infection by a pH-dependent endocytic pathway (Bertram *et al.*, 2021).

1.6.2. Tissue Residing Conventional Dendritic Cells 1

Conventional dendritic cells 1 (cDC1) cells are characterised by low/no expression of CD1c, CD11c, CD11b, CD14, CCR5, and Signal Regulatory Protein (SIRP)α, moderate expression of XCR1, C-Type Lectin Domain Containing (Clec)9A and Cell Adhesion Molecule (CADM)1 and high expression of CD141 (Watchmaker *et al.*, 2014, Haniffa *et al.*, 2012). cDC1s have been identified in blood and both peripheral and lymphoid tissues, all originating from similar precursor cells; within type I and II mucosal surfaces as well as skin, cDC1s reside in the underlying submucosa (Haniffa *et al.*, 2012). cDC1s express a limited TLR profile compared to conventional dendritic cells 2, however, they express TLR-7, TLR-9 and high amounts of TLR-3 (Pigni *et al.*, 2018). Compared to other dermis residing DC subsets, cDC1s have an increased ability to cross-present antigens to $CD8^+$ T cells, which is enhanced upon TLR-3 stimulation (Haniffa *et al.*, 2012). Tissue cDC1s produce little to no IL-1, IL-6, IL-8, IL-10, IL-12, and IL-23, however, produce high levels of CXCL10 and TNF-α upon stimulation (Haniffa *et al.*, 2012). The isolation and identification of cDC1s from tissue is challenging as many of the markers used for there definition: CD141, CADM1 and CD11c, are expressed by conventional dendritic cells 2 during migration from tissue (Botting *et al.*, 2017).

1.6.3. Tissue Residing Conventional Dendritic Cells 2

Conventional dendritic cells 2 (cDC2s) located in tissue typically express more C-type lectin receptors than those located in the blood and are 10 times more frequent than cDC1s; they also show a more activated phenotype including increased expression of maturation markers, notably CD80, CD86, and CD83 (Haniffa *et al.*, 2012, Watchmaker *et al.*, 2014). Tissue cDC2s are defined by their expression of SIRPα, CD1c, and CD11c as well as an absence of Dendritic Cell-Specific Intercellular Adhesion Molecule 3 Grabbing Non-integrin (DC-SIGN). This demonstrates that DC-SIGN is not universally expressed by DCs as once thought (Harman *et al.*, 2013a, Schlitzer *et al.*, 2013). cDC2s can express Langerin but are differentiated from LCs that are migrating through the dermis by expression of CD11c and CD11b as well as an absence of Birbeck granules (De Monte *et al.*, 2016, Harman *et al.*, 2013a). cDC2s express TLR-1 through to 9 and can produce a wide range of cytokines, notably IL-6, IL-8, IL-23, TNF-α, IL-1β and CXCL-10 (Lundberg *et al.*, 2013, Harman *et al.*, 2013a). Within the intestine, cDC2s stimulate a strong $CD4^+$ T_H17 response, while the presentation of antigen by MHC-II induces a strong T_{FH} response (Eisenbarth, 2019, Watchmaker *et al.*, 2014).

1.6.3.1. Epidermal Langerin$^+$ CD11c$^+$ cDC2s

Until recently, LCs have been the only MNP described in the epidermis of healthy tissue (Nasr *et al.*, 2014) however it has been demonstrated that the traditional methods employed to isolate MNPs from tissue, enzymatic digestion with trypsin, cleaves key MNP surface markers (Yoshida *et al.*, 2014). A recent study employing collagenase digestion reported the presence of three new MNP subsets residing in the healthy epidermis that had unique phenotypes and transcriptional profiles that resembled dermal cDC2s (Bertram *et al.*, 2019). Of significant interest, was an epidermal MNP subset characterised by low Langerin expression which is not traditionally thought to be a cDC2 marker, and high CD11c expression termed Epi-DCs; as a result of their high expression of CCR5 they are more efficient at acquiring and transferring

HIV to $CD4^+$ T cells (Bertram *et al.*, 2019). Furthermore, a recent study published by the host lab demonstrated that Epi-DCs can support higher levels of HSV1 infection compared to LCs or keratinocytes, despite similar levels of viral uptake and expressing similar HSV entry receptors (Bertram *et al.*, 2021). Unlike LCs, HSV entry into Epi-DCs is pH-independent, contrasting with entry into LCs, likely contributing to enhanced infection by HSV. However Epi-DCs likely follow the same apoptosis and dermal migration processes seen in LCs (Bertram *et al.*, 2021). Further investigation is required to understand the functional differences between Epi-DCs and both LCs and $Langerin^-$ cDC2s, especially in relation to the stimulation of T cells.

1.6.4. Tissue Residing Conventional Dendritic Cells 3

Also recently, unbiased high-dimensional transcriptomic and proteomics demonstrated the existence of a pro-inflammatory, cDC2 like, MNP population that express CD163, CD14, CD1c, CD11b and CD64 termed conventional dendritic cells 3 (cDC3) (Girard *et al.*, 2020). Expansion of cDC3 populations is believed to correlate with an increased risk of acquiring an autoimmune disease as demonstrated by studies on patients with systemic lupus erythematosus (Villani *et al.*, 2017). cDC3 maturation is driven by IFNβ secretion and relative to cDC2s they express less CD86 and higher levels of Glucocorticoid-induced tumour necrosis factor receptor family-related protein ligand (GITRL) (Girard *et al.*, 2020). Similar to cDC2s, cDC3s stimulate a strong $CD4^+$ T_h17 and T_h2 immune response (Dutertre *et al.*, 2019) and an *in vitro* and *in vivo* study has demonstrated that they are potent activators of $CD8^+CD103^+CD69^+$ TRM cells (Bourdely *et al.*, 2020). Some of the current literature and discussion among researchers supports claims that the newly discovered cDC3s are actually a previously described pDC population that expresses Sialic Acid-Binding Immunoglobulin-Type Lectin (SIGLEC)-1 and Axl, often termed ASDCs (Villani *et al.*, 2017, Wilhelm *et al.*, 2016, Gerl, 2020). Finally, it

remains to be determined if the before mentioned Epi-DCs are derived from dermal cDC3s rather than dermal cDC2s, Investigations into this by the host lab are currently underway.

Table 1.1. Summary of significant tissue residing MNPs

MNP Population	Markers		TLRs	Secretion	
LCs	Birbeck granules	CD1c	1-3	IL-8	CXCL10
	HLA-DR	EpCAM	6		
	Langerin	E-Cadherin	10		
cDC1s	HLA-DR	XCR1	7	CXCL10	TNF-α
	CD141	CADM1	9		
	Clec9a	CD103- (intestine)	3		
Langerin$^-$ cDC2s	HLA-DR	CD11c	1-9	IL-6	TNF-α
	CD1a	CD1c		IL-8	IL-1β
	SIRPα	CD103-(intestine)		CXCL-10	IL-23
Langerin$^+$ cDC2s	CD11b	Langerin$^{+/-}$			
cDC3s	CD163	CD1c	Not defined	Not defined however is pro-inflammatory	
	CD14	CD11b			
	CD64				
CD1c$^+$ MDDCs	DC-SIGN	CD11c	1-9	IL-1β	IL-8
	CD141- (activated)	CD11b		IL-10	IL-6
		CX3CR1			
	CD14	CD1c$^{+/-}$			
	CD86	CD80			
CD1c$^-$ MDMs	CD163	SIRPα			
Macrophages	Auto-fluorescent	CD64	Not defined	IL-1	TNFα
	FXIIIa	SIRPα		IL-6	IL-23
	CD14	DC-SIGN		IL-10	
Inflammatory Dendritic Epidermal Cells (IDEC)	CD1a	CD36	1-9	TNFα	IL-12
	CD11c	CD32		IL-6	IL-1β
	FceR1	CD11b		IL-23	
	HLA-DR				

1.7. HIV and HSV Coinfection in the Context of MNPs and T Lymphocytes

As mentioned previously, prior HSV2 infection increases the risk of HIV acquisition by as an average of 3-fold, and if the HSV2 infection was recent this increases to as much as a 5-fold increase (Reynolds *et al.*, 2003, Looker *et al.*, 2017). It is hypothesised that this occurs as a result of inflammation and ulceration of the anogenital mucosa (Passmore *et al.*, 2016). It has also been shown that in sub-Saharan Africa over 50% of HIV infections in women, and 37% globally are associated with prior HSV2 infection (Looker *et al.*, 2017, Masese *et al.*, 2015). It

is also well established that herpetic lesions shed HIV virions during coinfection (Augenbraun *et al.*, 1995). As such, understanding the association between prior HSV infection and HIV acquisition is a priority for HIV researchers as it may lead to approaches that reduce the transmission of HIV and negate the effects of prior HSV infection.

1.7.1. Mechanisms of Increased HIV Acquisition During HSV-HIV Coinfection

The mechanisms by which HSV2 enhances HIV transmission is complex and not completely defined. The genital ulcers formed by HSV2 in the epidermis disrupt the stratum corneum, providing easier entry into the epidermis (Abu-Raddad *et al.*, 2008). Furthermore, phenotyping of the inflammatory infiltrate in type II mucosa demonstrated that activated $CD4^+$ T cells and macrophages accumulate at the base of herpetic lesions and persist even after recovery, increasing the number of HIV target cells in the epidermis (Cunningham *et al.*, 1985). A study examining HIV replication in cellular infiltrate isolated from biopsied HSV2 lesions showed significant populations of $CD8^+$ and $CD4^+$ T cells as well as myeloid DCs; the isolated $CD4^+$ T cells had enriched expression of CCR5 and showed increased integrated HIV DNA (Zhu *et al.*, 2009). These cells are highly persistent, and HSV2 infection likely facilitates both HIV replication and infection in the anogenital mucosa (Zhu *et al.*, 2009). As most $CD4^+$ T cells are in the dermis and HSV lesions are confined to the epidermis, it is hypothesised that coinfection or adjacent infection of Epi-DCs or LCs provide a route for HIV to reach the dermis to infect $CD4^+$ T cells during coinfection (Marsden *et al.*, 2015, Nasr *et al.*, 2014).

While it is well established that LCs residing in type II mucosa are major targets for HIV or HSV infection the viruses have different, potentially converging, interactions with $CD4^+$ T cells and DCs (Nasr *et al.*, 2014). HSV infection results in the apoptosis of many DC populations for uptake and presentation to T cells by bystander DCs as HSV antigen (Kim *et al.*, 2015, Bosnjak *et al.*, 2005). However, HIV employs DCs as trojan horses facilitating its

transfer to $CD4^+$ T cells resulting in explosive replication (Nasr *et al.*, 2014). It is hypothesised that due to the persistent inflammatory environment associated with HSV infection there is also an increase in the number of $CD4^+$ TRM cells in the dermis to control recurrent lesion formation (O'Neil *et al.*, 2021). SIV infected macaques demonstrate that there are both resting and activated $CD4^+$ T memory cells in the dermis/submucosa, however while the majority of activated cells migrate to the lymph nodes the resting cells may become latently infected (Van der Sluis *et al.*, 2020). Thus, as HSV infection may increase the number of $CD4^+$ TRM cells, even in through asymptomatic viral shedding, it can assist the HIV latent reservoir in becoming established even in the absence of the characteristic lesions associated with infection (O'Neil *et al.*, 2021). Finally, a study has demonstrated that DCs exposed to HSV secrete cytokines with potent HIV latency reversal properties, exacerbating disease progression (Marsden *et al.*, 2015).

It has also been demonstrated that antiretroviral drugs taken as part of HIV pre-exposure prophylaxis (PrEP), notably topically applied tenofovir gel, have efficacies dependent on inflammation: 75% of women with minimal to no vaginal inflammation applying tenofovir gel were protected against HIV (McKinnon *et al.*, 2018). However, those with moderate to severe inflammation experienced no protection. Since genital herpes caused by both HSV1 and HSV2 is associated with significant inflammation (O'Neil *et al.*, 2021), it probable that HSV infection reduces the efficacy of certain antiretroviral drugs taken as part of PrEP.

1.8. Aims and Hypothesis

The host lab has previously studied how HSV is transported within LCs to dermal DCs to form distinct clusters (Kim *et al.*, 2015) which has lead us to hypothesise that HIV may also travel along the same route, by either coinfection or adjacent infection of activated epidermal DCs/LCs that are migrating to the dermis due to the presence of HSV. We have also shown

that upon HSV infection, MDDCs and LCs produce TNFα, which upregulates expression of the HIV infection coreceptor CCR5 enhancing the establishment of epidermal HIV in local LCs (Marsden *et al.*, 2015), and possibly epi-DCs. However, there is still a significant gap in the literature surrounding the migration after viral uptake and subsequent cell interactions that take place during HSV-HIV coinfection, and those that take place in HSV infection that create an environment conducive for later HIV infection. As such, this thesis had two key aims:

1. To identify changes HSV infection induces in type II mucosa that have the potential to increase the acquisition of HIV upon exposure.
2. To design an optimised HSV2-HIV coinfection explant model utilising tissue taken from the anogenital tract that can be used to address some of the most significant questions in the HSV2-HIV coinfection field.

In order to address aim 1, we employed a HSV1 explant infection model that has previously been optimised by the host lab that utilises inner foreskin specimens donated by patients of surgeons in the Western Sydney and Blue Mountains Local Health Districts after circumcisions. To address aim 2, we took the principles of the HSV1 foreskin explant model, adapted it to vaginal tissue in addition to foreskin tissue, and shifted from the use of HSV1 to HSV2 to ultimately design an optimised novel HSV2- HIV coinfection explant model to accurately simulate the events that occur during coinfection at the anogenital mucosa. Both the HSV1 and the HSV2-HIV coinfection explant model use High Density Microarray Patches designed by Vaxxas for intraepidermal dermal vaccine delivery, allowing us to simulate the microtrauma that occurs during sexual intercourse that contributes to HSV/HIV infection. Both HSV and HIV were visualised by highly sensitive DNAscope or RNAscope respectively while the distribution of cells was visualised and quantified by rounds of cyclic immunofluorescence. Cyclic immunofluorescence allows us to generate images that circumvent many of the traditional limitations that immunofluorescence panels face. The increased understanding of

the role prior HSV infection plays in HIV acquisition by MNPs and $CD4^+$ T cells ascertained by the execution of the methodology detailed in this thesis, is hoped to contribute to curative approaches and vaccine design against HIV.

Chapter 2: Materials and Methods

2.1. General Solutions and Comments

All filter sterilisations were performed with 0.22 μm filters (Merck Millipore; Darmstadt, Germany). All plasticware was supplied by Corning (CA, USA), Greiner Bio-One (Kremsmunster, Austria) or Eppendorf (Hamburg, Germany) unless otherwise specified.

2.1.1. Human Antibody Serum

Human Ab (hAb) serum was heat-inactivated at 56 °C for 30 minutes, followed by storage at -20 °C until use. Before use, hAb serum was filter sterilised.

2.1.2. Foetal Bovine Serum

Foetal bovine serum (FBS; Sigma-Aldrich; MO, USA) was filter sterilised and stored at 4 °C until use.

2.1.3. Blocking Solution

Unless otherwise specified, microscopy blocking steps were completed with 1% bovine serum albumin (BSA; w/v; Sigma-Aldrich), 0.1% saponin (w/v; Sigma-Aldrich) and 10% donkey serum (v/v; Sigma-Aldrich) in tris buffered saline (TBS; Sigma-Aldrich).

2.1.4. Cyclic Immunofluorescence Photobleaching Solution

Photobleaching of microscopy sections was completed with 5% hydrogen peroxide (Advanced Cell Diagnostics; ACD; CA, USA) and 20 mM sodium hydroxide (Sigma-Aldrich) in TBS.

2.1.5. High-Density Microarray Patch Coating Solution

High-density microarray patch coating solution used as a wetting agent during HSV1/2 infection by intraepidermal injection with Vaxxas High-Density Microarray Patches was prepared as 50% sucrose (w/v; Sigma-Aldrich) and 0.05% poloxamer188 (v/v; Sigma-Aldrich) dissolved in Milli-Q water.

2.1.6. Cell/Tissue Culture Media

Continuous cell lines were cultured in Dulbecco's Modified Eagle Medium (DMEM) which contains glucose (4.5 g/L) and L-glutamine (4 mM), supplied by Lonza (Basel, Switzerland), and was supplemented with 10% (v/v) FBS, referred to as DMEM10.

Tissue explants were cultured in DC culture medium (DCM): Roswell Park Memorial Institute (RPMI) containing L-glutamine (Lonza), supplemented with 10 µM HEPES (Gibco; MA, USA), 1 x non-essential amino acids (Gibco), 10 µg/mL gentamicin (Gibco), 50 µM 2-mercaptoethanol (Gibco), 1 mM sodium pyruvate (Gibco), and 10% (v/v) FBS.

Transformed bacteria were cultured in Luria-Bertani (LB) broth (Sigma-Aldrich) supplemented with 100 µg/mL of ampicillin (Sigma-Aldrich).

2.1.7. Cell Lines

HEK293T cells, a transfectable human embryonic kidney immortal cell line, were cultured in 150 cm^2 flasks with DMEM10 and passaged when the cells reached 80% confluency (approximately every two days).

Vero cells, an immortal cell line derived from monkey epithelial kidney cells, were cultured in 150 cm^2 flasks with DMEM10 and passaged when the cell reached 80% confluency (approximately every three days).

TZMbl cells (NID AIDs Research and Reference Reagent Program), a HeLa cell derivative used as a HIV infection reporter cell line, were cultured in 75 or 150 cm^2 flasks with DMEM10 and passaged when they reached 80% confluency (approximately every three days).

Stbl. 2 *E. coli* (Invitrogen; CA, USA) cells, a high-transformation competent clone, were cultured in either LB broth or agar supplemented with ampicillin.

2.2. Experimental Rationale

Prior work performed by the host lab involving HSV1 infection of donated inner foreskin specimens has led to the optimisation of an explant model in which tissue is infected by the injection of the virus past the stratum corneum and into the mid-epidermis by application of High-Density Microarray Patches coated with virus (Rana *et al.*, 2024). After culture in DCM, at 24 hours post infection (hpi), tissue was removed from culture and snap-frozen for cryosectioning. Immunofluorescent microscopy and RNAscope amplification were used to visualise HSV1 interactions with immune cells. In some cases, culture supernatants were retained to assess the inflammatory cytokine-chemokine environment by the LEGENDplex assay. The principles underlying the HSV1 infection explant model were adapted in this project to design a new model utilising vaginal and inner foreskin tissues to visualise and assess virus-cell interactions during HSV2-HIV coinfection. The concentration of HIV to be added, method of HIV infection following HSV-2 infection, and duration of culture post HIV inoculation required optimisation prior to the successful use of the coinfection model.

2.3. Preparation of Viral Stocks

2.3.1. Growth of HIV Stock

Frozen glycerol stocks of Stbl. 2 *E. coli* transformed to contain the HIV_{Bal} plasmid (pBal; NIH AIDS Research and Reference Reagent Program) were thawed and spiked into LB broth starter cultures supplemented with ampicillin and incubated at 250 revolutions per minute (rpm) at 37 °C for 16 hours. pBal presence was confirmed by 1) isolation of plasmid DNA by the PureYield Plasmid Miniprep System (Promega; WI, USA), 2) enzymatic digestion with EcoRI-HF and KnpI-HF (New England Biolabs; NEB; MA, USA) using the CutSmart Buffer system (NEB), and 3) visualised by gel electrophoresis. Maxicultures were spiked at a ratio of 1:100 (starter culture: LB broth supplemented with ampicillin) and incubated as above. Transfection grade pBal was collected using the NucleoBond Xtra Maxi kit (Macherey-Nagel; Duren, Germany)

and concentration and purity were assessed by nanodrop (Victor X3 203 Multi-Label Reader; PerkinElmer; MA, USA).

HEK293T cells were cultured in 150 cm^2 flasks in DMEM10 at eight million cells per 20 mL for transfection. Once the cells reached a confluence of 60-70% the media was changed to 15 mL of DMEM supplemented with 2% FBS. 1 mL of transfection solution A: 1 mL HEPES buffered saline (HBS; Lonza) and 10 µL 150 mM Na_2HPO_4, and 1 mL of transfection solution B: 50 µg of plasmid DNA and 128 µL 2M $CaCl_2$ (Sigma-Aldrich) were brought to 1 mL with 10% TE buffer (ThermoFisher Scientific; MA, USA) were prepared per flask. Solutions A and B were combined just before transfection and the resulting 2 mL solution was added to each flask and incubated at 37 °C for 18 hours, after which the media was replaced with 13 mL of fresh DMEM supplemented with 2% FBS. The virus-containing media (VCM) was collected, replaced with fresh media everyday for 5 days and concentrated in 300 kDa molecular cut-off filters (Vivaspin 20; Sartorius; Gottingen, Germany) by centrifugation at 3000 xg. The concentrated virus was pelleted by ultracentrifugation (Beckman Optima XL-100 K Ultracentrifuge) for 2 hours at 28 000 rpm and resuspended in 100 µL of PBS, left at 4 °C to solubilise overnight, and then aliquoted and frozen at -80 °C. Infectivity was assessed with the HIV infection reporter TZMbl cell line to determine the 50% tissue culture infectious dose (TCID50). the virus titre was confirmed in primary cells by titration with activated $CD4^+$ T cells. The calculated TCID50 was $10^{7.07}$ per mL.

2.3.2. Growth of HSV1-GFP and HSV2 Stocks

Vero cells in 850 cm^2 roller bottles were cultured in DMEM10 at twenty million cells per 200 mL for infection. Once the cells reached an 80% confluency, 20 mL of DMEM supplemented with 2% FBS, 1% penicillin, and HSV at a multiplicity of infection (MOI) of 0.001 was added and gently rocked over the cell monolayer for 1 hour at 37 °C. The roller bottles were then

topped up to 200 mL with the above DMEM solution and incubated at 37 °C until 90-100% of the cells exhibited cytopathic effects (approximately three days). Cells were scraped into the VCM and collected in falcon tubes, centrifuged at 4000 rpm for 10 minutes, and resuspended in 0.5 mL of the VCM. The remainder of the VCM was retained for ultracentrifugation at 12 000 rpm for 2 hours, aliquoted, and frozen at -80 °C. The virus associated cells were sonicated (Branson 450 Digital Sonifier; Marshall Scientific; NH, USA) in four cycles of 60 second bursts at maximum power, with 30 second rests and centrifuged at 875 xg for 10 minutes, and the resulting supernatant was aliquoted and frozen at -80 °C. The titre of HSV1 bound to Green fluorescent protein (GFP) and HSV2 cell-associated virus and the concentrated VCM was obtained by a crystal violet plaque assay using Vero cells and were calculated to be 1.03×10^9 plaque forming units (PFU)/mL for HSV1 strain F with GFP tagged at US9 (HSV1-GFP), and 2.83×10^8 PFU/mL for HSV2 strain 186.

2.4. Preparation of Anogenital Tissue Explants and Microscopy Slides

The host lab has collaborations with surgeons operating at hospitals and private practices within the Western Sydney Local Health District (WSLHD) and Nepean Blue Mountains Local Health District providing us with mucosal tissues of the anogenital tract, particularly vaginal mucosa and inner foreskin, which being common sites of HSV1/2 and HIV infection, are the focus of this thesis. The use of this tissue was approved by the WSLHD Human Research Ethics Committee (HREC), with reference number (4192) AU RED HREC/15 WMEAD/11.

2.4.1. Preparation of Tissue Explants and Infection by HSV

Vagina and inner foreskin specimens were infected with HSV1-GFP or HSV2 by intraepidermal application via proprietary 9 x 9 mm silicon magnetic micropatches known as High-Density Microarray Patches (HD-MAPs) generously donated by Vaxxas (QLD, Australia; **Figure 2.1a-b**). HD-MAP Coating Solution (**Section 2.1.5)** was spiked with 10^8

PFU/mL of HSV1-GFP or HSV2 and was prepared at a total volume of 1 mL within a 12-well plate. HD-MAPs were dipped 10-20 times in the coating solution using forceps to allow the solution to soak up between the microneedles. The addition of Poloxamer188 and Sucrose Solution reduced the surface tension of the coating solution, increasing the amount of virus-containing solution coating the HD-MAP. Using a mechanical applicator supplied by Vaxxas **(Figure 2.1c)**, soaked HD-MAPs were magnetically transferred, and ejected onto the taut tissue specimen. The HD-MAPs remained attached to the tissue for 1 minute while a scalpel was used to cut around HD-MAP treated tissue. Following this, HD-MAPs were removed, and the tissue was cut into anywhere from 1 to 4 equal segments and placed in a twenty-four-well plate with 300 µL of DCM resting on 1 cm x 1 cm gelfoam sponges (Pfizer; Sydney, Australia) pre-soaked in DCM with the epidermis of the tissue facing up and the dermis making contact with the gelfoam. After being left in culture for 18-24 hours, tissue could either be infected with HIV for co-infection optimisations or placed in optimal cutting temperature compound (OCT; SciGen Pte. Ltd; Singapore), snap-frozen in isopentane that was pre-cooled in liquid nitrogen, and stored at -80 °C until cryosectioned or, if paraffin embedded, fixed in 4% paraformaldehyde (PFA; Electron Microscopy Sciences; PA, USA). In some experiments, the culture supernatants of explants were retained and stored at -80 °C for interrogation by LEGENDplex.

2.4.2. Infection of Explants by HIV

Following the application of Vaxxas HD-MAPs coated in mock (coating solution without virus) or HSV2 coating solution, vaginal and foreskin explants were infected with HIV. The method of virus application, the concentration of HIV used (measured by TCID50), and the collection time post-HIV infection were optimised. At 18 after application of a HD-MAP, HIV was either topically applied to the epidermis by a paintbrush, or pipetted onto the surface within 6 mm cloning cylinders (Sigma-Aldrich) adhered to the epidermis of the explant via the use of

surgical glue (B.Braun; Melsungen, Germany; **Figure 2.1d**). Application by paint brush involved dipping the brush in a single well of a 96 well plate containing 60 µL of RPMI with a known TCID50 of HIV, and painting the explant until no RPMI remained in the well. Cloning cylinder application involved pipetting the 60 µL of HIV-containing RPMI directly into the cloning cylinder following its adherence to the tissue. Concentrations of 7 000 and 70 000 TCID50 per 60 uL were tested as advised by previous work with anogenital mucosa infection performed by the host lab. Following HIV infection, explants were collected at either 2, 12, 24, 36, or 48 hpi and fixed for 24 hours in 4% PFA followed by freezing in OCT or paraffin embedding.

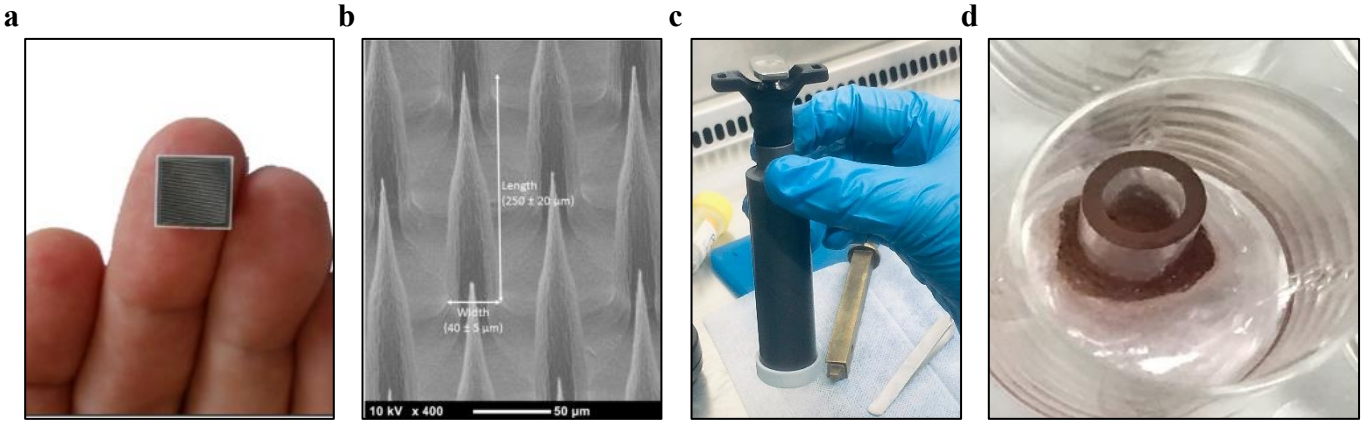

Figure 2.1. Key equipment used during explant preparation. To infect explants with HSV and puncture the epidermis of anogenital tissue, HD-MAPs supplied by Vaxxas, typically used for intradermal vaccine delivery, were used. **(a & b)** HD-MAPs contain 10K silicon microneedles 250 ± 50 µm in length, with a width of 40 ± 5 µm and 100 µm between needles. **(c)** The HD-MAPs were magnetic and could be applied with an applicator that utilised a spring-loaded release to embed the HD-MAP into the explant. **(d)** For HIV infection, after the epithelium had been punctured with an HD-MAP, 6 mm cloning cylinders were glued to the surface of the explant for topical administration of HIV or (not pictured) administered by painting HIV onto the epidermis. **(a & b)** Images were supplied by Griffin *et al*. (2017).

2.4.3. Microscopy Slide Preparation and Selection

Frozen samples were cryosectioned at 7 μm using a CryoStar Nx70 or HM-505E Cryostat, while PFA fixed paraffin embedded (FFPE) blocks were sectioned at 4 μm with a microtome provided by the Histology Core Facility at the Westmead Research Hub (WRH). A light microscope with high contrast was used to check the quality and transverse orientation (cross-section of epidermis and underlying dermis) of the sections prior to storage at -80 °C (OCT frozen) or RT (FFPE) until immunofluorescent microscopy and RNAscope were performed. Before staining, FFPE slides were baked for approximately 1 hour at 60 °C, then dewaxed and rehydrated by immersion in Xylene followed by 100% ethanol three times. The first immersion was 2 minutes while the 2 following immersions were 1 minute each.

2.5. Immunofluorescence Microscopy Staining

Note: All washes were performed in TBS for 2.5 minutes at 70 rpm on an orbital shaker unless otherwise stated.

Frozen slides selected for immunofluorescent microscopy were washed twice in TBS to remove OCT. Sections were then dried and encircled with a hydrophobic DAKO fixation pen (Aligent Dako; CA, USA) followed by fixation with 2% PFA for 20 minutes in the dark at room temperature and washed twice. For FFPE sections, slides underwent antigen retrieval in a Decloaking Chamber immersed in RNAscope Target Retrieval buffer at 95 °C for 20 minutes and cooled indirectly with running water. Sections were then dried and encircled with a hydrophobic DAKO fixation pen. All sections were blocked with Blocking Solution (**Section 2.1.3**) for 30 minutes, followed by staining with the primary antibodies from **Table 2.1. & 2.2.** as specified in figure legends for 1 hour at 37 °C or overnight at 4 °C in the dark. Sections were washed twice and stained with secondary antibodies (**Table 2.1. & 2.2**) for 30 minutes in the dark at room temperature followed by another two washes. When primary fluorophore-

conjugated antibodies were also used, a second identical fixation step was performed followed by incubation of the slides with the conjugated antibodies for 1 hour at 37 °C. Nuclear staining of cells was performed with DAPI for 3 minutes at room temperature in the dark. Following another two washes with TBS, autofluorescence within the tissue was quenched by a precise 1.5-minute incubation at room temperature with reagents supplied in the TrueView Autofluorescence Quenching Kit (Vector Labs; Ca, USA). Sections were washed twice with TBS and once with Milli-Q water as described above and allowed to air dry before coverslipping using Slowfade Gold Antifade Reagent Without DAPI (Invitrogen; MA, USA). Slides were sealed before imaging with nail polish only if no further rounds of immunofluorescence or RNAscope staining was required. Imaging was performed using the VS120 Virtual Slide Microscope (Olympus; Tokyo, Japan) at 20x magnification and the generated images were acquired using version 2.9 of VS-Desktop (Olympus).

In the case of multiple rounds of immunofluorescence staining (cyclic immunofluorescence) or RNAscope, slides were not sealed with nail polish and were washed in TBS for 30 minutes to remove the coverslips. Mounting media was removed by two washes with TBS as described above, and the fluorescent signal from previous rounds of staining was bleached by incubation with Cyclic Immunofluorescence Photobleaching Solution (**Section 2.1.4**) for 1 hour under a 15W 2700K light bulb (Sansai, Australia). Slides were then washed and immunofluorescent staining as described above or RNAscope as described in the next section was performed. The antibodies used and what round they were used in is summarised in **Table 2.3.**

Table 2.1. Antibodies used for IF microscopy before Section 4.8.1 re-optimisation

	Ligand	Species	Clone	Conjugate	Source	Dilution
Primary antibody	CD3	Mouse	OKT3	Cy3	Sigma Aldrich	1:100
	Langerin	Goat	Polyclonal	-	R&D Systems	1:100
	CD4	Rabbit	EPR6855	-	Abcam	1:100
	CD11c	Mouse	3.9	-	Invitrogen	1:50
Secondary antibody	Mouse IgG	Donkey	Polyclonal	AF647	Invitrogen	1:400
	Rabbit IgG	Donkey	Polyclonal	Dylight755	Invitrogen	1:400
	Goat IgG	Donkey	Polyclonal	AF488	Invitrogen	1:400

Table 2.2. Antibodies used for IF microscopy after Section 4.8.1. re-optimisation

	Ligand	Species	Clone	Conjugate	Source	Dilution
Primary antibody	CD3	Rabbit	Polyclonal	Cy3	Dako	1:20
	Langerin	Goat	Polyclonal	-	R&D Systems	1:50
	CD4	Rabbit	EPR6855	-	Abcam	1:50
	CD11c	Rabbit	EP1347Y	AF647	Abcam	1:20
Secondary antibody	Rabbit IgG	Donkey	Polyclonal	Dylight755	Invitrogen	1:200
	Goat IgG	Donkey	Polyclonal	Dylight755	Invitrogen	1:400

Table 2.3. Summary of employed cyclic IF panel

Panel before re-optimisation of IF panel (**Section 4.8.1**)		
Channel	**Cycle 1**	**Cycle 2**
DAPI	DAPI	DAPI
FITC	-	Goat anti-Langerin (primary) Donkey anti-goat IgG AF488 (secondary)
TRITC	Mouse anti-CD3 Cy3 (conjugated)	HSV1/2 DNA FastRed
Cy5	Mouse anti-CD11c (primary) Donkey anti-Mouse IgG AF647 (secondary)	-
Cy7	Rabbit anti-CD4 (primary) Donkey anti-Rabbit IgG Dylight755 (secondary)	-
Panel after re-optimisation of IF panel (Section 4.8.1.)		
Channel	**Cycle 1**	**Cycle 2**
DAPI	DAPI	DAPI
FITC	-	HIV RNA Tyramide FITC
TRITC	Rabbit anti-CD3 Cy3 (conjugated)	HSV-2 DNA RNAscope FastRed
Cy5	Rabbit anti-CD11c AF647 (conjugated)	-
Cy7	Rabbit anti-CD4 (primary) Donkey anti-rabbit-Dylight755 (secondary)	Goat anti-Langerin (primary) Donkey anti-goat Dylight755 (secondary)

2.6. HSV1/2 and HIV RNAscope

In order to visualise viral DNA/RNA in a tissue infected with a single virus, the RNAscope 2.5 HD Manual Assay – RED kit (ACDBio) was utilised with ACDBio supplied probes specific to HSV1 DNA (Gene Target: UL30/GU734771.1; Base Pairs: 63215-64488; Catalogue Number: 498861), HSV2 DNA (Gene Target: UL29; Base Pairs: 1180-2758; Catalogue Number: 440121), and a probe specific to HIV_{Bal} RNA (Gene Target: HIV-Bal; Base Pairs: 1144-8431; Catalogue Number: 486631) following a host lab optimised version of the manufacturer's protocol for fluorescent (rather than chromogenic) staining. Similarly, to visualise viral DNA/RNA in tissue coinfected with HSV2 and HIV, the RNAscope 2.5 HD Duplex Assay kit (ACDBio) was employed with the previously described probes following an optimised version of the protocol supplied by the manufacturer for fluorescent staining.

2.6.1. Visualisation of Either HSV1/2 or HIV

Note: All washes were performed in 0.5x RNAscope Wash Buffer (ACDBio) for 2 minutes at room temperature at 70 rpm unless otherwise stated.

Endogenous enzymes within sections were blocked by incubation with BLOXALL (Vector Laboratories) for 10 minutes at room temperature. Following two washes with TBS for 2.5 minutes each, sections were incubated with Protease Plus (ACDBio) at a 1:5 dilution in TBS for 20 minutes at 40 °C using a HybEZ hybridisation oven (220 VAC;ACDBio) and washed twice with Milli-Q water for 2.5 minutes. Prewarmed probes specific for HSV1 or HSV2 DNA or HIV RNA or positive control (targeting the housekeeping gene PPIB) or negative control (targeting bacterial gene DAPB) probes were added to sections and incubated for 2 hours at 40 °C followed by two washes. Following this, signal amplification was performed using the RNAscope 2.5 HD Assay kit – Red amps 1-6, as described in **Table 2.4.** with two washes after each incubation step. FastRed solution was prepared by the addition of Red B to A at a B:A

ratio of 1:60, and 50 µL was added to each section for incubation for precisely 1.5 minutes at room temperature in the dark. Sections were washed once with TBS and twice with Milli-Q water each for 2.5 minutes, followed by coverslipping as described in **Section 2.5**. or additional rounds of staining. Imaging was performed with the VS120 Virtual Slide Microscope using VS-Desktop software.

Table 2.4. Optimised Probe Amplification by RNAscope 2.5 HD Assay - Red

Amp	Volume added per section (µL)	Time (Minutes)	Temperature (°C)
1	50	30	40
2	75	15	40
3	50	30	40
4	75	15	40
5	75	30	Room Temperature
6	50	15	Room Temperature

2.6.2. Visualisation of HSV2 and HIV Coinfected Tissue

Note: All washes were performed in 0.5x RNAscope Wash Buffer twice for 2 minutes at room temperature at 70 rpm unless otherwise stated.

Following BLOXALL and Protease Plus treatments as described in the previous section, HSV2 and HIV probes were mixed at a ratio of 1:50 (HSV2:HIV) and added to each section for a 2-hour incubation at 40 °C followed by 2 washes. Amplification and detection were performed as described in **Table 2.4.** and the previous section, however, using reagents from the RNAscope 2.5 HD Duplex Assay kit to detect both HIV RNA and HSV2 DNA simultaneously within a single tissue section. HIV RNA probes were amplified by a second round of amplification at the conditions described in **Table 2.5.** with washing performed in between the addition of each amp. HIV RNA signal detection solution was prepared by 1:750 dilution of Tyramide-FITC with PLUS diluent (Tyramide:PLUS diluent, Akoya Biosciences) and 50 µL

of the solution was added to each section for a 30 minute incubation at room temperature in the dark. Sections were washed once with TBS and twice with Milli-Q water each for 2.5 minutes, followed by coverslipping as described previously or additional rounds of immunofluorescent staining and imaged.

Table 2.5. Optimised Probe Amplification by RNAscope 2.5 HD Duplex Assay

Amp	Volume Added (µL)	Time (Minutes)	Temperature (°C)
7	75	15	40
8	75	30	40
9	75	30	Room Temperature
10	75	15	Room Temperature

2.7. Analysis of Microscopy Images

Fluorescent microscopy images were analysed using VS-Desktop and version 2.0.0 of Fiji ImageJ software (National Institutes of Health; NIH; WI, USA). VS-Desktop was used to convert microscopy images to high resolution 'tif' files for manual counting using ImageJ. Prior to analysis, the image registration function of ImageJ used the DAPI signal from the same tissue across multiple rounds of staining to merge images of the same tissue and show an overlay of all fluorescent markers from each round within a single image (**Appendix A**).

2.7.1. Determining $CD3^+$ Lymphocyte and MNP Distribution and Density

In infected sections, sites of HSV/HIV epidermal infection and the underlying dermis were outlined with rectangular boxes referred to as 'frames' and the length of the epidermis of the largest infection site within the tissue was measured (**Figure 2.2a**). Regions of tissue designated as 'far from infection' within infected tissue sections were at least this measured epidermal distance away from any detected virus. For non-infected sections, frames of the epidermis and underlying dermis were selected at random. The epidermis of frames designated as healthy or infected were outlined, and a distance map from the basement membrane between

the epidermis and dermis was applied and used to create an outline of the first 120 μm of the dermis (**Figure 2.2b**). The number of $CD3^+$ lymphocytes, $CD3^+CD4^+$, $CD3^+CD4^-$, $CD3^-CD11c^+$, and $CD11c^-Langerin^+$ cells within the first 120 μm of the dermis of frames taken from explant sections that were not treated with a HD-MAP (no HD-MAP), explants treated with HD-MAP without virus (mock HD-MAP), and both sites of infection and far from infection in HSV infected explants were quantified by manually counting cells in a known area and converted to density/mm^2.

Following this, the dermis and accompanying counts and cell densities were split into three segments: the first 30 μm from the epidermis (Dermis 0-30 μm), the next 30 μm of the dermis (Dermis 30-60 μm), and finally the 60 μm of the dermis that followed these regions (Dermis 60-120 μm; **Figure 2.2c**). The first 60 μm of the dermis was selected as an area of increased interest (and hence split into 0-30 μm and 30-60 μm) as a previous study has demonstrated that the $CD3^+$ lymphocytes and $CD11c^+$ MNPs preferentially home to this region of the dermis in healthy skin (Wang *et al.*, 2014). Finally, the distance map function of Fiji (ImageJ) was used to determine the average distance from the basement membrane of the cell populations of interest that resided in the first 120 μm of the underlying dermis (**Figure 2.2d**).

2.7.2. Spatial Analysis of $CD11c^+$ MNPs and $CD3^+CD4^+$ Lymphocytes

The cartesian coordinates of MNPs and lymphocytes were obtained using Fiji during the manual counting performed in the previous section and exported for use with an R based spatial analysis software package – Spatstat (v2.3). Using the coordinates, a two-dimensional cartesian plane consisting of the point patterns of the MNP and lymphocyte populations was generated, and a matrix of the cross distances was calculated for the two-point patterns (i.e. $CD3^-CD11c^+$ cells against $CD3^+CD4^+$ cells etc). Finally, the mean of the cross distances in the resulting

matrix was calculated and converted from pixels to microns. This provided an effective measure of the average distance between cells of one population to cells of another population.

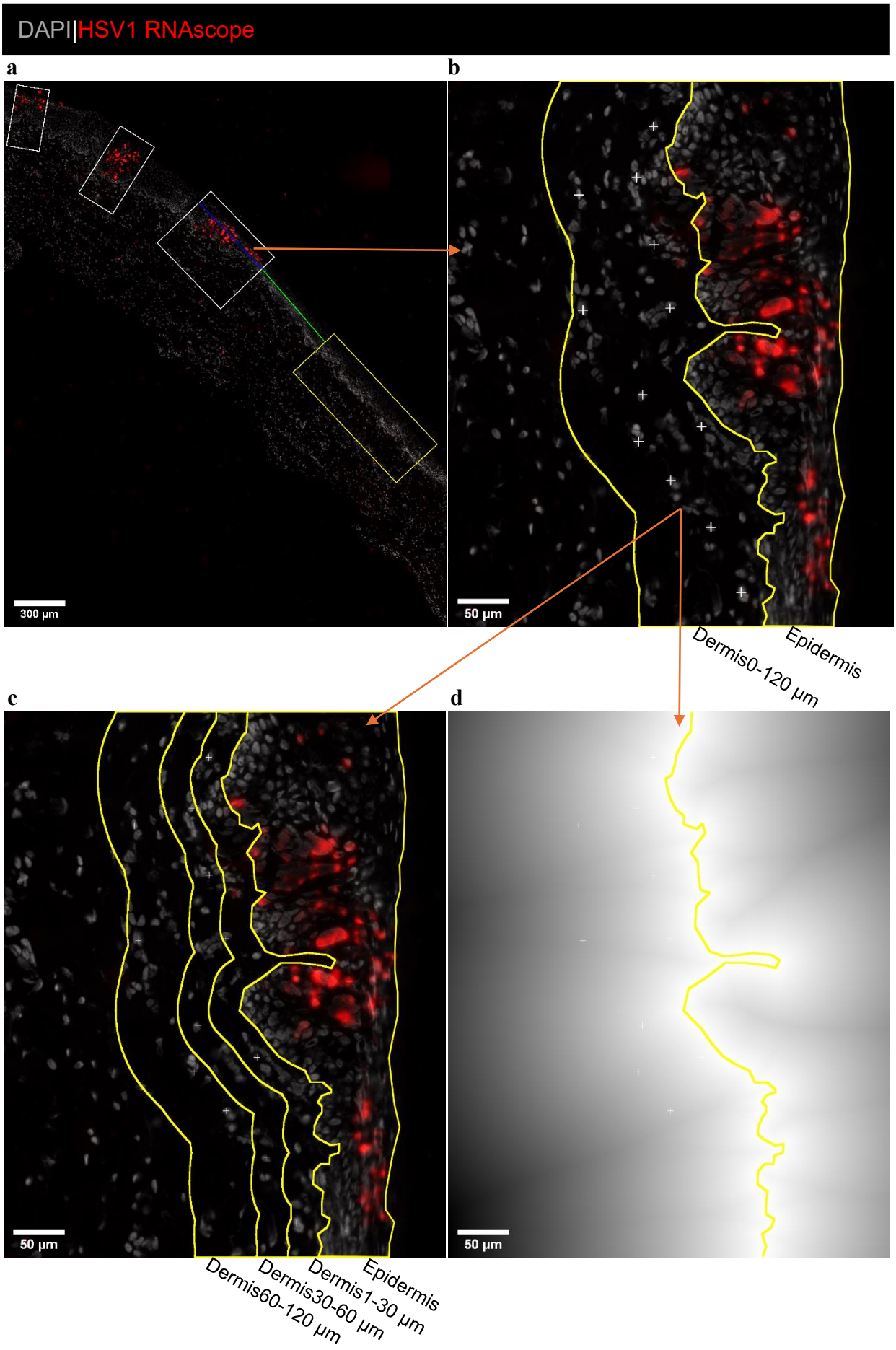
DAPI|HSV1 RNAscope
a
b
300 µm
50 µm
Epidermis
Dermis0-120 µm
c
d
50 µm
50 µm
Epidermis
Dermis1-30 µm
Dermis30-60 µm
Dermis60-120 µm

Figure 2.2. ImageJ analysis pipeline for cell distributions and densities in the dermis. (a) Sites where virus was detected by RNAscope in infected tissue were outlined with rectangular boxes (white) to generate frames and the length of the epidermis of the largest infection site was measured (blue). Regions within infected tissue that were designated as 'far from infection' were also outlined with rectangles (yellow) and had an epidermal distance from the nearest infection site (green) that exceeded the length of the epidermis of the largest infection site. **(b)** Following the outlining of the epidermis, the dermis was distance mapped and cells of interest were counted in the first 120 μm of the underlying dermis and converted to densities. **(c)** Densities were also determined for different segments of the underlying dermis: Dermis 1-30 μm, Dermis 30-60 μm, and Dermis 60-120 μm. **(d)** Finally, distance mapping was used to determine the average distance of the cells of interest from the basement membrane within the first 120 μm of the dermis. **(a-d)** This process was also performed on explants that were not treated with a HD-MAP, and explants treated with HD-MAP without any virus, however frames were selected at random.

2.8. LEGENDplex

Supernatants from select foreskin explants were retained and frozen at -80 °C for assessment of the inflammatory cytokines and chemokines by LEGENDplex. Two LEGENDplex plates were setup in accordance with the manufacturer's protocols with reagents supplied as part of the Proinflammatory Chemokine Assay and LEGENDplex Multiplex Inflammatory Panel 1 kits (BioLegend; USA, CA). 25 μL of Assay Buffer was added to 25 μL of explant supernatant and added to a 96-well V-bottom plate in duplicate. Similarly, standards were added to separate control wells and 25 μL of capture bead solution was added to each well and incubated for 2 hours in the dark at room temperature on a shaker. Following this, the solution was aspirated from the wells, then washed with 200 μL of supplied wash buffer, and 25 μL of detection antibodies were added to each well followed by a 1 hour incubation as above. 25 μL of Streptavidin PE was then added to each well and incubated for 30 minutes, followed by a final two washes with 200 μL of wash buffer and resuspension of the beads on a plate shaker for 1

minute. The samples were acquired on a BD LSRFortessa using FACSDiva and analysed with FlowJo. The Flow Cytometry Core Facility at the WRH performed the LEGENDplex assay and acquisition as a paid service.

2.9. Data Representation and Statistical Analysis

All data in this thesis is reported as mean ± standard deviation (SD) unless otherwise specified. All statistical analyses were completed using GraphPad 10 (version 10.4.2; Prism; USA, CA). Cells densities and distances within the epidermis were assumed to be parametric and where single comparisons between two experimental conditions were made paired Student T-tests were utilised (**Figures 3.4, 3.5, and 3.12**). Similarly, dermal densities and distributions were assumed to be parametric, however, to account for uneven sample numbers across experimental conditions and the need for multiple pair-wise comparisons, Mixed-effects analysis (ANOVA) with Tukey's Multiple Comparisons was utilised (**Figures 3.7-3.11 panels a & c**). Finally, to examine the differences in cell densities at both different depths of the dermis (dermis 0-30 μm, dermis 30-60 μm, and dermis 60-120 μm) and different experimental conditions (site of infection and far from infection), Two-way repeated measures ANOVAs were used (**Figures 3.7-3.11 panel b**).

Chapter 3: Identifying HSV Induced Changes in Anogenital Tissues that Enhance HIV Acquisition and Infection

3.1. Introduction

To determine how prior HSV1 and HSV2 infection increases HIV acquisition, it is necessary to examine the immunological changes that occur in the anogenital mucosa during HSV1/2 infection. Epi-DCs were recently identified in the epidermis of human abdominal tissue and anogenital mucosae, which along with LCs may act as HIV 'trojan horses' by using C-type lectin receptors to take up and traffic the virus to the dermis or lymph nodes for transfer to $CD4^+$ T cells (Bertram *et al.*, 2019, Nasr *et al.*, 2014). It has also been shown by microscopy of biopsied HSV1 lesions that LCs carrying virus antigen migrate to the dermis which apoptose and the fragments are taken up by dermal DCs, which in turn likely emigrate to the lymph node for antigen presentation (Kim *et al.*, 2015). HSV1 also infects both LCs and Epi-DCs by different mechanisms of entry and induces apoptosis in both (Bertram *et al.*, 2021).

While the healthy epidermis only hosts two known MNP populations, the dermis contains many different macrophage and DC populations such as cDC1s, cDC2s, MDDCs, MDMs, pro-inflammatory macrophages, and anti-inflammatory macrophages (Rhodes *et al.*, 2021). Although most studies focus on epithelial MNPs in the context of inflammation such as IDECs, sub-epithelial cells such as the $CD14^+CD1c^+$ MDDC and $Langerin^+$ cDC2 take up HIV at increased frequencies (Rhodes *et al.*, 2021). This highlights the importance of looking at factors that impact not just epidermal MNP populations, but also those that reside in the dermis.

Of particular interest, is how HSV1/2 infection alters the distribution of $CD4^+$ T cells, the main target cells of HIV infection and explosive replication (Garg and Blumenthal, 2008). Although both the dermis and the epidermis are populated with $CD4^+$ or $CD8^+$ T lymphocytes, their numbers are low in the epidermis relative to the dermis where they are most frequent in the 60 μm closest to the basement membrane (Wang *et al.*, 2014). Understanding the changes in the distributions and densities of both $CD4^+$ T cells and MNPs in the anogenital mucosa due to HSV1/2 infection is of great importance. Finally, as changes in the secretion of cytokines and

cellular infiltration inducing chemokines during HSV1/2 infection may alter the risk of HIV acquisition, this is also an area of interest for investigation. Thus, in this chapter we employ an inner foreskin explant infection model previously optimised by the host lab to examine the distributions of T lymphocyte, DC, and LC populations in both the epidermis and dermis in addition to the cytokine-chemokine environment within the first 24 hours of HSV1 infection of anogenital mucosa **(Figure 3.1.)**. This explant model was optimised with inner foreskin over other anogenital tissue types as it is a common site of HSV infection, only contains a thin layer of keratinisation (the stratum corneum), and also typically has a slightly thinner epidermis than other type II mucosae, reducing the distance for cells to traffic to the dermis (Ganor and Bomsel, 2011, Lemos *et al.*, 2014).

3.2. Summary of Key Methodology

GFP expressing HSV1 passaged and titred by the host lab **(Section 2.3.2)** was administered intraepidermally into inner foreskin explants through the use of HD-MAPs with the aid of an optimised coating solution to reduce surface tension **(Figure 3.1)**. HD-MAP treated tissue was excised out of the specimen and was cut into a maximum of 4 pieces for culturing in DC media, ensuring that the dermis of the inner foreskin was in contact with a DC media pre-soaked gelfoam **(Section 2.4.1)**. The inner foreskin explant model has previously been optimised by the host lab. At 24 hpi the tissue was frozen in OCT for sectioning and the supernatants were retained for the LEGENDplex assay **(Section 2.8)**. Immunofluorescent staining and subsequent imaging were performed on the slides to visualise: CD3, CD4, CD11c and langerin **(Section 2.5)**. Slides were then photobleached with a sodium hydroxide and hydrogen peroxide solution under direct light. RNAscope was performed to detect HSV1 DNA **(Section 2.6.1)** followed by a second round of immunofluorescent staining to detect Langerin^{+} cells. Immunofluorescent

microscopy was selected as this allowed us to visualise cell-cell and cell-virus spatial interactions *in situ* which flow cytometry cannot do.

Images from different rounds of Cyclic IF were merged based on aligning the DAPI staining from both rounds by a script written by the host lab that utilises the Registration and Alignment tools in Fiji (ImageJ; **Appendix A)**. Merged images of the controls, foreskin explants cultured but not treated with a HD-MAP (no HD-MAP), and explants treated with a HD-MAP coated with sucrose solution without virus (mock HD-MAP), or the test condition, foreskin explants coated with HSV1 containing sucrose (HSV1 HD-MAP) were analysed by manually counting as described in **Section 2.7.** In brief, ImageJ was used to generate frames of the epidermis and underlying dermis from no HD-MAP, mock HD-MAP, and HSV1 HD-MAP treated explants. For images of infected explants, frames were generated at both sites of HSV1 infection (site of infection) and sites far from any signs of HSV1 (far from infection). Densities and the average distance of cells in the epidermis, the most superficial 30 μm of the dermis (dermis 0-30), the next 30 μm (dermis 30-60 μm), and finally the 60 μm of dermis deep to this (dermis 60-120 μm) were calculated **(Section 2.7.1)**, and the average cross distance between MNP and lymphocyte populations was determined by the R statistical package Spatstat **(Section 2.7.2)**. This depth of the dermis was selected as the focus region as it has been demonstrated that the immune cells of interest preferentially home to this region of the dermis (Wang *et al.*, 2014).

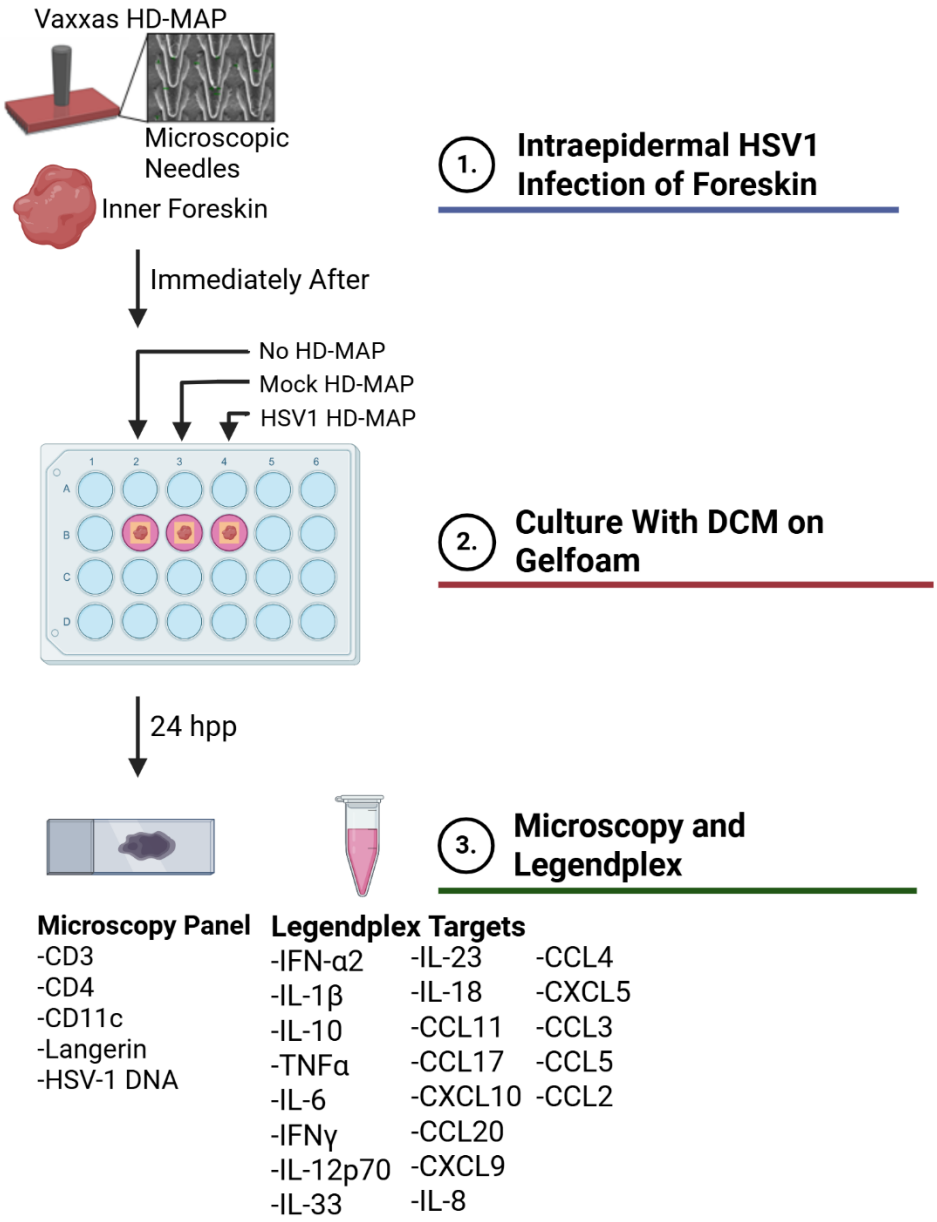

Figure 3.1. Inner foreskin infection explant model workflow. HSV1 was administered intraepidermally using HD-MAPs which penetrate the keratinised outer layer of the inner foreskin (stratum corneum). Tissue that was either left untreated (no HD-MAP), treated with HD-MAP Coating Solution only (mock HD-MAP), or with HSV1 coated HD-MAPs (HSV1 HD-MAP) was placed in DC Culture Medium (DCM) on gel foam. At 24 after application of a HD-MAP (hours post patch/hpp), the tissue was snap-frozen for sectioning to perform Cyclic IF microscopy including RNAscope, while the supernatants were retained for the LEGENDplex Assay.

3.2.1. Selection of Inner Foreskin Donors

To replicate the natural course of HSV1 infection, stringent criteria was put in place for the selection of tissue donors. Inner foreskin donors selected were aged 5 years and above as previous observations by the host lab have demonstrated that inner foreskins from donors aged less than 5 years old had much thinner foreskins resulting in accidental injection of the virus directly into the dermis, and thus does not model the natural course of HSV1/2 infection *in vivo* (Rana et al., 2024). Furthermore, it is well established that the cell types and densities found in the skin of young children do not reflect what is seen in the age groups that are most typically exposed to STIs such as HSV1/2 and HIV (Vreman *et al.*, 2021, Razavi *et al.*, 2015, Gadsbøll *et al.*, 2021). All foreskin specimens were received directly from surgeons in operating theatres located across the Western Sydney Local Health District within 30 minutes of removal from patients and transported to the lab on ice for immediate preparation of the explant model. Finally, collected foreskins were inspected by the surgical team and the host lab for signs of macroscopic inflammation or disease. Foreskins that were severely inflamed were excluded. Donors selected for the inner foreskin explant infection model are described in **Table 3.1.**

Table 3.1. Summary of donors selected for the inner foreskin explant infection model.

Donor	Shape	Reason for removal	Inflammatory Status	Age	Surgeon
1	●	Circumcision	Healthy	9	Dr Cohen
2	■	Circumcision	Mild	21	Dr Ferguson
3	▲	Circumcision	Healthy	12	Dr Cohen
4	◆	Lichen sclerosus	Mild-moderate	41	Dr Wines
5	⬣	Circumcision	Mild	5	Dr Cohen
6	★	Circumcision	Mild-moderate	22	Dr Ferguson

3.3. Validation of the Cyclic Immunofluorescence Bleaching Solution

As observing interactions between DCs and $CD4^+$ T cells is important due to the transfer of HIV between them (Bertram *et al.*, 2019, Rhodes *et al.*, 2021), both these cell populations needed to be visualised in the same microscopy section. However, the limits of traditional immunofluorescent microscopy make this challenging. Cyclic IF allows us to visualise DCs, lymphocytes, HSV1 virions in the same image, and will allow follow up studies to add markers to identify different DC and $CD4^+$ T cell subsets. Also, to visualise lymphocytes, DCs and both HSV2 and HIV virions in co-infected explants **(Chapter 4)** Cyclic IF becomes essential. For Cyclic IF to be used to visualise multiple cell markers, it is necessary to validate that the antibodies selected for cell visualisation can be bleached by the Cyclic IF photobleaching process described in **Section 2.1.4.** To compare the staining of cells before and after photobleaching, images of antibody-stained sections were taken before and after photobleaching and aligned (**Figure 3.2**). CD11c, CD4, and CD3 expressing cells were not identified in the images taken after photobleaching. However, Langerin expression was detected **(Figure 3.2)**. This demonstrates that the antibodies anti-CD4 with secondary Dylight755, anti-CD11c with secondary AF647 and anti-CD3 conjugated to Cy3 can be photobleached and can therefore be used in either round of Cyclic IF, while use of Langerin AF488 should be limited to the final round of immunofluorescent staining. The host lab has previously tried bleaching the fluorescent signal associated with RNA/DNAscope, but this was also unsuccessful; thus RNA/DNAscope staining must also be limited to the final round of Cyclic IF.

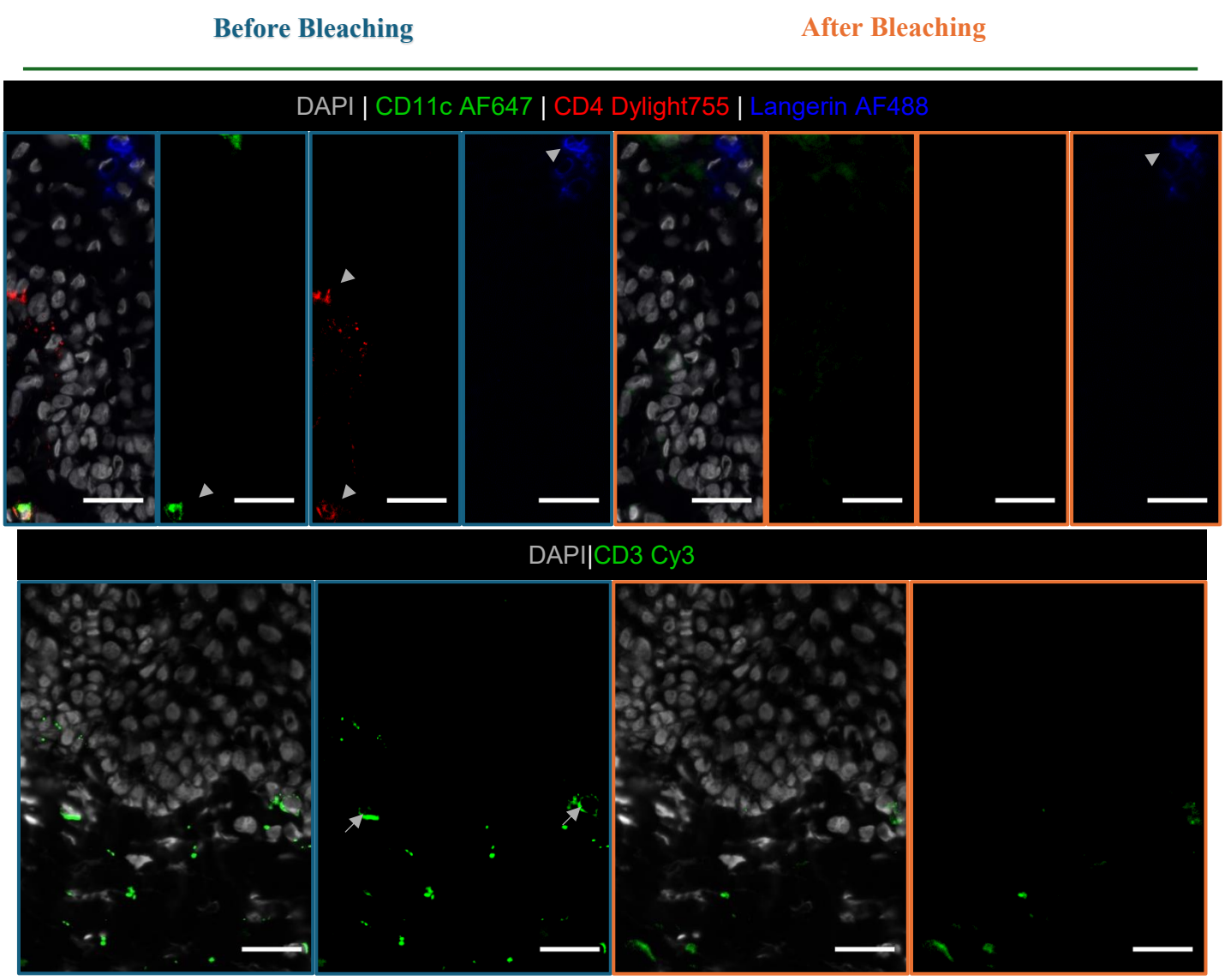

Figure 3.2. Assessment of the efficacy of the Cyclic IF photobleaching process. Untreated inner foreskin specimens were cultured in DCM on gelfoam for 24 hours and snap-frozen in OCT for sectioning. Sections underwent a round of staining consisting of: fixation with 2% PFA; blocking with Blocking Solution; addition of the primary antibodies rabbit anti-CD4 (1:100), mouse anti-CD11c (1:50) and goat anti-Langerin (1:100); addition of the secondary antibodies anti-rabbit Dylight755 (1:400), anti-mouse AF647 (1:400) and anti-goat AF488 (1:400); and finally DAPI nuclear staining, use of the TrueView Autofluorescence Quenching kit, and cover-slipping with Slow Fade Diamond Antifade Mountant for imaging. Alternatively, the primary round of staining consisted of rabbit anti-CD3 conjugated to Cy3. Sections were decover-slipped, bleached using the Cyclic IF photobleaching solution under direct light for 1 hour, re-stained with DAPI and cover-slipped again with Slow Fade Diamond Antifade Mountant for imaging. Cells stained by antibodies are indicated with grey arrows. Scale bars = 30 µm.

3.4. Analysis of Epidermal LC and Epi-DC Density and Distribution

Our lab has previously employed immunofluorescent microscopy staining for CD11c and Langerin expression to examine the density and distribution of epidermal LCs and the newly discovered CD11c^{+} Epi-DCs (Bertram *et al.*, 2021, Rana *et al.*, 2024) at sites of infection and sites far from infection in HSV1 infected foreskin explants. At 24 hpi, HSV1 infection is restricted to the epidermis, and it has been demonstrated that LCs may traffic the virus to the dermis while they apoptose (Kim *et al.*, 2015). This section reanalysed images acquired by Dr Hafsa Rana to determine the distributions and densities of Epi-DCs and LCs in the epidermis at sites of infection **(Figure 3.3a)** and sites far from infection **(Figure 3.3b)** (Rana *et al.*, 2024) using the analysis approach described in **Sections 3.4.2 and 3.4.3** and described in **Section 2.7.1.**

a

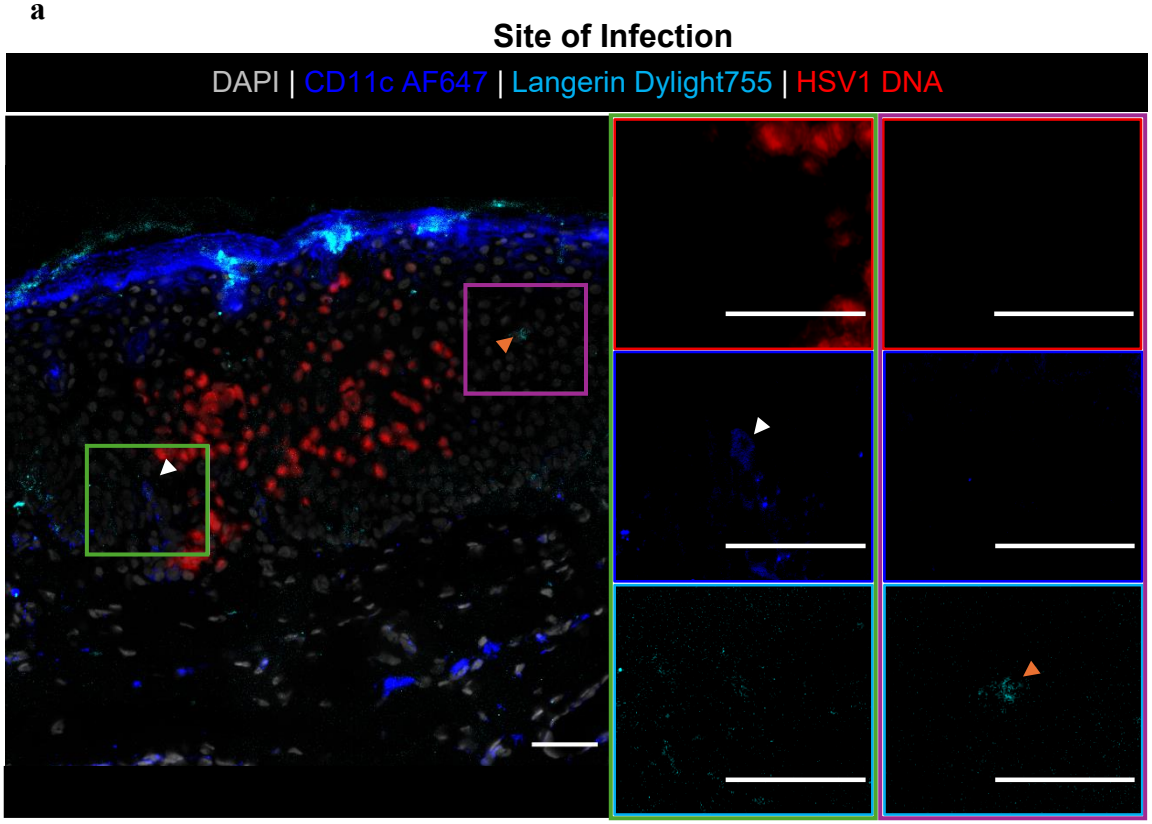

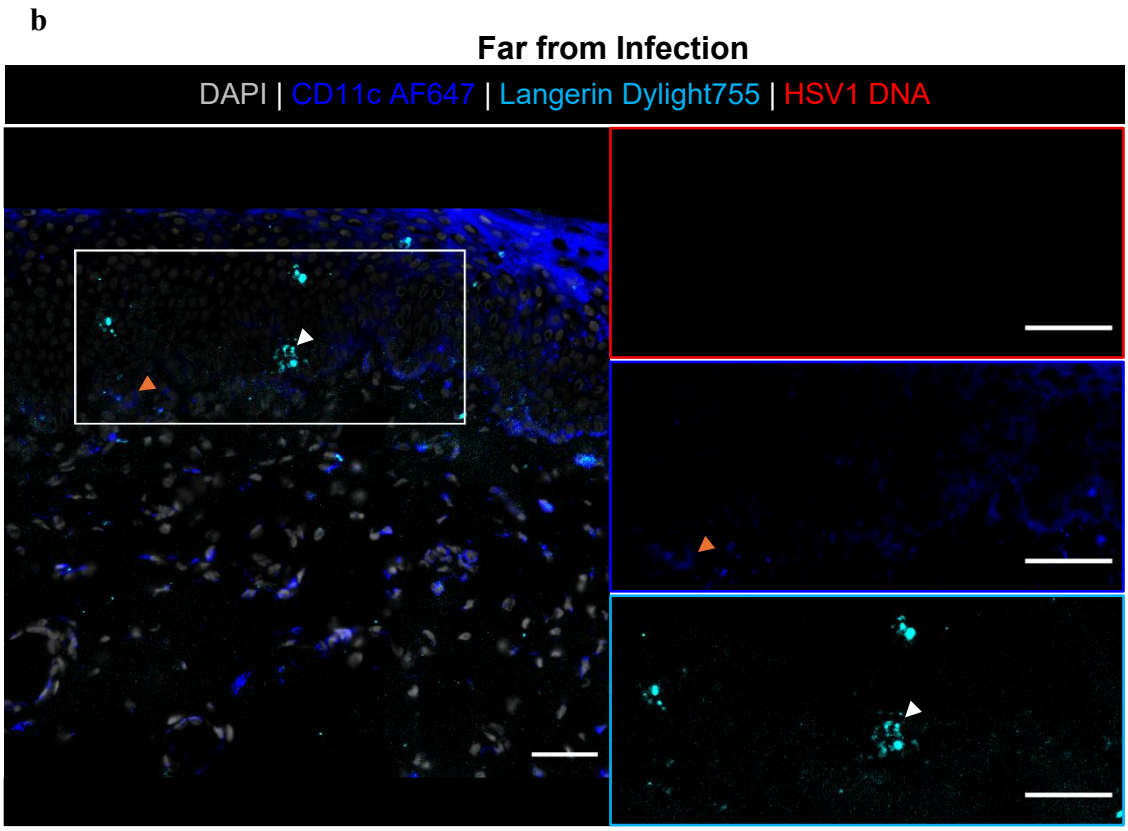

Figure 3.3. Representative images of foreskin explants stained for epidermal counting. Inner foreskin specimens were treated with a HD-MAP coated with HSV1 and were then placed in DCM on gelfoam. 24 hpi specimens were frozen in OCT and sectioned, followed by a round of staining consisting of: fixation with 2% PFA; blocking with Blocking Solution; addition of the primary antibodies mouse anti-CD11c (1:50) and goat anti-Langerin (1:100); addition of the secondary antibodies rabbit anti-mouse AF647 (1:400) and donkey anti-goat Dylight755 (1:400); and finally, DAPI staining and application of the TrueView Autofluorescence Quenching Kit. HSV1 was visualised with RNAscope in which endogenous enzymes were blocked with BLOXALL; Protease Plus (1:5) was applied to sections; and finally, the RNAscope 2.5 HD assay with HSV1 DNA probe was added to detect virus using FastRed. Slides were cover-slipped with Slow Fade Diamond Antifade Mountant for imaging. Images were aligned and merged using the registration function in Fiji (ImageJ). **(a-b)** Arrows denote: epidermal $CD11c^+$ (orange) cells, LCs (white) and Scale bars = 50 µm.

3.4.1. Epi-DCs were Sparsely Distributed and Closer to the Basement Membrane at Sites of HSV1 Infection

To identify how HSV1 infection alters the density and distance of Epi-DCs from the basement membrane at sites of infection and sites far from infection, Epi-DC cell density and distance from the basement membrane were determined by manual counting. Epi-DCs had a significantly lower number of cells per mm^2 at sites of HSV1 infection (13.4 ± 9.4 cells/mm^2) relative to sites far from infection (35.7 ± 19.1 cells/mm^2; p = 0.017; **Figure 3.4a**). At sites of infection (59.3 ± 12.6 µm) the average distance of Epi-DCs from the basement membrane was less than half the distance of Epi-DCs residing at sites far from HSV1 (130.4 ± 129.6 µm; p = 0.266; **Figure 3.4b**). In summary, HSV1 infection caused epidermal DCs to migrate from epidermal sites of infection, either laterally to epidermal sites far from infection, or more likely, into the dermis, as suggested by the reduced distance from the basement membrane.

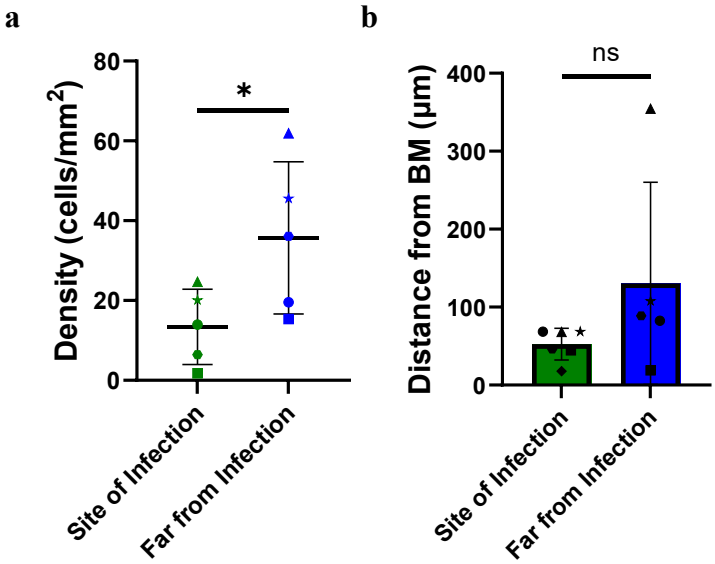

Figure 3.4. The density and average distance from the basement membrane of Epi-DCs. Inner foreskin explants were infected with HSV1 via HD-MAP and cultured in DCM for 24 hours before being frozen in OCT and sectioned. Immunofluorescent microscopy was performed as described in **Figure 3.3**. $CD3^-CD11c^+$ cells were manually counted using Fiji (ImageJ) at sites of HSV1 infection, and sites far from infection. **(a)** The density at sites of HSV1 infection and sites far from infection. **(b)** The average distance of Epi-DCs from the basement membrane. **(a & b)** Statistical analysis performed by Paired T-Tests (n = 5; ns p > 0.05, * p < 0.05), graphs depict the mean ± standard deviation (SD).

3.4.2. Epidermal LCs were Less Dense at Sites of HSV1 Infection

As performed with the Epi-DCs, epidermal LCs at sites of HSV1 infection and sites far from infection were quantified by manual counting to determine the density and average distance from the basement membrane. Similar to Epi-DCs, LCs were significantly less densely distributed at sites of HSV1 infection (22.8 ± 27.1 cells/mm^2) compared to sites far from infection (90.2 ± 62.5 cells/mm^2; p = 0.042; **Figure 3.5a**). Unlike Epi-DCs, epidermal LCs were not located closer to the basement membrane at sites of HSV1 infection (117.0 ± 135.9 µm) when compared to sites far from infection (111.4 ± 94.7 µm; p = 0.834; **Figure 3.5b**). In summary, epidermal LCs have a lower density at sites of HSV1 infection compared to sites far from infection, however rather than being closer, their distance from the basement membrane is unaltered.

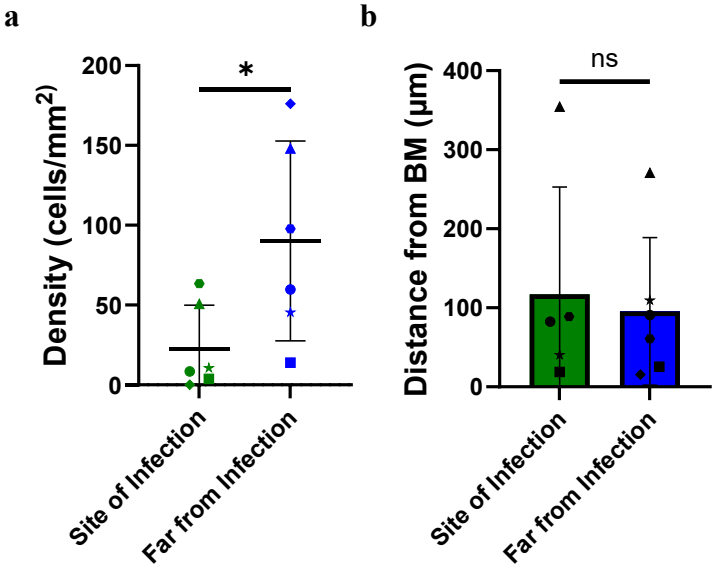

Figure 3.5. Density and the average distance from the basement membrane of LCs residing in the epidermis. See **Figure 3.4.** however, cells that were only Langerin$^+$ were manually counted. (a) n=6, (b) n=5.

3.5. T Lymphocyte and MNP Distribution in the Dermis

As **Section 3.4.** demonstrated that epidermal MNPs reduce in density in the epidermis, during HSV1 infection, we next investigated whether this corresponded to a change in the density and distance of dermal T lymphocytes and MNP cells (**Figure 3.6a-d).** $CD3^{-}CD11c^{+}$ cells were counted as DCs and $CD11c^{-}Langerin^{+}$ cells were considered LCs. $CD3^{+}$ cells were counted as T lymphocytes, $CD3^{+}CD4^{+}$ were classified as $CD4^{+}$ T cells, and $CD3^{+}CD4^{-}$ cells were also examined as cell subsets with this phenotype are immunologically relevant to HSV1 and HIV infection. The $CD3^{+}CD8^{+}$ T cell subset have been shown to have an important role in controlling reactivation of HSV (van Velzen *et al.*, 2013) and accumulate near HSV reactivation sites (Zhu *et al.*, 2007), while $CD3^{+}CD4^{-}CD8^{-}$ T cells form an important part of the HIV and HSV immune response (Cunningham *et al.*, 1985, Meziane *et al.*, 2020). In HSV1 infected sections, HSV1 DNA was exclusively seen in the epidermis as large indistinct clumps overlapping with DAPI staining in small regions of dense infection which typically spanned the entire epidermal width **(Figure 3.6a)**; HSV1 infected foci were interspaced by regions of tissue that lacked HSV1 DNA **(Figure 3.6b)**. As expected, no HD-MAP and mock HD-MAP explants did not show any positive staining for HSV1 DNA by RNAscope **(Figure 3.6c & d)**. The employed cyclic IF panel allowed for CD3, CD4, CD11c, and Langerin expressing cells to be discretely stained with appropriate colocalisation of markers within the dermis. This enabled the visualisation and quantification **(Section 3.6.1-3.6.2)** of $CD3^{+}$, $CD3^{+}CD4^{+}$, and $CD3^{+}CD4^{-}$ T cells, and the MNP subsets: $CD3^{-}CD11c^{+}$ DCs and $CD11c^{-}Langerin^{+}$ LCs.

a

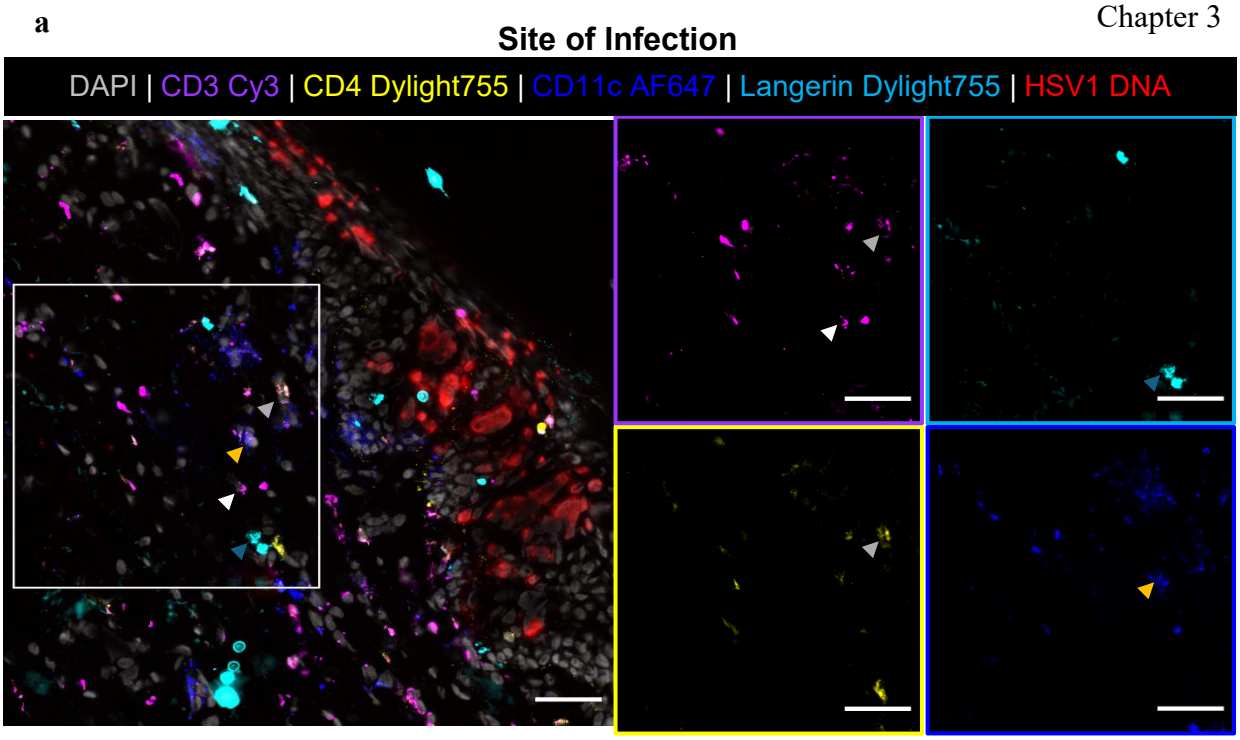
Site of Infection
DAPI | CD3 Cy3 | CD4 Dylight755 | CD11c AF647 | Langerin Dylight755 | HSV1 DNA

c

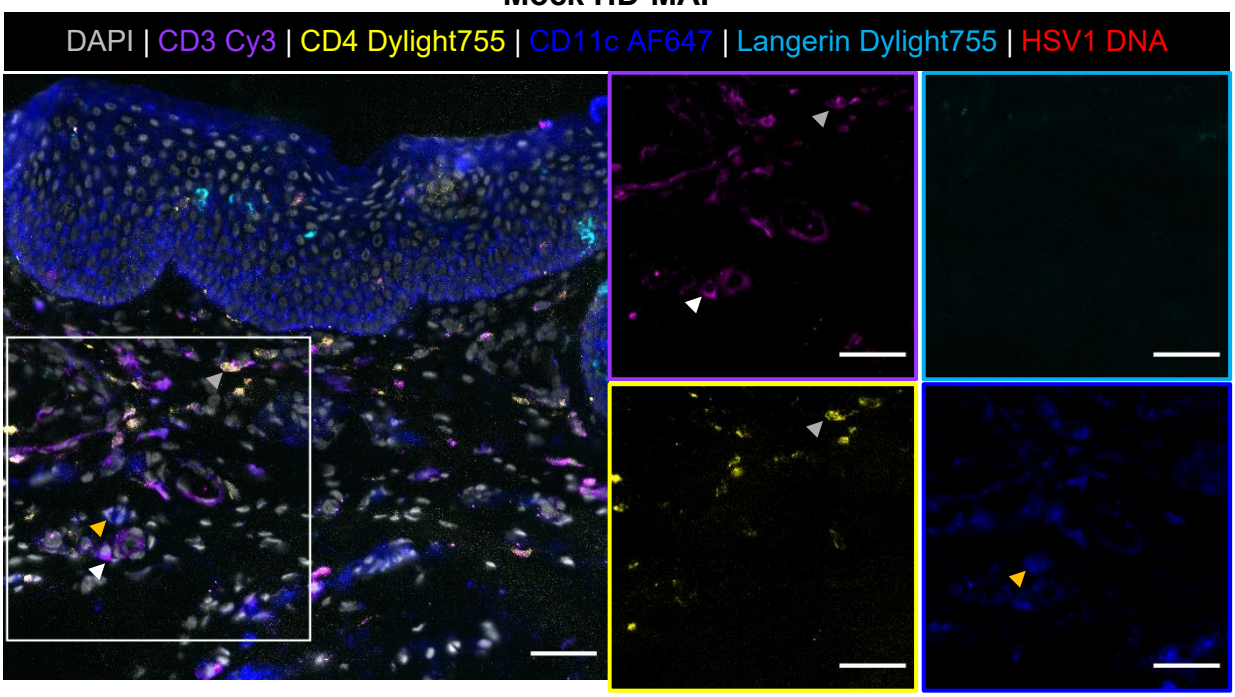
Mock HD-MAP
DAPI | CD3 Cy3 | CD4 Dylight755 | CD11c AF647 | Langerin Dylight755 | HSV1 DNA

b

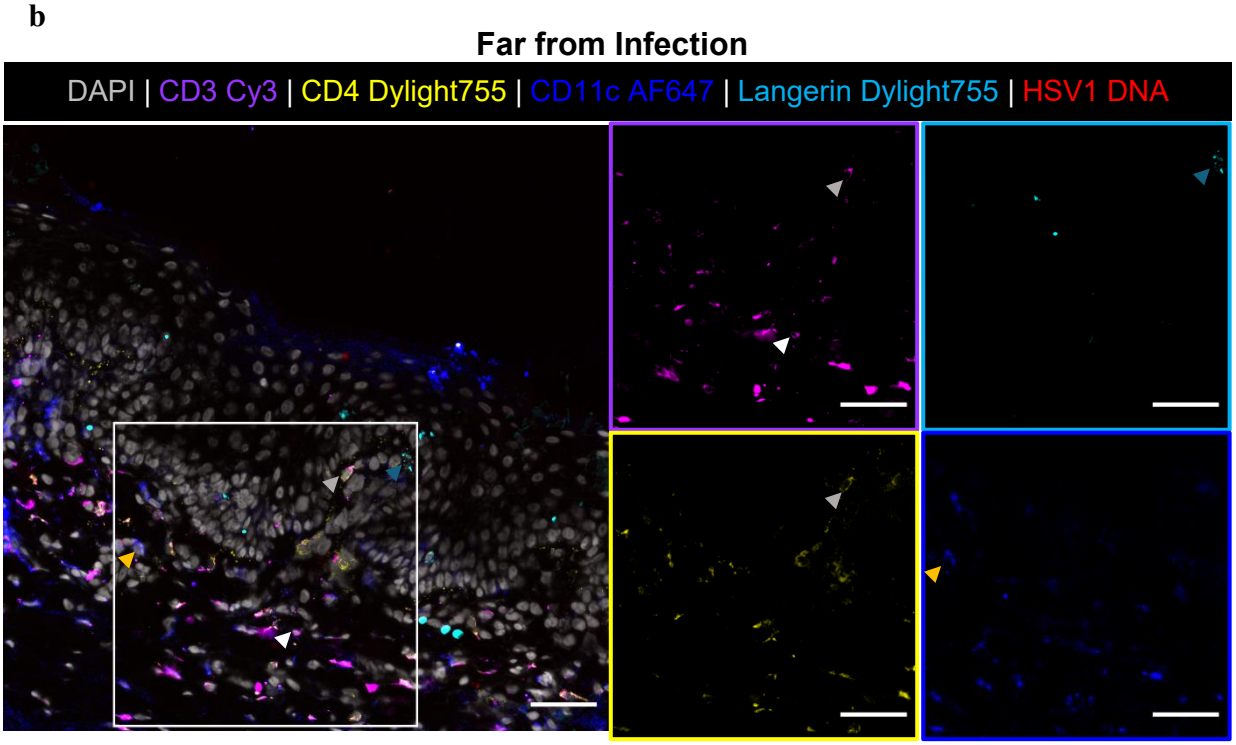
Far from Infection
DAPI | CD3 Cy3 | CD4 Dylight755 | CD11c AF647 | Langerin Dylight755 | HSV1 DNA

d

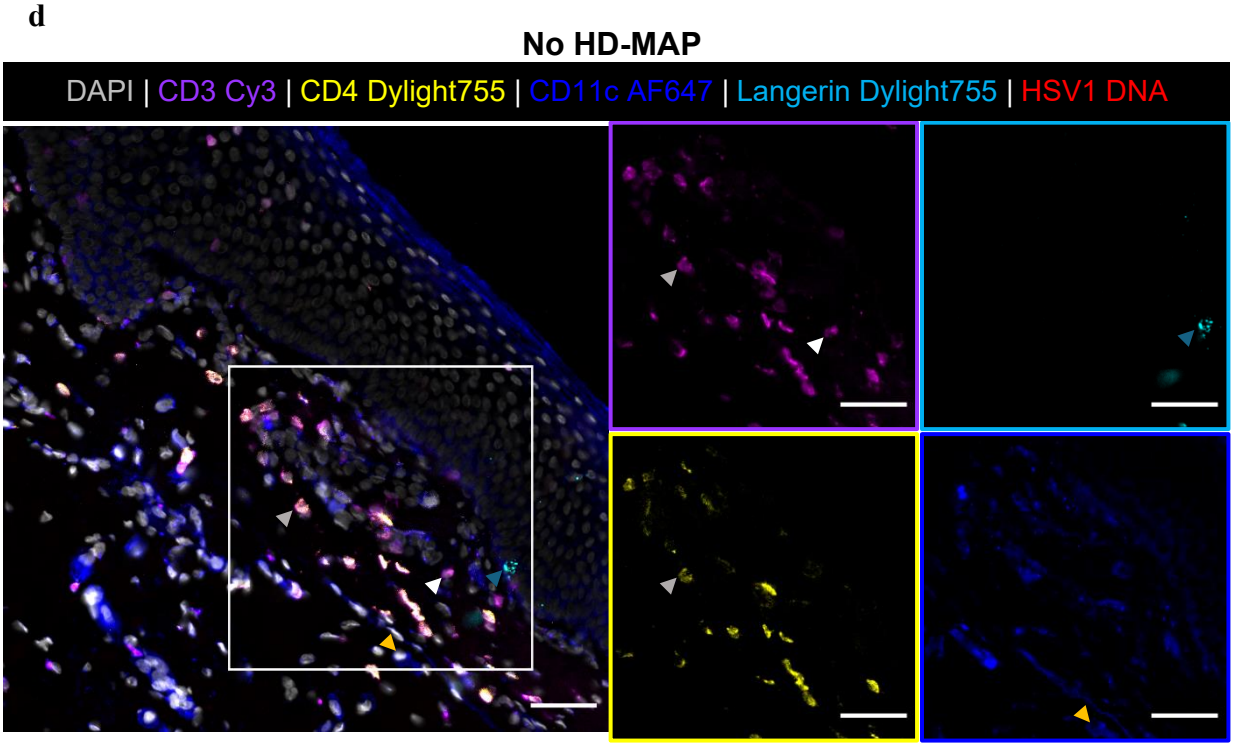
No HD-MAP
DAPI | CD3 Cy3 | CD4 Dylight755 | CD11c AF647 | Langerin Dylight755 | HSV1 DNA

Figure 3.6. Representative images of foreskin explants stained for dermal manual counting. Inner foreskin specimens were either treated with **(a-b)** a HD-MAP coated with HSV1, **(c)** a HD-MAP with no virus (mock HD-MAP), or **(d)** untreated (no HD-MAP). They were then placed in DCM on gelfoam. 24 hpi specimens were frozen in OCT and sectioned followed by a round of staining consisting of: fixation with 2% PFA; blocking with Microscopy Blocking Solution; addition of the primary antibodies anti-CD3-Cy3 (1:100), mouse anti-CD11c (1:50), and rabbit anti-CD4 (1:100); addition of the secondary antibodies anti-mouse AF647 (1:400) and anti-rabbit Dylight755 (1:400); and finally DAPI staining, application of the TrueView Autofluorescence Quenching Kit, and cover-slipping with Slow Fade Diamond Antifade Mountant for imaging. Sections were decover-slipped for photobleaching prior to a second round of staining consisting of the above steps except: endogenous enzymes were blocked with BLOXALL; Protease Plus (1:5) was applied to sections; the RNAscope 2.5 HD assay with HSV1 DNA probe was employed to detect virus; the primary antibody goat anti-Langerin (1:100) was used followed by secondary antibody donkey anti-goat Dylight755 (1:400). Images were aligned and merged using the registration function in Fiji (ImageJ). Arrows denote: $CD3^+CD4^+$ (grey), $CD3^+CD4^-$ (white), or $CD11c^+$ (orange) cells, LCs (blue) **(a-d)** Scale bars = 50 μm.

3.5.1. Distribution and Density of LCs and DCs in the Dermis

As HSV1 is relayed from the epidermis to the dermis by LCs (Kim *et al.*, 2015) and we demonstrated that epidermal $CD11c^+$ cells seemingly also migrated towards the dermis (**Section 3.4)**, we first investigated whether the densities and distributions of LCs ($Langerin^+$ cells) and $CD11c^+$ DCs ($CD3^-CD11c^+$ cells) in the dermis were impacted by HSV1 infection.

3.5.1.1. Dermal $CD11c^+$ DCs were Denser at Sites of HSV1 Infection and Closer to the Basement Membrane

We first examined the density of $CD11c^+$ DCs in the most superficial 120 μm of the dermis in no HD-MAP, mock HD-MAP, and HSV1 HD-MAP inner foreskin explants **(Figure 3.7a)**. In contrast with the epidermis, the average number of DCs per mm^2 (385.8 ± 124.4 cells/mm^2) directly below sites of HSV1 infection, was significantly higher than sites far from infection

(139.3 ± 39.3 cells/mm^2; p = 0.011) and mock HD-MAP treated explants (162.4 ± 69.8 cells/mm^2; p = 0.012). There was no significant difference in the density of DCs at sites far from infection in HSV1 infected explants compared to mock HD-MAP treated explants (p = 0.613), nor between mock HD-MAP treated explants and no HD-MAP explants (p = 0.673).

Next, we examined if the density of DCs varied at different depths of the dermis by segmenting the dermis into regions based on distance from the basement membrane: 0-30 µm, 30-60 µm and 60-120 µm **(Figure 3.7b)**. In the first 0-30 µm of the dermis, sites of infection in HSV1 infected explants had the most significant increase in the number of DCs per mm^2 (675 ± 204.4 cells/mm^2) relative to sites far from infection (103.9 ± 36.2 cells/mm^2; p = 0.0006). The next 30 µm of the dermis (dermis 30-60 µm) also had an increase in DC density at sites of HSV1 infection (367.9 ± 209.7 cells/mm^2) compared to sites far from infection (157.9 ± 34.8 cells/mm^2), however, this did not reach statistical significance (p = 0.053). DCs in the deepest region of dermis examined (dermis 60-120 µm) were also significantly more densely distributed at sites of HSV1 infection (231.9 ± 86.8 cells/mm^2) relative to sites far from infection (152.3 ± 57.6 cells/mm^2; p=0.039). At sites of HSV1 infection, DCs were most densely distributed in the 30 µm most proximal to the basement membrane, followed by the next 30-60 µm of the dermis (0-30 µm vs. 30-60 µm p=0.032), and finally, the deepest 60 µm of dermis examined which had the lowest cell density (0-30 µm vs. 60-120 µm p=0.0038). However, there were no significant differences in cell density at the different depths at sites far from infection.

To determine if the distance of DCs from the basement membrane was altered by HSV1 infection in the foreskin explant model, the average distance of DCs residing in the first 120 µm of the dermis from the basement membrane was determined **(Figure 3.7c)**. DCs directly below sites of HSV1 infection in HSV1 HD-MAP explants were significantly closer to the

basement membrane (39.8 ± 8.1 µm) relative to both sites far from infection (62.7 ± 4.6 µm; p = 0.008) and no HD-MAP explants (61.5 ± 5.7 µm; p = 0.024). Compared to mock HD-MAP explants (60.5 ± 11.2 µm), DCs at sites of HSV1 infection were also closer to the basement membrane, however, this trend was not statistically significant (p = 0.169). In summary, HSV1 infection increased the number of DCs in the dermis in a distance specific manner, with increased numbers in regions closer to the basement membrane than deeper segments, which resulted in a reduction in the average distance of DCs from the basement membrane.

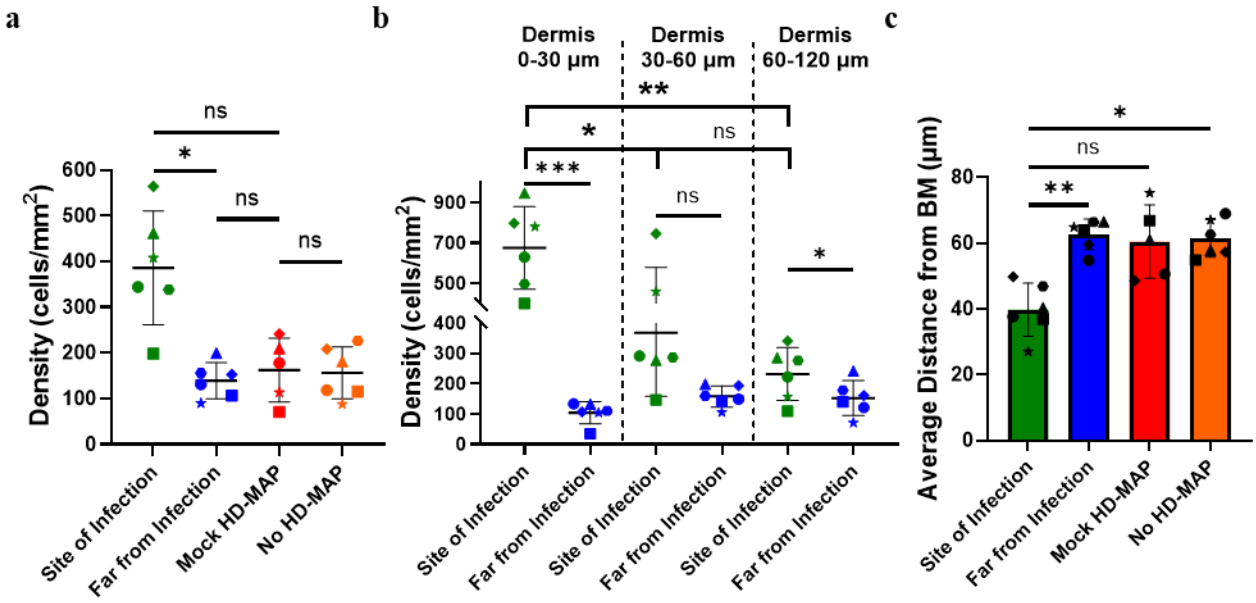

Figure 3.7. Distribution and density of DCs in the most superficial 120 µm of the dermis. Cyclic IF was employed to detect $CD3^{-}CD11c^{+}$ cells within foreskin explants as described in **Figure 3.6**. Using ImageJ, the epidermis was outlined and the most proximal 120 µm of the dermis was distance mapped and outlined allowing for DCs in this region to be manually counted. **(a)** The average density of DCs within the first 120 µm of the dermis from the basement membrane. **(b)** The average density of DCs in different segments of the first 120 µm of the dermis from the basement membrane: 0-30 µm, 30-60 µm, and 60-120 µm. **(c)** The average distance of DCs that reside in the first 120 µm of the dermis from the basement membrane. **(a-c)** Statistical analysis was performed by **(a & c)** Mixed-effects analysis (ANOVA) with Tukey's Multiple Comparisons, Mock HD-MAP n=5, all other groups n=6 or **(b)** Two-way repeated measures ANOVA, n=6; ns $p > 0.05$, * $p < 0.05$, ** $p < 0.01$, *** $p < 0.001$), graphs depict the mean ± SD

3.5.1.2. Dermal LCs were Denser at Sites of HSV1 Infection and Closer to the Basement Membrane

As done for the dermal DCs, we examined the density of LCs residing in the most superficial 120 μm of the dermis, counting cells that were only positive for Langerin **(Figure 3.8a)**. Sites of infection in HSV1 infected explants (157.7 ± 54.9 cells/mm^2) harboured significantly more LCs per mm^2 compared to sites far from infection (86.8 ± 43.1 cells/mm^2; p = 0.042) and mock HD-MAP explants (92.8 ± 37.9 cells/mm^2; p = 0.012). There was no significant difference in the density of LCs at sites far from infection in HSV1 infected explants compared to mock HD-MAP treated explants (p=0.999), nor between mock HD-MAP treated explants and no HD-MAP explants (p = 0.770).

The density of LCs in the dermis was next assessed at different depths from the basement membrane: 0-30 μm, 30-60 μm and 60-120 μm **(Figure 3.8b)**. The first 0-30 μm below sites of infection in HSV1 HD-MAP explants (315.3 ± 120 cells/mm^2) harboured significantly more LCs per mm^2 than sites far from infection (64.6 ± 26.9 cells/mm^2; p = 0.003). The next 30 μm of the dermis (dermis 30-60 μm) showed a slight increase in the density of LCs at sites of infection (124.3 ± 65.2 cells/mm^2) relative to sites far from infection (102.9 ± 57.9 cells/mm^2), but this was not statistically significant (p = 0.570). For the deepest segment of dermis examined (dermis 60-120 μm), there was no difference in the LC density at sites of infection (87.4 ± 42.7 cells/mm^2) compared to sites far from infection (92.4 ± 54.5 cells/mm^2, p = 0.710). At sites of HSV1 infection, LC density was highest in the segment of dermis directly bordering the basement membrane (dermis 0-30 μm), followed by dermis 30-60 μm (0-30 μm vs. 30-60 μm p = 0.007), and finally dermis 60-120 μm which had the lowest density of LCs (0-30 μm vs. 60-120 μm p = 0.009). Contrasting this at sites far from infection, the average LC density was highest in dermis 30-60 μm, followed by dermis 60-120 μm and finally dermis 0-30 μm, however these trends were not significant.

Finally, the average distance from the basement membrane of LCs residing within the first 120 µm of the dermis was quantified **(Figure 3.8c)**. Similar to our observations of DCs, LCs were significantly closer to the basement membrane at sites of infection in HSV1 HD-MAP explants (38.3 ± 6.4 µm) compared to sites far from infection (60.4 ± 7.3 µm; p = 0.016), no HD-MAP explants (62.5 ± 8.9 µm; p = 0.005), and mock HD-MAP explants (63.2 ± 9.8 µm; p = 0.024) which harboured LCs that were the furthest from the basement membrane. In summary, similar to our observations of dermal DCs, HSV1 infection of the epidermis increased the density of LCs in the subjacent dermis, with the effect being confined to the first 30 µm of the dermis, resulting in a reduction in the average distance of LCs from the basement membrane.

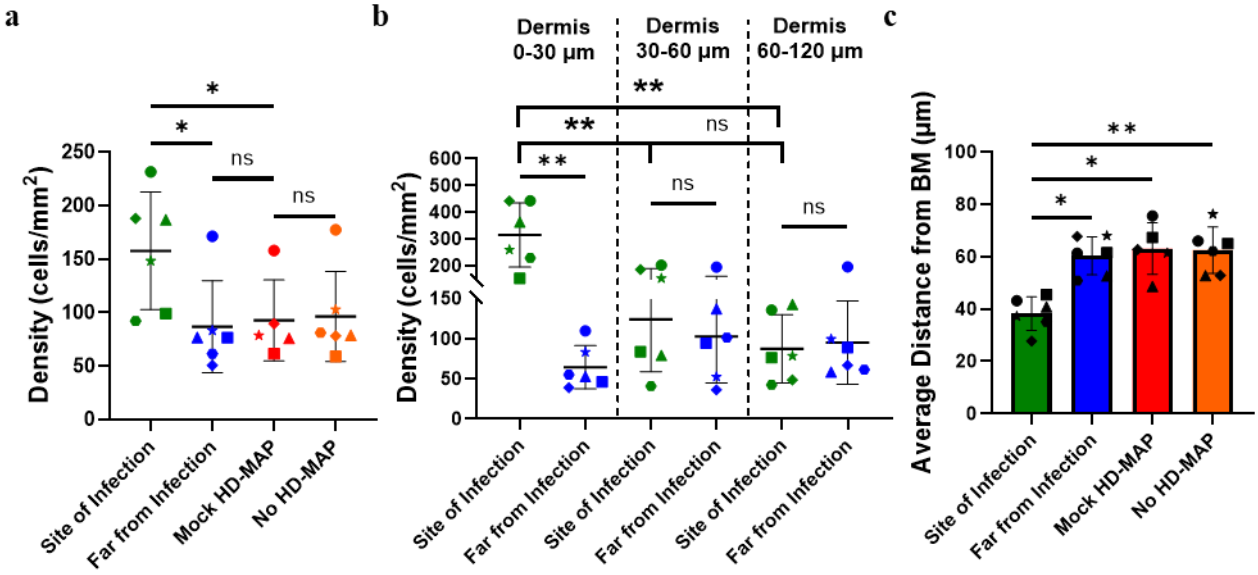

Figure 3.8. Distribution and density of LCs in the first 120 µm of the dermis. See **Figure 3.7.** however, cells that were exclusively Langerin$^+$ were manually counted.

3.5.2. Distributions and Densities of T Lymphocyte Populations in the Dermis

Both types of T lymphocytes play critical roles during initial HIV infection. HIV undergoes explosive replication in CD4$^+$ T cells (Buzon *et al.*, 2014), and CD8$^+$ T cells play an important role in the immune response against HIV (Migueles *et al.*, 2002), although both the CD4$^+$ and

$CD8^+$ T cells residing in the dermis will not be specific for HIV. Therefore, it is important to understand how prior HSV infection affects the distribution of these cells (most importantly $CD4^+$ T cells) to understand how HSV impacts the acquisition of HIV. This distribution is also important for understanding the pathogenesis of HSV itself. The host lab has previously shown that tissue resident $CD4^+$ and $CD8^+$ T are found at low density in the epidermis of inner foreskin (O'Neil, 2023). However, their numbers are not sufficient to allow for their counting in the small regions of infection that the inner foreskin infection explant model generates. As such, the distributions of T lymphocytes in the epidermis were not examined.

3.5.2.1. Dermal T Lymphocytes Were Uniformly Denser at Sites of HSV1 Infection

We first looked at changes in the density of the total $CD3^+$ T cell population residing in the first 120 μm of the dermis of HSV1 HD-MAP explants **(Figure 3.6a)**. As observed with the dermal MNPs, at sites of HSV1 infection, the average number of $CD3^+$ T cells per mm^2 (380.8 ± 155.1 cells/mm^2) was significantly higher compared to sites far from HSV1 infection within infected explants (111.4 ± 42.1 cells/mm^2; $p = 0.015$), mock HD-MAP (154.6 ± 69.8 cells/mm^2; $p = 0.017$) and no HD-MAP explants (121.7 ± 34.2 cells/mm^2; $p = 0.029$). However, there was no significant difference in the number of $CD3^+$ T cells per mm^2 in mock HD-MAP explants compared to no HD-MAP treated explants ($p = 0.649$).

To identify whether the observed change in $CD3^+$ T cell density varies at different depths of the dermis, the first 120 μm of the dermis was segmented into different depths from the basement membrane: 0-30 μm, 30-60 μm, and 60-120 μm **(Figure 3.9b)**. In the first 0-30 μm, sites of HSV1 infection showed the most significant increase in T cells per mm^2 (421.8 ± 194.5 cells/mm^2) compared to sites far from infection (110.3 ± 69.9 cells/mm^2; $p = 0.003$). Similarly, albeit to a lesser degree of significance, the next 30-60 μm of the dermis harboured significantly more T cells per mm^2 (376.9 ± 179.6 cells/mm^2) compared to sites far from HSV1 infection

(134.8 ± 36.1 cells/mm^2; p = 0.010). The final segment of 60-120 µm also demonstrated a significant increase in the number of T cells per mm^2 (360.1 ± 170.1 cells/mm^2) compared to sites far from HSV1 infection (101.0 ± 42.9 cells/mm^2; p = 0.011). In contrast to dermal MNPs, there were no significant differences in the densities of T cells at sites of infection between the segments of dermis examined. At sites of HSV1 infection the density of T cells was highest in the first 0-30 µm, followed by 30-60 µm (0-30 µm vs. 30-60 µm p=0.640), and finally 60-120 µm (0-30 µm vs. 60-120 µm p=0.754). At sites far from HSV1 infection there were no significant differences or trends in the density of T lymphocytes between the segments of dermis examined.

Unlike what we saw with dermal MNPs, the average distance of T cells from the basement membrane was not impacted by HSV1 infection in the foreskin explant model **(Figure 3.9c)**. For all conditions the average distance was within 2 microns of 55 (55 ± 2 µm) from the basement membrane and were therefore not statistically significant (summary p value = 0.696).

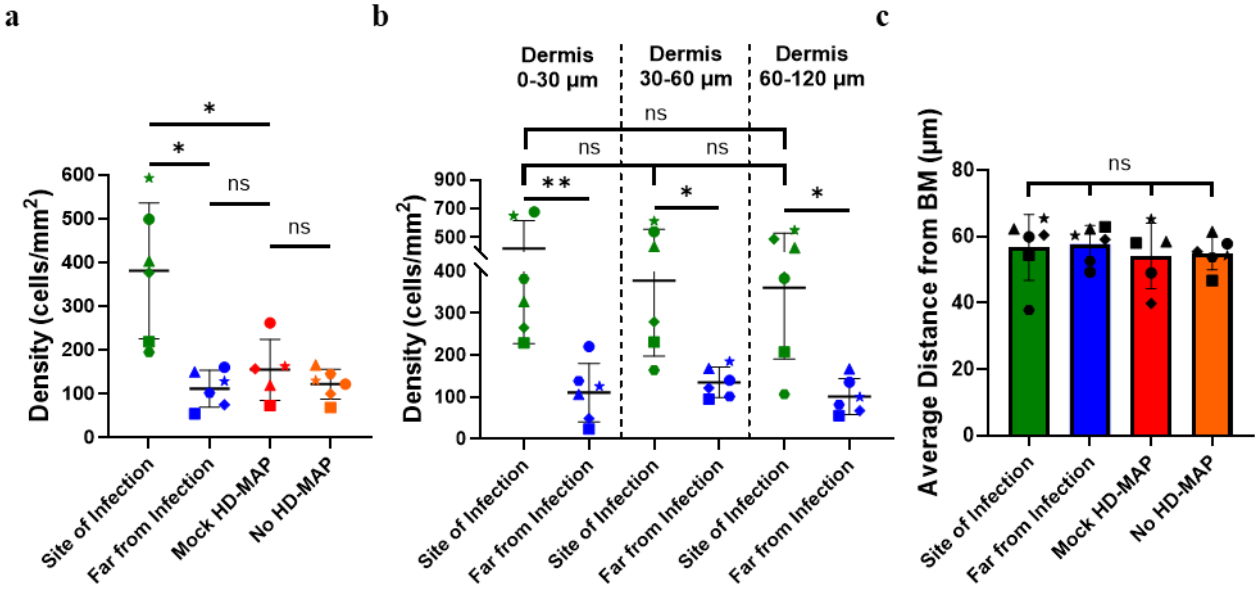

Figure 3.9. Distribution and density of CD3$^+$ T cells in the first 120 µm of the dermis. See **Figure 3.7.** however, cells that were CD3$^+$ were manually counted and **(c)** Statistical analysis was performed by a Mixed-effects analysis (ANOVA) reporting the summary p value only, Mock HD-MAP n=5, all other groups n=6.

3.5.2.2. Dermal CD4$^+$ T cells Were Uniformly Denser at Sites of HSV1 Infection

Next, the distributions and densities of the CD4$^+$ T cell subpopulation were analysed (**Figure 3.10a)**. As observed with the MNP and total T lymphocyte populations, at sites of infection in HSV1 HD-MAP explants the average number of CD4$^+$ T cells per mm^2 (206.2 ± 73.7 cells/mm^2) was significantly higher than both sites far from infection (55.0 ± 21.5 cells/mm^2; $p = 0.008$) and mock HD-MAP treated explants (77.9 ± 49.8 cells/mm^2; $p = 0.020$). There was no significant difference in the density of CD4$^+$ lymphocytes at sites far from HSV1 infection compared to mock HD-MAP explants ($p = 0.618$), nor between mock HD-MAP explants compared to no HD-MAP explants (59.2 ± 22.1 cells/mm^2; $p = 0.653$).

As before, the first 120 µm of the dermis was segmented (0-30 µm, 30-60 µm, and 60-120 µm) and the distribution of the density of CD4$^+$ T cells was investigated (**Figure 3.10b)**. The 0-30 µm dermal segment demonstrated the most significant increase in the density of CD4$^+$ T cells at sites of infection in HSV1 HD-MAP explants (221.5 ± 118 cells/mm^2) relative to sites far from infection (51.3 ± 43.8 cells/mm^2; $p = 0.007$). The 30-60 µm dermal segment also had a significant increase in the number of CD4$^+$ T cells per mm^2 at sites of HSV1 infection (222.6 ± 77.3 cells/mm^2) compared to sites far from infection (80.1 ± 35.2 cells/mm^2; $p = 0.010$). As seen in the previous two segments, the 60-120 µm segment showed a significant increase in the density of CD4$^+$ T cells at sites of HSV1 infection (188.5 ± 103.5 cells/mm^2) relative to sites far from infection (51 ± 29.7 cells/mm^2; $p = 0.020$). At both sites of HSV1 infection and sites far from infection, there were no significant differences in the density of CD4$^+$ T cells between the segment depths of dermis examined.

Finally, the average distance of CD4$^+$ T cells in the first 120 µm of the dermis from the basement membrane was determined to identify any impact on CD4$^+$ T cell distribution by HSV1 infection **(Figure 3.10c)**. CD4$^+$ T cells at sites far from infection in HSV1 HD-MAP explants had the lowest average distance from the basement membrane (54.7 ± 11.9 µm),

followed by sites of HSV1 infection (57.2 ± 10.6 µm), no HD-MAP explants (57.3 ± 3.8 µm), and finally, mock HD-MAP explants (61 ± 7.9 µm). None of the variations in cell distances were statistically significant (summary p value = 0.639).

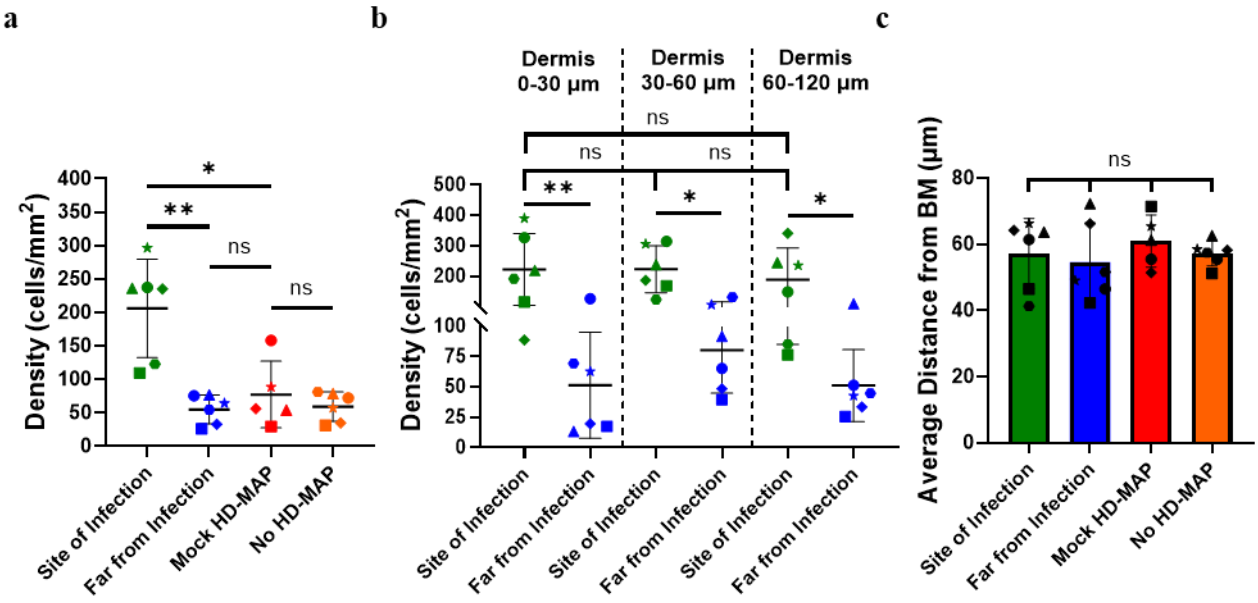

Figure 3.10. Distribution and density of CD4$^+$ T cells in the first 120 µm of the dermis. See **Figure 3.7.** however, cells that were CD3$^+$CD4$^+$ were manually counted and **(c)** Statistical analysis was performed by a Mixed-effects analysis (ANOVA) reporting the summary p value only, Mock HD-MAP n=5, all other groups n=6.

3.5.2.3. Dermal CD3$^+$CD4$^-$ T cells Were Uniformly Denser at Sites of HSV1 Infection

Following the analysis of CD4$^+$ T cells in the first 120 µm of the dermis, the distributions and densities of CD4$^-$ T cell subpopulation were analysed **(Figure 3.11a)**. At sites of infection in HSV1 HD-MAP explants, the average number of CD4$^-$ T cells per mm^2 (174.5 ± 87.6 cells/mm^2) was significantly higher than sites far from infection (59.0 ± 23.1 cells/mm^2; p = 0.036) and non-significantly higher than mock HD-MAP treated explants (76.2 ± 24.2 cells/mm^2; p = 0.068). Albeit not significant, there was a consistent reduction in the average density of CD4$^-$ T cells at sites far from infection in HSV1 infected explants compared to mock

HD-MAP explants (p = 0.570). Finally, there was a small non-significant increase in the average number of $CD4^-$ T cells per mm^2 in mock HD-MAP treated explants compared to no HD-MAP explants (61.9 ± 17.9 cells/mm^2; p = 0.717).

The dermis was segmented into dermis 0-30 µm, dermis 30-60 µm, and dermis 60-120 µm to compare the density of $CD4^-$ T cells at different depths of the dermis (**Figure 3.11b**). The density of $CD4^-$ T cells at sites of HSV1 infection (200.3 ± 91.9 cells/mm^2) increased most significantly compared to sites far from HSV1 infection (60.0 ± 33.6 cells/mm^2; p = 0.009) in the first 0-30 µm of the dermis. Dermis 30-60 µm had a non-significant increase in the density of $CD4^-$ T cells at sites of infection (154.3 ± 104.7 cells/mm^2) compared to sites far from infection (67.3 ± 21.3 cells/mm^2; p = 0.061), while in the dermis 60-120 µm $CD4^-$ T cells at sites of infection (171.7 ± 99.1 cells/mm^2) increased significantly compared to sites far from infection (54.6 ± 23.6; p = 0.016). Again, there were no significant differences in the $CD4^-$ T cell densities between dermal segments when examined at sites of HSV1 infection and sites far from infection.

The average distance from the basement membrane of $CD4^-$ T cells residing in the first 120 µm of the dermis was lowest in mock HD-MAP explants (44.6 ± 13.6 µm), followed by no HD-MAP treated explants (51.2 ± 11.5 µm), sites far from HSV1 infection (52.5 ± 11.5 µm) and finally sites of HSV1 infection, which had the highest average distance from the basement membrane (54.1 ± 9.8; **Figure 3.11c**). However the differences in the average distance from the basement membrane were not statistically significant (summary p value = 0.282).

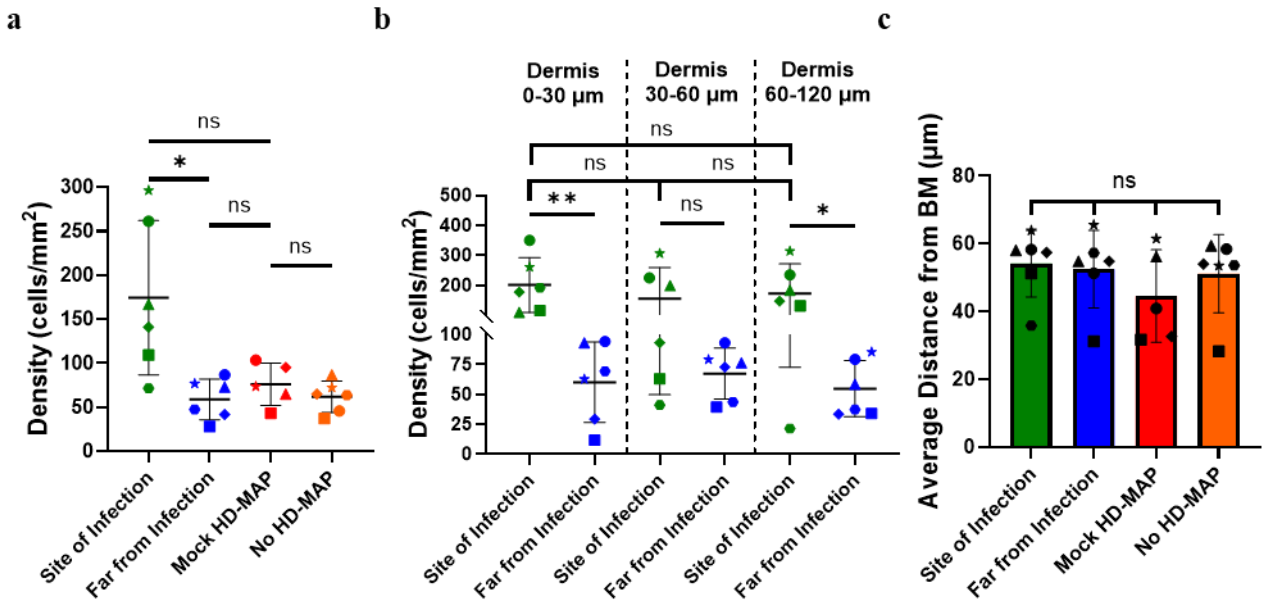

Figure 3.11. Distribution and density of CD4$^-$ T cells in the first 120 µm of the dermis. See **Figure 3.7.** however, cells that were CD3$^+$CD4$^-$ were manually counted and **(c)** Statistical analysis was performed by a Mixed-effects analysis (ANOVA) reporting the summary p value only, Mock HD-MAP n=5, all other groups n=6.

3.5.2.4. Summary of the T Cell Distributions in the HSV1 Inner Foreskin Explant Model

As the CD3$^+$, CD3$^+$CD4$^-$, CD3$^+$CD4$^+$ T cell populations exhibited similar trends, this section will briefly summarise the trends that were consistent in **Figures 3.9-3.11.**

1. All T cell populations showed increased density at sites of HSV1 infection in the first 120 µm of the dermis compared to sites far from infection that are significant compared to mock HD-MAP explants that were only statistically significant in the CD3$^+$ and CD3$^+$CD4$^+$ T cell subsets.
2. Sites far from HSV1 infection exhibited a small non-significant reduction in T cell density compared to mock HD-MAP explants in the first 120 µm of the dermis.
3. T cell density had a trend of being highest in either the first 0-30 or 30-60 µm at sites of HSV1 infection and far from infection. However, differences in the T cells between any dermal segments were not statistically significant.

4. HSV1 infection did not induce a statistically significant change in the average distance from the basement membrane for any T cell population.

Collectively, these results indicate that HSV1 infection of anogenital tissue uniformly increases the density of T lymphocytes in the first 120 μm of the dermis at sites of infection without reducing the average distance of cells from the basement membrane, suggesting lateral migration towards sites of HSV1 infection.

3.5.3. HSV1 Infection Reduced the Lymphocyte-MNP Cross Distance in the Dermis

As mentioned previously, HIV is typically transferred to $CD4^+$ T cells by MNPs that have taken up the virus. As a result of this, we next took the same microscopy images that were generated and utilised in **Section 3.5.1 & 3.5.2** to investigate if the increase in the density of dermal MNPs and dermal T cell populations resulted in a change in the average distance between MNPs and lymphocytes (cross distance), as this may have implications for the probability of HIV transfer to $CD4^+$ T cells. We measured the average cross distance within each donor and saw that at sites of HSV1 infection, the average cross distance between $CD4^+$ T cells and $CD11c^+$ DCs (67.4 ± 49.1 μm) was significantly lower than at sites far from infection (108.7 ± 23.8 μm; $p = 0.031$; **Figure 3.12a**). Similarly, there was a significant reduction in the average cross distance between $CD4^-$ T cells and DCs at sites of infection (65.5 ± 44.1 μm) relative to sites far from infection in HSV1 HD-MAP explants (109.3 ± 30.4 μm; $p = 0.025$; **Figure 3.12b**). The average cross distance between LCs and $CD4^+$ T cells was significantly reduced at sites of HSV1 infection (66.4 ± 44.2) compared to sites far from infection (112.2 ± 19.5 μm; $p = 0.013$; **Figure 3.12c**). Finally, there was also a significant reduction in the average cross distance between $CD3^+CD4^-$ T cells and LCs at sites of infection (67.7 ± 47.1 μm) relative to sites far from infection (109.2 ± 27.2 μm; $p = 0.036$; **Figure 3.12d**).

Interestingly, regardless of which two populations of cells were examined, the average cross distance at sites of infection typically fell between 60-70 μm, while at sites far from infection the average cross distance was typically two times higher (105-115 μm). Also, a large increase in the density of cell populations at sites of infection relative to sites far from infection did not always translate to a reduction in the average cross distance: For a single donor, despite an increase in the density of both MNP and T lymphocyte populations, the average cross distance was larger at sites of infection compared to sites far from infection. In summary, this data indicates that HSV1 infection of the foreskin explant model resulted in a reduction in the average cross distance between MNPs and T cell populations.

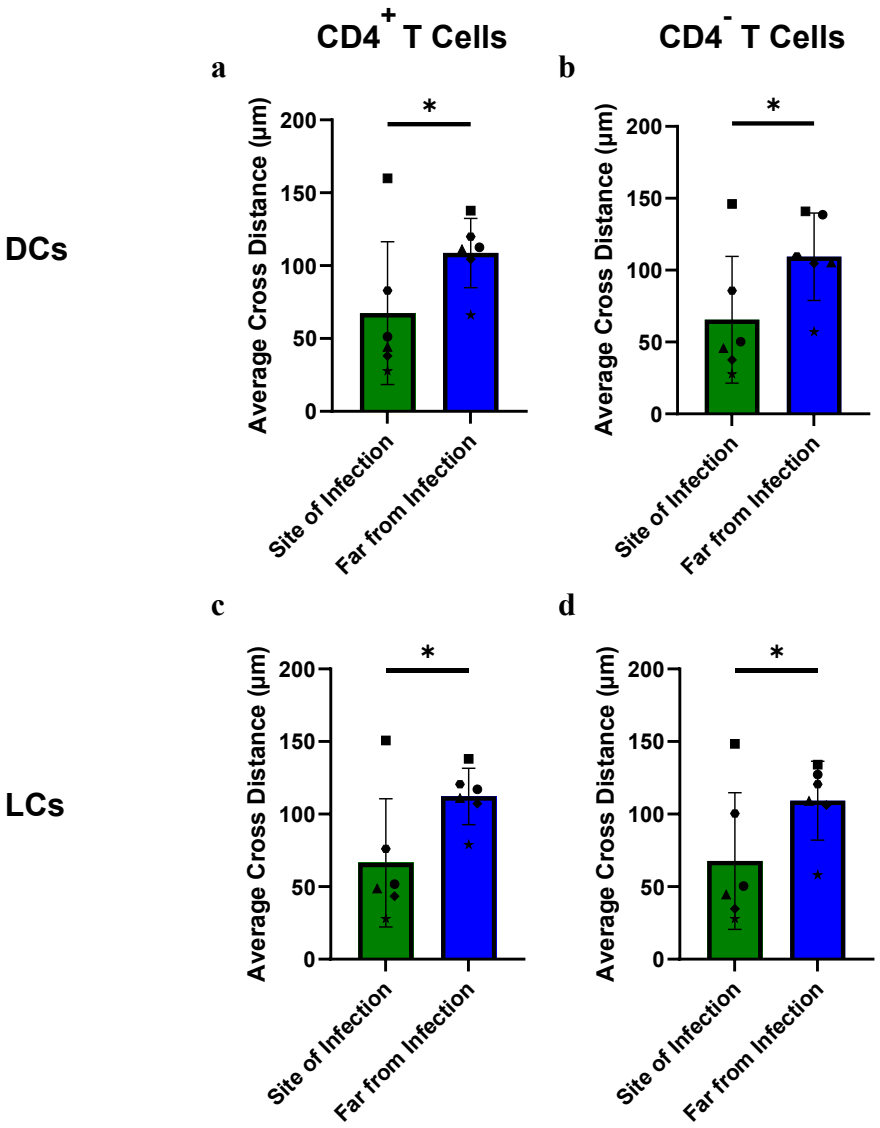

Figure 3.12. The average cross distance between T Cell and MNP populations. $CD4^+$ T cells, $CD3^+CD4^-$ T Cells, $CD11c^+$ DCs, and LCs were counted in the first 120 µm of the dermis at sites of infection and sites far from infection in HSV1 HD-MAP foreskin explants using ImageJ and the cartesian coordinates were exported. Using the R software package Spatstat, point patterns were generated for each cell population and the average **(a)** DC-$CD4^+$ T cell, **(b)** DC-$CD4^-$ T cell, **(c)** LC-$CD4^+$ T cell, and **(d)** LC-$CD4^-$ T cell cross distance was calculated. **(a-d)** All statistical analysis was performed by Paired T-Tests ($n = 6$; * $p < 0.05$).

3.6. HSV1 Infection Altered the Chemokine/Cytokine Environment of Inner Foreskin Explants

It is well established that the migration of cells in the skin and mucosa is influenced by the release of chemokines and proinflammatory cytokines during an immune response, such as after virus infection (Hernández-Ruiz *et al.*, 2017). Additionally, recent studies investigating proinflammatory cytokines have demonstrated that certain chemokine and proinflammatory cytokines such as IL-1β, TNFα, IL-8, CXCL9, CXCL10, CCL3, CCL4, CCL5 and CCL2, correlate with an increased risk of HIV acquisition (Liebenberg *et al.*, 2017, Prodger *et al.*, 2016, Sabo *et al.*, 2020). As such, we next quantified chemokines and proinflammatory cytokines in supernatants retained from mock HD-MAP and HSV1 HD-MAP treated inner foreskin explants using LEGENDplex assays to identify any chemokines/cytokines that may be responsible for the observed cell migrations and also those implicated in increased HIV acquisition.

As inflammation of tissue is associated with increased HIV infection (Liebenberg *et al.*, 2017), the LEGENDplex Multiplex Inflammatory Panel 1 Kit was used to quantify: IFN-α2, IL-1β, IL-10, TNFα, IL-6, IFNγ, IL-12p70, IL-33, IL-23, and IL-18 in supernatants from mock and infected explants. **(Figure 3.13a)**. Relative to mock HD-MAP explant supernatants, HSV1 HD-MAP explant supernatants showed consistent upregulation of: IFN-α2 (8.9-13.6 pg/mL to 14.6-16.2 pg/mL), IL-1β (105.3-155.7 pg/mL to 478.7-2067.8 pg/mL), IL-10 (45.4-107.2 pg/mL to 165.5-224.1 pg/mL), TNFα (10.7-12 pg/mL to 37-61.3 pg/mL), IL-6 (199291.2-202409.3 pg/mL to 378287.5-393503 pg/mL), IFNγ (13-17.4 pg/mL to 17.6-18.9 pg/mL), IL-12p70 (14.7-17.5 pg/mL to 19.1-19.3 pg/mL), IL-33 (65.4-107.3 pg/mL to 138.1-269.4 pg/mL), IL-23 (19-25.4 pg/mL to 28.3-35.4 pg/mL), and IL-18 (341.5-2553.4 pg/mL to 1181.8-2759.9 pg/mL).

As many chemokines such as CCL11, CCL17, CXCL10, CCL20, CXCL9, IL-8, CCL4, CXCL5, CCL3, CCL5, and CCL2 are also implicated in cell migration, these were also quantified by LEGENDplex, using the Proinflammatory Chemokine Assay **(Figure 3.13b)**. Relative to mock HD-MAP explant supernatants, HSV1 HD-MAP explant supernatants showed consistent upregulation of: CCL11 (6.1-6.1 pg/mL to 8.2-11.7 pg/mL), CCL17 (3.9-11.1 pg/mL to 6.6-47.5 pg/mL), CXCL10 (34.1-1076.9 pg/mL to 49.8-7214 pg/mL), CCL20 (2.5-5.6 pg/mL to 19.7-26.8 pg/mL), CXCL9 (34.1-1076.9 pg/mL to 49.8-7214 pg/mL), IL-8 (18313.26-18886.6 pg/mL to 23128.4-24124.3 pg/mL), CCL4 (3.8-21.7 pg/mL to 58.3-74.1 pg/mL), CXCL5 (143.8-280.5 pg/mL to 193.2-752.1 pg/mL), CCL3 (68.1-121 pg/mL to 630.2-662.5 pg/mL), CCL5 (5.5-7.6 pg/mL to 12.2-35.6 pg/mL), and CCL2 (10757.9-14969.5 pg/mL to 29910.9-19806.33 pg/mL).

In summary, these results demonstrated that HSV1 upregulated all inflammatory cytokines and chemokines that were assessed by the LEGENDplex chemokine and cytokine assays. As many of these proinflammatory cytokines and chemokines are associated with cell migration and increased HSV1 acquisition (Looker *et al.*, 2017, Mikloska *et al.*, 1998) this upregulation likely contributes to the changes in cell distributions and may also contribute to the increased risk of HIV acquisition that is observed in HSV positive individuals.

a

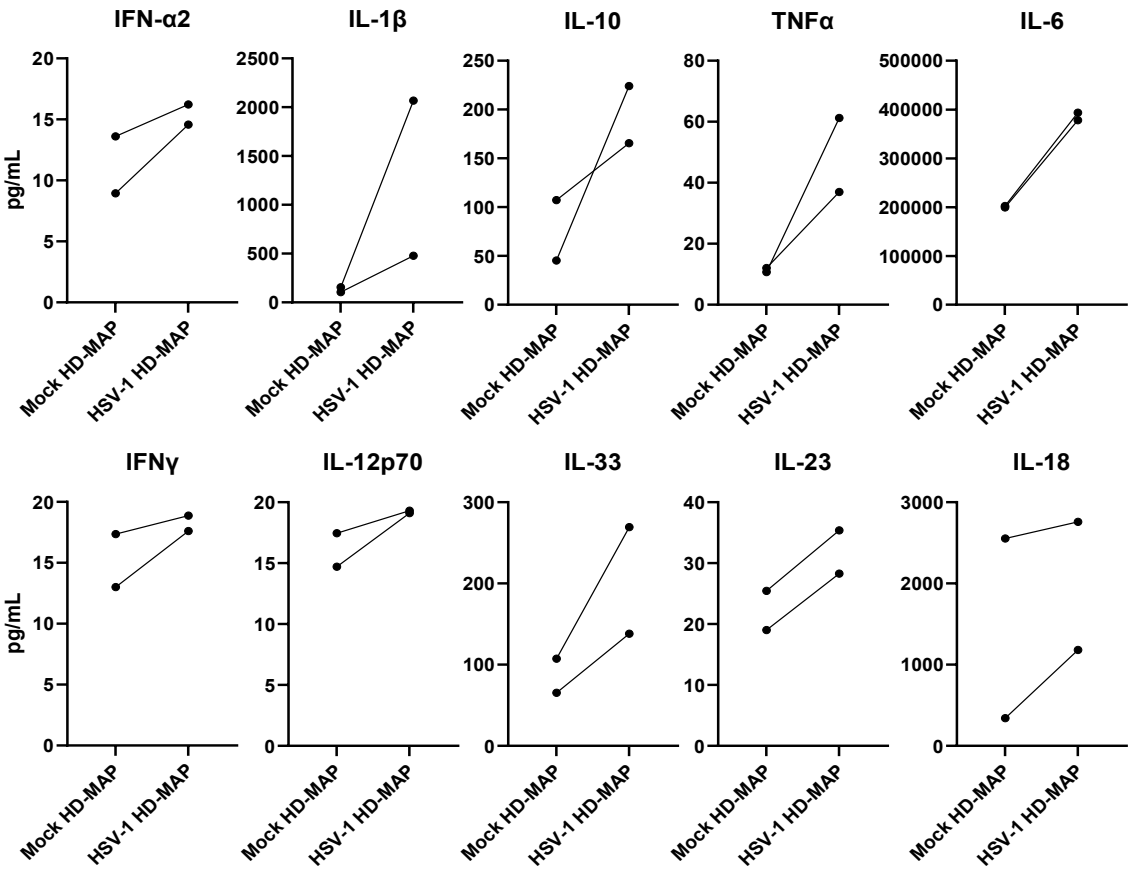
IFN-α2
IL-1β
IL-10
TNFα
IL-6
IFNγ
IL-12p70
IL-33
IL-23
IL-18
pg/mL
Mock HD-MAP
HSV-1 HD-MAP

b

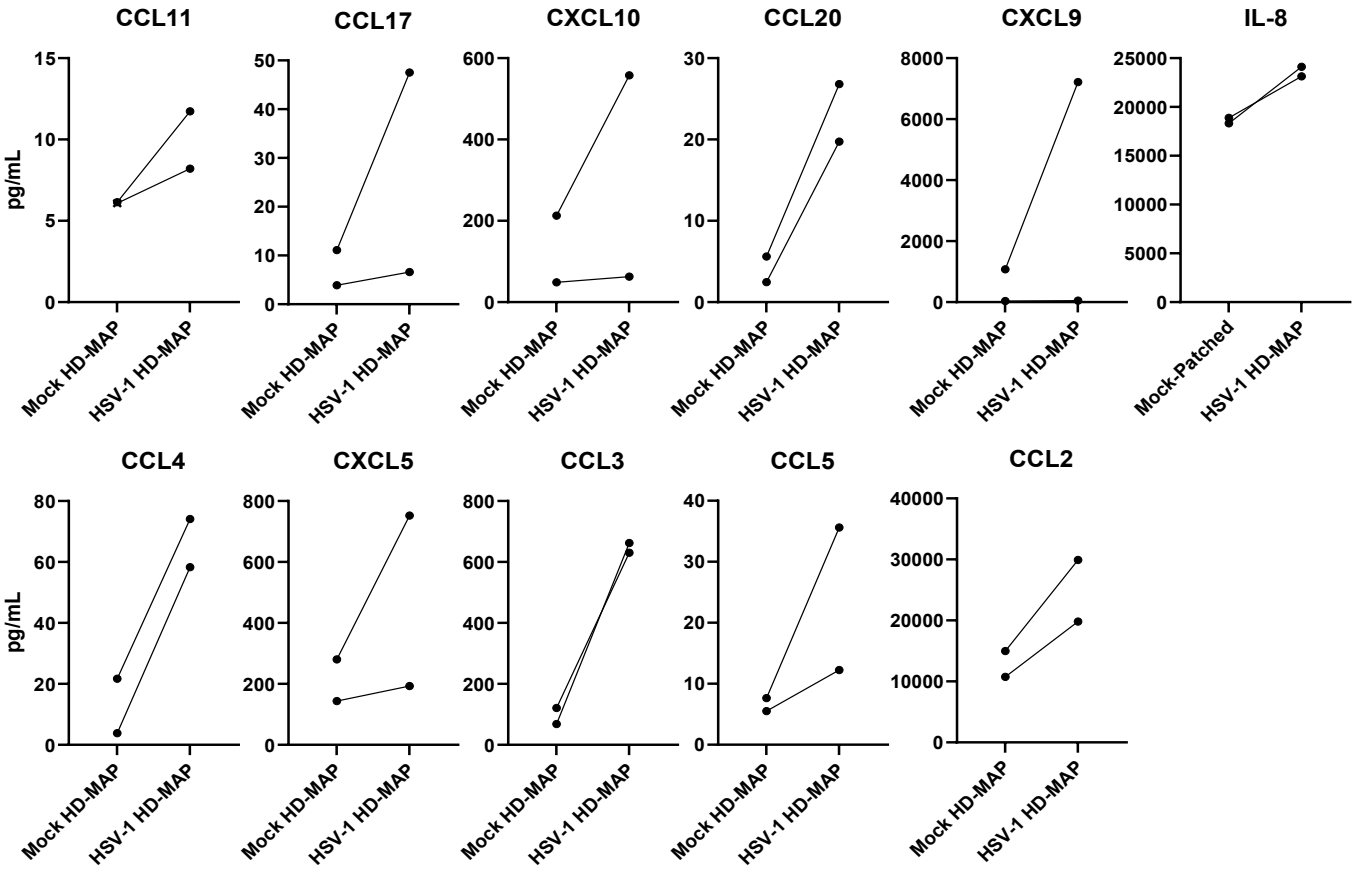
CCL11
CCL17
CXCL10
CCL20
CXCL9
IL-8
CCL4
CXCL5
CCL3
CCL5
CCL2
pg/mL
Mock HD-MAP
HSV-1 HD-MAP
Mock-Patched

Figure 3.13. Quantification of inflammatory cytokines and chemokines in foreskin explant supernatants. (a) Inflammatory cytokines and **(b)** chemokines in mock HD-MAP and HSV1 HD-MAP foreskin explant supernatants were quantified using the LEGENDplex Multiplex Inflammatory Panel 1 kit and the Proinflammatory Chemokine Assay respectively. Retained supernatants and standards were combined with assay buffer and added to a 96-well V-bottom plate with capture bead solution and incubated in the dark at room temperature for two hours. Following a wash with supplied wash buffer, detection antibodies were added for a 1-hour incubation as above and Streptavidin PE was then added for a further 30 minutes. This was followed by two washes and bead acquisition by flow cytometry. **(a-b)** n = 2.

3.7. Chapter Three Discussion

STIs such as HSV1/2 and HIV1 are transmitted at sites of microtrauma in the anogenital mucosa where they enter the epithelium and encounter epidermal residing MNPs; they may eventually be transported to the submucosa where they encounter dermal residing MNPs and a range of $CD3^+$ T cell populations (Bertram *et al.*, 2019, Bertram *et al.*, 2021, Harman *et al.*, 2013b). It has been demonstrated that prior HSV infection increases the risk of HIV acquisition, however the mechanisms behind this remain undefined (Looker *et al.*, 2017). In this chapter, we employed an inner foreskin HSV1 infection explant model designed and optimised by the host lab to investigate changes HSV may induce in the anogenital mucosa that increases the risk of HIV acquisition. We observed that epidermal MNPs such as LCs and $CD11c^+$ Epi-DCs were significantly less frequent at sites of HSV1 infection and were typically closer to the basement membrane (although this was not significant) than MNPs in the epidermis of far from infection sites. This correlated with our second major observation, LCs and DCs residing in the dermis at sites of infection were significantly closer to the basement membrane and significantly denser relative to sites far from infection, where these MNPs were more evenly distributed in the first 120 µm of the dermis and less frequent. Collectively, these findings suggest that within the first 24 hours of HSV infection epidermal MNPs 'flee' sites of infection

to migrate and accumulate in the dermis underlying the infection. An alternative, although less likely explanation given the increase in dermal MNPs, is that the decrease in epidermal MNPs at sites of HSV infection is not due to migration to the epidermis, but rather exclusively due to apoptosis within the epidermis. Further clarity could be provided with the inclusion of mock and mock HD-MAP treated tissue samples as used within **Section 3.5.**

The migration of LCs is consistent with previous work performed by the host lab which utilised primary biopsies from sites of HSV1 3 days after symptom onset to show that HSV1 infected epidermal LCs apoptose and migrate to the dermis where they are taken up by BDCA3$^+$ dermal DCs for antigen presentation (Kim *et al.*, 2015). More recently, *in vitro* experiments demonstrated that 18 hpi with HSV1 Epi-DCs begin to show signs of apoptosis, suggesting they share a similar fate to epidermal LCs (Bertram *et al.*, 2021). We have previously demonstrated that while HSV1 infects LCs by pH-dependent pathways, CD11c$^+$ Epi-DC infection utilises a pH-independent pathway which allows for enhanced infection (Bertram *et al.*, 2021). Of the cells we classified as dermal CD11c$^+$ DCs, the vast majority are likely DC2s (Rhodes *et al.*, 2021), with the remainder being CD14$^+$ monocyte-derived DCs and the density of dermal DCs we reported in healthy tissue is consistent with previous findings (Rhodes *et al.*, 2021). As DC2s and CD14$^+$ monocyte-derived DCs express very similar functional markers (Rhodes *et al.*, 2021) regardless of which dermal cell CD11c is staining it is expected they would behave very similarly. Therefore, our findings of a greater concentration of DC2s in the dermis, especially the upper dermis, under foci of HSV1 infection may be due to Epi-DC migration from the epidermis or concentration from the dermis. It is important to note that as we did not utilise a marker that allows for differentiating between epidermal and dermal DC2s and LCs within the dermis, migration from the epidermis cannot be definitively proven with the current staining panel.

We also reported that LC density at sites of HSV1 infection increased significantly in the 30 µm of the dermis closest to the basement membrane, however there was no increase in deeper dermal segments, while there was an increase in DC density across all dermal depths that was statistically significant at 0-30 µm and 60-120 µm. This could be explained by higher rates of Epi-DC migration from the epidermis to the dermis allowing them to reach deeper segments of the dermis than LCs at 24 hpi. An alternative explanation to this is that the migrating LCs apoptose before reaching deeper segments of the dermis for DCs to uptake fragments as shown in Kim *et al*., (2015). However, it is important to note that despite the significant increase in DC density at all depths of the dermis, HSV1 infected Epi-DCs have also been shown to undergo apoptosis (Bertram *et al.*, 2021).

We also reported that both major populations of $CD3^+$ lymphocytes, $CD3^+CD4^+$ cells and $CD3^+CD4^-$ cells, increased significantly in density at sites of HSV1 infection relative to sites far from infection and relative to explants that were mock HD-MAP (significant for $CD3^+$ and $CD3^+CD4^+$ subsets). However, contrasting what we saw with the MNPs, there was no significant difference in the distance from the basement membrane between conditions. Although the host lab have previously reported that $CD3^+$ T cells can be found in the epidermis (O'Neil, 2023), their numbers are too low to reliably quantify.

The increase in the density of dermal T cell populations at sites of HSV1 infection relative to sites far from infection in the absence of any migration of lymphocytes from the epidermis or changes in the average distance from the basement membrane suggests that this is a product of lateral migration within the dermis. This explanation is supported by the small and non-significant, but highly consistent trend of a lower density of lymphocyte populations at sites far from infection relative to mock HD-MAP treated explants. At sites of HSV1 infection the different dermal segments examined had near-uniform densities. This suggests that whatever

chemotactic gradient induces $CD3^+$ lymphocyte migration is either: 1) by 24 hpi is reaching a limit of effect/range on attracting cells from the surrounding tissue and the migrating cells are uniformly distributing in the underlying dermis; or 2) by 24 hpi there are opposing chemokines/mechanisms preventing a further increase in cell density. Mechanisms that temporarily inhibit T cell migration to sites rich in antigen to allow for emigration of activated T cells have been demonstrated (Dustin *et al.*, 1997) which is consistent with a range of mathematical models that show a limit to the range of chemotaxis in the absence of inflammatory infiltrate from blood vessels (Painter, 2019).

We also observed that the average cross distance between the MNP and $CD3^+$ T cell populations investigated was significantly lower in the dermis of sites of infection compared to sites far from infection in HSV1 HD-MAP treated foreskin explants, likely because of the increase in density of cells in the dermis. The increase in density of the different cell populations examined in the dermis has significant implications for the risk of HIV acquisition, as it has been demonstrated that regions of tissue that are richer in HIV target cells due to inflammation are more susceptible to infection (Abu-Raddad *et al.*, 2008, Zhu *et al.*, 2007) The uptake of HIV virions by MNPs typically results in the eventual degradation of the virion (or in some cases immunological evasion and productive infection of DCs) unless it encounters a $CD4^+$ T cell for antigen presentation resulting in the transfer of the virion to the T cell and which becomes highly productively infected (Piguet and Steinman, 2007). As epidermal MNPs are closer to the basement membrane, and the dermal MNP-$CD4^+$ T cell cross distance is reduced during HSV infection, perhaps during HSV-HIV coinfection MNPs that have taken up HIV virions encounter $CD4^+$ T cells for antigen presentation more frequently and earlier, increasing the risk of an intact HIV virion being passed to the $CD4^+$ T cell for productive infection.

The chemokines and proinflammatory cytokines we investigated by LEGENDplex were either upregulated in HSV1 HD-MAP explants relative to mock HD-MAP explants or had concentrations out of the range of the assay (not shown). Statistical significance could not be assessed due to the sample size (n=2). The function of each chemokine/cytokine investigated is summarised in **Table 3.2.** The inflammatory environment caused by the upregulation of IL-1β, TNFα, IL-8, CXCL9, CXCL10, CCL4 and CCL2 is associated with an increase in the risk of acquiring HIV (Sabo *et al.*, 2020, Liebenberg *et al.*, 2017, Prodger *et al.*, 2016); this may partially explain why prior HSV infection increases the risk of HIV acquisition. The excessive inflammation induced by these chemokines and cytokines likely enhances T cell and MNP migration and activation allowing for HIV infection. Furthermore, both CCL5 and CCL3 are ligands to the HIV coreceptor CCR5, the upregulation of these ligands can upregulate the receptor, resulting in increased HIV infection (Gonzalez *et al.*, 2001). Many of these inflammatory cytokines and chemokines are associated with the migration of lymphocytes and MNPs, notably CCL17, CXCL10, CCL3/4 and CCL2 (Sokol and Luster, 2015, Zaid *et al.*, 2017); therefore these chemokines could explain the increase in MNPs and T cells in the dermis underlying sites of HSV infection. It is worth noting that our LEGENDplex kit did not quantify anti-inflammatory cytokines such as TGF-β which act to counter the effects of these pro-inflammatory cytokines (Walter, 2020). Future investigations should examine whether there is also a significant increase in anti-inflammatory cytokines such as TGF-β as they may resist changes that could be caused by a rise in the studied inflammatory cytokines and chemokines.

Our LEGENDplex data was consistent with previous work done by the host lab looking at chemokine and inflammatory cytokine production in a HSV infected keratocyte cell line (HaCaTs) and another study that examined HSV1 infected primary keratinocytes and vesicle fluid in recurrent herpes infection (Mikloska *et al.*, 1998, Rana *et al.*, 2024). The concentrations we reported were higher than the cell line study by the host lab, however, were similar or

slightly lower than what Mikloska *et al* (1998) found. This is consistent with the fact that higher levels of cytokines/chemokines are known to be produced by primary keratinocytes than cell lines (Olaru and Jensen, 2010). It is important to note that the explant model only contains resident immune cells and therefore does not measure the input from an inflammatory infiltrate as in vesicle fluid from lesions. Furthermore, the explant model mimics initial infection rather than the formation of a recurrent lesion, which is where resident memory T cells and an inflammatory infiltrate may synergise in cytokine production. Unfortunately, we only retained supernatants from two inner foreskin donors, and therefore were unable to test for statistical significance on the data obtained from the LEGENDplex due to a limited sample size. Although the LEGENDplex allowed us to assess a wide range cytokines and chemokines, it does not allow us to visualise what cells are responsible for their secretion and localisation. Performing RNAscope with probes specific to the cytokines/chemokines that show the largest fold change would allow us to visualise which cells are responsible and whether the production of the cytokines/chemokines was localised to sites of infection or present throughout the entire explant.

Table 3.2. Function of the chemokines and inflammatory cytokines investigated

Chemokine/Cytokine	Function	Reference
IFN-α2	Secreted by virally infected cells to inhibit viral infection of surrounding cells.	(Gresser, 2015)
IL-1β	Produced by activated macrophages and is a lymphocyte inflammation marker	(Lopez-Castejon and Brough, 2011)
IL-10	Proinflammatory and survival cytokine that induces antibody production.	(Iyer and Cheng, 2012)
TNFα	Produced by macrophages during acute infection and induces inflammation	(Idriss and Naismith, 2000)
IL-6	Produced by macrophages to mediate the production of neutrophils and lymphocytes.	(Tanaka *et al.*, 2014)
IFNγ	Activates macrophages and MHC-II expression as part of anti-viral responses.	(Schoenborn and Wilson, 2007)
IL-12p70	Secreted by MNPs during infection to regulate of the T cell response.	(Gee *et al.*, 2009)
IL-33	Induces a type 2 immune response in $CD4^+$ T cells, eosinophils, and basophils.	(Miller, 2011)
IL-23	Proinflammatory cytokine particularly important to $CD4^+$ T_h17 cell expansion.	(Tang *et al.*, 2012)
IL-18	Produced by macrophages and induces cell-mediated type I immunity.	(Dinarello *et al.*, 2013)
CCL11	Responsible for the recruitment of eosinophils during inflammation.	(Rankin *et al.*, 2000)
CCL17	Induces a $CD4^+$ T_h2 T cell response at infection sites.	(Saeki and Tamaki, 2006)
CXCL10	Chemoattractant for MNPs and T cells; promotes adhesion to endothelial cells.	(Liu *et al.*, 2011)
CCL20	Chemoattractant for lymphocytes and neutrophils in mucosal lymphoid tissues.	(Iwata *et al.*, 2013)
CXCL9	Responsible for the recruitment of $CD8^+$ T cells, NK cells, and $CD4^+$ T_h1 cells.	(Schoenborn and Wilson, 2007)
IL-8	Responsible for the recruitment and activation of neutrophils.	(Bickel, 1993)
CCL4	Chemoattractant for lymphocytes and MNPs and induces a type 2 response.	(Maurer and von Stebut, 2004)
CXCL5	Neutrophil chemoattractant and activator.	(Mostafa and Al-Ayadhi, 2015)
CCL3	Secreted by macrophages and plays an important role in wound healing.	(Bhavsar *et al.*, 2015)
CCL5	Induces proliferation of NK ells and a chemoattractant for leukocytes.	(Appay and Rowland-Jones, 2001)
CCL2	Key chemokine for the recruitment of monocytes and lymphocytes.	(Deshmane *et al.*, 2009)

The strengths of the foreskin explant model are that it utilises healthy tissue removed from donors which is this then infected with HSV1; this allows us to control the amount of virus delivered, the time since infection, and allows definition of the initial interaction with resident immune cells. Its limitations are that it does not include the effects of inflammatory infiltrate during HSV infection. It is likely that the differences we observed between sites of infection and sites far from infection would be much more significant if an inflammatory infiltrate was able to migrate to sites of infection from blood vessels. As was done in the past, obtaining new biopsies of primary and recurrent herpes lesions would allow us to compare the findings observed in our explant model, but also capture the inflammatory infiltrate and understand the more complex immunology in true herpetic lesions. Another limitation of the explant model in its current form, is that our staining panel does not distinguish between DC2s residing in the dermis, and those that migrate from the epidermis to the dermis during HSV1 infection, as mentioned above. Follow-up studies could include an IF marker specific for HSV infected Epi-DCs, such as capase-3 for apoptosis or ICP27 indicative of productive HSV infection, or the implementation of a topically applied epidermal staining fluorescent dye for the Epi-DCs to take up and carry as they migrate, as utilised by Fernandez and Marull-Tufeu (2019). Furthermore, working with excised tissue from diverse donors introduces a wide range of variation in the cell numbers within the tissue, which could obscure trends unless an impractically large sample size is achieved. Although our cytokine studies were only performed in duplicate, they were consistent, although we will need further replicates for significance. Finally, whilst we presumed the vast majority of $CD3^{+}CD4^{-}$ cells residing in the dermis to be $CD8^{+}$ T cells, $CD3^{+}CD4^{-}$ natural killer T cells share this phenotype and with limited data on their numbers in the dermis during HSV infection, they limit our ability to draw conclusions about $CD8^{+}$ T cells densities and distribution. This uncertainty can be readily resolved by

including CD8 and CD56 as additional markers for $CD8^+$ T cells and NK/T cells respectively in future IF experiments.

Overall, we have demonstrated in our *ex vivo* HSV1 explant model that resident T lymphocytes and MNPs accumulate in the dermis underlying sites of HSV1 infection resulting in a reduced MNP-T cell cross distance, while epidermal MNPs likely migrate from the epidermis to the dermis, along with changes in the chemokine-cytokine environment; this has significant implications for the risk of HIV acquisition in individuals with prior HSV infection.

Chapter 4: Optimisation and Implementation of an HSV2 and HIV Coinfection Explant Model

4.1. Introduction

Epidemiological evidence has demonstrated that prior HSV1/2 infection increases the risk of HIV acquisition: Individuals with HSV are 3-5 fold more likely to acquire HIV and over 50% of new infections in sub-Saharan Africa occur in women infected with HSV2 (Looker *et al.*, 2017, Masese *et al.*, 2015). Genital ulcers caused by HSV2 disrupt the stratum corneum and provide HIV with easy entry to the underlying epidermis (Abu-Raddad *et al.*, 2008) while activated $CD4^+$ T cells expressing increased CCR5, can accumulate in the underlying dermis and in the epidermis at the base of herpetic lesions and remain after recovery (Zhu *et al.*, 2009, Cunningham *et al.*, 1985). Furthermore, consistent with previous findings on biopsied HSV1 lesions (Kim *et al.*, 2015), in **Chapter 3** we showed that during HSV1 infection MNPs that take up HIV, such as epidermal LCs, migrate to the dermis along with the newly discovered $CD11c^+$ epi-DC2s. The latter are more susceptible to HIV uptake and infection (Bertram *et al.*, 2019). Our findings in **Chapter 3** also suggest that inflammatory cytokines and chemokines associated with an increased risk of HIV acquisition are secreted during HSV1 infection and the average cross distance between $CD4^+$ T cells and MNPs is reduced in the dermis.

Despite this knowledge, the *ex vivo* visualisation of HSV and HIV coinfection has not yet been achieved, leaving much to elucidate on how prior HSV infection increases the risk of HIV acquisition. The host laboratory has optimised a HSV1 infection in the inner foreskin explant model, which we used in **Chapter 3** however, attempts at adapting this model for HSV-HIV coinfection have been limited. This chapter aims to adapt the principles employed by the inner foreskin infection explant model to design and optimise a coinfection explant model that will allow for the *ex vivo* visualisation of HSV2 and HIV coinfection and the accompanying immunological changes that may be responsible for increased mucosal HIV acquisition and targeting of resident CD4 T cells. We hypothesize that a newly optimised HSV2-HIV coinfection explant model could answer major questions in the field of HSV-HIV coinfection:

3. Do HIV and HSV colocalise in epidermal MNPs, either by coinfection or infection of cells within a cluster?
4. Are epidermal MNPs more likely to ferry HIV to the dermis during HSV infection?
5. Does prior HSV infection increase the likelihood of HIV virions encountering $CD4^+$ T cells in dermis?

4.2. Summary of Key Methodology

HSV2, passaged and titrated by the host laboratory **(Section 2.3.2.),** was administered intraepidermally into donated vaginal tissue specimens using silicon HD-MAPs dipped in HD-MAP Coating Solution, optimised to reduce surface tension **(Section 2.4.1.)**. Although the host laboratory previously worked with GFP expressing HSV1 viruses (Kim et al., 2015, Bertram et al., 2021, Rana et al., 2024), we used HSV2 for optimisation of the coinfection explant as HSV2 is more commonly associated with genital herpes and thus, associated with HIV acquisition (Looker *et al.*, 2017). HD-MAP treated tissue was excised from the specimen and split into 4 pieces and cultured in DCM with the submucosa in contact with gelfoam pre-soaked with DCM. At 24 hpi the tissue was fixed with 4% PFA and frozen in OCT for sectioning and assessment of the degree of infection **(Section 2.4.1)**.

To optimise HIV infection, vaginal or foreskin explants were treated with HD-MAPs that were coated with mock coating solution (mock HD-MAP) and at 18 hours after application of a mock HD-MAP (hours post patch or hpp), either a second mock HD-MAP was applied or HIV_{Bal} **(Section 2.3.1)** was applied by a paintbrush or a cloning cylinder at a TCID50 of 7 000 or 70 000 **(Section 2.4.2)**. These methods and the TCID50 were selected based on previous explant models using various type I and II anogenital mucosa to investigate the early events of HIV uptake and infection performed by the host laboratory (Baharlou *et al.*, 2022). At 12, 24, 36, and 48 hpi with HIV the tissue was fixed with 4% PFA and frozen in OCT for sectioning and assessment of infection **(Section 2.4.3)**. These steps allowed us to select the optimal

TCID50, HIV infection method, and time point post HIV exposure that resulted in optimal infection. To visualise virus in infected explants, we used RNAscope with either a probe for HSV2 DNA or HIV_{Bal} RNA **(Section 2.6)**. All manual counting was performed following the methodology employed in **Chapter 3** and is as described in **Section 2.7.1.** The key methodology employed within **Chapter 4** is summarised in **Figure 4.1.**

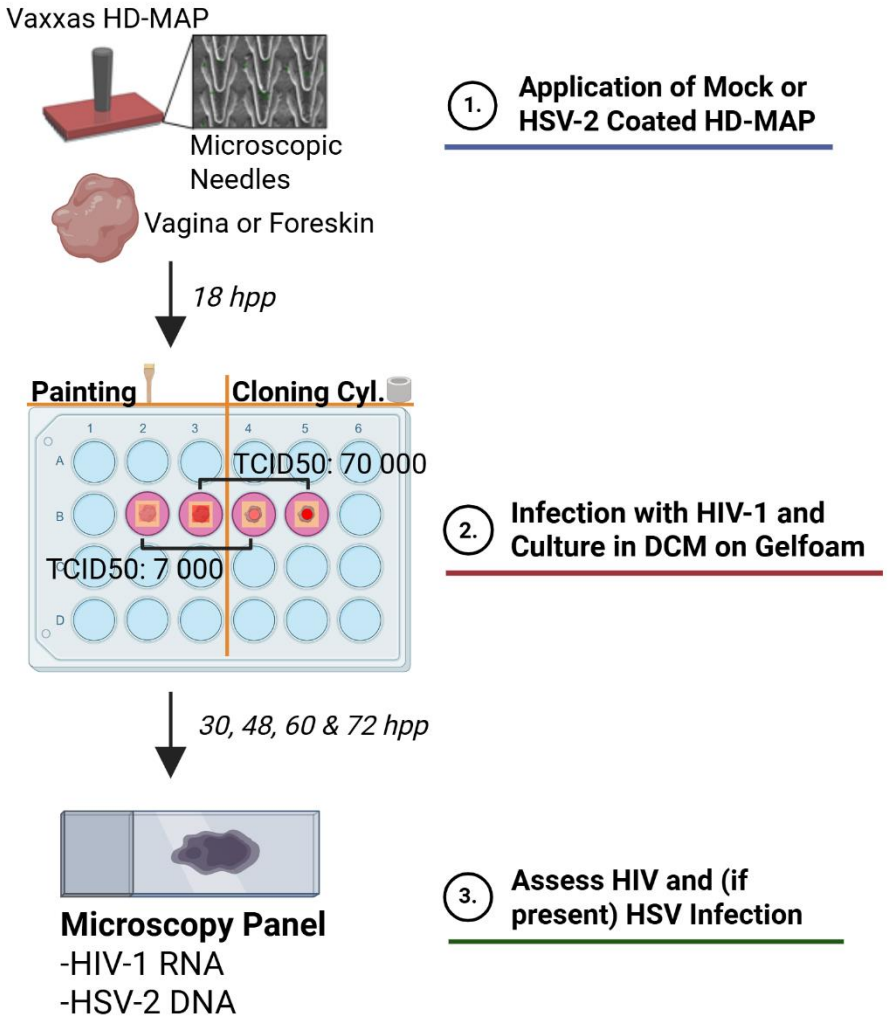

Figure 4.1. Optimisation of HSV2-HIV coinfection explant model. Tissue was infected with HSV2 intraepidermally using the HD-MAPs that were used in **Chapter 3** to penetrate the partly keratinised outer layer of the vaginal or foreskin mucosa. 18 hours after application of the HD-MAP various methods were trialled to administer HIV at different TCID50s such as: the application of a second HD-MAP, viral painting, or applying HIV within a cloning cylinder attached to the epidermis. Once a method of infection and TCID50 were selected, various time points post HIV infection were examined to determine the best time balance between detectable virus and tissue integrity, and finally HSV2-HIV coinfections were trialled.

4.2.1. Selection of Tissue Donors

Due to the increased availability of vaginal tissue via new collaborations with gynaecological surgeons, optimisation of the HSV2-HIV coinfection explant largely took place using vaginal tissue as well as inner foreskin tissue. Interchangement of inner foreskin and vaginal tissue in this chapter depended on what tissue was available, meaning to progress our model of coinfection we accepted both foreskin and vaginal tissue as they are both relevant human anatomical sites of infection in male and female respectively. In women, one of the most common site for genital herpes to present is the vagina, which has a type II mucosal structure and T cell population best-resembling foreskin tissue (Malkin, 2004, Duluc *et al.*, 2013). Discarded healthy vaginal and foreskin tissue was received from surgeons based in the WSLHD within 30 minutes of tissue removal from the body and were transferred to the laboratory on ice for immediate use. Tissue was inspected macroscopically for signs of disease or inflammation by members of the host laboratory and the surgical team following the screening criteria described in **Chapter 3.** The clinical details of donors are described in **Table 4.1.**

Table 4.1. Summary of donors used for the optimisation of a coinfection explant model

Donor	Tissue Type	Reason for Removal	Inflammatory Status	Age	Use
1	Vagina	Vaginoplasty	Healthy	56	Section 4.3. Section 4.4.
2	Vagina	Vaginal prolapse	Healthy	80	Section 4.5.
3	Vagina	Vaginal prolapse	Healthy	53	Section 4.6.1.
4	Vagina	Vaginoplasty	Healthy	Not disclosed	Section 4.6.2.
5	Inner Foreskin	Phimosis	Minimally Inflamed	43	Section 4.7.2.
6	Inner Foreskin	Phimosis	Minimally Inflamed	25	Section 4.8.

4.3. Assessment of HSV2 Infection in Vaginal Tissue

To assess whether vaginal explants could be infected with HSV2 infection they were exposed to 10^8 PFU/mL of HSV2 for 24 hours and visualised using RNAscope to qualitatively compare them to the inner foreskin HSV1 infection explant model **(Section 3.3; Figure 3.2.)**. Mock infected vaginal tissue explants stained for HSV2 were devoid of any background signal **(Figure 4.2a)**, facilitating easy identification of viral signals in HSV2 infected vagina **(Figure 4.2b)**. Detecting HSV1 was more difficult in the inner foreskin infection explant model due to the higher level of autofluorescence **(Section 3.3.)**. While staining of HSV1 by RNAscope produced large indistinct regions of HSV1 DNA **(Section 3.3.)**, staining for HSV2 within vaginal tissue produced more frequent discrete points of staining at sites of infection **(Figure 4.2b)**. In summary, we successfully demonstrated that similar to the inner foreskin, vaginal tissue can be infected with HSV by intraepidermal injection with HD-MAPs to create foci of HSV2 infection. Furthermore, RNAscope HSV2 DNA probes can be used to visualise HSV in the infected tissue in a highly specific manner.

a

No Virus HD-MAP Treatment

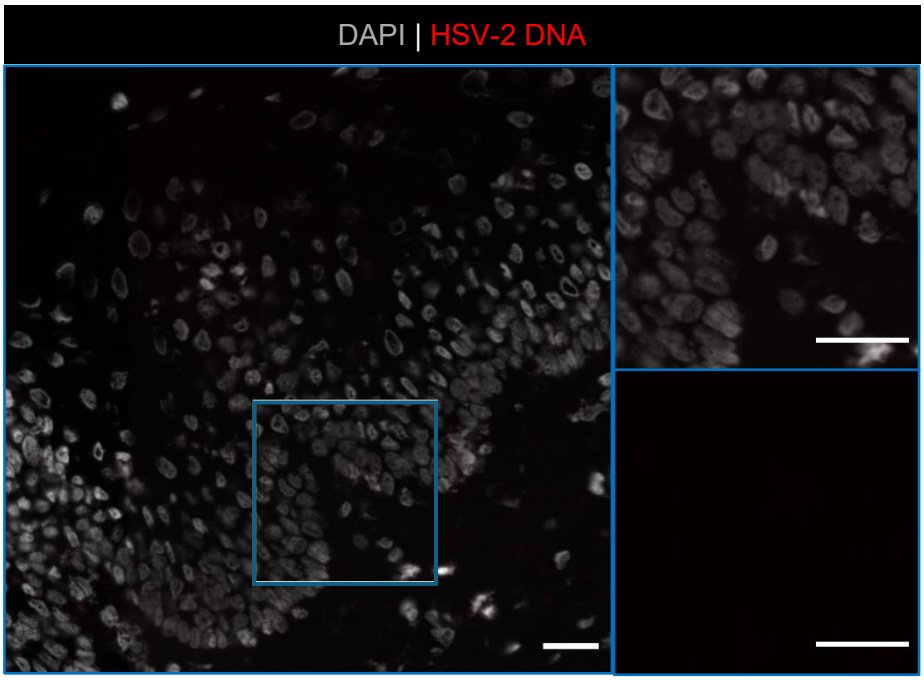

b

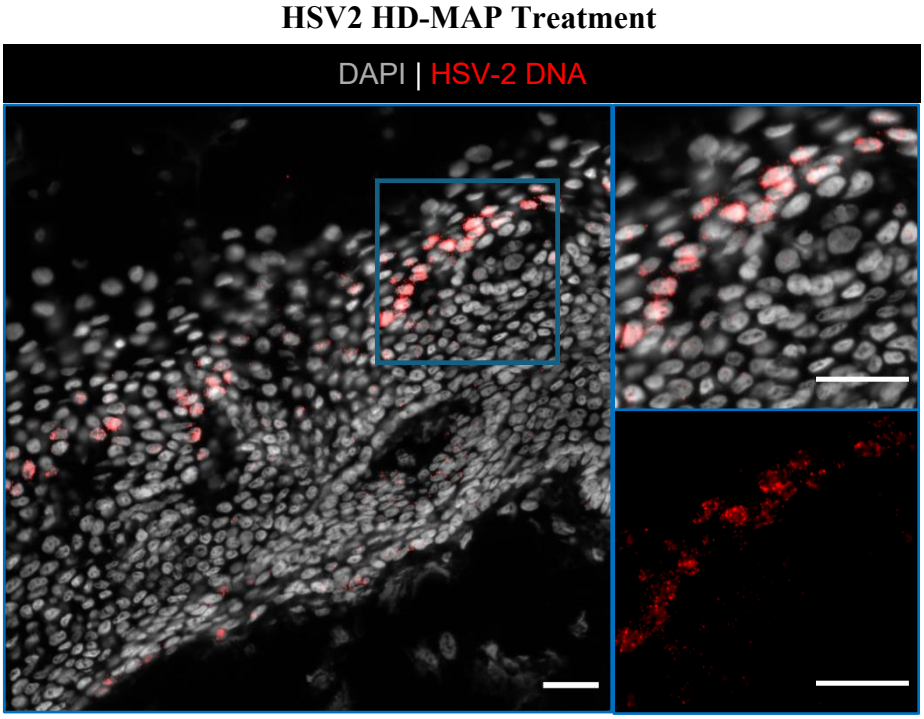

Figure 4.2. Visualisation of HSV2 infection in vaginal tissue explants. Vaginal tissue was treated with HD-MAPs coated with either **(a)** a mock coating solution or **(b)** HSV2 containing coating solution, then placed in DC culture medium on gelfoam. 24 hpi specimens were fixed in 4% PFA, frozen in OCT and sectioned. Sections were treated with BLOXALL to inhibit endogenous enzymes, followed by application of Protease Plus diluted with TBS (1:5). HSV2 infection was visualised using the RNAscope 2.5 HD RED assay with an HSV2 UL29 DNA probe. Following this, sections were stained with DAPI, subjected to the TrueView Autofluorescence Quenching Kit, and cover-slipped with SlowFade Diamond Antifade Mountant for imaging at 20x. **(a-b)** Scale bars = 30 µm.

4.4. Changes in Cell Distributions in HSV2 Infected Vaginal Tissue

As we were now using HSV2 rather than HSV1 to infect tissue, we next attempted to confirm that some key observations we made in **Chapter 3** using the HSV1 infected inner foreskin were similar in HSV2 infected vaginal tissue. Therefore, human vaginal tissue was treated with HSV2 HD-MAPs, then dermal $CD3^{+}CD4^{+}$ T cells and $CD3^{+}CD4^{-}$ T cells at sites of HSV2 infection and sites far from infection were stained and their densities and distributions quantified as in **Chapter 3.** Within the HSV2 infected inner foreskin explant, the density of

dermal lymphocytes was increased at sites of HSV2 infection relative to sites far from infection ($CD4^+$ T cells: 178.83 to 231.6; $CD3^+CD4^-$ T cells: 134.13 to 180.2; **Figure 4.3b**). These densities fell within the range of the densities we observed in HSV1 infected explants performed in **Chapter 3** (**Table 4.2**).

In the dermis, the average distance of $CD4^+$ and $CD3^+CD4^-$ T cells from the basement membrane at sites far from infection and sites of HSV2 infection was similar for both $CD4^+$ (61.1 and 53.4) and $CD3^+CD4^-$ (54.3 and 46.5) T cells **(Figure 4.3c)**. Similar to the densities, our observed cell distances also fell within the range of the average cell distances from the basement membrane for both $CD4^+$ and $CD3^+CD4^-$ T cells obtained from the HSV1 infected foreskin explants performed in **Chapter 3** (**Table 4.2**). Overall, these preliminary findings suggest that infecting vaginal tissue with HSV2 induces a change in lymphocyte density similar to what we observed in HSV1 infected foreskin.

a

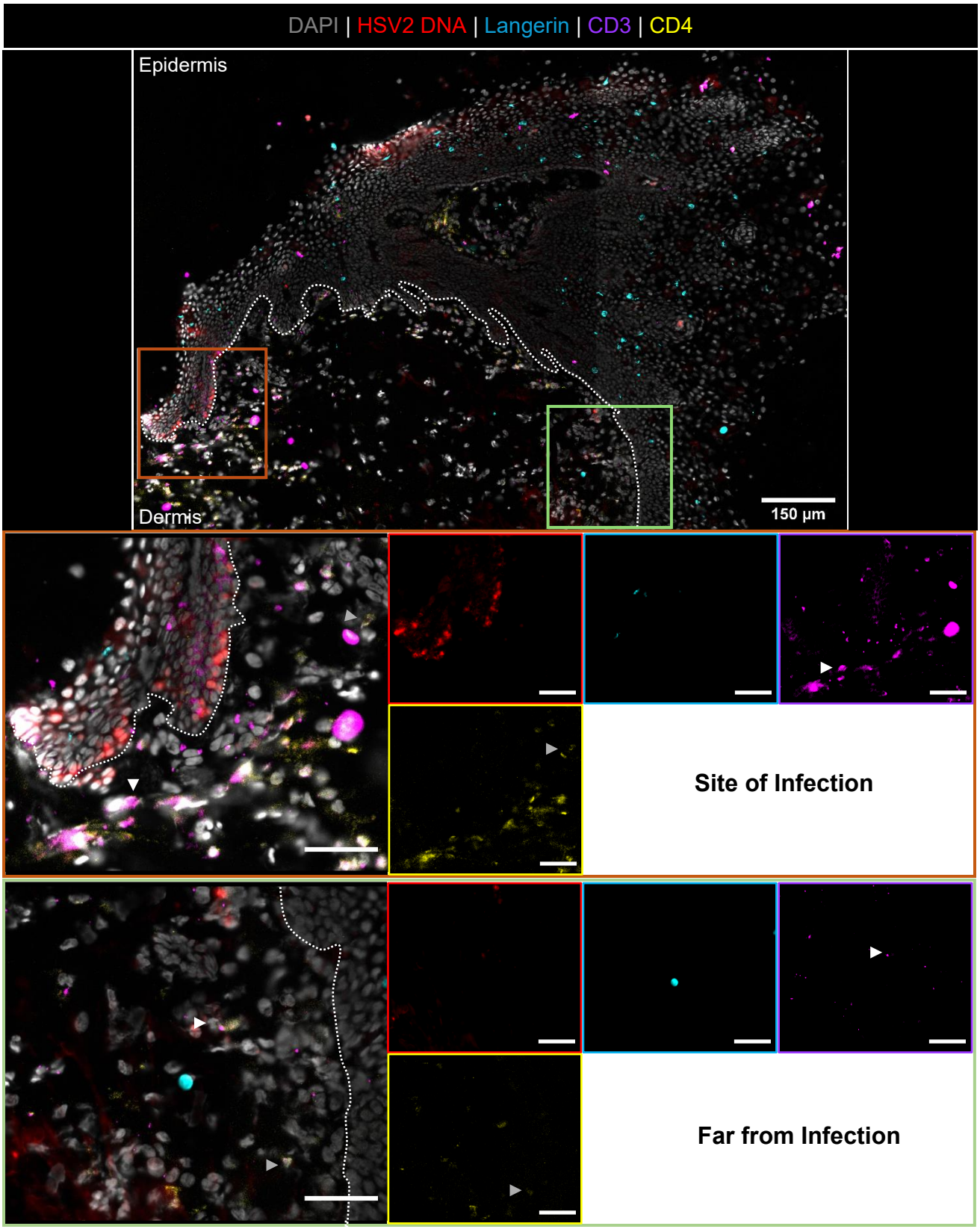
DAPI | HSV2 DNA | Langerin | CD3 | CD4
Epidermis
Dermis
150 µm
Site of Infection
Far from Infection

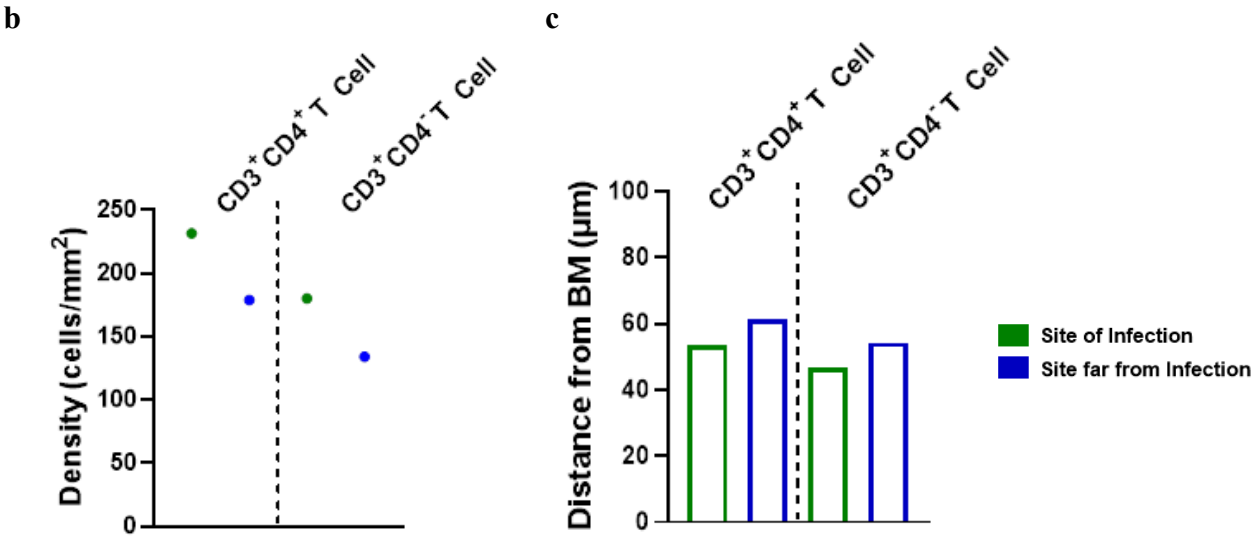

Figure 4.3. Density and distribution of lymphocytes in the epidermis and dermis. a) Vaginal tissue was infected with HSV2 by HD-MAP and cultured in DCM for 24 hours then frozen in OCT and sectioned. RNAscope to detect HSV2 and immunofluorescent microscopy to detect CD3, CD4 and Langerin was performed. Scale bars = 50 µm unless otherwise specified. White arrows = $CD3^+$ cells, grey arrows = $CD4^+$ cells (n=1). **b & c)** $CD3^+CD4^+$ T and $CD3^+CD4^-$ cells, were manually counted using ImageJ at sites of HSV2 infection and sites far from infection. **(a)** The density and **(b)** the average distance of cells from the basement membrane of the manually counted cells were determined.

Table 4.2. Range of Densities and average cell distances from the basement membrane reported in Chapter 3

Metric	Sample	Cell Type	Minimum	Maximum	Figure
Density (cells/mm²)	Site of Infection	$CD3^-CD4^+$	109.46	237.51	**Figure 3.10a**
	Site far from infection		76.85	26.16	
	Site of Infection	$CD3^-CD4^-$	71.72	296.48	**Figure 3.11a**
	Site far from infection		28.03	86.79	
Distance (µm)	Site of Infection	$CD3^-CD4^+$	41.3	66.3	**Figure 3.10c**
	Site far from infection		42.3	72.3	
	Site of Infection	$CD3^-CD4^-$	35.8	63.9	**Figure 3.11c**
	Site far from infection		31.2	65.6	

4.5. Application of Two HD-MAPs to the Same Explant

Due to the successful application of HSV in the inner foreskin explant model using HD-MAPs, we initially decided that application of a second HD-MAP would be the best way to infect a vaginal tissue explant with HIV. However, as the effects of applying two silicon HD-MAPs on the same piece of tissue had not been characterised, we first took vaginal tissue explant and applied either no HD-MAPs, one HD-MAP, or one HD-MAP followed by a second HD-MAP 24 hpp **(Figure 4.4)**. Vaginal tissue that was treated with one HD-MAPs was structurally intact, with no tearing with the epidermis or lifting of the epidermis from the dermis (**Figure 4.4**). Furthermore, autofluorescence, was frequent throughout tissue treated with one HD-MAP as vertical lines starting at the stratum corneum through approximately 25-75% of the epidermis. These autofluorescent lines are the result of needle punctures from the HD-MAP after it penetrates the tougher partly keratinised superficial layer.

Vaginal tissue treated with two HD-MAPs had signs of significant structural damage (**Figure 4.4)**. Much of the epidermis had been torn away from the dermis leading to autofluorescence of the basement membrane. The remaining cells of the epidermis were loosely distributed above the basement membrane and were also often associated with significant autofluorescence. Overall, these findings suggest that while application of one HD-MAP does not significantly disrupt the structure of the tissue, application of a second HD-MAP 24 hours after the initial HD-MAP resulted in significant damage to the epidermis rendering it unusable. Thus, the design of a vaginal tissue coinfection explant model cannot involve infection with HIV that is facilitated by the application of a second silicon HD-MAP.

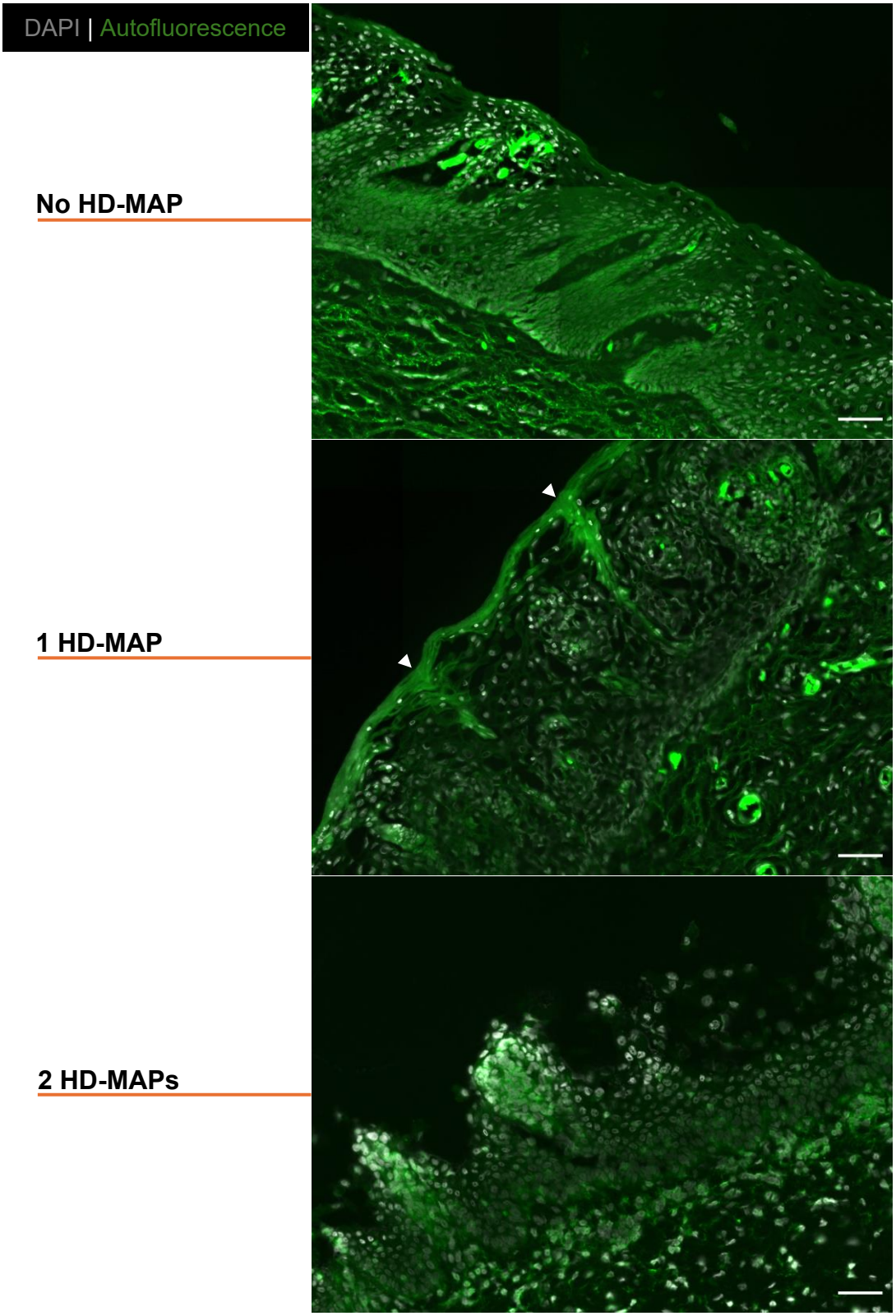

Figure 4.4. The structural integrity of tissue following HD-MAP application. Segments taken from a vaginal specimen were either treated with one silicon HD-MAP that did not contain virus or left untreated **(No HD-MAP)** and were placed on gelfoam in DCM. 24 hours after initiation of the explant model, tissue treated with HD-MAPs either had a second HD-MAP **(Two HD-MAPs)** applied or were left untreated **(One HD-MAP)**. Tissue was fixed in

4% PFA for 24 h, frozen in OCT, and sectioned for visualisation of the structural integrity of the tissue. Sections were stained with DAPI before being cover-slipped with Slow Fade Diamond Antifade Mountant for imaging. To identify the structural integrity of the tissue, autofluorescence was visualised using an empty channel (FITC) as well as DAPI. Arrows indicate puncture marks and scale bars = 50 μm.

4.6. Optimisation of HIV Infection of Vaginal Tissue

We next optimised HIV infection of vaginal tissue to: 1) determine the virus concentration that should be added to the tissue; 2) the route to intraepidermally deliver HIV as the application of a second virus coated HD-MAP was not feasible, and 3) the time of HIV exposure that will provide the highest level of infection without tissue degradation.

4.6.1. Titration and Selection of a Route of Delivery for HIV

To identify the optimal concentration of HIV and a route of delivery that will induce high level of HIV infection, vaginal tissue was treated with one HD-MAP and left in culture for 18 hours (to simulate infection with HSV), then infected with HIV using either a cloning cylinder or a paintbrush at TCID50s of 7 000 and 70 000. At 2 hpi, the tissue was prepared for sectioning and stained for HIV RNA using RNAscope. In both vaginal tissue explants infected by either cloning cylinder or paint brush, HIV RNA was detected **(Figure 4.5a-b).** The explants infected by cloning cylinder showed HIV RNA within the epidermis of the tissue, at a depth consistent with virus uptake after 2 hours **(Figure 4.5a).** In contrast, HIV within explants infected by paintbrush was evenly distributed superficially on vaginal epidermis without penetrating into the epidermis **(Figure 4.5b).** Similar to HSV2 infection of vaginal explants **(Figure 4.2b)** and HSV1 infection of inner foreskin explants **(Figure 3.2a),** vaginal explants infected with HIV by cloning cylinder had areas of tissue containing significant amounts of HIV RNA interspaced by regions of minimal to no virus **(Figure 4.5a)**. This contrasts with the inability of painted virus to penetrate the epidermis **(Figure 4.5b)**.

Vaginal explants infected with a TCID50 of 7 000 contained much less HIV RNA in the epidermis compared to the explants infected with a TCID50 of 70 000 **(Figure 4.5a-b)**. Within explants infected with a TCID50 of 7 000, the presence of HIV RNA was limited throughout the tissue to the extent that it would be difficult to identify it in a coinfection explant. Contrasting this, explants infected at a TCID50 of 70 000 had distinct foci of HIV RNA. Interestingly, the amount of virus present seemed to also be affected by the method of infection: Explants infected at either TCID50 by cloning cylinder contained much more virus than the explants infected by paint brush at identical TCID50s. In summary, this data demonstrates that the best route to infect vaginal tissue explants with HIV is through the utilisation of cloning cylinders as it leads to better HIV uptake into the epidermis. Furthermore, a TCID50 of 70 000 should be used as it produces distinct foci of HIV infection which can be compared with and without HSV coinfection. Finally, regardless of concentration and route, virus that made it into the tissue was largely present as extracellular aggregate particles, consistent with virus uptake without infection.

a

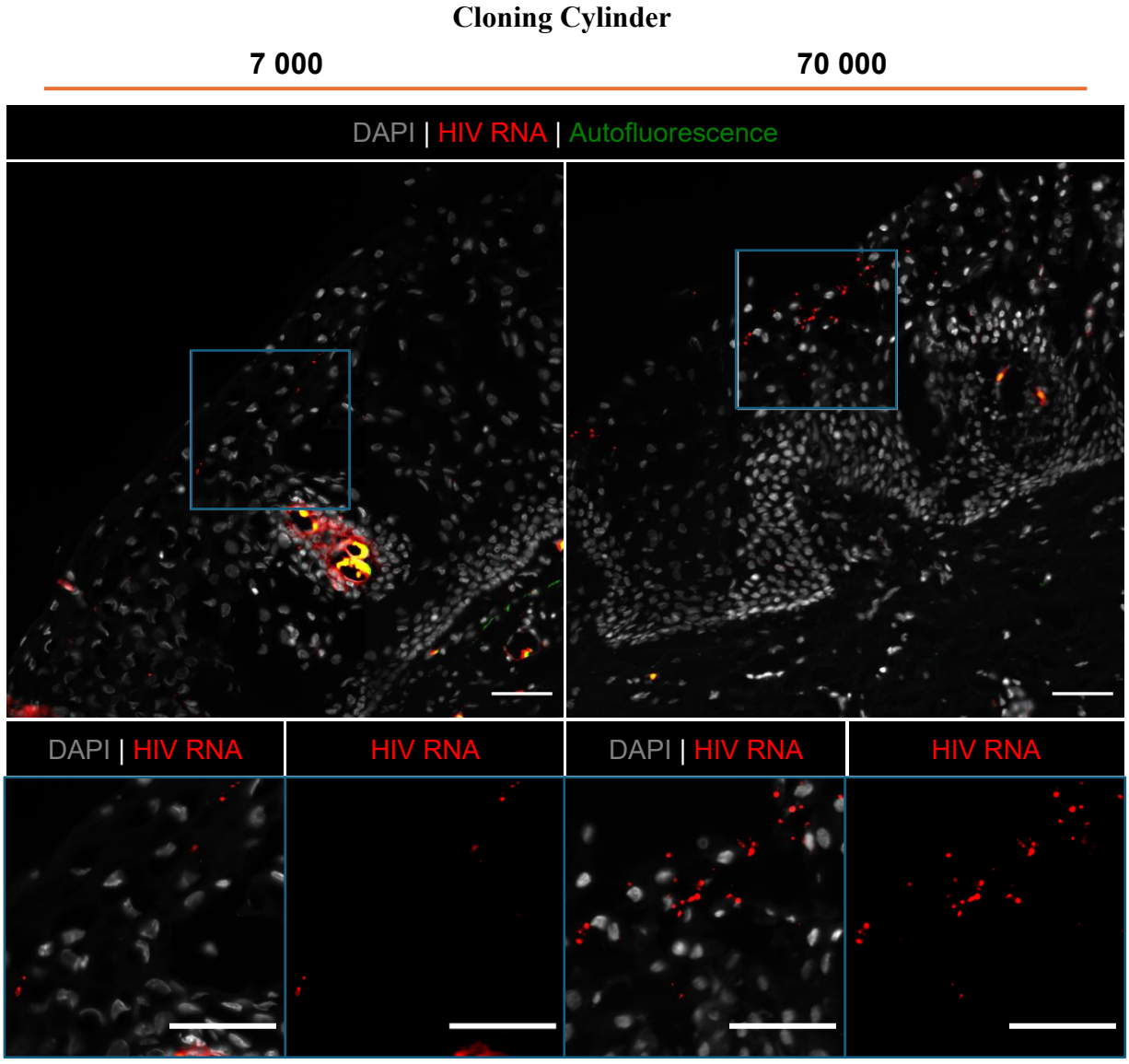
Cloning Cylinder
7 000
70 000
DAPI | HIV RNA | Autofluorescence
DAPI | HIV RNA
HIV RNA
DAPI | HIV RNA
HIV RNA

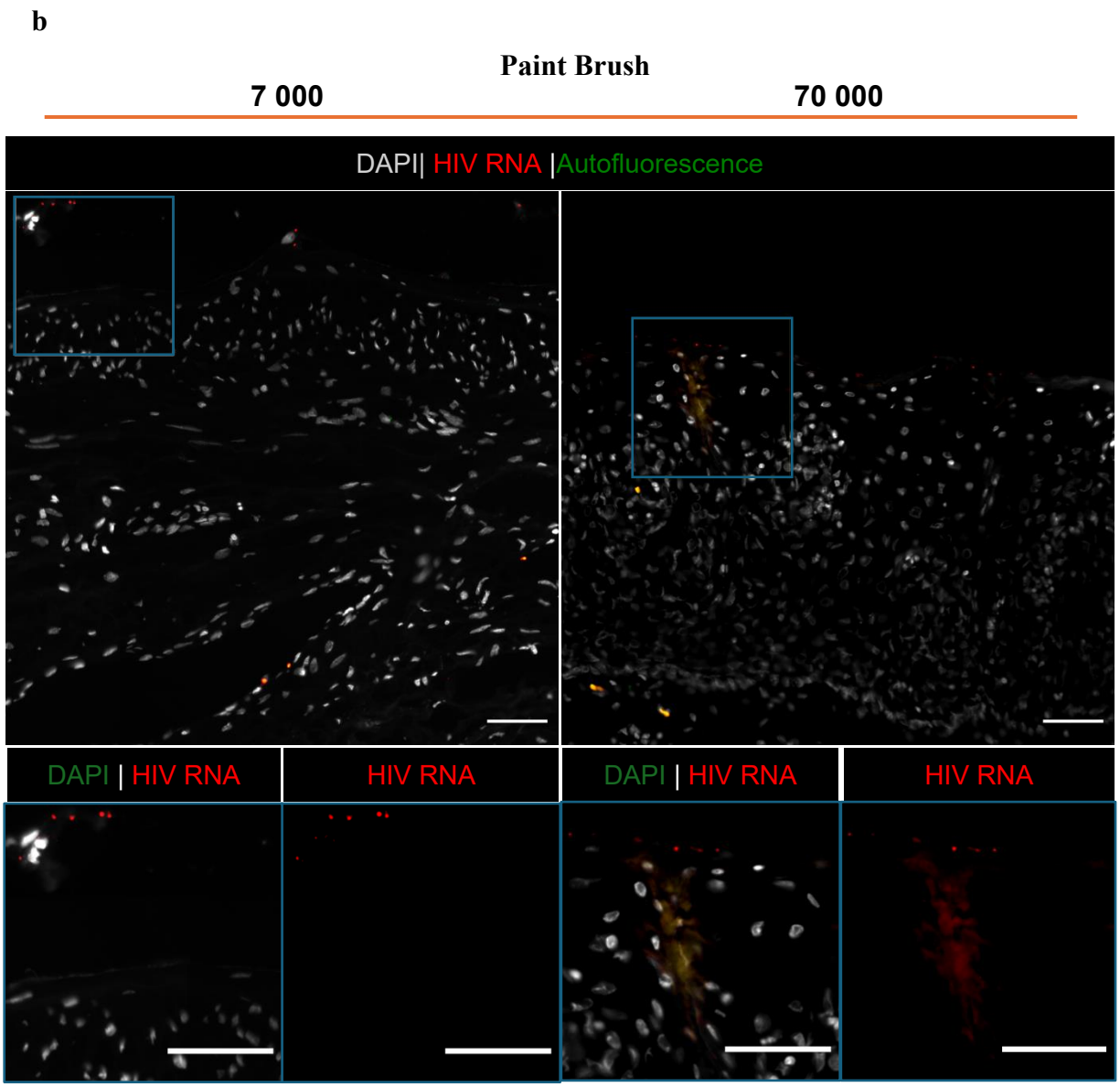

Figure 4.5. Optimisation of method of infection and TCID50. A vaginal explant was treated with HD-MAPs without virus and segmented. The HD-MAP treated tissue segments were placed in DCM on gelfoam and 18 hpp HIV_{BaL} was topically administered at a TCID50 of 7 000 and 70 000 by either **(a)** cloning cylinders adhered to the epidermis or **(b)** use of a paint brush soaked in virus. At 2 hpi tissue was fixed in 4% PFA for 24 hours, frozen in OCT, and sectioned for visualisation of infection by RNAscope consisting of: blocking of endogenous enzymes using BLOXALL; application of Protease Plus (1:5) to all sections; use of the RNAscope 2.5 HD assay with an $HIV1_{BaL}$ RNA probe, DAPI staining and cover-slipping with Slow Fade Diamond Antifade Mountant for imaging. To differentiate between autofluorescence and true staining, slides were also imaged with an unstained channel (FITC). **(a-b)** Scale bars = 50 µm.

4.6.2. Defining the Optimal Time Post HIV Treatment to Visualise Infection

We next performed a time course to visualise HIV infection as it was unknown what time point would result in the best HIV infection, and for how long after application of a HD-MAP and subsequent HIV infection the tissue would maintain its integrity in culture before degrading. Vaginal tissue was mock HD-MAP treated to simulate the microtrauma induced during HSV2 infection and at 18 hpp infected with HIV at a TCID50 of 70 000 using a cloning cylinder. Samples were cultured for 12, 24, 36 or 48 hpi with total culture times of 30, 42, 56 and 66 hours, respectively. HIV infection was then visualised by RNAscope **(Figure 4.6)**.

Twelve hours after HIV exposure, RNAscope revealed that most of the epidermis contained HIV RNA, with the highest density being approximately halfway between the epidermis and basement membrane. At 24 hpi, HIV RNA was closer to the basement membrane than it was at 12 hpi and appeared slightly more widespread. In contrast to the extracellular viral staining particles seen at 2 hpi in the HIV viral uptake experiment performed in **Section 4.6.1,** viral staining in **Figure 4.6** was far more discrete and largely co-localised to cell nuclei. At both 12 and 24 hpi, the epidermis and dermis of the vaginal tissue explants were not degraded and were structurally intact. At 36 hpi, HIV RNA was still mostly found in the epidermis and infrequently in the dermis, typically closely co-localising with cells. At this time point, the epidermis was generally thinner than earlier time points. At 48 hpi, the epidermis was almost completely absent, however compared to 12, 24 and 36 hpi larger quantities of HIV RNA could be seen localising to the basement membrane. At this time point, HIV RNA could also be seen in the dermis deeper than at 36 hpi. This data has demonstrated that while the structural integrity of the dermis remains unchanged overtime, by 36 hpi the epidermis appeared partially missing, and was completely degraded by 48 hpi. Finally, HIV infection was clearly visible at all investigated time points, with the best time balance between tissue integrity and infection being 24 hpi (total culture time of 42 hours).

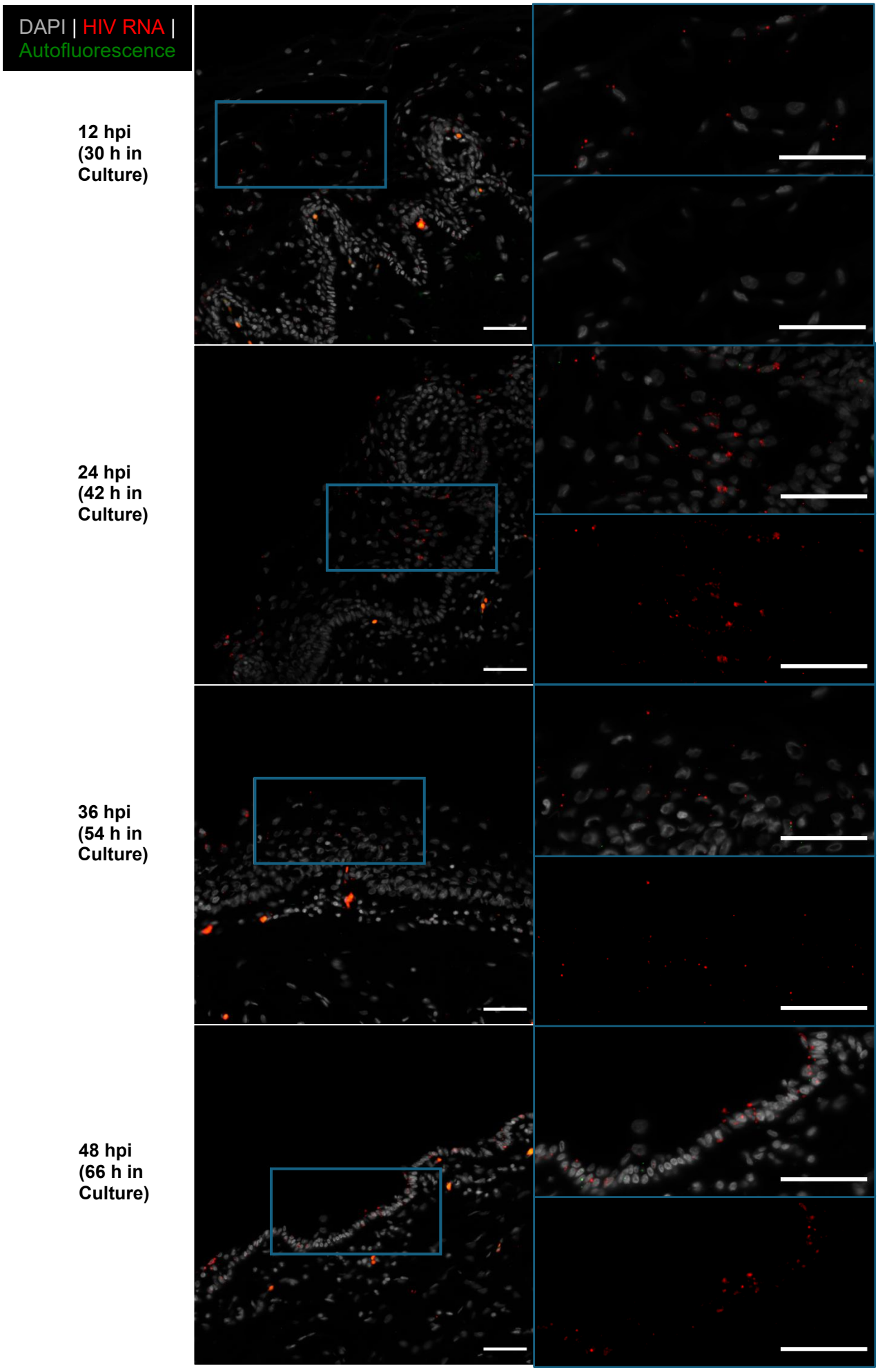
DAPI | HIV RNA | Autofluorescence
12 hpi (30 h in Culture)
24 hpi (42 h in Culture)
36 hpi (54 h in Culture)
48 hpi (66 h in Culture)

Figure 4.6. Selection of the best time point after HIV infection. Human vaginal mucosal explants were treated with a HD-MAP coated in mock coating solution and left in culture with DCM for 18 hours. HIV_{Bal} at a TCID50 of 70 000 was administered by a cloning cylinder glued to the epidermis and left in culture for either a further 12 (a), 24 (b), 36 (c), or 48 (d) hpi. Following this, cloning cylinders were removed, and the explants were fixed with 4% PFA for 24 hours. RNAscope was used to detect HIV RNA consisting of: blocking of endogenous enzymes using BLOXALL; application of Protease Plus (1:5); use of the RNAscope 2.5HD assay with $HIV1_{BaL}$ RNA probes, DAPI staining and cover-slipping with Slow Fade Diamond Antifade Mountant for imaging. To differentiate between autofluorescence and true staining, slides were also imaged with an unstained channel (FITC). Scale bars = 50 μm.

4.7. Updates to the Cyclic Immunofluorescent Microscopy Panel and the HD-MAP for the Coinfection Explant

To progress to co-infected explants containing HIV rather than HSV alone, it became necessary to shift embedding our samples from the fixed-frozen (PFA-OCT) approach to formaldehyde fixed paraffin-embedded (FFPE). FFPE tissue is more compatible with other techniques used in the host laboratory such as Imaging Mass Cytometry (IMC) and spatial transcriptomics, which we plan to use in our HSV and HIV coinfection studies in future experiments. This shift in experimental design required re-optimisation of several antibodies in the cyclic IF microscopy panel. Furthermore, due to recent manufacturing changes in the material (silicon to polymer) and needle density of HD-MAPs, we needed to compare the punctures generated by the silicon and polymer HD-MAPs in explant tissues to understand the impact the change in material might have on experimental outcomes.

4.7.1. Optimisation of a New Immunofluorescent Microscopy Panel

Antibodies validated by their manufacturers to be compatible with the FFPE tissue preservation were titrated to identify optimal concentrations for staining. The optimisation of the new cyclic IF microscopy panel was performed by Honours student Xinyi Ding as a component of her 2023 honours thesis and is summarised below:

A new commercially conjugated rabbit anti-CD11c-AF647 antibody and an in-house conjugated rabbit anti-CD3-Cy3 antibody were tested at 1:20, 1:50 and 1:100 dilutions. Acquired images revealed 1:20 as the optimal dilution for both conjugated antibodies in foreskin tissue **(Figure 4.7)**. A primary rabbit anti-CD4 antibody was tested at 1:50 and 1:100 dilutions with a donkey anti-rabbit Dylight755 secondary at 1:200 and 1:400 dilutions. The 1:50 for the primary and 1:200 for the secondary were selected as the optimal dilutions **(Figure 4.7).** The primary goat anti-Langerin and secondary donkey anti-goat-Dylight755 antibodies were used at 1:50 and 1:200 dilutions respectively. A summary of the cyclic IF panel employed in all future experiments is shown in **Table 4.3.**

Table 4.3. Summary of re-optimised cyclic IF panel for FFPE explant infections

	Round 1		Round 2	
Channel	**Stain**	**Dilution**	**Stain**	**Dilution**
DAPI	DAPI	1:1000	DAPI	1:1000
FITC	-	-	HIV RNA RNAscope Tyramide FITC	-
TRITC	Rabbit anti-CD3-Cy3	1:20	HSV2 DNA RNAscope Fast Red	-
Cy5	Rabbit anti-CD11c-AF647	1:20	-	-
Cy7	Rabbit anti-CD4 (primary) Donkey anti-rabbit-Dylight755 (secondary)	1:50 1:200	Goat anti-Langerin (primary) Donkey anti-goat Dylight755 (secondary)	1:50 1:200

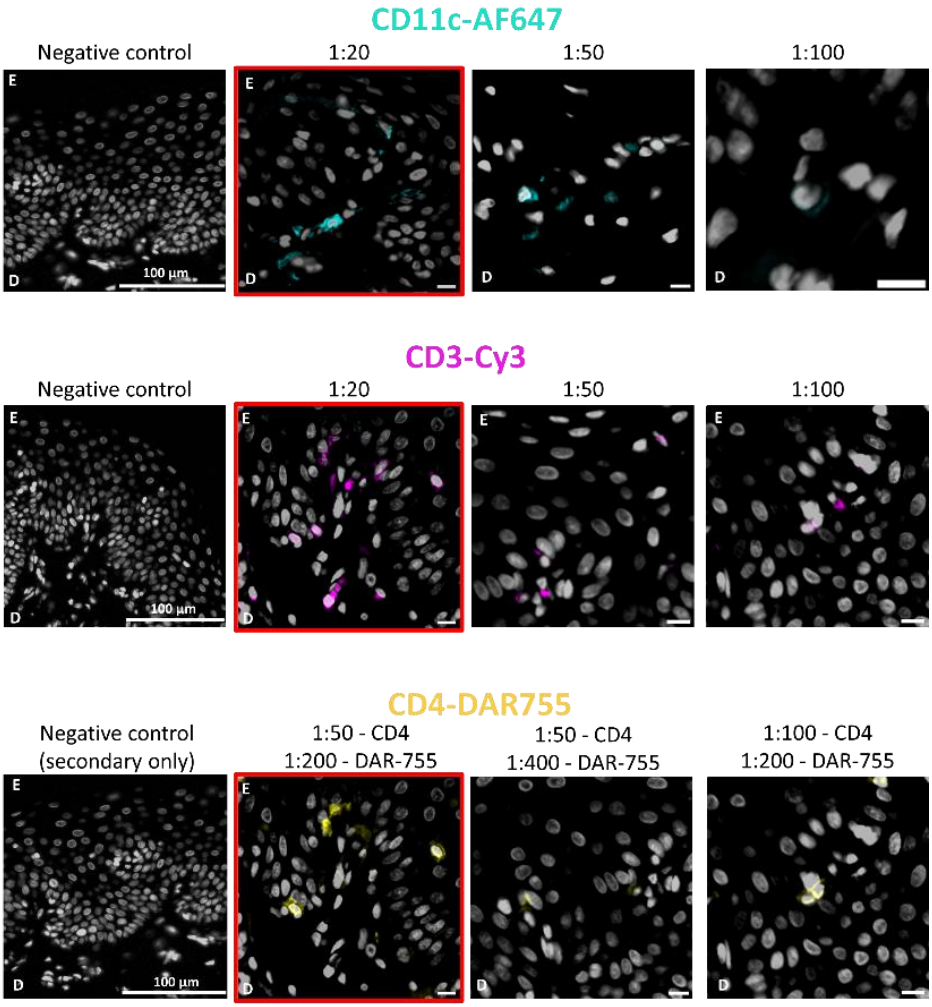

Figure 4.7. Titration of antibodies for FFPE preserved foreskin tissue. Inner foreskin specimens that did not receive a HD-MAP treatment were fixed using 4% PFA and paraffin embedded. Following sectioning, antigen retrieval, and blocking with blocking buffer; the primary antibodies anti-CD11c AF647, anti-CD3 Cy3, and rabbit anti-CD4 were added at dilutions of 1:20 (not used for anti-CD4), 1:50, or 1:100; the secondary antibody donkey anti-rabbit Dylight755 was added at dilutions of 1:200 and 1:400; and finally DAPI staining and cover-slipping with Slow Fade Diamond Antifade Mountant for imaging. The dilutions determined to have the best cellular staining are indicated with red boxes. Scale bars = 10 µm unless otherwise indicated, D = dermis and E = epidermis. Figure generated by Xinyi Ding as part of her Honours thesis (2023).

4.7.2. Polymer HD-MAP Punctures Were More Frequent and Deeper Than Silicon

We have previously used silicon HD-MAPs with a density of 10 000 microneedles per 1 cm^2 and average needle length of 250 ± 20 µm for the HSV1 explant model in **Chapter 3** and for the optimisations of the HSV2-HIV coinfection explant in **Chapter 4** prior to **Section 4.7**. However, Vaxxas discontinued manufacturing silicon HD-MAPs and required us to use their polymer HD-MAP which have a density of 5 000 microneedles per 1 cm^2 and average needle length of 250 ± 50 µm. Due to this, we compared the number and depth of punctures introduced by the new polymer HD-MAPs to the old silicon HD-MAPs by treating regions of a single foreskin donor with either a polymer or silicon HD-MAP and visualising sections from each region with a H&E stain **(Figure 4.8a)**. After excluding sections without any punctures, we determined the average: 1) number of punctures per section, 2) length of punctures per section, and 3) the number of punctures penetrating 30% of the epidermal thickness, as reaching 30% of the epidermal thickness is required to reliably establish infection (Rana *et al.*, 2024).

The average number of punctures per section in inner foreskin where the polymer HD-MAPs was applied (7.2 ± 1.32) was significantly higher ($p=0.042$) than the region where the silicon HD-MAPs was applied (4.25 ± 0.58; **Figure 4.8b**). Critically, the number of these punctures reaching deep in the epidermis (30% of the epidermal thickness) using the HD-MAPs (4.8 ± 1.11) was also significantly higher ($p=0.0002$) than the number of punctures obtained using the silicon HD-MAPs (0.25 ± 0.13; **Figure 4.8c**). Consistent with this, the average length of punctures generated by the polymer HD-MAPs (206.21 ± 12.09 µm) was also significantly higher ($p < 0.0001$) than the punctures generated by the silicon HD-MAPs (90.62 ± 6.21 µm: **Figure 4.8d**). No punctures were seen reaching the dermis from either polymer or silicon HD-MAP. In summary, the polymer HD-MAP more consistently penetrated the epidermis of anogenital tissue than the silicon HD-MAP, and more frequently reached the depth required

for a high probability of a successful (established) viral infection, likely increasing the reliability of the explant model.

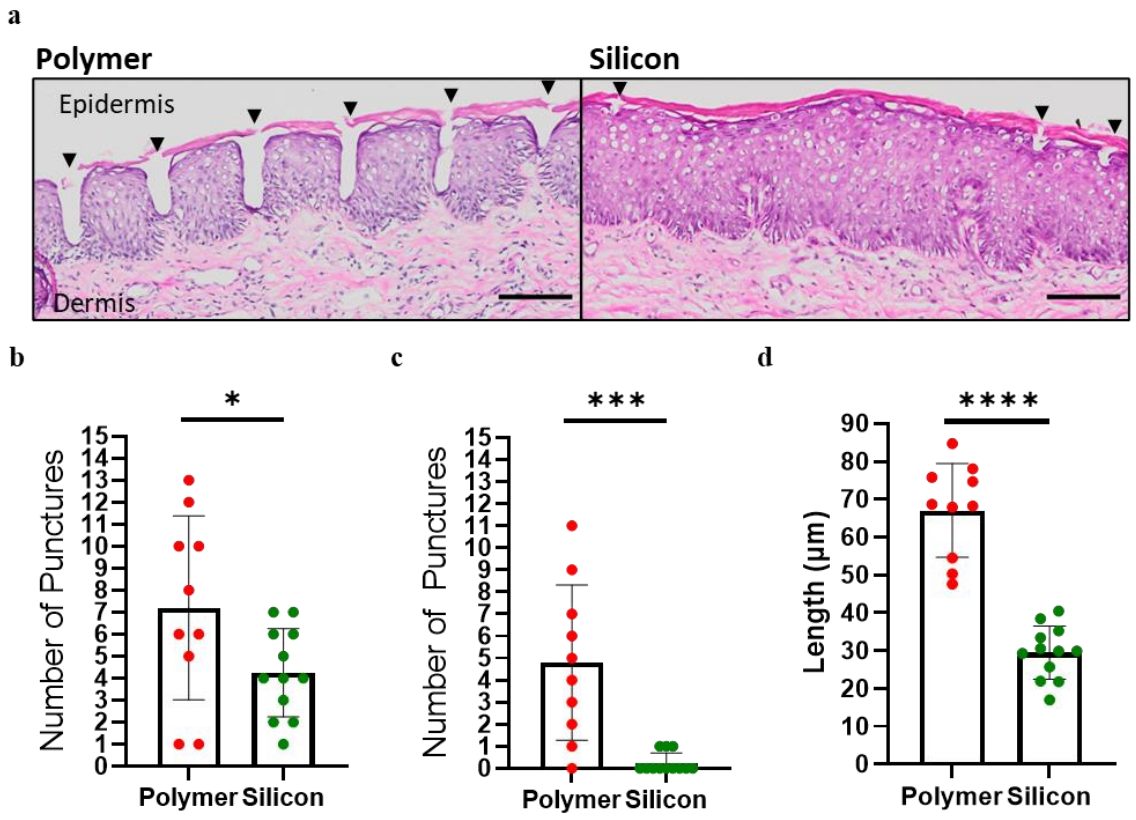

Figure 4.8. Comparison of the frequency and depth of punctures generated by different HD-MAP materials. Inner foreskin tissue was treated with either a polymer or silicon HD-MAP. **(a)** Following cryopreservation in OCT, punctures in sections taken from each treatment were visualised using a H&E stain, and the frequency and average length of punctures per section was measured. Scale bars = 100 µm. **(b-d)** Graphs show **(b)** The number of punctures per section, **(c)** The number of punctures per section that exceed 30% of the epidermal thickness, and **(d)** The average depth of the punctures that were identified in each section. Each data point represents a different tissue section, and the column graph represents the mean ± standard deviation. Statistical significance was determined by unpaired Student's T-Test (n = 10/12, *p<0.05, ***p<0.001, ****p<0.0001).

4.8. Trialling the HSV2 and HIV Coinfection Foreskin Explant Model

After performing various experiments to determine the optimal conditions to achieve a HSV-HIV coinfection, we attempted to demonstrate coinfection of HSV2 and HIV in foreskin tissue. We opted to swap from a 24 hour HIV infection to a 6 hour as we expected a preestablished HSV infection would create a viral relay (Kim *et al.*, 2015) to allow for rapid HIV transfer to dermal MNPs. The mock infected tissue demonstrated cellular staining consistent with the newly optimised cyclic IF panel **(Section 4.8.1)** and good tissue integrity following application of a mock coated HD-MAP and the gluing and removal of a cloning cylinder (**Figure 4.9a)**. The HSV2 only infection revealed a single focus of HSV2 infection deep in the epidermis (**Figure 4.9b).** This focus of infection was surrounded by CD4, Langerin, and CD11c expressing cells, however, HSV2 was not detected in any of these cells.

The HIV only specimen showed that the majority of the viral signal was concentrated on the epidermal surface, with small foci of infection within the epidermis and no detectable viral signal in the dermis. **(Figure 4.9c)**. **Figures 4.9a-c** also showed that mock-infected tissues lacked RNAscope signal for either HSV2 or HIV, demonstrating the reliability of our staining protocol to identify HSV2 and HIV. The HSV2 HIV coinfected tissue showed very limited HSV2 and HIV infection within the dermis, and importantly no regions within the tissue where the viruses were co-localised **(Figure 4.9d)**. However, we were able to identify two regions of significant interest: 1) a langerin^{+} cell lining the basement membrane, that co-expressed HSV2; and 2) an epidermal CD3^{+}CD4^{+} T cell that co-expressed HIV. Despite these interesting and rare visualised interactions, our inability to produce large amounts of epidermal HSV2/HIV infection and coinfected foci suggests future optimisation of the co-infection explant model is required.

a

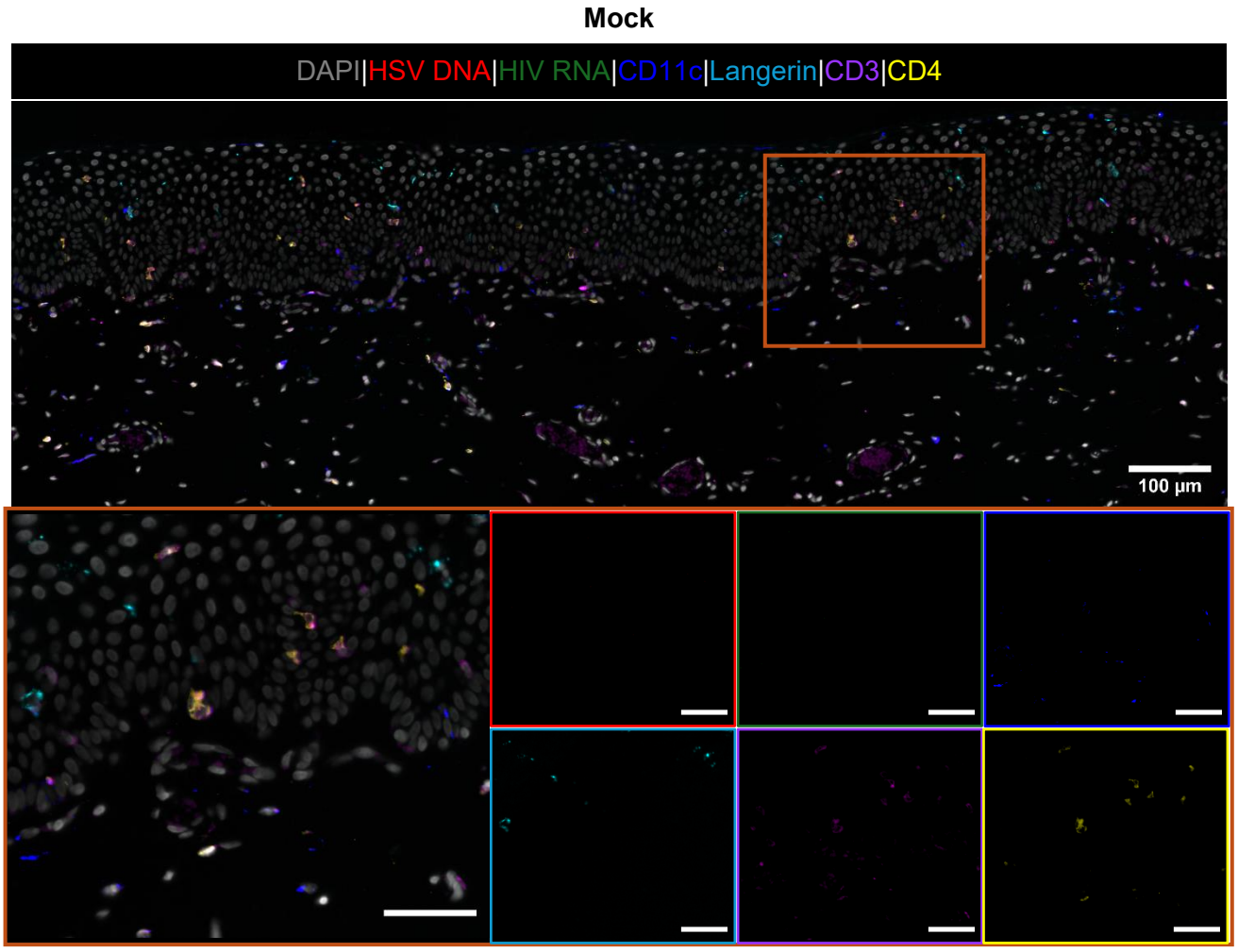

b

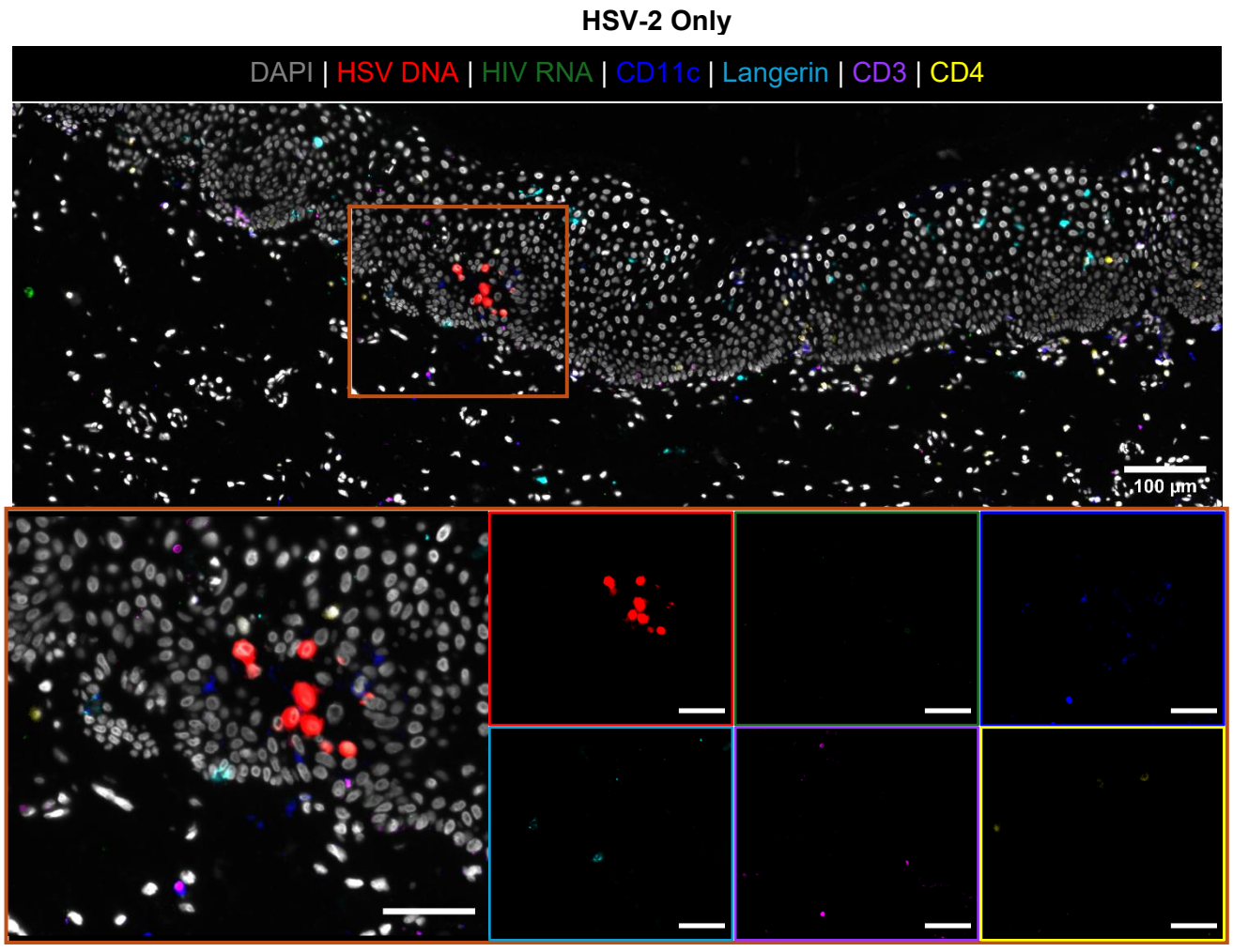

c

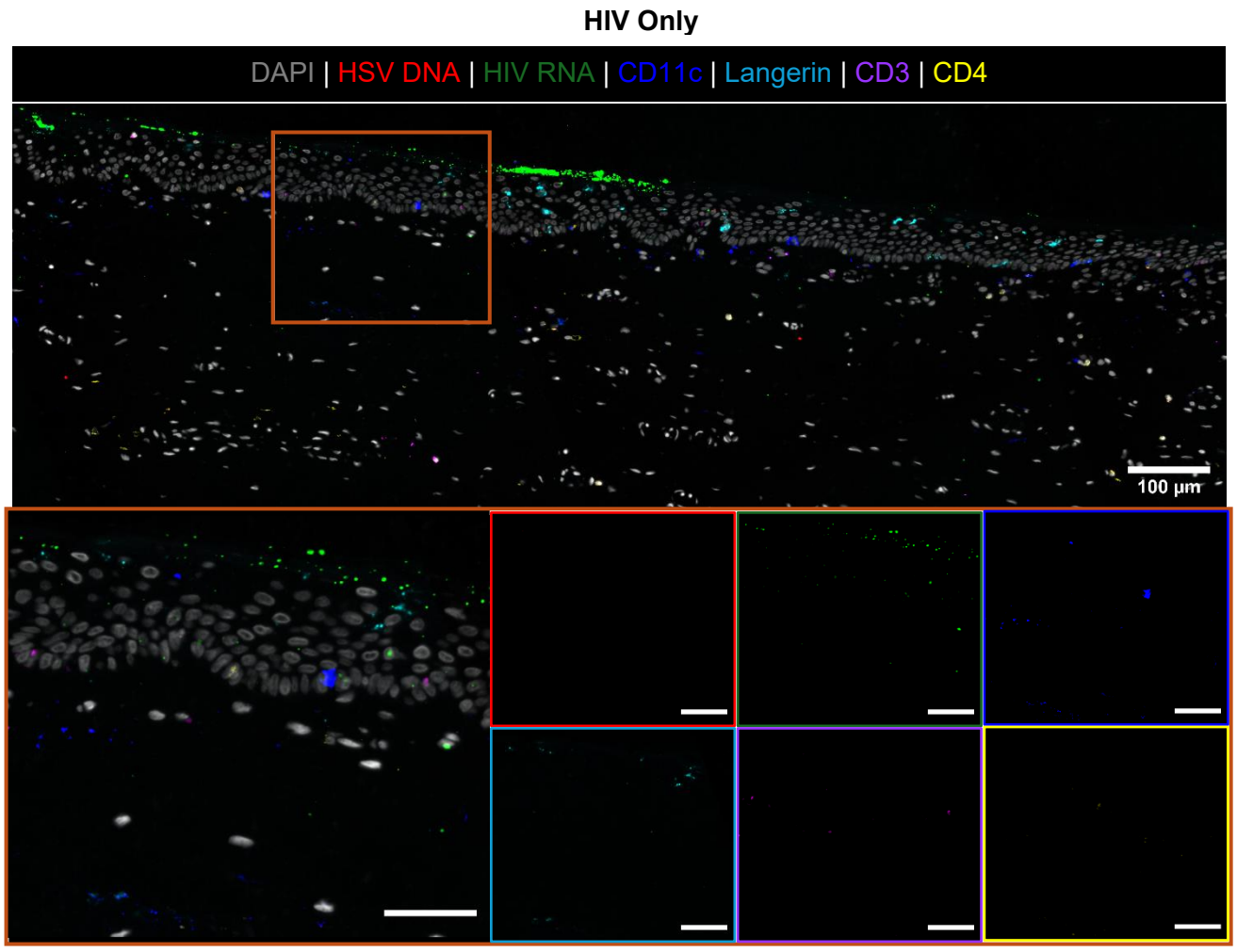

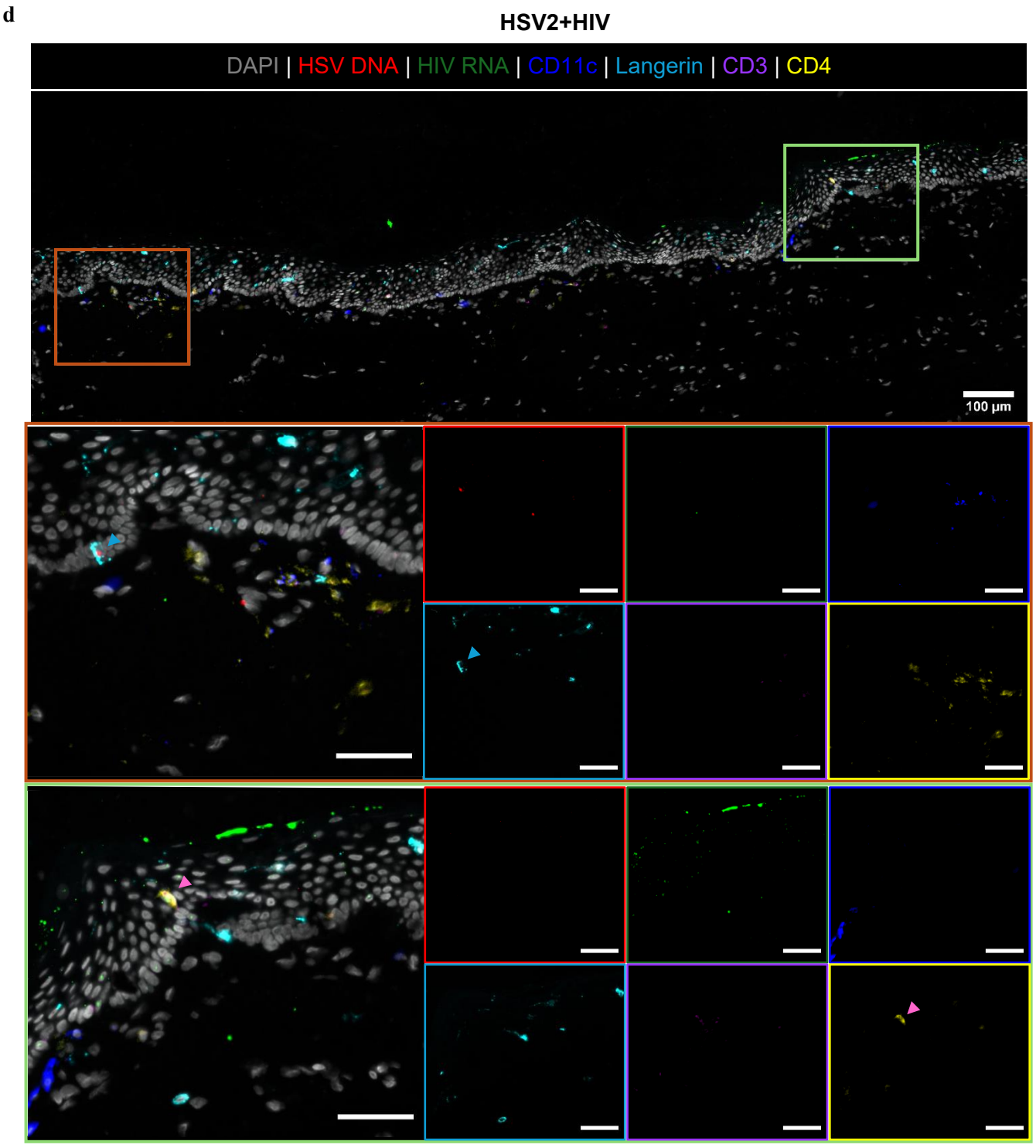

Figure 4.9. HSV2 and HIV coinfection and visualisation attempt. Inner foreskin tissue explants were treated with either a HD-MAP coated with HSV2 (HSV2 only and HSV2+HIV images) or a mock HD-MAP (mock and HIV only images) and left in culture for 18 hours with DCM. HIV_{Bal} at a TCID50 of 70 000 was administered by a cloning cylinder glued to the epidermis and left in culture for a further 6 hours. Following cloning cylinder removal, the explants were fixed with 4% PFA for 24 hours, and cells were visualised using the new cyclic IF panel **(Table 4.3).** HSV2 DNA and HIV RNA were visualised using Duplex RNAscope

which consisted of: blocking of endogenous enzymes using BLOXALL; application of Protease Plus (1:5); and use of the RNAscope 2.5 HD Duplex Assay kit with HSV2 UL29 DNA and $HIV1_{BaL}$ RNA probes. Slides underwent DAPI staining, autofluorescent quenching, and cover-slipping with Slow Fade Diamond Antifade Mountant for imaging. The two rounds of imaging were aligned using the image registration script in Fiji (ImageJ). Scale bars = 50 μm unless otherwise specified, gold arrow = HSV2 infected $Langerin^+$ cell, and pink arrow = HIV infected $CD3^+CD4^+$ T cell.

4.9. Chapter Four Discussion

Despite strong evidence that HSV1/2 infection is a significant risk factor for developing a HIV infection upon exposure (Masese *et al.*, 2015, Looker *et al.*, 2017), the exact mechanisms why this is the case are yet to be elicited and there is a paucity of publications in this field. A major barrier to research in this area is the lack of a high-quality model that can visualise cell and virus interactions during HSV-HIV coinfection in tissue. In this chapter, we aimed to take the HSV1 inner foreskin tissue explant model that has been extensively validated by the host lab and utilised in **Chapter 3** and optimise it to include HIV infection to create a HSV2-HIV coinfection tissue explant that would allow us to track and visualise $CD4^+$ T cells, LCs, Epi-DC2s, and (in future) dermal DC subtypes interactions with both viruses.

As the host lab traditionally used HSV1 to infect inner foreskin tissue, we first demonstrated that the T cell changes observed in **Chapter 3** were analogous to the changes observed when using HSV2 to infect vagina tissue. This was important as prior HSV2 infection of vaginal tissue is the most epidemiologically relevant to HSV-HIV coinfection (Masese *et al.*, 2015, Looker *et al.*, 2017). While we also attempted to demonstrate this for MNPs examined in **Chapter 3**, we were unable to quantify these in at sites of HSV2 infection, attributable to the small foci of infection and only performing the experiment in one donor. A 2012 study that compared the immune responses between HSV1 and HSV2 in mice infected vaginally

suggested significantly more cell infiltration to the vagina in HSV2 infected mice, suggesting HSV2 is associated with a similar but greatly exaggerated immune response compared to HSV1 (Zheng *et al.*, 2012). Their use of *in vivo* infected mice versus our *ex vivo* human tissue infection (preventing blood vessel to tissue migration) and our lack of replicates could explain why we did not see an obviously exaggerated immune response to HSV2 as Zheng *et al*. reported. A study focusing on individuals infected with HSV1 or HSV2 showed that HSV2 infection likely induces more T cell migration than HSV1 (Schmid *et al.*, 1997) which, as the primary HIV target cell, could suggest that moving forward HSV2 may provoke more T cell migration making it more useful to the coinfection explant.

Our microscopy data showed that the vagina is more keratinised and exhibits greater variability in keratin thickness than the inner foreskin, a finding consistent with the literature (Dinh *et al.*, 2010, Schaller, 1990). This observation aligns with recent findings from our host lab, which demonstrated that successful HSV infection in *ex vivo* tissue explants requires delivery of the virus to a depth exceeding 30% of the epidermis of inner foreskin (Rana *et al.*, 2024). Such penetration is more readily achievable in inner foreskin tissue, as its thinner outer keratin layer presents less of a barrier compared to the vagina. Although we observed HSV infection and cell migration with both inner foreskin **(Chapter 3)** and vaginal tissue, with vaginal tissue being particularly relevant to *in vivo* HSV-HIV coinfection in sub-Saharan Africa, the use of inner foreskin may maximise the chances of successful viral infection in the explant model as it is easier for the HD-MAPs to penetrate to 30% the thickness of the epidermis.

Just like with HSV, we investigated whether HIV-coated HD-MAPs could be used to simulate the microtrauma that occurs during sexual acquisition of HIV (Harman *et al.*, 2013b). However, the application of a second HD-MAP to tissue (24 hours after the first HD-MAP) resulted in the destruction of the epidermis due to either: 1) the tissue notwithstanding the trauma caused

by the application of a second HD-MAP; or 2) after 24 hours in culture after excision from the body, the tissue became highly friable, making it unsuitable for the second application of HD-The donor utilised for this experiment was 80 years old, which is much older than other donors used in this chapter, which could also contribute to such significant tissue destruction. This experiment was also performed utilising Vaxxas' older silicon HD-MAPs which have double the number of needle density present than the newer polymer HD-MAPs; therefore, it is possible repeating the experiment on a younger donor, and with the less dense polymer HD-MAPs would have resulted in better tissue integrity after the application of a second HD-MAP, allowing for the use of a HD-MAP to deliver HIV into the tissue 24 hours after HSV infection. However, due to time constraints and limited availability of tissues, this was not performed.

We next demonstrated that the use of a cloning cylinder with a HIV TCID50 of 70 000 resulted in the best viral uptake into the tissue. A 2007 study demonstrated that the HIV TCID50 in seminal plasma during an acute HIV1 infection ranges from 10 000-100 000 (Pilcher *et al.*, 2007), highlighting the physiological relevance of HIV infection at a TCID50 of 70 000 to the natural course of HIV transmission. Previous work by the host lab has however demonstrated at TCID50s as low as 3500 can result in HIV uptake in type I anogenital mucosa sometimes just as reliably as infection with a higher TCID50 (Bertram *et al.*, 2019, Rhodes *et al.*, 2021) which is why we attempted infection with a lower TCID50. As the actual amount of virus delivered into our tissue explants depends greatly on the tissue surface integrity during explant preparation, spending large amounts of time and multiple tissue replicates on the optimisation of the best HIV TCID50 is not justifiable, so we proceeded with a high physiologically relevant HIV dose (Pilcher *et al.*, 2007) that allowed us to successfully visualise HIV viral uptake into the tissue.

The success of the cloning cylinder to deliver HIV into vaginal tissue is consistent with previous work done by the lab utilising cloning cylinders to deliver HIV into type I mucosa (Baharlou *et al.*, 2022). However, in type II mucosa such as the keratinised vagina, it is more challenging for the virus to enter the tissue. A 2022 study using Vaxxas HD-MAPs showed *in vivo* skin punctures began to heal at 24 hours and was completed by 48 hours (Henricson *et al.*, 2022). We hypothesise that the application of the HD-MAP 24 hours before HIV infection as part of the HSV infection protocol, induces breaks in the stratum corneum that are still present when HIV was added to the tissue, thus simulating microtrauma and allowing the virus to pass the keratinised outer barrier into the deeper layers of the epidermis. Some explanations for why the paintbrush did not allow HIV viral uptake in the tissue include: 1) A large amount of virus may have been retained by the paintbrush reducing the true TCID50 that was applied to the tissue, and 2) the virus-containing solution that was painted onto the tissue dried out before the virus enters the tissue.

We determined that a 24 hour period of culture with HIV, 18 hours after the application of a HD-MAP to the explant (thus representing a total of 42 hours explant culture time) led to the best balance of HIV infection and tissue integrity. The substantial tissue damage we observed after 54 hours of explant culture (36 hpi with HIV) contrasted with similar *ex vivo* explant models in the literature: these utilised human skin placed on top of gelfoam in contact with media and demonstrated that skin explants can maintain structural integrity for 4 weeks (Steinstraesser *et al.*, 2009) and also maintain some of their wound healing properties for 1-2 weeks (Xu *et al.*, 2012, Neil *et al.*, 2020). Our inability to maintain tissue integrity for this long is likely attributed to the significant tissue trauma induced by HD-MAPs, the removal of the cloning cylinders which are glued to the tissue, the increased fragility of anogenital mucosa compared to skin, and our lack of use of Human Keratinocyte Growth Supplement in the media, compared to the previous studies.

The fact that transcription (*de novo* RNA production) starts at approximately 24 hpi (Mohammadi *et al.*, 2013) is consistent with our observation of some increased HIV RNA staining at 24 hpi compared to 12 hpi. However, at a time point as early as 24 hpi it is more likely that what we visualised was cellular uptake of HIV virions, as true productive infection would likely have produced more diffuse RNAscope staining of HIV, consistent with similar studies visualising HIV infection *ex vivo* (Deleage *et al.*, 2016). Uptake of HIV into cells with the epithelium also explains our observation that there was a shift from the extracellular viral staining 'aggregate viral particles at 2 hpi to discrete intracellular viral RNA in the nucleus at 24 hpi. Previous work by host lab has demonstrated that once HIV has been taken up by a HIV target cell and internalised into a virus containing compartment, productive infection typically ensues (Nasr *et al.*, 2014). Alternatively, as HIV virions can travel along tissue abrasions into tissue without true internalisation into cells, it is possible that this has occurred at the 24 hpi time point (Maher *et al.*, 2005). Finally, our observation that most of the HIV RNA associated with epidermal cells, can be explained by studies reporting that the time from HIV infection of myeloid cells to export of *de novo* virions is approximately 52 hours (Murray *et al.*, 2011, Nasr *et al.*, 2014).

Our attempt at HSV2-HIV coinfection explant included a HSV2 only control, a HIV only control with largely epidermal and some intraepidermal HIV infection, and a co-infected explant. The coinfected tissue had very limited presence of both viruses and no region where they co-localised. However despite, this we observed a HSV2 infected langerin^{+} cell lining the basement membrane, and an epidermal CD3^{+}CD4^{+} T cell that expressed HIV. Demonstration of an HSV infected epidermal langerin^{+} cell at the basement membrane, and an epidermal CD3^{+}CD4^{+} T cell that expressed HIV supports previous work demonstrating HSV infected epidermal MNPS ferry HSV from the epidermis into the dermis (Kim *et al.*, 2015). The HSV2 infected LC's proximity to the basement membrane, is also consistent with our conclusions in

Chapter 3 that HSV1 infection causes epidermal MNPs to migrate from superficial to deeper regions of the epidermis (towards the basement membrane). It is established that the majority of epidermal $CD3^+CD4^+$ T cells in the anogenital mucosa are CD69 expressing TRM cells (O'Neil *et al.*, 2021), mainly present in the dermis but also in the epidermis of anogenital mucosa (O'Neil, 2023). Therefore, the presence of a HIV infected $CD3^+CD4^+$ T cell in the epidermis suggests that $CD4^+$ TRM cells can likely be directly infected in the epidermis and likely contribute to the viral reservoir during latent HIV infection. Our visualisation of HIV infection in an epidermal $CD4^+$ T cell in foreskin that is likely a TRM cell, is also consistent with previous reports of HIV infection of CD4 TRMs in the human cervix (Cantero-Pérez *et al.*, 2019). However, it is important to note that as our microscopy panel did not utilise CD69 staining, we are unable to definitively confirm that the visualised $CD4^+$ T cell infected with HIV in the foreskin epidermis is a TRM. As vagina has more epidermal and dermal $CD4^+$ TRM cells than inner foreskin (O'Neil, 2023), HIV infection of epidermal $CD4^+$ TRM cells may prove to be more relevant in this tissue type.

We noted that successful HIV infection is far more challenging and infrequent in our explant model than HSV2 infection. This is consistent with studies that have demonstrated that HSV1/2 requires only mucosal contact and subsequent keratinocyte uptake for successful infection (Clarke, 2015) while HIV infection necessitates interaction with less frequently encountered $CD4^+$ T cells or CD4/CCR5 expressing myeloid or dendritic cells (Bertram *et al.*, 2019, Rhodes *et al.*, 2021). One technical issue to avoid in future explants is that the use of surgical glue to fix cloning cylinders to the tissue which can result in a barrier forming over the tissue preventing HIV infection, as well as causing the epidermis to be stripped from the tissue when the cloning cylinder is removed. Although we appeared to overcome this as evidenced by visualisation of numerous HIV particles in the upper epidermis, a potential future direction to allow better HIV infection of the tissue could involve experimenting with other adhesives such

as waxes to attach the cloning cylinders to tissue. Importantly any new adhesives used to fix the cloning cylinder to tissue should be assessed with trypan blue to determine if the adhesive forms an adequate seal with. In the coinfection studies we opted to swap to a 6 hour HIV infection despite demonstrating the best results with single HIV infection at 24 hpi, as we expected a preestablished HSV infection would create a viral relay (Kim *et al.*, 2015) to allow for rapid HIV transfer to dermal MNPs by this time point. However instead we saw HIV infection limited to the superficial epidermis and coating the epidermal surface, likely due to a lack of HSV2 infection of LCs/DCs at these very superficial sites. A longer HSV infection may be needed for deeper diffusion of the HIV particles.

While working with excised human tissue provides the ideal *in situ* model for investigating interactions of HSV1/2, HIV and cells in the anogenital mucosa, it has some key limitations. Due to the limited availability of tissue, we adopted a flexible approach to specimen selection. This often required the use of vaginal tissue, which while epidemiologically relevant and structurally similar to foreskin, had not previously been utilised in the host lab's *ex vivo* tissue explant model which has implications for achieving tissue infection. It has been demonstrated that the lactobacilli dominated vaginal microbiota coats the vaginal wall with antimicrobial acid and hydrogen peroxide which inhibits HSV2 and HIV1 replication (Zabihollahi *et al.*, 2012). However as our explant model use HDMAPs to bypass the surface of the epithelium, the impact of these secreted antimicrobials is likely reduced or eliminated. Furthermore, vaginal tissue may be more difficult to infect with HIV than foreskin tissue, especially if obtained during the estrogenic part of the of the menstrual cycle as progesterone treatment enhances vaginal SIV infection in macaque models (Marx *et al.*, 1996) and thickness of the vaginal wall is known to vary throughout the menstrual cycle (Wang *et al.*, 2024). The host lab has observed that HD-MAP application to inner foreskin may potentially result in a greater number of punctures reaching the depth within the epidermis required for HSV infection to

take place compared to vaginal tissue, although this has not been formally investigated. Foreskin tissue is also well established to be highly susceptible to HIV infection, to the extent that in high-risk areas, circumcision as a public health measure significantly reduces transmission (Moses, 2009). Furthermore limited tissue supply meant key optimisation steps were performed only once, without repetition to confirm results, and required us to accept tissue from donors who varied greatly in age, menstrual cycle stage, inflammation status, and health. In future we will check the cycle stage by H&E staining and glycogen staining (Ayre, 1951).

The challenges we faced in achieving HIV infection may mean that rather than focusing on non-simultaneous HSV and HIV infection of tissue, we could shift towards designing a model that utilises one HD-MAP coated in both HSV and HIV to produce simultaneous HSV-HIV coinfection in the explant. Although this is a less likely occurrence and will not best replicate how HSV induced cell changes increase HIV acquisition, it is indeed feasible that both viruses may be present during an active herpes lesion. This less experimentally challenging approach could still provide valuable insight into the interactions between the two viruses and cells. Finally, as discussed in **Chapter 3**, as the infection takes place in tissue after it is excised from the body, our explant model cannot capture the impact of inflammatory cells circulating within the vasculature that would typically infiltrate the mucosa.

4.9.1. Conclusions

Despite not demonstrating HSV2 and HIV coinfection, in our *ex vivo* tissue explant model, the optimisations detailed in this chapter significantly contribute to the development of a HSV2-HIV coinfection explant:

1. We demonstrated that HSV2 infection of human vaginal epithelial explants was shown to produce very similar results to HSV1 infection of inner foreskin explants **(Chapter**

3), with a similar migration of dermal CD4 T cells to regions subjacent to foci of epidermal HSV infection.

2. The following protocol was suggested for attempts at producing HSV2 HIV coinfected explants: HSV2 is delivered by HD-MAP followed 24 hours later by HIV added at a concentration of 70 000 TCID50 within a cloning cylinder. HSV2 and HIV particles and foci within cells will be visualised using RNAscope staining 24 hours after HIV inoculation and the locations of virus and cells of interest within in the dermis and epidermis can be identified.
3. Should our current approach to HSV2-HIV coinfection continue to be unsuccessful, an alternative backup plan is to coinfect with both simultaneously with a single HD-MAP coated with HSV2 and HIV, simulating the effect of microtrauma during intercourse and the presence of both viruses.

Chapter 5: Overall Discussion

The global rate of new HIV infections has held steady, adding continuously to the number of people living with HIV requiring lifelong ART. With 600,000 death related to AIDS and 1.3 million new infections in 2023 (HIVGov, 2025), HIV/AIDS remains a significant public health concern. There is growing evidence that prior HSV2 infection makes individuals 3-5 times more likely to acquire HIV via sexual transmission (Looker *et al.*, 2017, Reynolds *et al.*, 2003). While it is hypothesised that this is related to ulceration and inflammation of the anogenital mucosa (Passmore *et al.*, 2016), the precise mechanisms underlying this increased risk have not yet been elucidated. Since HIV infection largely occurs through sexual transmission (HIVGov, 2025), and HSV1/2 are two of the most prevalent STIs globally, understanding the mechanisms by which HSV1/2 infection increases HIV acquisition risk could contribute to novel prevention approaches in populations with high HSV1/2 prevalence.

In **Chapter 3**, we first utilised a preexisting *ex vivo* HSV1 infected inner foreskin explant model optimised by the host lab to visualise and quantify cellular and cytokine/chemokine alterations that may increase susceptibility to mucosal acquisition of HIV. We found that epidermal LCs and $CD11c^+$ Epi-DCs were less dense and closer to the basement membrane at sites of epidermal HSV1 infection, and that dermal LCs and $CD11c^+$ DCs were more densely distributed under foci of HSV1 infection compared to sites far from infection. In contrast, when examining $CD3^+$ lymphocyte populations ($CD3^+CD4^+$ and $CD3^+CD4^-$) in the dermis under sites of infection, we found that although their density increased at sites of HSV1 infection, there was no change in the average distance of lymphocytes from the basement membrane compared to sites far from infection. We finally showed that the average cross distance between dermal MNPs and $CD3^+$ lymphocyte populations was reduced in the dermis underlying sites of infection, and that HSV1 infected foreskins upregulated the production of all inflammatory cytokines and chemokines that we examined.

These findings of **Chapter 3** have several implications for understanding how early HSV infection affects the cellular landscape and reveals multiple mechanisms by which prior HSV can facilitate enhanced HIV transmission. The fact that epidermal MNPs decreased in density and were closer to the basement membrane while dermal MNPs increased in density and were also closer to the basement membrane led us to hypothesise that within the early hours of HSV infection epidermal MNPs migrate from the epidermis and accumulate in the dermis under foci of infection. This is supported by previous literature examining LC (Kim *et al.*, 2015) and $CD11c^+$ Epi-DC (Bertram *et al.*, 2021) migration during HSV infection where these cells act as a viral relay to carry virus into the dermis of the anogenital mucosa. In contrast, as lymphocytes increased in density in the dermis under sites of infection uniformly in the first 0-120 μm without a reduction in distance from basement membrane, we hypothesise that HSV infection induces lymphocyte populations to migrate laterally within the dermis rather than from the epidermis. However, given that $CD3^+$ cells are rare in the epidermis (O'Neil, 2023), this may be the primary reason why our observations with T cells do not align with epidermal to dermal LC and DC cell migration.

The fact that the average cross distance between MNP and lymphocyte subsets is reduced has significant implications when considering that: 1) regions enriched in HIV target cells are more likely to acquire HIV when exposed to the virus (Abu-Raddad *et al.*, 2008, Zhu *et al.*, 2007), and 2) if the hypothesised migration of epidermal MNPs to the dermis potentially acts as a viral relay for HIV (Bertram *et al.*, 2019), this will allow HIV to be transported from the epidermis into the more target cellrich dermis underlying sites of HSV infection. Therefore, the changes in the cellular landscape between potentially HIV carrying MNPs and $CD4^+$ T cells could facilitate the latent or productive infection of these target cells.

Although our analysis was limited to supernatants from only two donors, the upregulation of several chemokines and proinflammatory cytokines known to mediate lymphocyte and MNP migration may explain the patterns of cell migration we observed. This is consistent with previous work examining chemokines and inflammatory cytokines performed in HaCaTs (Rana *et al.*, 2024) and HSV1 infected primary keratinocytes (Mikloska *et al.*, 1998). The cell distributions we observed with the upregulation of chemokines and proinflammatory cytokines suggest that HSV induces inflammation within the anogenital mucosa that could create a chemotactic environment, which could contribute to the recruitment and redistribution of key HIV target cells, lowering the threshold for HIV sexual transmission.

In **Chapter 4** we adapted our explant model for use with vaginal tissue and HSV-2, establishing a HSV2 HIV coinfection explant model to visualise viral and cellular interactions in both vaginal and foreskin tissue. Despite limited tissue supplies and technical challenges, we demonstrated that vaginal tissue could be infected with HSV2 using a method similar to that used for generating HSV1 infected foreskin explants. This resulted in a redistribution in lymphocyte populations consistent with our findings in **Chapter 3.** Optimal HIV infection in vaginal tissue was achieved with a TCID50 of 70 000, delivered by cloning cylinder, with the tissue preserved 24 post HIV infection. Finally, despite the challenges we faced, we produced a foreskin explant which while lacking regions of overlapping HSV2 and HIV infection, contained a region of HSV2 infection and a separate region of HIV infection which allowed us to observe a HSV2 carrying Langerin$^+$ cell lining the basement membrane and a HIV infected CD4$^+$ T cell residing in the epidermis.

While not achieving HSV2 HIV coinfection, we significantly optimised the coinfection model which will be used for a variety of experiments to: 1) examine early interactions between HSV2 and HIV with CD4$^+$ T cells and other immune cells in the anogenital mucosa, and 2) directly

visualise how mucosal acquisition of HIV is enhanced by prior HSV infection. Most importantly, our observation of a HSV2 carrying Langerin$^+$ cell lining the basement membrane contributes to the conclusions we drew in **Chapter 3** and other reports (Kim *et al.*, 2015) showing that HSV2 forms a viral relay that HIV could utilise to reach the dermis as discussed above. The HIV infected epidermal CD4$^+$ T cell we identified was most likely a TRM cell (O'Neil *et al.*, 2021), which is consistent with the literature that demonstrates that these cells contribute to the HIV viral reservoir (Cantero-Pérez *et al.*, 2019), however without a marker of tissue residency such as CD69, this cell cannot be confirmed to be a TRM cell. An alternative explanation for this is that chemokines CCL3, CCL4, and CCL5, which induce T cell migration and were upregulated in our HSV1 infected tissue, could cause dermal residing CD4$^+$ T cells to migrate to the epidermis. These cells could therefore be part of the HSV lesion inflammatory infiltrate that contribute to the heightened risk of HIV acquisition in the epidermis.

Before future work can take place, the HSV2 HIV infection explant model will require further optimisation in order to ensure more reliable HSV2 HIV coinfection can be achieved. An area of significant interest to the lab is the optimisation of HD-MAP application to tissue, as we demonstrated that polymer HD-MAPs more frequently produced punctures that were > 30% the epidermal depth which are associated with better infection, while more recent data has suggested silicon HD-MAPs are superior. This is likely due to polymer HD-MAPs having thicker tips, which limit skin deformation, thereby reducing puncture formation and depth (Zhang *et al.*, 2018). Changes to the spring velocity and the material underlying tissue during HD-MAP application have also been explored by the host lab to further optimise puncture formation. Such works have since proven to be successful during the writing of this thesis, with the host lab producing HSV2 infected foreskins with significantly more punctures and virus detection than previously seen using the explant system.

Concerns about puncture sites closing and tissue integrity led us to reduce the interval between HSV and HIV inoculation from 24 hours to 18 hours in **Chapter 4**. However, even at this reduced time length, there is a significant risk of puncture closure (Nuutila *et al.*, 2012). Therefore, moving forward, the host lab will assess whether coinfection explants with a shorter culture time between HSV2 and HIV infection (1-6 hours) can be used to produce useful results. Furthermore, experiments will be conducted to identify a new adhesive for securing cloning cylinders to tissue, one that is gentler to the tissue while still providing an effective seal. Once fully optimised, we hope to use this novel coinfection explant model with technologies that assess 30-40 markers such as imaging mass cytometry or high parameter sequential IF. These advanced methodologies will produce high-quality staining of a large panel of immune markers to identify more immune subsets, their functional markers, and their interactions with HSV and HIV.

Our study was strengthened by our exclusive use of human anogenital mucosa such as foreskin and vagina which is physiologically relevant when investigating the landscape of tissue residing immune cells during early HSV and HIV infection. Previous models have replicated microtrauma with scalpel incisions (Rhodes *et al.*, 2021), however this method resulted in less consistent depths and frequencies compared to our use of HD-MAPs. Traditionally visualisation of HSV and HIV has been achieved with virus tagged with fluorescent protein (such as GFP) or IF. However, our use of RNAscope is significantly more sensitive and allows the visualisation of individual virions or aggregates as GFP is not typically detectable until replication occurs which is 18-24 hpi. Finally, our use of cyclic IF allowed us to visualise both lymphocytes and MNPs within the same panel due to the increased number of markers we could visualise, and allows for additional markers to be added without significant further optimisations of a staining and imaging protocol.

Despite the significant advantage of using human tissue to closely mimic the *in vivo* cellular response to HSV and HIV infection, a major limitation encountered in Chapter 4 was the limited availability of such tissue. This led us to first shift from inner foreskin to vaginal tissue despite our concerns about its menstrual cycle-dependent thickness and the more keratinised epidermis (Schaller, 1990), and then based on availability we ultimately accepted both foreskin and vaginal tissue from donors of varying health, age, and tissue size. These variations and supply challenges meant that confirming optimisations in multiple donors was not feasible, and a large number of replicates was required to achieve statistical significance. Our tissue explant system also currently limits us from examining early mucosal infection, as cells and tissue degrade significantly after 48 hours in culture, and as the tissue is excised from the body prior to infection we are unable to observe the impact of circulating inflammatory cells which are known to migrate to sites of HSV infection (Cunningham *et al.*, 1985, Zhu *et al.*, 2009).

In conclusion, this thesis demonstrated some of the mechanisms and changes induced by HSV in the anogenital mucosa that potentially contribute to an increased risk of HIV acquisition and made significant progress in optimising a novel HSV2 HIV coinfection explant. Once fully optimised, this coinfection explant could pave the way for exciting new avenues of research and ultimately contribute to reducing or preventing mucosal acquisition of HIV.

References

ABRAM, M. E., FERRIS, A. L., DAS, K., QUINOÑES, O., SHAO, W., TUSKE, S., ALVORD, W. G., ARNOLD, E. & HUGHES, S. H. 2014. Mutations in HIV-1 reverse transcriptase affect the errors made in a single cycle of viral replication. *Journal of virology,* 88**,** 7589-7601.

ABU-RADDAD, L. J., MAGARET, A. S., CELUM, C., WALD, A., LONGINI JR, I. M., SELF, S. G. & COREY, L. 2008. Genital herpes has played a more important role than any other sexually transmitted infection in driving HIV prevalence in Africa. *PloS one,* 3**,** e2230.

ACCHIONI, C., REMOLI, A. L., MARSILI, G., ACCHIONI, M., NARDOLILLO, I., ORSATTI, R., FARCOMENI, S., PALERMO, E., PERROTTI, E. & BARRECA, M. L. 2019. Alternate NF-κB-independent signaling reactivation of latent HIV-1 provirus. *Journal of virology,* 93**,** e00495-19.

AGOSTINI, S., MANCUSO, R., BAGLIO, F. & CLERICI, M. J. E. R. O. A.-I. T. 2017. A protective role for herpes simplex virus type-1-specific humoral immunity in Alzheimer's disease. 15**,** 89-91.

AHMADZADEH, M. & ROSENBERG, S. A. 2005. TGF-β1 attenuates the acquisition and expression of effector function by tumor antigen-specific human memory CD8 T cells. *The Journal of Immunology,* 174**,** 5215-5223.

AKHTAR, J. & SHUKLA, D. 2009. Viral entry mechanisms: cellular and viral mediators of herpes simplex virus entry. *The FEBS journal,* 276**,** 7228-7236.

AL-SHURA, A. 2020. Lymphocytes. *Advanced hematology in integrated cardiovascular Chinese medicine***,** 41-46.

ALMUKDAD, S., FAROOQUI, U. S., HARFOUCHE, M., ALDOS, L. & ABU-RADDAD, L. J. 2022. Epidemiology of herpes simplex virus type 2 in Canada, Australia, and New Zealand: systematic review, meta-analyses, and meta-regressions. *Sexually transmitted diseases,* 49**,** 403-413.

ALMUKDAD, S., HARFOUCHE, M., FAROOQUI, U. S., ALDOS, L. & ABU-RADDAD, L. J. 2023. Epidemiology of herpes simplex virus type 1 and genital herpes in Australia and New Zealand: Systematic review, meta-analyses and meta-regressions. *Epidemiology & Infection,* 151**,** e33.

ALVAREZ, Y., TUEN, M., SHEN, G., NAWAZ, F., ARTHOS, J., WOLFF, M. J., POLES, M. A. & HIOE, C. E. 2013. Preferential HIV infection of CCR6+ Th17 cells is associated with higher levels of virus receptor expression and lack of CCR5 ligands. *Journal of virology,* 87**,** 10843-10854.

APPAY, V. & ROWLAND-JONES, S. L. 2001. RANTES: a versatile and controversial chemokine. *Trends Immunol,* 22**,** 83-7.

ARAKELYAN, A., PETERSEN, J. D., BLAZKOVA, J. & MARGOLIS, L. 2019. Macrophage-derived HIV-1 carries bioactive TGF-beta. *Scientific reports,* 9**,** 1-8.

ARTHUR, J. L., SCARPINI, C. G., CONNOR, V., LACHMANN, R. H., TOLKOVSKY, A. M. & EFSTATHIOU, S. 2001. Herpes simplex virus type 1 promoter activity during latency establishment, maintenance, and reactivation in primary dorsal root neurons in vitro. *J Virol,* 75**,** 3885-95.

ASHKAR, A. A. & ROSENTHAL, K. L. 2003. Interleukin-15 and natural killer and NKT cells play a critical role in innate protection against genital herpes simplex virus type 2 infection. *Journal of virology,* 77**,** 10168-10171.

AUGENBRAUN, M., FELDMAN, J., CHIRGWIN, K., ZENILMAN, J., CLARKE, L., DEHOVITZ, J., LANDESMAN, S. & MINKOFF, H. 1995. Increased genital shedding of herpes simplex virus type 2 in HIV-seropositive women. *Annals of internal medicine,* 123**,** 845-847.

AYOUB, H. H., CHEMAITELLY, H. & ABU-RADDAD, L. J. J. B. M. 2019. Characterizing the transitioning epidemiology of herpes simplex virus type 1 in the USA: model-based predictions. 17**,** 1-12.

AYRE, W. B. 1951. The glycogen-estrogen relationship in the vaginal tract. *J Clin Endocrinol Metab,* 11**,** 103-10.

BADER, C., CRUMPACKER, C. S., SCHNIPPER, L. E., RANSIL, B., CLARK, J. E., ARNDT, K. & FREEDBERG, I. M. 1978. The natural history of recurrent facial-oral infection with herpes simplex virus. *J Infect Dis,* 138**,** 897-905.

BAHARLOU, H., CANETE, N., VINE, E. E., HU, K., YUAN, D., SANDGREN, K. J., BERTRAM, K. M., NASR, N., RHODES, J. W. & GOSSELINK, M. P. 2022. An in situ analysis pipeline for initial host-pathogen interactions reveals signatures of human colorectal HIV transmission. *Cell Reports,* 40.

BAIYEGUNHI, O., NDLOVU, B., OGUNSHOLA, F., ISMAIL, N., WALKER, B. D., NDUNG'U, T. & NDHLOVU, Z. M. 2018. Frequencies of Circulating Th1-Biased T Follicular Helper Cells in Acute HIV-1 Infection Correlate with the Development of HIV-Specific Antibody Responses and Lower Set Point Viral Load. *Journal of virology,* 92.

BARRÉ-SINOUSSI, F., CHERMANN, J. C., REY, F., NUGEYRE, M. T., CHAMARET, S., GRUEST, J., DAUGUET, C., AXLER-BLIN, C., VÉZINET-BRUN, F., ROUZIOUX, C., ROZENBAUM, W. & MONTAGNIER, L. 1983. Isolation of a T-lymphotropic retrovirus from a patient at risk for acquired immune deficiency syndrome (AIDS). *Science,* 220**,** 868-71.

BECKER, S., WARREN, M. & HASKILL, S. 1987. Colony-stimulating factor-induced monocyte survival and differentiation into macrophages in serum-free cultures. *The Journal of Immunology,* 139**,** 3703-3709.

BELL, N. M. & LEVER, A. M. 2013. HIV Gag polyprotein: processing and early viral particle assembly. *Trends in microbiology,* 21**,** 136-144.

BENEDETTI, J. K., ZEH, J. & COREY, L. 1999. Clinical reactivation of genital herpes simplex virus infection decreases in frequency over time. *Annals of internal medicine,* 131**,** 14-20.

BENNETT, S. R., CARBONE, F. R., KARAMALIS, F., FLAVELL, R. A., MILLER, J. F. & HEATH, W. R. 1998. Help for cytotoxic-T-cell responses is mediated by CD40 signalling. *Nature,* 393**,** 478-480.

BERNSTEIN, D. I., BELLAMY, A. R., HOOK, E. W., III, LEVIN, M. J., WALD, A., EWELL, M. G., WOLFF, P. A., DEAL, C. D., HEINEMAN, T. C., DUBIN, G. & BELSHE, R. B. 2012. Epidemiology, Clinical Presentation, and Antibody Response to Primary Infection With Herpes Simplex Virus Type 1 and Type 2 in Young Women. *Clinical Infectious Diseases,* 56**,** 344-351.

BERTRAM, K. M., BOTTING, R. A., BAHARLOU, H., RHODES, J. W., RANA, H., GRAHAM, J. D., PATRICK, E., FLETCHER, J., PLASTO, T. M., TRUONG, N. R., ROYLE, C., DOYLE, C. M., TONG, O., NASR, N., BARNOUTI, L., KOHOUT, M. P., BROOKS, A. J., WINES, M. P., HAERTSCH, P., LIM, J., GOSSELINK, M. P., CTERCTEKO, G., ESTES, J. D., CHURCHILL, M. J., CAMERON, P. U., HUNTER, E., HANIFFA, M. A., CUNNINGHAM, A. L. & HARMAN, A. N. 2019. Identification of HIV transmitting CD11c + human epidermal dendritic cells. *Nature communications,* 10**,** 2759-15.

BERTRAM, K. M., TRUONG, N. R., SMITH, J. B., KIM, M., SANDGREN, K. J., FENG, K. L., HERBERT, J. J., RANA, H., DANASTAS, K. & MIRANDA-SAKSENA, M. 2021. Herpes Simplex Virus type 1 infects Langerhans cells and the novel epidermal

dendritic cell, Epi-cDC2s, via different entry pathways. *PLoS Pathogens,* 17**,** e1009536.

BEYNON, V., QUINTANA, F. J. & WEINER, H. L. 2012. Activated human CD4+CD45RO+ memory T-cells indirectly inhibit NLRP3 inflammasome activation through downregulation of P2X7R signalling. *PloS one,* 7**,** e39576-e39576.

BHAVSAR, I., MILLER, C. S. & AL-SABBAGH, M. 2015. Macrophage Inflammatory Protein-1 Alpha (MIP-1 alpha)/CCL3: As a Biomarker. *General Methods in Biomarker Research and their Applications***,** 223-249.

BICKEL, M. 1993. The role of interleukin-8 in inflammation and mechanisms of regulation. *J Periodontol,* 64**,** 456-60.

BIGLEY, V., MCGOVERN, N., MILNE, P., DICKINSON, R., PAGAN, S., COOKSON, S., HANIFFA, M. & COLLIN, M. 2015. Langerin-expressing dendritic cells in human tissues are related to CD1c+ dendritic cells and distinct from Langerhans cells and CD141high XCR1+ dendritic cells. *Journal of leukocyte biology,* 97**,** 627-634.

BOHANNON, K. P., JUN, Y., GROSS, S. P. & SMITH, G. A. J. P. O. T. N. A. O. S. 2013. Differential protein partitioning within the herpesvirus tegument and envelope underlies a complex and variable virion architecture. 110**,** E1613-E1620.

BOLDOGKŐI, Z., SZŰCS, A., BALÁZS, Z., SHARON, D., SNYDER, M. & TOMBÁCZ, D. J. S. D. 2018. Transcriptomic study of Herpes simplex virus type-1 using full-length sequencing techniques. 5**,** 1-14.

BORROW, P., LEWICKI, H., HAHN, B. H., SHAW, G. M. & OLDSTONE, M. B. 1994. Virus-specific CD8+ cytotoxic T-lymphocyte activity associated with control of viremia in primary human immunodeficiency virus type 1 infection. *The Journal of Virology,* 68**,** 6103.

BOSNJAK, L., MIRANDA-SAKSENA, M., KOELLE, D. M., BOADLE, R. A., JONES, C. A. & CUNNINGHAM, A. L. 2005. Herpes simplex virus infection of human dendritic cells induces apoptosis and allows cross-presentation via uninfected dendritic cells. *The Journal of Immunology,* 174**,** 2220-2227.

BOTTING, R. A., RANA, H., BERTRAM, K. M., RHODES, J. W., BAHARLOU, H., NASR, N., CUNNINGHAM, A. L. & HARMAN, A. N. 2017. Langerhans cells and sexual transmission of HIV and HSV. *Reviews in medical virology,* 27**,** e1923.

BOURDELY, P., ANSELMI, G., VAIVODE, K., RAMOS, R. N., MISSOLO-KOUSSOU, Y., HIDALGO, S., TOSSELO, J., NUÑEZ, N., RICHER, W. & VINCENT-SALOMON, A. 2020. Transcriptional and functional analysis of CD1c+ human dendritic cells identifies a CD163+ subset priming CD8+ CD103+ T cells. *Immunity,* 53**,** 335-352. e8.

BRÜGGEN, M.-C., BAUER, W. M., REININGER, B., CLIM, E., CAPTARENCU, C., STEINER, G. E., BRUNNER, P. M., MEIER, B., FRENCH, L. E. & STINGL, G. 2016. In situ mapping of innate lymphoid cells in human skin: evidence for remarkable differences between normal and inflamed skin. *Journal of Investigative Dermatology,* 136**,** 2396-2405.

BURCH, A. D. & WELLER, S. K. 2005. Herpes simplex virus type 1 DNA polymerase requires the mammalian chaperone hsp90 for proper localization to the nucleus. *Journal of virology,* 79**,** 10740-10749.

BURNETT, J. C., LIM, K.-I., CALAFI, A., ROSSI, J. J., SCHAFFER, D. V. & ARKIN, A. P. 2010. Combinatorial latency reactivation for HIV-1 subtypes and variants. *Journal of virology,* 84**,** 5958-5974.

BURREL, S., BOUTOLLEAU, D., RYU, D., AGUT, H., MERKEL, K., LEENDERTZ, F. H. & CALVIGNAC-SPENCER, S. 2017. Ancient Recombination Events between Human Herpes Simplex Viruses. *Molecular biology and evolution,* 34**,** 1713-1721.

BUZON, M. J., SUN, H., LI, C., SHAW, A., SEISS, K., OUYANG, Z., MARTIN-GAYO, E., LENG, J., HENRICH, T. J. & LI, J. Z. 2014. HIV-1 persistence in CD4+ T cells with stem cell–like properties. *Nature medicine,* 20**,** 139.

CABRERA JORGE, R., CHARRON AUDRA, J. & LEIB DAVID, A. 2018. Neuronal Subtype Determines Herpes Simplex Virus 1 Latency-Associated-Transcript Promoter Activity during Latency. *Journal of Virology,* 92**,** 10.1128/jvi.00430-18.

CACCAMO, N., JOOSTEN, S. A., OTTENHOFF, T. H. M. & DIELI, F. 2018. Atypical Human Effector/Memory CD4(+) T Cells With a Naive-Like Phenotype. *Frontiers in immunology,* 9**,** 2832-2832.

CAGNO, V., TSELIGKA, E. D., JONES, S. T. & TAPPAREL, C. 2019. Heparan Sulfate Proteoglycans and Viral Attachment: True Receptors or Adaptation Bias? *Viruses,* 11.

CALLÉ, A., UGRINOVA, I., EPSTEIN, A. L., BOUVET, P., DIAZ, J.-J. & GRECO, A. 2008. Nucleolin is required for an efficient herpes simplex virus type 1 infection. *Journal of virology,* 82**,** 4762-4773.

CAMARENA, V., KOBAYASHI, M., KIM, J. Y., ROEHM, P., PEREZ, R., GARDNER, J., WILSON, A. C., MOHR, I. & CHAO, M. V. 2010. Nature and duration of growth factor signaling through receptor tyrosine kinases regulates HSV-1 latency in neurons. *Cell host & microbe,* 8**,** 320-330.

CANTERO-PÉREZ, J., GRAU-EXPÓSITO, J., SERRA-PEINADO, C., ROSERO, D. A., LUQUE-BALLESTEROS, L., ASTORGA-GAMAZA, A., CASTELLVÍ, J., SANHUEZA, T., TAPIA, G., LLOVERAS, B., FERNÁNDEZ, M. A., PRADO, J. G., SOLÉ-SEDENO, J. M., TARRATS, A., LECUMBERRI, C., MAÑALICH-BARRACHINA, L., CENTENO-MEDIAVILLA, C., FALCÓ, V., BUZON, M. J. & GENESCÀ, M. 2019. Resident memory T cells are a cellular reservoir for HIV in the cervical mucosa. *Nature communications,* 10**,** 4739-4739.

CARDONE, G., WINKLER, D. C., TRUS, B. L., CHENG, N., HEUSER, J. E., NEWCOMB, W. W., BROWN, J. C. & STEVEN, A. C. 2007. Visualization of the herpes simplex virus portal in situ by cryo-electron tomography. *Virology,* 361**,** 426-434.

CARMICHAEL, J. C., YOKOTA, H., CRAVEN, R. C., SCHMITT, A. & WILLS, J. W. 2018. The HSV-1 mechanisms of cell-to-cell spread and fusion are critically dependent on host PTP1B. *PLoS pathogens,* 14**,** e1007054.

CARUSO, M. P., FALIVENE, J., HOLGADO, M. P., ZURITA, D. H., LAUFER, N., CASTRO, C., NICO, Á., MAETO, C., SALIDO, J. & PÉREZ, H. 2019. Impact of HIV-ART on the restoration of Th17 and Treg cells in blood and female genital mucosa. *Scientific reports,* 9**,** 1-16.

CASTELLINO, F., HUANG, A. Y., ALTAN-BONNET, G., STOLL, S., SCHEINECKER, C. & GERMAIN, R. N. 2006. Chemokines enhance immunity by guiding naive CD8+ T cells to sites of CD4+ T cell–dendritic cell interaction. *Nature,* 440**,** 890-895.

CDC 1981. Kaposi's sarcoma and Pneumocystis pneumonia among homosexual men--New York City and California. *MMWR Morb Mortal Wkly Rep.* 1981/07/03 ed.

CHANG, H.-C., SEHRA, S., GOSWAMI, R., YAO, W., YU, Q., STRITESKY, G. L., JABEEN, R., MCKINLEY, C., AHYI, A.-N. & HAN, L. 2010. The transcription factor PU. 1 is required for the development of IL-9-producing T cells and allergic inflammation. *Nature immunology,* 11**,** 527-534.

CHAYAVICHITSILP, P., BUCKWALTER, J., KRAKOWSKI, A. & FRIEDLANDER, S. 2009. Herpes simplex. *Pediatrics in review,* 30 4**,** 119-29; quiz 130.

CHEGE, D., SHETH, P. M., KAIN, T., KIM, C. J., KOVACS, C., LOUTFY, M., HALPENNY, R., KANDEL, G., CHUN, T.-W. & OSTROWSKI, M. 2011. Sigmoid

Th17 populations, the HIV latent reservoir, and microbial translocation in men on long-term antiretroviral therapy. *Aids,* 25**,** 741-749.
CHESLOCK, S. R., POON, D. T., FU, W., RHODES, T. D., HENDERSON, L. E., NAGASHIMA, K., MCGRATH, C. F. & HU, W. S. 2003. Charged assembly helix motif in murine leukemia virus capsid: an important region for virus assembly and particle size determination. *J Virol,* 77**,** 7058-66.
CHOUDHARY, S. K., ARCHIN, N. M., CHEEMA, M., DAHL, N. P., GARCIA, J. V. & MARGOLIS, D. M. 2012. Latent HIV-1 infection of resting $CD4^+$ T cells in the humanized $Rag2^{-/-}$ $\gamma c^{-/-}$ mouse. *Journal of virology,* 86**,** 114-120.
CHRISTENSEN-QUICK, A., LAFFERTY, M., SUN, L., MARCHIONNI, L., DEVICO, A. & GARZINO-DEMO, A. 2016. Human Th17 cells lack HIV-inhibitory RNases and are highly permissive to productive HIV infection. *Journal of virology,* 90**,** 7833-7847.
CICALA, C., ARTHOS, J. & FAUCI, A. S. 2011. HIV-1 envelope, integrins and co-receptor use in mucosal transmission of HIV. *Journal of translational medicine,* 9 Suppl 1**,** S2-S2.
CLARKE, R. W. 2015. Forces and Structures of the Herpes Simplex Virus (HSV) Entry Mechanism. *ACS Infectious Diseases,* 1**,** 403-415.
CLEMENT, C., TIWARI, V., SCANLAN, P. M., VALYI-NAGY, T., YUE, B. Y. & SHUKLA, D. 2006. A novel role for phagocytosis-like uptake in herpes simplex virus entry. *The Journal of cell biology,* 174**,** 1009-1021.
COHEN, E. A., TERWILLIGER, E. F., SODROSKI, J. G. & HASELTINE, W. A. 1988. Identification of a protein encoded by the vpu gene of HIV-1. *Nature,* 334**,** 532-534.
COHEN, J. I. 2020. Herpesvirus latency. *The Journal of clinical investigation,* 130**,** 3361-3369.
CONNICK, E., MATTILA, T., FOLKVORD, J. M., SCHLICHTEMEIER, R., MEDITZ, A. L., RAY, M. G., MCCARTER, M. D., MAWHINNEY, S., HAGE, A. & WHITE, C. 2007. CTL fail to accumulate at sites of HIV-1 replication in lymphoid tissue. *The Journal of Immunology,* 178**,** 6975-6983.
COOPER, R. S. & HELDWEIN, E. E. J. V. 2015. Herpesvirus gB: a finely tuned fusion machine. 7**,** 6552-6569.
COPE, A., LE FRIEC, G., CARDONE, J. & KEMPER, C. 2011. The Th1 life cycle: molecular control of IFN-γ to IL-10 switching. *Trends in immunology,* 32**,** 278-286.
CRAWFORD, D. H. 2013. *Virus hunt : the search for the origin of HIV/AIDs,* Oxford, OUP Oxford.
CROTTY, S. 2014. T follicular helper cell differentiation, function, and roles in disease. *Immunity,* 41**,** 529-542.
CUNNINGHAM, A. & NOBLE, J. 1989. Role of keratinocytes in human recurrent herpetic lesions. Ability to present herpes simplex virus antigen and act as targets for T lymphocyte cytotoxicity in vitro. *The Journal of clinical investigation,* 83**,** 490-496.
CUNNINGHAM, A. L., TURNER, R., MILLER, A. C., PARA, M. F. & MERIGAN, T. C. 1985. Evolution of recurrent herpes simplex lesions. An immunohistologic study. *The Journal of clinical investigation,* 75**,** 226-233.
CYSTER, J. G. 2005. Chemokines, sphingosine-1-phosphate, and cell migration in secondary lymphoid organs. *Annu. Rev. Immunol.,* 23**,** 127-159.
D'ETTORRE, G., BARONCELLI, S., MICCI, L., CECCARELLI, G., ANDREOTTI, M., SHARMA, P., FANELLO, G., FIOCCA, F., CAVALLARI, E. N., GIUSTINI, N., MALLANO, A., GALLUZZO, C. M., VELLA, S., MASTROIANNI, C. M., SILVESTRI, G., PAIARDINI, M., VULLO, V. & CECCHERINI-SILBERSTEIN, F. 2014. Reconstitution of Intestinal CD4 and Th17 T Cells in Antiretroviral Therapy

Suppressed HIV-Infected Subjects: Implication for Residual Immune Activation from the Results of a Clinical Trial. *PLoS ONE,* 9.

DAGENAIS-LUSSIER, X., AOUNALLAH, M., MEHRAJ, V., EL-FAR, M., TREMBLAY, C., SEKALY, R.-P., ROUTY, J.-P. & VAN GREVENYNGHE, J. 2016. Kynurenine reduces memory CD4 T-cell survival by interfering with interleukin-2 signaling early during HIV-1 infection. *Journal of virology,* 90**,** 7967-7979.

DAMBACHER, J., BEIGEL, F., ZITZMANN, K., DE TONI, E., GÖKE, B., DIEPOLDER, H. M., AUERNHAMMER, C. J. & BRAND, S. 2009. The role of the novel Th17 cytokine IL-26 in intestinal inflammation. *Gut,* 58**,** 1207-1217.

DAVEY, R., BHAT, N. & YODER, C. 1999. HIV-1 and T cell dynamics after interruption of highly active antiretroviral therapy (HAART) in patients with a history of sustained viral suppression. *Proceedings of the National Academy of Sciences of the United States of America,* 96**,** 15109-15114.

DE MONTE, A., OLIVIERI, C.-V., VITALE, S., BAILLEUX, S., CASTILLO, L., GIORDANENGO, V., MARYANSKI, J. L., SEGURA, E. & DOGLIO, A. 2016. CD1c-related DCs that express CD207/langerin, but are distinguishable from langerhans cells, are consistently present in human tonsils. *Frontiers in immunology,* 7**,** 197.

DEEKS, S. G., OVERBAUGH, J., PHILLIPS, A. & BUCHBINDER, S. 2015. HIV infection. *Nature reviews Disease primers,* 1**,** 1-22.

DEEKS, S. G. & WALKER, B. D. 2007. Human immunodeficiency virus controllers: mechanisms of durable virus control in the absence of antiretroviral therapy. *Immunity,* 27**,** 406-416.

DEEPAK, A. R., MICHAEL, F. G., JENNIFER, L. M., KAMIL, S., CHAMITH, Y. F., YANYAN, L., LAURA, T. D., LAUREN, A. H., KEVIN, W., FUMITAKA, M., NIKOLA, C. T., MICHAEL, E. W., ELENA, M. M., JONATHAN, S. C., SIMON, M. H., YVONNE, C. L., DERRICK, J. T., VIVIAN, P. B., SUSAN, M. G., ALESSANDRA, B. P., LIONEL, B. I., ELIZABETH, W. K., PETER, A. N., ANDREW, F., CHRISTOPHER, D. B., JAMES, A. L., SOUMYA, R. & MICHAEL, B. B. 2017. Pathologically expanded peripheral T helper cell subset drives B cells in rheumatoid arthritis. *Nature,* 542**,** 110.

DELEAGE, C., WIETGREFE, S. W., DEL PRETE, G., MORCOCK, D. R., HAO, X. P., PIATAK, M., JR., BESS, J., ANDERSON, J. L., PERKEY, K. E., REILLY, C., MCCUNE, J. M., HAASE, A. T., LIFSON, J. D., SCHACKER, T. W. & ESTES, J. D. 2016. Defining HIV and SIV Reservoirs in Lymphoid Tissues. *Pathog Immun,* 1**,** 68-106.

DESHMANE, S. L., KREMLEV, S., AMINI, S. & SAWAYA, B. E. 2009. Monocyte chemoattractant protein-1 (MCP-1): an overview. *Journal of interferon & cytokine research : the official journal of the International Society for Interferon and Cytokine Research,* 29**,** 313-326.

DINARELLO, C., NOVICK, D., KIM, S. & KAPLANSKI, G. J. F. I. I. 2013. Interleukin-18 and IL-18 binding protein. 4**,** 289.

DINH, M. H., ANDERSON, M. R., MCRAVEN, M. D., CIANCI, G. C., MCCOOMBE, S. G., KELLEY, Z., GIOIA, C. J., FOUGHT, A. J., RADEMAKER, A. W. & VEAZEY, R. S. 2015. Visualization of HIV-1 interactions with penile and foreskin epithelia: clues for female-to-male HIV transmission. *PLoS Pathog,* 11**,** e1004729.

DINH, M. H., HIRBOD, T., KIGOZI, G., OKOCHA, E. A., CIANCI, G. C., KONG, X., PRODGER, J. L., BROLIDEN, K., KAUL, R. & SERWADDA, D. 2012. No difference in keratin thickness between inner and outer foreskins from elective male circumcisions in Rakai, Uganda. *PLoS One,* 7**,** e41271.

DINH, M. H., MCRAVEN, M. D., KELLEY, Z., PENUGONDA, S. & HOPE, T. J. 2010. Keratinization of the adult male foreskin and implications for male circumcision. *AIDS (London, England),* 24**,** 899.

DONOVAL, B. A., LANDAY, A. L., MOSES, S., AGOT, K., NDINYA-ACHOLA, J., NYAGAYA, E. A., MACLEAN, I. & BAILEY, R. C. 2006. HIV-1 target cells in foreskins of African men with varying histories of sexually transmitted infections. *American journal of clinical pathology,* 125**,** 386-391.

DORFMAN, T., MAMMANO, F., HASELTINE, W. A. & GÖTTLINGER, H. G. 1994. Role of the matrix protein in the virion association of the human immunodeficiency virus type 1 envelope glycoprotein. *J Virol,* 68**,** 1689-96.

DOTIWALA, F. & LIEBERMAN, J. 2019. Granulysin: killer lymphocyte safeguard against microbes. *Current opinion in immunology,* 60**,** 19-29.

DUHEN, T., GEIGER, R., JARROSSAY, D., LANZAVECCHIA, A. & SALLUSTO, F. 2009. Production of interleukin 22 but not interleukin 17 by a subset of human skin-homing memory T cells. *Nature immunology,* 10**,** 857-863.

DULUC, D., GANNEVAT, J., ANGUIANO, E., ZURAWSKI, S., CARLEY, M., BOREHAM, M., STECHER, J., DULLAERS, M., BANCHEREAU, J. & OH, S. 2013. Functional diversity of human vaginal APC subsets in directing T-cell responses. *Mucosal immunology,* 6**,** 626-638.

DUSTIN, M. L., BROMLEY, S. K., KAN, Z., PETERSON, D. A. & UNANUE, E. R. 1997. Antigen Receptor Engagement Delivers a Stop Signal to Migrating T Lymphocytes. *Proceedings of the National Academy of Sciences - PNAS,* 94**,** 3909-3913.

DUTERTRE, C.-A., BECHT, E., IRAC, S. E., KHALILNEZHAD, A., NARANG, V., KHALILNEZHAD, S., NG, P. Y., VAN DEN HOOGEN, L. L., LEONG, J. Y. & LEE, B. 2019. Single-cell analysis of human mononuclear phagocytes reveals subset-defining markers and identifies circulating inflammatory dendritic cells. *Immunity,* 51**,** 573-589. e8.

EDWARDS, J. & MORRIS, H. 1985. Langerhans' cells and lymphocyte subsets in the female genita1 tract. *BJOG: An International Journal of Obstetrics & Gynaecology,* 92**,** 974-982.

EGAN, K. P., WU, S., WIGDAHL, B. & JENNINGS, S. R. 2013. Immunological control of herpes simplex virus infections. *Journal of neurovirology,* 19**,** 328-345.

EINKAUF, K. B., LEE, G. Q., GAO, C., SHARAF, R., SUN, X., HUA, S., CHEN, S. M. Y., JIANG, C., LIAN, X., CHOWDHURY, F. Z., ROSENBERG, E. S., CHUN, T.-W., LI, J. Z., YU, X. G. & LICHTERFELD, M. 2019. Intact HIV-1 proviruses accumulate at distinct chromosomal positions during prolonged antiretroviral therapy. *The Journal of Clinical Investigation,* 129**,** 988-998.

EISENBARTH, S. 2019. Dendritic cell subsets in T cell programming: location dictates function. *Nature Reviews Immunology,* 19**,** 89-103.

EL BILALI, N., DURON, J., GINGRAS, D. & LIPPÉ, R. J. J. O. V. 2017. Quantitative evaluation of protein heterogeneity within herpes simplex virus 1 particles. 91**,** e00320-17.

ELLER, M. A., GOONETILLEKE, N., TASSANEETRITHEP, B., ELLER, L. A., COSTANZO, M. C., JOHNSON, S., BETTS, M. R., KREBS, S. J., SLIKE, B. M., NITAYAPHAN, S., RONO, K., TOVANABUTRA, S., MAGANGA, L., KIBUUKA, H., JAGODZINSKI, L., PEEL, S., ROLLAND, M., MAROVICH, M. A., KIM, J. H., MICHAEL, N. L., ROBB, M. L. & STREECK, H. 2016. Expansion of Inefficient HIV-Specific CD8 T Cells during Acute Infection. *Journal of Virology,* 90**,** 4005.

EROSCHENKO, V. P. & DI FIORE, M. S. 2013. *DiFiore's atlas of histology with functional correlations*, Lippincott Williams & Wilkins.

EVANS, V. A., VAN DER SLUIS, R. M., SOLOMON, A., DANTANARAYANA, A., MCNEIL, C., GARSIA, R., PALMER, S., FROMENTIN, R., CHOMONT, N., SÉKALY, R.-P., CAMERON, P. U. & LEWIN, S. R. 2018. Programmed cell death-1 contributes to the establishment and maintenance of HIV-1 latency. *AIDS (London, England),* 32**,** 1491-1497.

FATAHZADEH, M. & SCHWARTZ, R. A. 2007. Human herpes simplex virus infections: epidemiology, pathogenesis, symptomatology, diagnosis, and management. *Journal of the American Academy of Dermatology,* 57**,** 737-763.

FEINGOLD, K. R. 2012. Lamellar bodies: the key to cutaneous barrier function. *Journal of Investigative Dermatology,* 132**,** 1951-1953.

FERNANDEZ, E. & MARULL-TUFEU, S. 2019. 3D imaging of human epidermis micromorphology by combining fluorescent dye, optical clearing and confocal microscopy. *Skin Research and Technology,* 25**,** 735-742.

FERNANDEZ, M. A., PUTTUR, F. K., WANG, Y. M., HOWDEN, W., ALEXANDER, S. I. & JONES, C. A. 2008. T regulatory cells contribute to the attenuated primary CD8+ and CD4+ T cell responses to herpes simplex virus type 2 in neonatal mice. *The Journal of immunology,* 180**,** 1556-1564.

FLACHER, V., BOUSCHBACHER, M., VERRONÈSE, E., MASSACRIER, C., SISIRAK, V., BERTHIER-VERGNES, O., DE SAINT-VIS, B., CAUX, C., DEZUTTER-DAMBUYANT, C. & LEBECQUE, S. 2006. Human Langerhans cells express a specific TLR profile and differentially respond to viruses and Gram-positive bacteria. *The Journal of Immunology,* 177**,** 7959-7967.

FONSECA, R., BEURA, L. K., QUARNSTROM, C. F., GHONEIM, H. E., FAN, Y., ZEBLEY, C. C., SCOTT, M. C., FARES-FREDERICKSON, N. J., WIJEYESINGHE, S. & THOMPSON, E. A. 2020. Developmental plasticity allows outside-in immune responses by resident memory T cells. *Nature immunology,* 21**,** 412-421.

FRADETTE, J., LAROUCHE, D., FUGÈRE, C., GUIGNARD, R., BEAUPARLANT, A., COUTURE, V., CAOUETTE-LABERGE, L., ROY, A. & GERMAIN, L. 2003. Normal human Merkel cells are present in epidermal cell populations isolated and cultured from glabrous and hairy skin sites. *J Invest Dermatol,* 120**,** 313-7.

FRANKEL, A. D. & YOUNG, J. A. 1998. HIV-1: fifteen proteins and an RNA. *Annual review of biochemistry,* 67**,** 1-25.

FRITSCH, R. D., SHEN, X., SIMS, G. P., HATHCOCK, K. S., HODES, R. J. & LIPSKY, P. E. 2005. Stepwise differentiation of CD4 memory T cells defined by expression of CCR7 and CD27. *The Journal of Immunology,* 175**,** 6489-6497.

FUJITA, H., NOGRALES, K. E., KIKUCHI, T., GONZALEZ, J., CARUCCI, J. A. & KRUEGER, J. G. 2009. Human Langerhans cells induce distinct IL-22-producing CD4+ T cells lacking IL-17 production. *Proceedings of the National Academy of Sciences,* 106**,** 21795-21800.

FURIO, L., BRIOTET, I., JOURNEAUX, A., BILLARD, H. & PÉGUET-NAVARRO, J. 2010. Human Langerhans cells are more efficient than CD14− CD1c+ dermal dendritic cells at priming naive CD4+ T cells. *Journal of investigative dermatology,* 130**,** 1345-1354.

GADSBØLL, A. S. Ø., JEE, M. H., AHLSTRÖM, M. G., DYRING-ANDERSEN, B., WOETMANN, A., ØDUM, N., JOHANSEN, J. D., GEISLER, C. & BONEFELD, C. M. J. C. D. 2021. Epidermal T cell subsets—Effect of age and antigen exposure in humans and mice. 84**,** 375-384.

GALIWANGO, R. M., YEGOROV, S., JOAG, V., PRODGER, J., SHAHABI, K., HUIBNER, S., MUYANJA, E., KABUUBI, B. R., NAMUNIINA, A. &

NALUTAAYA, A. 2019. Characterization of CD4+ T cell subsets and HIV susceptibility in the inner and outer foreskin of Ugandan men. *American Journal of Reproductive Immunology,* 82**,** e13143.
GANOR, Y. & BOMSEL, M. 2011. HIV-1 transmission in the male genital tract. *American Journal of Reproductive Immunology,* 65**,** 284-291.
GANOR, Y., ZHOU, Z., TUDOR, D., SCHMITT, A., VACHER-LAVENU, M., GIBAULT, L., THIOUNN, N., TOMASINI, J., WOLF, J. & BOMSEL, M. 2010. Within 1 h, HIV-1 uses viral synapses to enter efficiently the inner, but not outer, foreskin mucosa and engages Langerhans–T cell conjugates. *Mucosal immunology,* 3**,** 506-522.
GANSER-PORNILLOS, B. K., YEAGER, M. & SUNDQUIST, W. I. 2008. The structural biology of HIV assembly. *Current opinion in structural biology,* 18**,** 203-217.
GARG, H. & BLUMENTHAL, R. 2008. Role of HIV Gp41 mediated fusion/hemifusion in bystander apoptosis. *Cellular and molecular life sciences,* 65**,** 3134-3144.
GATTINONI, L., LUGLI, E., JI, Y., POS, Z., PAULOS, C. M., QUIGLEY, M. F., ALMEIDA, J. R., GOSTICK, E., YU, Z. & CARPENITO, C. 2011. A human memory T cell subset with stem cell–like properties. *Nature medicine,* 17**,** 1290-1297.
GATTINONI, L., SPEISER, D. E., LICHTERFELD, M. & BONINI, C. 2017. T memory stem cells in health and disease. *Nature medicine,* 23**,** 18-27.
GEE, K., GUZZO, C., CHE MAT, N. F., MA, W. & KUMAR, A. 2009. The IL-12 family of cytokines in infection, inflammation and autoimmune disorders. *Inflamm Allergy Drug Targets,* 8**,** 40-52.
GEISSMANN, F., PROST, C., MONNET, J.-P., DY, M., BROUSSE, N. & HERMINE, O. 1998. Transforming growth factor β1, in the presence of granulocyte/macrophage colony-stimulating factor and interleukin 4, induces differentiation of human peripheral blood monocytes into dendritic Langerhans cells. *The Journal of experimental medicine,* 187**,** 961-966.
GERL, V. 2020. RE: Single-cell RNA-seq reveals new types of human blood dendritic cells, monocytes, and progenitors.
GHEBREMICHAEL, M., LARSEN, U. & PAINTSIL, E. J. S. T. D. 2009. Association of age at first sex with HIV-1, HSV-2 and other sexual transmitted infections among women in northern Tanzania. 36**,** 570.
GILLIAM, A. C., KREMER, I. B., YOSHIDA, Y., STEVENS, S. R., TOOTELL, E., TEUNISSEN, M. B., HAMMERBERG, C. & COOPER, K. D. 1998. The human hair follicle: a reservoir of CD40+ B7-deficient Langerhans cells that repopulate epidermis after UVB exposure. *Journal of investigative dermatology,* 110**,** 422-427.
GIRARD, M., LAW, J. C., EDILOVA, M. I. & WATTS, T. H. 2020. Type I interferons drive the maturation of human DC3s with a distinct costimulatory profile characterized by high GITRL. *Science Immunology,* 5.
GONÇALVES, J., MOREIRA, E., SEQUEIRA, I. J., RODRIGUES, A. S., RUEFF, J. & BRÁS, A. 2016. Integration of HIV in the Human Genome: Which Sites Are Preferential? A Genetic and Statistical Assessment. *International Journal of Genomics,* 2016**,** 2168590.
GONZALEZ, E., DHANDA, R., BAMSHAD, M., MUMMIDI, S., GEEVARGHESE, R., CATANO, G., ANDERSON, S. A., WALTER, E. A., STEPHAN, K. T. & HAMMER, M. F. J. P. O. T. N. A. O. S. 2001. Global survey of genetic variation in CCR5, RANTES, and MIP-1α: impact on the epidemiology of the HIV-1 pandemic. 98**,** 5199-5204.
GOSSELIN, A., MONTEIRO, P., CHOMONT, N., DIAZ-GRIFFERO, F., SAID, E. A., FONSECA, S., WACLECHE, V., EL-FAR, M., BOULASSEL, M.-R. & ROUTY, J.-

P. 2010. Peripheral blood CCR4+ CCR6+ and CXCR3+ CCR6+ CD4+ T cells are highly permissive to HIV-1 infection. *The Journal of Immunology,* 184**,** 1604-1616.
GOTO, T., NAKAI, M. & IKUTA, K. 1998. The life-cycle of human immunodeficiency virus type 1. *Micron,* 29**,** 123-138.
GRESSER, I. 2015. On intuition and the discovery of interferon. *Cytokine growth factor reviews,* 26**,** 99-101.
GRICE, E. A. & SEGRE, J. A. 2011. The skin microbiome. *Nature reviews microbiology,* 9**,** 244-253.
GROVES, M. J. J. A. F. P. 2016. Genital herpes: a review. 93**,** 928-934.
GRÜNEWALD, K., DESAI, P., WINKLER, D. C., HEYMANN, J. B., BELNAP, D. M., BAUMEISTER, W. & STEVEN, A. C. 2003. Three-Dimensional Structure of Herpes Simplex Virus from Cryo-Electron Tomography. *Science,* 302**,** 1396.
GUILLIAMS, M., DUTERTRE, C.-A., SCOTT, C. L., MCGOVERN, N., SICHIEN, D., CHAKAROV, S., VAN GASSEN, S., CHEN, J., POIDINGER, M. & DE PRIJCK, S. 2016. Unsupervised high-dimensional analysis aligns dendritic cells across tissues and species. *Immunity,* 45**,** 669-684.
GUILLIAMS, M., GINHOUX, F., JAKUBZICK, C., NAIK, S. H., ONAI, N., SCHRAML, B. U., SEGURA, E., TUSSIWAND, R. & YONA, S. 2014. Dendritic cells, monocytes and macrophages: a unified nomenclature based on ontogeny. *Nature Reviews Immunology,* 14**,** 571-578.
GUNN, M., TANGEMANN, K., TAM, C. & CYSTER, J. 1998. A chemokine expressed in lymphoid high endothelial venules promotes the adhesion and chemotaxis of naive T lymphocytes. *Proceedings of the National Academy of Sciences of the United States of America,* 95**,** 258-263.
HALFORD, W. P. & SCHAFFER, P. A. 2001. ICP0 is required for efficient reactivation of herpes simplex virus type 1 from neuronal latency. *Journal of virology,* 75**,** 3240-3249.
HAMOUDI, M., SIMON-LORIERE, E., GASSER, R. & NEGRONI, M. 2013. Genetic diversity of the highly variable V1 region interferes with Human Immunodeficiency Virus type 1 envelope functionality.(Report). *Retrovirology,* 10.
HANIFFA, M., SHIN, A., BIGLEY, V., MCGOVERN, N., TEO, P., SEE, P., WASAN, P. S., WANG, X.-N., MALINARICH, F. & MALLERET, B. 2012. Human tissues contain CD141hi cross-presenting dendritic cells with functional homology to mouse CD103+ nonlymphoid dendritic cells. *Immunity,* 37**,** 60-73.
HARMAN, A. N., BYE, C. R., NASR, N., SANDGREN, K. J., KIM, M., MERCIER, S. K., BOTTING, R. A., LEWIN, S. R., CUNNINGHAM, A. L. & CAMERON, P. U. 2013a. Identification of lineage relationships and novel markers of blood and skin human dendritic cells. *The Journal of Immunology,* 190**,** 66-79.
HARMAN, A. N., KIM, M., NASR, N., SANDGREN, K. J. & CAMERON, P. U. 2013b. Tissue dendritic cells as portals for HIV entry. *Reviews in medical virology,* 23**,** 319-333.
HEATH, W. R. & CARBONE, F. R. 2013. The skin-resident and migratory immune system in steady state and memory: innate lymphocytes, dendritic cells and T cells. *Nature immunology,* 14**,** 978.
HELDWEIN, E. & KRUMMENACHER, C. 2008. Entry of herpesviruses into mammalian cells. *Cellular and molecular life sciences,* 65**,** 1653-1668.
HENRICSON, J., MULLER, D. A., BAKER, S. B., IREDAHL, F., TOGÖ, T. & ANDERSON, C. D. 2022. Micropuncture closure following high density microarray patch application in healthy subjects. *Skin Res Technol,* 28**,** 305-310.

HERNÁNDEZ-RUIZ, M., ZLOTNIK, A. J. J. O. I. & RESEARCH, C. 2017. Mucosal chemokines. 37**,** 62-70.

HIENER, B., HORSBURGH, B. A., EDEN, J.-S., BARTON, K., SCHLUB, T. E., LEE, E., VON STOCKENSTROM, S., ODEVALL, L., MILUSH, J. M., LIEGLER, T., SINCLAIR, E., HOH, R., BORITZ, E. A., DOUEK, D., FROMENTIN, R., CHOMONT, N., DEEKS, S. G., HECHT, F. M. & PALMER, S. 2017. Identification of Genetically Intact HIV-1 Proviruses in Specific CD4+ T Cells from Effectively Treated Participants. *Cell Reports,* 21**,** 813-822.

HILL, J. M., GARZA, H., HELMY, M. F., COOK, S. D., OSBORNE, P. A., JOHNSON, M., THOMPSON, H. W., GREEN, L. C., O'CALLAGHAN, R. J. & GEBHARDT, B. M. 1997. Nerve growth factor antibody stimulates reactivation of ocular herpes simplex virus type 1 in latently infected rabbits. *Journal of neurovirology,* 3**,** 206-211.

HILL, M., TACHEDJIAN, G. & MAK, J. 2005. The packaging and maturation of the HIV-1 Pol proteins. *Current HIV research,* 3**,** 73-85.

HIVGOV. 2025. *The Global HIV/AIDS Epidemic* [Online]. Available: https://www.hiv.gov/hiv-basics/overview/data-and-trends/global-statistics [Accessed 10/05/2025].

HLADIK, F. & HOPE, T. J. 2009. HIV infection of the genital mucosa in women. *Current HIV/AIDS Reports,* 6**,** 20-28.

HLADIK, F. & MCELRATH, M. J. 2008. Setting the stage: host invasion by HIV. *Nature Reviews Immunology,* 8**,** 447-457.

HLADIK, F., SAKCHALATHORN, P., BALLWEBER, L., LENTZ, G., FIALKOW, M., ESCHENBACH, D. & MCELRATH, M. J. 2007. Initial events in establishing vaginal entry and infection by human immunodeficiency virus type-1. *Immunity,* 26**,** 257-270.

HORSBURGH, B. A., LEE, E., HIENER, B., EDEN, J.-S., SCHLUB, T. E., VON STOCKENSTROM, S., ODEVALL, L., MILUSH, J. M., LIEGLER, T. & SINCLAIR, E. 2020. High levels of genetically intact HIV in HLA-DR+ memory T cells indicates their value for reservoir studies. *Aids,* 34**,** 659-668.

HOWLEY, P. M., KNIPE, D. M., COHEN, J. L. & DAMANIA, B. A. 2021. *Fields Virology: DNA Viruses*, Lippincott Williams & Wilkins.

HYMES, K. B., CHEUNG, T., GREENE, J. B., PROSE, N. S., MARCUS, A., BALLARD, H., WILLIAM, D. C. & LAUBENSTEIN, L. J. 1981. Kaposi's sarcoma in homosexual men-a report of eight cases. *Lancet,* 2**,** 598-600.

IBIRICU, I., MAURER, U. E. & GRÜNEWALD, K. 2013. Characterization of herpes simplex virus type 1 L-particle assembly and egress in hippocampal neurones by electron cryo-tomography. *Cellular microbiology,* 15**,** 285-291.

IDRISS, H. T. & NAISMITH, J. H. 2000. TNF alpha and the TNF receptor superfamily: structure-function relationship(s). *Microsc Res Tech,* 50**,** 184-95.

IIJIMA, N. & IWASAKI, A. 2014. A local macrophage chemokine network sustains protective tissue-resident memory CD4 T cells. *Science,* 346**,** 93-98.

ILDGRUBEN, A. K., SJÖBERG, I. M. & HAMMARSTRÖM, M.-L. K. 2003. Influence of hormonal contraceptives on the immune cells and thickness of human vaginal epithelium. *Obstetrics & Gynecology,* 102**,** 571-582.

IWASAKI, A. 2010. Antiviral immune responses in the genital tract: clues for vaccines. *Nature Reviews Immunology,* 10**,** 699-711.

IWATA, T., TANAKA, K., INOUE, Y., TOIYAMA, Y., HIRO, J., FUJIKAWA, H., OKUGAWA, Y., UCHIDA, K., MOHRI, Y. & KUSUNOKI, M. 2013. Macrophage inflammatory protein-3 alpha (MIP-3a) is a novel serum prognostic marker in patients with colorectal cancer. *J Surg Oncol,* 107**,** 160-6.

IYER, S. S. & CHENG, G. 2012. Role of interleukin 10 transcriptional regulation in inflammation and autoimmune disease. *Critical reviews in immunology,* 32**,** 23-63.
JAMES, C., HARFOUCHE, M., WELTON, N. J., TURNER, K. M., ABU-RADDAD, L. J., GOTTLIEB, S. L. & LOOKER, K. J. J. B. O. T. W. H. O. 2020. Herpes simplex virus: global infection prevalence and incidence estimates, 2016. 98**,** 315.
JEREB, M., LAINSCAK, M., MARIN, J. & POPOVIC, M. 2005. Herpes simplex virus infection limited to the brainstem. *Wien Klin Wochenschr,* 117**,** 495-9.
JIAO, Y.-M., LIU, C.-E., LUO, L.-J., ZHU, W.-J., ZHANG, T., ZHANG, L.-G., SU, L.-S., LI, H.-J. & WU, H. 2015. CD4+ CD25+ CD127 regulatory cells play multiple roles in maintaining HIV-1 p24 production in patients on long-term treatment: HIV-1 p24-producing cells and suppression of anti-HIV immunity. *International Journal of Infectious Diseases,* 37**,** 42-49.
JOERIS, T., MÜLLER-LUDA, K., AGACE, W. W. & MOWAT, A. M. 2017. Diversity and functions of intestinal mononuclear phagocytes. *Mucosal Immunology,* 10**,** 845-864.
JOHANSSON, M. E., SJÖVALL, H., HANSSON, G. C. J. N. R. G. & HEPATOLOGY 2013. The gastrointestinal mucus system in health and disease. 10**,** 352-361.
JULIEN, J.-P., CUPO, A., SOK, D., STANFIELD, R. L., LYUMKIS, D., DELLER, M. C., KLASSE, P.-J., BURTON, D. R., SANDERS, R. W., MOORE, J. P., WARD, A. B. & WILSON, I. A. 2013. Crystal structure of a soluble cleaved HIV-1 envelope trimer. *Science (New York, N.Y.),* 342**,** 1477-1483.
KANG, J., VOLKMANN, A. & RAULET, D. H. 2001. Evidence that γδ versus αβ T cell fate determination is initiated independently of T cell receptor signaling. *Journal of Experimental Medicine,* 193**,** 689-698.
KANITAKIS, J., MORELON, E., PETRUZZO, P., BADET, L. & DUBERNARD, J. M. 2011. Self-renewal capacity of human epidermal Langerhans cells: observations made on a composite tissue allograft. *Experimental dermatology,* 20**,** 145-146.
KAPLAN, D. H., JENISON, M. C., SAELAND, S., SHLOMCHIK, W. D. & SHLOMCHIK, M. J. 2005. Epidermal langerhans cell-deficient mice develop enhanced contact hypersensitivity. *Immunity,* 23**,** 611-620.
KARA, E. E., COMERFORD, I., BASTOW, C. R., FENIX, K. A., LITCHFIELD, W., HANDEL, T. M. & MCCOLL, S. R. 2013. Distinct chemokine receptor axes regulate Th9 cell trafficking to allergic and autoimmune inflammatory sites. *The Journal of Immunology,* 191**,** 1110-1117.
KIM, M., TRUONG, N. R., JAMES, V., BOSNJAK, L., SANDGREN, K. J., HARMAN, A. N., NASR, N., BERTRAM, K. M., OLBOURNE, N., SAWLESHWARKAR, S., MCKINNON, K., COHEN, R. C. & CUNNINGHAM, A. L. 2015. Relay of herpes simplex virus between Langerhans cells and dermal dendritic cells in human skin. *PLoS pathogens,* 11**,** e1004812-e1004812.
KIMBERLIN, D. W. & ROUSE, D. J. 2004. Genital herpes. *New England Journal of Medicine,* 350**,** 1970-1977.
KITCHEN, A., SHACKELTON, L. A. & HOLMES, E. C. 2011. Family level phylogenies reveal modes of macroevolution in RNA viruses. *Proceedings of the National Academy of Sciences,* 108**,** 238-243.
KLATT, N. R., BOSINGER, S. E., PECK, M., RICHERT-SPUHLER, L. E., HEIGELE, A., GILE, J. P., PATEL, N., TAAFFE, J., JULG, B. & CAMERINI, D. 2014. Limited HIV infection of central memory and stem cell memory CD4+ T cells is associated with lack of progression in viremic individuals. *PLoS Pathog,* 10**,** e1004345.
KLEBANOFF, S. J. & COOMBS, R. W. 1991. Viricidal effect of Lactobacillus acidophilus on human immunodeficiency virus type 1: possible role in heterosexual transmission. *The Journal of experimental medicine,* 174**,** 289-292.

KNICKELBEIN, J. E., KHANNA, K. M., YEE, M. B., BATY, C. J., KINCHINGTON, P. R. & HENDRICKS, R. L. 2008. Noncytotoxic lytic granule–mediated CD8+ T cell inhibition of HSV-1 reactivation from neuronal latency. *Science,* 322**,** 268-271.

KOCH, U. & RADTKE, F. 2011. Mechanisms of T cell development and transformation. *Annual review of cell and developmental biology,* 27**,** 539-562.

KÖK, A., HOCQUELOUX, L., HOCINI, H., CARRIÈRE, M., LEFROU, L., GUGUIN, A., TISSERAND, P., BONNABAU, H., AVETTAND-FENOEL, V. & PRAZUCK, T. 2015. Early initiation of combined antiretroviral therapy preserves immune function in the gut of HIV-infected patients. *Mucosal immunology,* 8**,** 127-140.

KOLB, A. W., ANÉ, C. & BRANDT, C. R. 2013. Using HSV-1 genome phylogenetics to track past human migrations. *PloS one,* 8**,** e76267-e76267.

KUCHROO, K. V., ANDERSON, C. A. & PETROVAS, C. C. 2014. Coinhibitory receptors and CD8 T cell exhaustion in chronic infections. *Current Opinion in HIV and AIDS,* 9**,** 439-445.

KUKHANOVA, M., KOROVINA, A. & KOCHETKOV, S. 2014. Human herpes simplex virus: life cycle and development of inhibitors. *Biochemistry (Moscow),* 79**,** 1635-1652.

KUMAR, B. V., MA, W., MIRON, M., GRANOT, T., GUYER, R. S., CARPENTER, D. J., SENDA, T., SUN, X., HO, S.-H. & LERNER, H. 2017. Human tissue-resident memory T cells are defined by core transcriptional and functional signatures in lymphoid and mucosal sites. *Cell reports,* 20**,** 2921-2934.

LAHOUASSA, H., DADDACHA, W., HOFMANN, H., AYINDE, D., LOGUE, E. C., DRAGIN, L., BLOCH, N., MAUDET, C., BERTRAND, M. & GRAMBERG, T. 2012. SAMHD1 restricts the replication of human immunodeficiency virus type 1 by depleting the intracellular pool of deoxynucleoside triphosphates. *Nature immunology,* 13**,** 223.

LANGERHANS, P. 1868. Über die Nerven der menschlichen Haut. *Archiv für pathologische Anatomie und Physiologie und für klinische Medicin,* 44**,** 325-337.

LANZAVECCHIA, A. 1998. Immunology. Licence to kill. *Nature,* 393**,** 413-4.

LE ROUZIC, E. & BENICHOU, S. 2005. The Vpr protein from HIV-1: distinct roles along the viral life cycle. *Retrovirology,* 2**,** 1-14.

LEE, G. Q., ORLOVA-FINK, N., EINKAUF, K., CHOWDHURY, F. Z., SUN, X., HARRINGTON, S., KUO, H.-H., HUA, S., CHEN, H.-R. & OUYANG, Z. 2017. Clonal expansion of genome-intact HIV-1 in functionally polarized Th1 CD4+ T cells. *The Journal of clinical investigation,* 127**,** 2689-2696.

LEE, S. W., PARK, Y., YOO, J. K., CHOI, S. Y. & SUNG, Y. C. 2003. Inhibition of TCR-induced CD8 T cell death by IL-12: regulation of Fas ligand and cellular FLIP expression and caspase activation by IL-12. *The Journal of Immunology,* 170**,** 2456-2460.

LEMOS, M. P., LAMA, J. R., KARUNA, S. T., FONG, Y., MONTANO, S. M., GANOZA, C., GOTTARDO, R., SANCHEZ, J. & MCELRATH, M. J. 2014. The inner foreskin of healthy males at risk of HIV infection harbors epithelial CD4+ CCR5+ cells and has features of an inflamed epidermal barrier. *PloS one,* 9**,** e108954.

LI, G., NUNOYA, J.-I., CHENG, L., RESZKA-BLANCO, N., TSAO, L.-C., JEFFREY, J. & SU, L. 2017. Regulatory T Cells Contribute to HIV-1 Reservoir Persistence in CD4+ T Cells Through Cyclic Adenosine Monophosphate–Dependent Mechanisms in Humanized Mice In Vivo. *The Journal of infectious diseases,* 216**,** 1579-1591.

LI, J. H., ROSEN, D., SONDEL, P. & BERKE, G. 2002. Immune privilege and FasL: two ways to inactivate effector cytotoxic T lymphocytes by FasL-expressing cells. *Immunology,* 105**,** 267-277.

LIAW, F.-Y., HUANG, C.-F., HSUEH, J.-T. & CHIANG, C.-P. J. C. F. P. 2012. Eczema herpeticum: a medical emergency. 58**,** 1358-1361.

LIEBENBERG, L. J., MASSON, L., ARNOLD, K. B., MCKINNON, L. R., WERNER, L., PROCTOR, E., ARCHARY, D., MANSOOR, L. E., LAUFFENBURGER, D. A. & KARIM, Q. A. J. J. O. A. I. D. S. 2017. Genital—systemic chemokine gradients and the risk of HIV Acquisition in Women. 74**,** 318.

LIJUN, W., NORMA, P. G., RICHARD, W., HYERYUN, C., CRISTINA, P., NANCY, R., ALESSÂNDRA, B., ANGELO, A. C., ELIZABETH, D., WALTER, N., CRAIG, G. & JOSEPH, S. 1996. CD4-induced interaction of primary HIV-1 gp120 glycoproteins with the chemokine receptor CCR-5. *Nature,* 384**,** 179.

LIKHOSHVAI, V. A., KHLEBODAROVA, T. M., BAZHAN, S. I., GAINOVA, I. A., CHERESHNEV, V. A. & BOCHAROV, G. A. 2014. Mathematical model of the Tat-Rev regulation of HIV-1 replication in an activated cell predicts the existence of oscillatory dynamics in the synthesis of viral components. *BMC genomics,* 15**,** 1-18.

LINTERMANS, L. L., RUTGERS, A., STEGEMAN, C. A., HEERINGA, P. & ABDULAHAD, W. H. 2017. Chemokine receptor co-expression reveals aberrantly distributed TH effector memory cells in GPA patients. *Arthritis research & therapy,* 19**,** 1-11.

LIU, A., YANG, Y., LIU, L., MENG, Z., LI, L., QIU, C., XU, J. & ZHANG, X. 2014a. Differential compartmentalization of HIV-targeting immune cells in inner and outer foreskin tissue. *PLoS One,* 9**,** e85176.

LIU, M., GUO, S., HIBBERT, J. M., JAIN, V., SINGH, N., WILSON, N. O. & STILES, J. K. 2011. CXCL10/IP-10 in infectious diseases pathogenesis and potential therapeutic implications. *Cytokine & growth factor reviews,* 22**,** 121-130.

LIU, R.-D., WU, J., SHAO, R. & XUE, Y.-H. 2014b. Mechanism and factors that control HIV-1 transcription and latency activation. *Journal of Zhejiang University. Science. B,* 15**,** 455-465.

LLOYD, J., CROUCH, N. S., MINTO, C. L., LIAO, L. M. & CREIGHTON, S. M. 2005. Female genital appearance:'normality'unfolds. *BJOG: An International Journal of Obstetrics & Gynaecology,* 112**,** 643-646.

LÖHNING, M., HEGAZY, A. N., PINSCHEWER, D. D., BUSSE, D., LANG, K. S., HÖFER, T., RADBRUCH, A., ZINKERNAGEL, R. M. & HENGARTNER, H. 2008. Long-lived virus-reactive memory T cells generated from purified cytokine-secreting T helper type 1 and type 2 effectors. *The Journal of experimental medicine,* 205**,** 53-61.

LOOKER, K. J., ELMES, J. A., GOTTLIEB, S. L., SCHIFFER, J. T., VICKERMAN, P., TURNER, K. M. & BOILY, M.-C. 2017. Effect of HSV-2 infection on subsequent HIV acquisition: an updated systematic review and meta-analysis. *The Lancet infectious diseases,* 17**,** 1303-1316.

LOOKER, K. J., GARNETT, G. P. & SCHMID, G. P. 2008. An estimate of the global prevalence and incidence of herpes simplex virus type 2 infection. *Bulletin of the World Health Organization,* 86**,** 805-812.

LOOKER, K. J., JOHNSTON, C., WELTON, N. J., JAMES, C., VICKERMAN, P., TURNER, K. M., BOILY, M.-C. & GOTTLIEB, S. L. J. B. G. H. 2020. The global and regional burden of genital ulcer disease due to herpes simplex virus: a natural history modelling study. 5**,** e001875.

LOPEZ-CASTEJON, G. & BROUGH, D. 2011. Understanding the mechanism of IL-1β secretion. *Cytokine & growth factor reviews,* 22**,** 189-195.

LU, K., HENG, X. & SUMMERS, M. F. 2011. Structural determinants and mechanism of HIV-1 genome packaging. *J Mol Biol,* 410**,** 609-33.

LUEBCKE, E., DUBOVI, E., BLACK, D., OHSAWA, K. & EBERLE, R. 2006. Isolation and characterization of a chimpanzee alphaherpesvirus. *Journal of General Virology,* 87**,** 11-19.

LUGLI, E., DOMINGUEZ, M. H., GATTINONI, L., CHATTOPADHYAY, P. K., BOLTON, D. L., SONG, K., KLATT, N. R., BRENCHLEY, J. M., VACCARI, M. & GOSTICK, E. 2013. Superior T memory stem cell persistence supports long-lived T cell memory. *The Journal of clinical investigation,* 123.

LUNDBERG, K., ALBREKT, A.-S., NELISSEN, I., SANTEGOETS, S., DE GRUIJL, T. D., GIBBS, S. & LINDSTEDT, M. 2013. Transcriptional profiling of human dendritic cell populations and models-unique profiles of in vitro dendritic cells and implications on functionality and applicability. *PloS one,* 8**,** e52875.

MACKAY, L. K., BRAUN, A., MACLEOD, B. L., COLLINS, N., TEBARTZ, C., BEDOUI, S., CARBONE, F. R. & GEBHARDT, T. 2015a. Cutting edge: CD69 interference with sphingosine-1-phosphate receptor function regulates peripheral T cell retention. *The Journal of Immunology,* 194**,** 2059-2063.

MACKAY, L. K., WYNNE-JONES, E., FREESTONE, D., PELLICCI, D. G., MIELKE, L. A., NEWMAN, D. M., BRAUN, A., MASSON, F., KALLIES, A. & BELZ, G. T. 2015b. T-box transcription factors combine with the cytokines TGF-β and IL-15 to control tissue-resident memory T cell fate. *Immunity,* 43**,** 1101-1111.

MAGARET, A. S., MUJUGIRA, A., HUGHES, J. P., LINGAPPA, J., BUKUSI, E. A., DEBRUYN, G., DELANY-MORETLWE, S., FIFE, K. H., GRAY, G. E. & KAPIGA, S. J. C. I. D. 2016. Effect of condom use on per-act HSV-2 transmission risk in HIV-1, HSV-2-discordant couples. 62**,** 456-461.

MAGARET, C. A., BENKESER, D. C., WILLIAMSON, B. D., BORATE, B. R., CARPP, L. N., GEORGIEV, I. S., SETLIFF, I., DINGENS, A. S., SIMON, N. & CARONE, M. 2019. Prediction of VRC01 neutralization sensitivity by HIV-1 gp160 sequence features. *PLoS computational biology,* 15**,** e1006952.

MAHER, D., WU, X., SCHACKER, T., HORBUL, J. & SOUTHERN, P. 2005. HIV binding, penetration, and primary infection in human cervicovaginal tissue. *Proc Natl Acad Sci U S A,* 102**,** 11504-9.

MAHNKE, Y. D., BRODIE, T. M., SALLUSTO, F., ROEDERER, M. & LUGLI, E. 2013. The who's who of T-cell differentiation: human memory T-cell subsets. *European journal of immunology,* 43**,** 2797-2809.

MALKIN, J.-E. J. H. T. J. O. T. I. 2004. Epidemiology of genital herpes simplex virus infection in developed countries. 11**,** 2A-23A.

MANTOVANI, A., BISWAS, S. K., GALDIERO, M. R., SICA, A. & LOCATI, M. 2013. Macrophage plasticity and polarization in tissue repair and remodelling. *The Journal of pathology,* 229**,** 176-185.

MARBAN, C., FOROUZANFAR, F., AIT-AMMAR, A., FAHMI, F., EL MEKDAD, H., DAOUAD, F., ROHR, O. & SCHWARTZ, C. 2016. Targeting the Brain Reservoirs: Toward an HIV Cure. *Frontiers in Immunology,* 7.

MARIEB, E. N. & HOEHN, K. 2007. *Human anatomy & physiology*, Pearson education.

MARSDEN, V., DONAGHY, H., BERTRAM, K. M., HARMAN, A. N., NASR, N., KEOSHKERIAN, E., MERTEN, S., LLOYD, A. R. & CUNNINGHAM, A. L. 2015. Herpes simplex virus type 2-infected dendritic cells produce TNF-α, which enhances CCR5 expression and stimulates HIV production from adjacent infected cells. *The Journal of immunology (1950),* 194**,** 4438-4445.

MARTÍNEZ-CINGOLANI, C., GRANDCLAUDON, M., JEANMOUGIN, M., JOUVE, M., ZOLLINGER, R. & SOUMELIS, V. 2014. Human blood BDCA-1 dendritic cells

differentiate into Langerhans-like cells with thymic stromal lymphopoietin and TGF-β. *Blood, The Journal of the American Society of Hematology,* 124**,** 2411-2420.
MARTINEZ-PICADO, J. & DEEKS, S. G. 2016. Persistent HIV-1 replication during antiretroviral therapy. *Current Opinion in HIV and AIDS,* 11**,** 417.
MARTINEZ, F. O. & GORDON, S. 2014. The M1 and M2 paradigm of macrophage activation: time for reassessment. *F1000prime reports,* 6.
MARX, P. A., SPIRA, A. I., GETTIE, A., DAILEY, P. J., VEAZEY, R. S., LACKNER, A. A., MAHONEY, C. J., MILLER, C. J., CLAYPOOL, L. E., HO, D. D. & ALEXANDER, N. J. 1996. Progesterone implants enhance SIV vaginal transmission and early virus load. *Nat Med,* 2**,** 1084-9.
MASESE, L., BAETEN, J. M., RICHARDSON, B. A., BUKUSI, E., JOHN-STEWART, G., GRAHAM, S. M., SHAFI, J., KIARIE, J., OVERBAUGH, J. & MCCLELLAND, R. S. 2015. Changes in the contribution of genital tract infections to HIV acquisition among Kenyan high-risk women from 1993 to 2012. *AIDS (London, England),* 29**,** 1077.
MASS, E., BALLESTEROS, I., FARLIK, M., HALBRITTER, F., GÜNTHER, P., CROZET, L., JACOME-GALARZA, C. E., HÄNDLER, K., KLUGHAMMER, J. & KOBAYASHI, Y. 2016. Specification of tissue-resident macrophages during organogenesis. *Science,* 353.
MATHERS, A. R., JANELSINS, B. M., RUBIN, J. P., TKACHEVA, O. A., SHUFESKY, W. J., WATKINS, S. C., MORELLI, A. E. & LARREGINA, A. T. 2009. Differential capability of human cutaneous dendritic cell subsets to initiate Th17 responses. *The Journal of Immunology,* 182**,** 921-933.
MAURER, M. & VON STEBUT, E. 2004. Macrophage inflammatory protein-1. *The International Journal of Biochemistry & Cell Biology,* 36**,** 1882-1886.
MCCOOMBE, S. G. & SHORT, R. V. 2006. Potential HIV-1 target cells in the human penis. *Aids,* 20**,** 1491-1495.
MCCORMACK, A. L., RABIE, N., WHITTEMORE, B., MURPHY, T., SITLER, C., MAGANN, E. J. O. & SURVEY, G. 2019. HSV hepatitis in pregnancy: a review of the literature. 74**,** 93-98.
MCCUNE, J. M. 2001. The dynamics of CD4+ T-cell depletion in HIV disease. *Nature,* 410**,** 974-979.
MCDONALD, D., WU, L., BOHKS, S. M., KEWALRAMANI, V. N., UNUTMAZ, D. & HOPE, T. J. 2003. Recruitment of HIV and its receptors to dendritic cell-T cell junctions. *Science,* 300**,** 1295-1297.
MCELWEE, M., VIJAYAKRISHNAN, S., RIXON, F. & BHELLA, D. J. P. B. 2018. Structure of the herpes simplex virus portal-vertex. 16**,** e2006191.
MCGARY, C. S., DELEAGE, C., HARPER, J., MICCI, L., RIBEIRO, S. P., PAGANINI, S., KURI-CERVANTES, L., BENNE, C., RYAN, E. S. & BALDERAS, R. 2017. CTLA-4+ PD-1− memory CD4+ T cells critically contribute to viral persistence in antiretroviral therapy-suppressed, SIV-infected rhesus macaques. *Immunity,* 47**,** 776-788. e5.
MCGOVERN, N., SCHLITZER, A., GUNAWAN, M., JARDINE, L., SHIN, A., POYNER, E., GREEN, K., DICKINSON, R., WANG, X.-N. & LOW, D. 2014. Human dermal CD14+ cells are a transient population of monocyte-derived macrophages. *Immunity,* 41**,** 465-477.
MCKINNON, L. R., LIEBENBERG, L. J., YENDE-ZUMA, N., ARCHARY, D., NGCAPU, S., SIVRO, A., NAGELKERKE, N., LERMA, J. G. G., KASHUBA, A. D. & MASSON, L. 2018. Genital inflammation undermines the effectiveness of tenofovir gel in preventing HIV acquisition in women. *Nature medicine,* 24**,** 491.

MELLORS, J. W., RINALDO, C. R., GUPTA, P., WHITE, R. M., TODD, J. A. & KINGSLEY, L. A. 1996. Prognosis in HIV-1 infection predicted by the quantity of virus in plasma. *Science,* 272**,** 1167-1170.

METTENLEITER, T. C., KLUPP, B. G. & GRANZOW, H. 2006. Herpesvirus assembly: a tale of two membranes. *Current Opinion in Microbiology,* 9**,** 423-429.

METTENLEITER, T. C., KLUPP, B. G. & GRANZOW, H. 2009. Herpesvirus assembly: an update. *Virus research,* 143**,** 222-234.

MEZIANE, O., SALAHUDDIN, S., PHAM, T. N., FARNOS, O., PAGLIUZZA, A., OLIVENSTEIN, R., THOMSON, E., ALEXANDROVA, Y., ORLOVA, M. & SCHURR, E. 2020. HIV infection and persistence in pulmonary mucosal double negative T cells in vivo. *Journal of Virology,* 94**,** 10.1128/jvi. 01788-20.

MIGUELES, S. A., LABORICO, A. C., SHUPERT, W. L., SABBAGHIAN, M. S., RABIN, R., HALLAHAN, C. W., VAN BAARLE, D., KOSTENSE, S., MIEDEMA, F. & MCLAUGHLIN, M. 2002. HIV-specific CD8+ T cell proliferation is coupled to perforin expression and is maintained in nonprogressors. *Nature immunology,* 3**,** 1061-1068.

MIGUELES, S. A., OSBORNE, C. M., ROYCE, C., COMPTON, A. A., JOSHI, R. P., WEEKS, K. A., ROOD, J. E., BERKLEY, A. M., SACHA, J. B. & COGLIANO-SHUTTA, N. A. 2008. Lytic granule loading of CD8+ T cells is required for HIV-infected cell elimination associated with immune control. *Immunity,* 29**,** 1009-1021.

MIKLOSKA, Z., DANIS, V. A., ADAMS, S., LLOYD, A. R., ADRIAN, D. L. & CUNNINGHAM, A. L. J. J. O. I. D. 1998. In vivo production of cytokines and β (CC) chemokines in human recurrent herpes simplex lesions—do herpes simplex virus-infected keratinocytes contribute to their production? 177**,** 827-838.

MILLER, A. M. 2011. Role of IL-33 in inflammation and disease. *Journal of inflammation (London, England),* 8**,** 22-22.

MILLER, C. J., LI, Q., ABEL, K., KIM, E.-Y., MA, Z.-M., WIETGREFE, S., LA FRANCO-SCHEUCH, L., COMPTON, L., DUAN, L., SHORE, M. D., ZUPANCIC, M., BUSCH, M., CARLIS, J., WOLINKSY, S. & HAASE, A. T. 2005. Propagation and Dissemination of Infection after Vaginal Transmission of Simian Immunodeficiency Virus. *The Journal of Virology,* 79**,** 9217.

MILLER, J. C., BROWN, B. D., SHAY, T., GAUTIER, E. L., JOJIC, V., COHAIN, A., PANDEY, G., LEBOEUF, M., ELPEK, K. G. & HELFT, J. 2012. Deciphering the transcriptional network of the dendritic cell lineage. *Nature immunology,* 13**,** 888.

MILNE, P., BIGLEY, V., GUNAWAN, M., HANIFFA, M. & COLLIN, M. 2015. CD1c+ blood dendritic cells have Langerhans cell potential. *Blood, The Journal of the American Society of Hematology,* 125**,** 470-473.

MINAYA, M. A., JENSEN, T. L., GOLL, J. B., KOROM, M., DATLA, S. H., BELSHE, R. B. & MORRISON, L. A. 2017. Molecular evolution of herpes simplex virus 2 complete genomes: comparison between primary and recurrent infections. *Journal of virology,* 91.

MIRANDA-SAKSENA, M., DENES, C. E., DIEFENBACH, R. J. & CUNNINGHAM, A. L. 2018. Infection and Transport of Herpes Simplex Virus Type 1 in Neurons: Role of the Cytoskeleton. *Viruses,* 10.

MO, Y., CHEUNG, A. K. L., LIU, Y., LIU, L. & CHEN, Z. 2020. Δ42PD1-TLR4 augments γδ-T cell activation of the transitional memory subset of CD4+ T cells. *Iscience,* 23**,** 101620.

MOHAMMADI, P., DESFARGES, S., BARTHA, I., JOOS, B., ZANGGER, N., MUNOZ, M., GÜNTHARD, H. F., BEERENWINKEL, N., TELENTI, A. & CIUFFI, A. 2013. 24 hours in the life of HIV-1 in a T cell line. *PLoS pathogens,* 9**,** e1003161.

MOSES, S. 2009. Male circumcision: a new approach to reducing HIV transmission. *Cmaj,* 181**,** E134-E135.

MOSTAFA, G. A. & AL-AYADHI, L. Y. 2015. The possible link between elevated serum levels of epithelial cell-derived neutrophil- activating peptide-78 (ENA-78/CXCL5) and autoimmunity in autistic children. *Behavioral and Brain Functions,* 11**,** 11.

MSELLE, T. F., MEADOWS, S. K., ERIKSSON, M., SMITH, J. M., SHEN, L., WIRA, C. R. & SENTMAN, C. L. 2007. Unique characteristics of NK cells throughout the human female reproductive tract. *Clinical immunology,* 124**,** 69-76.

MURRAY, A. J., KWON, K. J., FARBER, D. L. & SILICIANO, R. F. 2016. The latent reservoir for HIV-1: how immunologic memory and clonal expansion contribute to HIV-1 persistence. *The Journal of Immunology,* 197**,** 407-417.

MURRAY, J. M., KELLEHER, A. D. & COOPER, D. A. 2011. Timing of the components of the HIV life cycle in productively infected CD4+ T cells in a population of HIV-infected individuals. *J Virol,* 85**,** 10798-805.

MUSUMECI, A., LUTZ, K., WINHEIM, E. & KRUG, A. B. 2019. What Makes a pDC: Recent Advances in Understanding Plasmacytoid DC Development and Heterogeneity. *Front Immunol,* 10**,** 1222.

NAHMIAS, A., PLOWRIGHT, W., RAPP, F., SHELDRICK, P., TAKAHASHI, M. & WOLF, K. 1981. Herpesviridae. Definition, provisional nomenclature, and taxonomy. The Herpesvirus Study Group, the International Committee on Taxonomy of Viruses. *Intervirology,* 16**,** 201217.

NAKANISHI, Y., LU, B., GERARD, C. & IWASAKI, A. 2009. CD8+ T lymphocyte mobilization to virus-infected tissue requires CD4+ T-cell help. *Nature,* 462**,** 510-513.

NASR, N., LAI, J., BOTTING, R. A., MERCIER, S. K., HARMAN, A. N., KIM, M., TURVILLE, S., CENTER, R. J., DOMAGALA, T. & GORRY, P. R. 2014. Inhibition of two temporal phases of HIV-1 transfer from primary Langerhans cells to T cells: the role of langerin. *The Journal of Immunology,* 193**,** 2554-2564.

NAYRAC, M., REQUENA, M., LOISEAU, C., CAZABAT, M., SUC, B., CARRERE, N., BARANGE, K., ALRIC, L., MARTIN-BLONDEL, G. & IZOPET, J. 2021. Th22 cells are efficiently recruited in the gut by CCL28 as an alternative to CCL20 but do not compensate for the loss of Th17 cells in treated HIV-1-infected individuals. *Mucosal immunology,* 14**,** 219-228.

NEIL, J. E., BROWN, M. B. & WILLIAMS, A. C. 2020. Human skin explant model for the investigation of topical therapeutics. *Scientific Reports,* 10**,** 21192.

NEUMANN, L., KRAAS, W., UEBEL, S., JUNG, G. & TAMPÉ, R. 1997. The active domain of the herpes simplex virus protein ICP47: A potent inhibitor of the transporter associated with antigen processing (TAP). *Journal of molecular biology,* 272**,** 484-492.

NGUYEN, Q. P., DENG, T. Z., WITHERDEN, D. A. & GOLDRATH, A. W. 2019. Origins of CD 4+ circulating and tissue-resident memory T-cells. *Immunology,* 157**,** 3-12.

NICOLA, A. V. & STRAUS, S. E. 2004. Cellular and viral requirements for rapid endocytic entry of herpes simplex virus. *Journal of virology,* 78**,** 7508-7517.

NICOLL, M. P., PROENÇA, J. T. & EFSTATHIOU, S. 2012. The molecular basis of herpes simplex virus latency. *FEMS microbiology reviews,* 36**,** 684-705.

NUNO, R. F., ANDREW, R., MARC, A. S., GUY, B., TREVOR, B., MELISSA, J. W., ANDREW, J. T., JOÃO, D. S., NIMALAN, A., JACQUES, P., DAVID, P., MARTINE, P., OLIVER, G. P. & PHILIPPE, L. 2014. The early spread and epidemic ignition of HIV-1 in human populations. *Science (American Association for the Advancement of Science),* 346**,** 56-61.

NUUTILA, K., SILTANEN, A., PEURA, M., BIZIK, J., KAARTINEN, I., KUOKKANEN, H., NIEMINEN, T., HARJULA, A., AARNIO, P., VUOLA, J. & KANKURI, E. 2012. Human skin transcriptome during superficial cutaneous wound healing. *Wound Repair Regen,* 20**,** 830-9.

O'NEIL, T. R. 2023. *Defining the human mucosal CD4+ T cell and Mononuclear Phagocyte landscape by high parameter technologies.* Doctor of Philosophy, University of Sydney.

O'NEIL, T. R., HU, K., TRUONG, N. R., ARSHAD, S., SHACKLETT, B. L., CUNNINGHAM, A. L. & NASR, N. 2021. The Role of Tissue Resident Memory CD4 T Cells in Herpes Simplex Viral and HIV Infection. *Viruses,* 13**,** 359.

OH, J., IIJIMA, N., SONG, E., LU, P., KLEIN, J., JIANG, R., KLEINSTEIN, S. & IWASAKI, A. 2019. Migrant memory B cells secrete luminal antibody in the vagina. *Nature,* 571**,** 122-5.

OH, M. J., AKHTAR, J., DESAI, P. & SHUKLA, D. 2010. A role for heparan sulfate in viral surfing. *Biochem Biophys Res Commun,* 391**,** 176-81.

OKADA, R., KONDO, T., MATSUKI, F., TAKATA, H. & TAKIGUCHI, M. 2008. Phenotypic classification of human CD4+ T cell subsets and their differentiation. *International immunology,* 20**,** 1189-1199.

OLARU, F. & JENSEN, L. E. 2010. Chemokine expression by human keratinocyte cell lines after activation of Toll-like receptors. *Exp Dermatol,* 19**,** e314-6.

ORLOVA-FINK, N., CHOWDHURY, F. Z., XIAOMING, S., HARRINGTON, S., ROSENBERG, E. S., YU, X. G. & LICHTERFELD, M. 2017. Preferential susceptibility of Th9 and Th2 CD4 T cells to X4-tropic HIV-1 infection. *AIDS (London, England),* 31**,** 2211.

OUCHI, T., KUBO, A., YOKOUCHI, M., ADACHI, T., KOBAYASHI, T., KITASHIMA, D. Y., FUJII, H., CLAUSEN, B. E., KOYASU, S. & AMAGAI, M. 2011. Langerhans cell antigen capture through tight junctions confers preemptive immunity in experimental staphylococcal scalded skin syndrome. *Journal of Experimental Medicine,* 208**,** 2607-2613.

PAINTER, K. J. J. J. O. T. B. 2019. Mathematical models for chemotaxis and their applications in self-organisation phenomena. 481**,** 162-182.

PASSMORE, J.-A. S., JASPAN, H. B. & MASSON, L. 2016. Genital inflammation, immune activation and risk of sexual HIV acquisition. *Current opinion in HIV and AIDS,* 11**,** 156.

PEARCE, E. L., MULLEN, A. C., MARTINS, G. A., KRAWCZYK, C. M., HUTCHINS, A. S., ZEDIAK, V. P., BANICA, M., DICIOCCIO, C. B., GROSS, D. A. & MAO, C.-A. 2003. Control of effector CD8+ T cell function by the transcription factor Eomesodermin. *Science,* 302**,** 1041-1043.

PIGNI, M., ASHOK, D., STEVANIN, M. & ACHA-ORBEA, H. 2018. Establishment and characterization of a functionally competent type 2 conventional dendritic cell line. *Frontiers in immunology,* 9**,** 1912.

PIGUET, V. & STEINMAN, R. M. 2007. The interaction of HIV with dendritic cells: outcomes and pathways. *Trends in Immunology,* 28**,** 503-510.

PILCHER, C. D., JOAKI, G., HOFFMAN, I. F., MARTINSON, F. E., MAPANJE, C., STEWART, P. W., POWERS, K. A., GALVIN, S., CHILONGOZI, D., GAMA, S., PRICE, M. A., FISCUS, S. A. & COHEN, M. S. 2007. Amplified transmission of HIV-1: comparison of HIV-1 concentrations in semen and blood during acute and chronic infection. *Aids,* 21**,** 1723-30.

PING, Z., HANSPETER, W., ELENA, C., KENNETH, A. T. & KENNETH, H. R. 2008. Cryoelectron tomography of HIV-1 envelope spikes: further evidence for tripod-like legs. *PLoS Pathogens,* 4**,** e1000203.

PORTH, C. 2011. *Essentials of pathophysiology: concepts of altered health states*, Lippincott Williams & Wilkins.

POSAVAD, C. M., ZHAO, L., DONG, L., JIN, L., STEVENS, C. E., MAGARET, A. S., JOHNSTON, C., WALD, A., ZHU, J. & COREY, L. 2017. Enrichment of herpes simplex virus type 2 (HSV-2) reactive mucosal T cells in the human female genital tract. *Mucosal immunology,* 10**,** 1259-1269.

PRODGER, J. L., GRAY, R. H., SHANNON, B., SHAHABI, K., KONG, X., GRABOWSKI, K., KIGOZI, G., NALUGODA, F., SERWADDA, D. & WAWER, M. J. J. P. P. 2016. Chemokine levels in the penile coronal sulcus correlate with HIV-1 acquisition and are reduced by male circumcision in Rakai, Uganda. 12**,** e1006025.

PUDNEY, J., QUAYLE, A. J. & ANDERSON, D. J. 2005. Immunological microenvironments in the human vagina and cervix: mediators of cellular immunity are concentrated in the cervical transformation zone. *Biology of reproduction,* 73**,** 1253-1263.

PUROHIT, S. K., SAMER, C., MCWILLIAM, H. E. G., TRAVES, R., STEAIN, M., MCSHARRY, B. P., KINCHINGTON, P. R., TSCHARKE, D. C., VILLADANGOS, J. A., ROSSJOHN, J., ABENDROTH, A. & SLOBEDMAN, B. 2021. Varicella Zoster Virus Impairs Expression of the Nonclassical Major Histocompatibility Complex Class I–Related Gene Protein (MR1). *The Journal of infectious diseases*.

QUAYLE, A. 2002. The innate and early immune response to pathogen challenge in the female genital tract and the pivotal role of epithelial cells. *Journal of reproductive immunology,* 57**,** 61-79.

QUINN, T. C. 1996. Global burden of the HIV pandemic. *The lancet,* 348**,** 99-106.

RAJASURIAR, R., BOOTH, D., SOLOMON, A., CHUA, K., SPELMAN, T., GOUILLOU, M., SCHLUB, T. E., DAVENPORT, M., CROWE, S. & ELLIOTT, J. 2010. Biological determinants of immune reconstitution in HIV-infected patients receiving antiretroviral therapy: the role of interleukin 7 and interleukin 7 receptor α and microbial translocation. *The Journal of infectious diseases,* 202**,** 1254-1264.

RANA, H., TRUONG, N. R., JOHNSON, B., BAHARLOU, H., HERBERT, J. J., KANDASAMY, S., GODDARD, R., COHEN, R. C., WINES, M., NASR, N., HARMAN, A. N., BERTRAM, K. M., SANDGREN, K. J. & CUNNINGHAM, A. L. 2024. Herpes simplex virus spreads rapidly in human foreskin, partly driven by chemokine-induced redistribution of Nectin-1 on keratinocytes. *PLOS Pathogens,* 20**,** e1012267.

RANDOLPH, G. J., BEAULIEU, S., LEBECQUE, S., STEINMAN, R. M. & MULLER, W. A. 1998. Differentiation of monocytes into dendritic cells in a model of transendothelial trafficking. *Science,* 282**,** 480-483.

RANDOLPH, G. J., INABA, K., ROBBIANI, D. F., STEINMAN, R. M. & MULLER, W. A. 1999. Differentiation of phagocytic monocytes into lymph node dendritic cells in vivo. *Immunity,* 11**,** 753-761.

RANKIN, S. M., CONROY, D. M. & WILLIAMS, T. J. J. M. M. T. 2000. Eotaxin and eosinophil recruitment: implications for human disease. 6**,** 20-27.

RATHORE, U., SAHA, P., KESAVARDHANA, S., KUMAR, A. A., DATTA, R., DEVANARAYANAN, S., DAS, R., MASCOLA, J. R. & VARADARAJAN, R. 2017. Glycosylation of the core of the HIV-1 envelope subunit protein gp120 is not required for native trimer formation or viral infectivity. *J Biol Chem,* 292**,** 10197-10219.

RAZAVI, A., BAGHERI, N., AZADEGAN-DEHKORDI, F., SHIRZAD, M., RAHIMIAN, G., RAFIEIAN-KOPAEI, M. & SHIRZAD, H. J. J. O. I. R. 2015. Comparative immune response in children and adults with H. pylori infection. 2015.

REN, H. M., KOLAWOLE, E. M., REN, M., JIN, G., NETHERBY-WINSLOW, C. S. & WADE, Q. 2020. IL-21 from high-affinity CD4 T cells drives differentiation of brain-resident CD8 T cells during persistent viral infection. *Science immunology,* 5.

RENIERS, G., BLOM, S., CALVERT, C., MARTIN-ONRAET, A., HERBST, A. J., EATON, J. W., BOR, J., SLAYMAKER, E., LI, Z. R. & CLARK, S. J. 2017. Trends in the burden of HIV mortality after roll-out of antiretroviral therapy in KwaZulu-Natal, South Africa: an observational community cohort study. *The Lancet HIV,* 4**,** e113-e121.

REYNOLDS, S. J., RISBUD, A. R., SHEPHERD, M. E., ZENILMAN, J. M., BROOKMEYER, R. S., PARANJAPE, R. S., DIVEKAR, A. D., GANGAKHEDKAR, R. R., GHATE, M. V. & BOLLINGER, R. C. 2003. Recent herpes simplex virus type 2 infection and the risk of human immunodeficiency virus type 1 acquisition in India. *The Journal of infectious diseases,* 187**,** 1513-1521.

RHODES, J. W., BOTTING, R. A., BERTRAM, K. M., VINE, E. E., RANA, H., BAHARLOU, H., VEGH, P., O'NEIL, T. R., ASHHURST, A. S. & FLETCHER, J. J. N. C. 2021. Human anogenital monocyte-derived dendritic cells and langerin+ cDC2 are major HIV target cells. 12**,** 1-15.

RHODES, J. W., TONG, O., HARMAN, A. N. & TURVILLE, S. G. 2019. Human Dendritic Cell Subsets, Ontogeny, and Impact on HIV Infection. *Frontiers in Immunology,* 10.

RIZZUTO, C. D., WYATT, R., HERNÁNDEZ-RAMOS, N., SUN, Y., KWONG, P. D., HENDRICKSON, W. A. & SODROSKI, J. 1998. A Conserved HIV gp 120 Glycoprotein Structure Involved in Chemokine Receptor Binding. *Science,* 280**,** 1949-1953.

ROBERTS, E. R., CARNATHAN, D. G., LI, H., SHAW, G. M., SILVESTRI, G. & BETTS, M. R. 2016. Collapse of Cytolytic Potential in SIV-Specific CD8+ T Cells Following Acute SIV Infection in Rhesus Macaques.(Research Article)(simian immunodeficiency viruses)(Report). *PLoS Pathogens,* 12**,** e1006135.

RODRÍGUEZ, M. C., DYBAS, J. M., HUGHES, J., WEITZMAN, M. D. & BOUTELL, C. J. V. R. 2020. The HSV-1 ubiquitin ligase ICP0: Modifying the cellular proteome to promote infection. 285**,** 198015.

ROIZMAN, B. & SEARS, A. E. 1987. An inquiry into the mechanisms of herpes simplex virus latency. *Annual Reviews in microbiology,* 41**,** 543-571.

ROIZMAN, B. & WHITLEY, R. J. 2001. The nine ages of herpes simplex virus. *HERPES-CAMBRIDGE-,* 8**,** 23-26.

ROIZMAN, B. & WHITLEY, R. J. 2013. An inquiry into the molecular basis of HSV latency and reactivation. *Annual review of microbiology,* 67**,** 355-374.

ROYCHOUDHURY, P., SWAN, D. A., DUKE, E., COREY, L., ZHU, J., DAVÉ, V., SPUHLER, L. R., LUND, J. M., PRLIC, M. & SCHIFFER, J. T. 2020. Tissue-resident T cell–derived cytokines eliminate herpes simplex virus-2–infected cells. *The Journal of clinical investigation,* 130**,** 2903-2919.

RUEDA, C. M., VELILLA, P. A., CHOUGNET, C. A. & RUGELES, M. T. 2013. Incomplete normalization of regulatory t-cell frequency in the gut mucosa of Colombian HIV-infected patients receiving long-term antiretroviral treatment. *PLoS One,* 8**,** e71062.

RYAN, E. S., MICCI, L., FROMENTIN, R., PAGANINI, S., MCGARY, C. S., EASLEY, K., CHOMONT, N. & PAIARDINI, M. 2016. Loss of function of intestinal IL-17 and

IL-22 producing cells contributes to inflammation and viral persistence in SIV-infected rhesus macaques. *PLoS pathogens,* 12**,** e1005412.
SABO, M. C., LEHMAN, D. A., WANG, B., RICHARDSON, B. A., SRINIVASAN, S., OSBORN, L., MATEMO, D., KINUTHIA, J., FIEDLER, T. L. & MUNCH, M. M. J. S. T. I. 2020. Associations between vaginal bacteria implicated in HIV acquisition risk and proinflammatory cytokines and chemokines. 96**,** 3-9.
SAEKI, H. & TAMAKI, K. 2006. Thymus and activation regulated chemokine (TARC)/CCL17 and skin diseases. *J Dermatol Sci,* 43**,** 75-84.
SALLUSTO, F., GEGINAT, J. & LANZAVECCHIA, A. 2004. Central memory and effector memory T cell subsets: function, generation, and maintenance. *Annu. Rev. Immunol.,* 22**,** 745-763.
SAMRI, A., CHARPENTIER, C., DIALLO, M. S., BERTINE, M., EVEN, S., MORIN, V., OUDIN, A., PARIZOT, C., COLLIN, G. & HOSMALIN, A. 2019. Limited HIV-2 reservoirs in central-memory CD4 T-cells associated to CXCR6 co-receptor expression in attenuated HIV-2 infection. *PLoS pathogens,* 15**,** e1007758.
SANDGREN, K. J., TRUONG, N. R., SMITH, J. B., BERTRAM, K. & CUNNINGHAM, A. L. J. H. S. V. 2020. Vaccines for herpes simplex: Recent progress driven by viral and adjuvant immunology. 31-56.
SANDLER, N. G. & DOUEK, D. C. 2012. Microbial translocation in HIV infection: causes, consequences and treatment opportunities. *Nature Reviews Microbiology,* 10**,** 655-666.
SCHALLER, G. 1990. Changes in keratin expression of human vaginal epithelium during different female generation phases. Polyclonal antibody studies. *Gynecol Obstet Invest,* 29**,** 278-81.
SCHIFFER, J. T., ABU-RADDAD, L., MARK, K. E., ZHU, J., SELKE, S., KOELLE, D. M., WALD, A. & COREY, L. J. P. O. T. N. A. O. S. 2010. Mucosal host immune response predicts the severity and duration of herpes simplex virus-2 genital tract shedding episodes. 107**,** 18973-18978.
SCHIFFER, J. T., MAYER, B. T., FONG, Y., SWAN, D. A. & WALD, A. J. J. O. T. R. S. I. 2014. Herpes simplex virus-2 transmission probability estimates based on quantity of viral shedding. 11**,** 20140160.
SCHIPKE, J., POHLMANN, A., DIESTEL, R., BINZ, A., RUDOLPH, K., NAGEL, C.-H., BAUERFEIND, R. & SODEIK, B. J. J. O. V. 2012. The C terminus of the large tegument protein pUL36 contains multiple capsid binding sites that function differently during assembly and cell entry of herpes simplex virus. 86**,** 3682-3700.
SCHLITZER, A., MCGOVERN, N., TEO, P., ZELANTE, T., ATARASHI, K., LOW, D., HO, A. W., SEE, P., SHIN, A. & WASAN, P. S. 2013. IRF4 transcription factor-dependent CD11b+ dendritic cells in human and mouse control mucosal IL-17 cytokine responses. *Immunity,* 38**,** 970-983.
SCHMID, D., THIEME, M., GARY, H. & REEVES, W. 1997. Characterization of T cell responses to herpes simplex virus type 1 (HSV-1) and herpes simplex virus type 2 (HSV-2) using a TNF-β ELISpot cytokine assay. *Archives of virology,* 142**,** 1659-1671.
SCHOENBORN, J. R. & WILSON, C. B. J. A. I. I. 2007. Regulation of interferon-γ during innate and adaptive immune responses. 96**,** 41-101.
SCHUSTER, P., THOMANN, S., WERNER, M., VOLLMER, J. & SCHMIDT, B. J. F. I. M. 2015. A subset of human plasmacytoid dendritic cells expresses CD8α upon exposure to herpes simplex virus type 1. 6**,** 557.

SENESCHAL, J., CLARK, R. A., GEHAD, A., BAECHER-ALLAN, C. M. & KUPPER, T. S. 2012. Human epidermal Langerhans cells maintain immune homeostasis in skin by activating skin resident regulatory T cells. *Immunity,* 36**,** 873-884.

SEVERINI, A., TYLER, S. D., PETERS, G. A., BLACK, D. & EBERLE, R. 2013. Genome sequence of a chimpanzee herpesvirus and its relation to other primate alphaherpesviruses. *Archives of virology,* 158**,** 1825-1828.

SHARP, P. M. & HAHN, B. H. 2011. Origins of HIV and the AIDS pandemic. *Cold Spring Harbor perspectives in medicine,* 1**,** a006841-a006841.

SHARPE, A. H. & PAUKEN, K. E. 2018. The diverse functions of the PD1 inhibitory pathway. *Nature Reviews Immunology,* 18**,** 153.

SHAW, J. M., HUNT, P. W., CRITCHFIELD, J. W., MCCONNELL, D. H., GARCIA, J. C., POLLARD, R. B., SOMSOUK, M., DEEKS, S. G. & SHACKLETT, B. L. 2011. Increased frequency of regulatory T cells accompanies increased immune activation in rectal mucosae of HIV-positive noncontrollers. *Journal of virology,* 85**,** 11422-11434.

SHEDLOCK, D. J., WHITMIRE, J. K., TAN, J., MACDONALD, A. S., AHMED, R. & SHEN, H. 2003. Role of CD4 T cell help and costimulation in CD8 T cell responses during Listeria monocytogenes infection. *The Journal of Immunology,* 170**,** 2053-2063.

SHEN, R., RICHTER, H. E. & SMITH, P. D. 2011. Early HIV-1 target cells in human vaginal and ectocervical mucosa. *American journal of reproductive immunology,* 65**,** 261-267.

SICA, A. & MANTOVANI, A. 2012. Macrophage plasticity and polarization: in vivo veritas. *The Journal of clinical investigation,* 122**,** 787-795.

SKON, C. N., LEE, J.-Y., ANDERSON, K. G., MASOPUST, D., HOGQUIST, K. A. & JAMESON, S. C. 2013. Transcriptional downregulation of S1pr1 is required for the establishment of resident memory CD8+ T cells. *Nature immunology,* 14**,** 1285-1293.

SMITH, K. A. 2012. The molecular mechanisms of regulatory T cell immunosuppression. *Frontiers in immunology,* 3**,** 379.

SOKOL, C. L. & LUSTER, A. D. J. C. S. H. P. I. B. 2015. The chemokine system in innate immunity. 7**,** a016303.

SORIANO-SARABIA, N., BATESON, R. E., DAHL, N. P., CROOKS, A. M., KURUC, J. D., MARGOLIS, D. M. & ARCHIN, N. M. 2014. Quantitation of replication-competent HIV-1 in populations of resting CD4+ T cells. *Journal of virology,* 88**,** 14070-14077.

STEINMAN, R. M. & COHN, Z. A. 1973. Identification of a novel cell type in peripheral lymphoid organs of mice: I. Morphology, quantitation, tissue distribution. *The Journal of experimental medicine,* 137**,** 1142-1162.

STEINSTRAESSER, L., RITTIG, A., GEVERS, K., SORKIN, M., HIRSCH, T., KESTING, M., SAND, M., AL-BENNA, S., LANGER, S., STEINAU, H. U. & JACOBSEN, F. 2009. A human full-skin culture system for interventional studies. *Eplasty,* 9**,** e5.

STOEGER, T. & ADLER, H. 2019. "Novel" Triggers of Herpesvirus Reactivation and Their Potential Health Relevance. *Frontiers in microbiology,* 9**,** 3207-3207.

STRAYER, D. S. 2015. *Rubin's pathology: clinicopathologic foundations of medicine*.

TANAKA, T., NARAZAKI, M. & KISHIMOTO, T. 2014. IL-6 in inflammation, immunity, and disease. *Cold Spring Harbor perspectives in biology,* 6**,** a016295-a016295.

TANG, C., CHEN, S., QIAN, H. & HUANG, W. J. I. 2012. Interleukin-23: as a drug target for autoimmune inflammatory diseases. 135**,** 112-124.

THOME, J. J., YUDANIN, N., OHMURA, Y., KUBOTA, M., GRINSHPUN, B., SATHALIYAWALA, T., KATO, T., LERNER, H., SHEN, Y. & FARBER, D. L.

2014. Spatial map of human T cell compartmentalization and maintenance over decades of life. *Cell,* 159**,** 814-828.
TONG, O., DUETTE, G., O'NEIL, T. R., ROYLE, C. M., RANA, H., JOHNSON, B., POPOVIC, N., DERVISH, S., BROUWER, M. A. & BAHARLOU, H. 2021. Plasmacytoid dendritic cells have divergent effects on HIV infection of initial target cells and induce a pro-retention phenotype. *PLoS pathogens,* 17**,** e1009522.
TRUONG, N. R., SMITH, J. B., SANDGREN, K. J. & CUNNINGHAM, A. L. 2019. Mechanisms of immune control of mucosal HSV infection: A guide to rational vaccine design. *Frontiers in immunology,* 10**,** 373.
TURVILLE, S., WILKINSON, J., CAMERON, P., DABLE, J. & CUNNINGHAM, A. L. 2003. The role of dendritic cell C-type lectin receptors in HIV pathogenesis. *Journal of leukocyte biology,* 74**,** 710-718.
TURVILLE, S. G., CAMERON, P. U., HANDLEY, A., LIN, G., PÖHLMANN, S., DOMS, R. W. & CUNNINGHAM, A. L. 2002. Diversity of receptors binding HIV on dendritic cell subsets. *Nat Immunol,* 3**,** 975-83.
VAN DER SLUIS, R. M., ZERBATO, J. M., RHODES, J. W., PASCOE, R. D., SOLOMON, A., KUMAR, N. A., DANTANARAYANA, A. I., TENNAKOON, S., DUFLOO, J. & MCMAHON, J. 2020. Diverse effects of interferon alpha on the establishment and reversal of HIV latency. *PLoS pathogens,* 16**,** e1008151.
VAN VELZEN, M., JING, L., OSTERHAUS, A. D., SETTE, A., KOELLE, D. M. & VERJANS, G. M. 2013. Local CD4 and CD8 T-cell reactivity to HSV-1 antigens documents broad viral protein expression and immune competence in latently infected human trigeminal ganglia. *PLoS Pathog,* 9**,** e1003547.
VANHECKE, D., LECLERCQ, G., PLUM, J. & VANDEKERCKHOVE, B. 1995a. Characterization of distinct stages during the differentiation of human CD69+ CD3+ thymocytes and identification of thymic emigrants. *The Journal of Immunology,* 155**,** 1862-1872.
VANHECKE, D., VERHASSELT, B., DEBACKER, V., LECLERCQ, G., PLUM, J. & VANDEKERCKHOVE, B. 1995b. Differentiation to T helper cells in the thymus. Gradual acquisition of T helper cell function by CD3+ CD4+ cells. *The Journal of Immunology,* 155**,** 4711-4718.
VAROL, C., MILDNER, A. & JUNG, S. 2015. Macrophages: development and tissue specialization. *Annual review of immunology,* 33**,** 643-675.
VILLANI, A.-C., SATIJA, R., REYNOLDS, G., SARKIZOVA, S., SHEKHAR, K., FLETCHER, J., GRIESBECK, M., BUTLER, A., ZHENG, S. & LAZO, S. 2017. Single-cell RNA-seq reveals new types of human blood dendritic cells, monocytes, and progenitors. *Science,* 356.
VITALI, D., BAGRI, P., WESSELS, J. M., ARORA, M., GANUGULA, R., PARIKH, A., MANDUR, T., FELKER, A., GARG, S. & KUMAR, M. J. I. J. O. M. S. 2020. Curcumin can decrease tissue inflammation and the severity of HSV-2 infection in the female reproductive mucosa. 21**,** 337.
VITTONE, V., DIEFENBACH, E., TRIFFETT, D., DOUGLAS MARK, W., CUNNINGHAM ANTHONY, L. & DIEFENBACH RUSSELL, J. 2005. Determination of Interactions between Tegument Proteins of Herpes Simplex Virus Type 1. *Journal of Virology,* 79**,** 9566-9571.
VOLLMER, B. & GRÜNEWALD, K. 2020. Herpesvirus membrane fusion–a team effort. *Current Opinion in Structural Biology,* 62**,** 112-120.
VREMAN, S., REBEL, J. M., MCCAFFREY, J., LEDL, K., ARKHIPOVA, K., COLLINS, D., MCDAID, D., SAVELKOUL, H. F., SKOVGAARD, K. & MOORE, A. C. J. V.

2021. Early immune responses in skin and lymph node after skin delivery of Toll-like receptor agonists in neonatal and adult pigs. 39**,** 1857-1869.
WAKIM, L. M., WOODWARD-DAVIS, A. & BEVAN, M. J. 2010. Memory T cells persisting within the brain after local infection show functional adaptations to their tissue of residence. *Proceedings of the National Academy of Sciences,* 107**,** 17872-17879.
WALD, A., LANGENBERG, A. G., LINK, K., IZU, A. E., ASHLEY, R., WARREN, T., TYRING, S., DOUGLAS JR, J. M. & COREY, L. J. J. 2001. Effect of condoms on reducing the transmission of herpes simplex virus type 2 from men to women. 285**,** 3100-3106.
WALD, A., MATSON, P., RYNCARZ, A. & COREY, L. J. S. T. D. 1999. Detection of herpes simplex virus DNA in semen of men with genital HSV-2 infection. 26**,** 1-3.
WALKER, J. A. & MCKENZIE, A. N. 2018. T H 2 cell development and function. *Nature Reviews Immunology,* 18**,** 121.
WALTER, M. R. 2020. The role of structure in the biology of interferon signaling. *Frontiers in immunology,* 11**,** 606489.
WANG, Q. & PANG, S. 2008. An intercellular adhesion molecule-3 (ICAM-3) -grabbing nonintegrin (DC-SIGN) efficiently blocks HIV viral budding. *FASEB Journal,* 22**,** 1055-1064.
WANG, X.-N., MCGOVERN, N., GUNAWAN, M., RICHARDSON, C., WINDEBANK, M., SIAH, T.-W., LIM, H.-Y., FINK, K., LI, J. L. Y. & NG, L. G. J. J. O. I. D. 2014. A three-dimensional atlas of human dermal leukocytes, lymphatics, and blood vessels. 134**,** 965-974.
WANG, X., LIU, J., ZOU, J., LUO, C. & WEI, D. 2024. The study of vaginal wall thickness in adults based on histopathological measurements. *Scientific Reports,* 14**,** 18644.
WATCHMAKER, P. B., LAHL, K., LEE, M., BAUMJOHANN, D., MORTON, J., KIM, S. J., ZENG, R., DENT, A., ANSEL, K. M. & DIAMOND, B. 2014. Comparative transcriptional and functional profiling defines conserved programs of intestinal DC differentiation in humans and mice. *Nature immunology,* 15**,** 98-108.
WAYENGERA, M. 2011. Proviral HIV-genome-wide and pol-gene specific zinc finger nucleases: usability for targeted HIV gene therapy. *Theoretical Biology and Medical Modelling,* 8**,** 1-13.
WERTHEIM, J. O., SMITH, M. D., SMITH, D. M., SCHEFFLER, K. & KOSAKOVSKY POND, S. L. 2014. Evolutionary Origins of Human Herpes Simplex Viruses 1 and 2. *Molecular Biology and Evolution,* 31**,** 2356-2364.
WHITLEY, R., KIMBERLIN, D. W., PROBER, C. G. J. H. H. B., THERAPY, & IMMUNOPROPHYLAXIS 2007. Pathogenesis and disease.
WHITLEY, R. J., KIMBERLIN, D. W. & ROIZMAN, B. 1998. Herpes simplex viruses. *Clinical Infectious Diseases***,** 541-553.
WILCOX, C. L. & JOHNSON JR, E. M. J. J. O. V. 1987. Nerve growth factor deprivation results in the reactivation of latent herpes simplex virus in vitro. 61**,** 2311-2315.
WILHELM, T. R., TADDEO, A., WINTER, O., SCHULZ, A. R., MÄLZER, J.-N., DOMINGO, C., BIESEN, R., ALEXANDER, T., THIEL, A. & RADBRUCH, A. 2016. Siglec-1-positive plasmacytoid dendritic cells (pDCs) in human peripheral blood: A semi-mature and myeloid-like subset imbalanced during protective and autoimmune responses. *Clinical Immunology,* 163**,** 42-51.
WILSON, A. C. & MOHR, I. 2012. A cultured affair: HSV latency and reactivation in neurons. *Trends in Microbiology,* 20**,** 604-611.
WYSOCKA, J. & HERR, W. 2003. The herpes simplex virus VP16-induced complex: the makings of a regulatory switch. *Trends in biochemical sciences,* 28**,** 294-304.

XU, H., WANG, X. & VEAZEY, R. S. 2014. Th17 cells coordinate with Th22 cells in maintaining homeostasis of intestinal tissues and both are depleted in SIV-infected macaques. *Journal of AIDS & clinical research,* 5.

XU, S. & CAO, X. 2010. Interleukin-17 and its expanding biological functions. *Cellular & molecular immunology,* 7**,** 164-174.

XU, W., HONG, S. J., JIA, S., ZHAO, Y., GALIANO, R. D. & MUSTOE, T. A. 2012. Application of a partial-thickness human ex vivo skin culture model in cutaneous wound healing study. *Laboratory investigation,* 92**,** 584-599.

XU, Y., PHETSOUPHANH, C., SUZUKI, K., AGGRAWAL, A., GRAFF-DUBOIS, S., ROCHE, M., BAILEY, M., ALCANTARA, S., CASHIN, K. & SIVASUBRAMANIAM, R. 2017. HIV-1 and SIV predominantly use CCR5 expressed on a precursor population to establish infection in T follicular helper cells. *Frontiers in immunology,* 8**,** 376.

YANG, C. Y., BEST, J. A., KNELL, J., YANG, E., SHERIDAN, A. D., JESIONEK, A. K., LI, H. S., RIVERA, R. R., LIND, K. C., D'CRUZ, L. M., WATOWICH, S. S., MURRE, C. & GOLDRATH, A. W. 2011. The transcriptional regulators Id2 and Id3 control the formation of distinct memory CD8+ T cell subsets. *Nature Immunology,* 12**,** 1221-1229.

YOSHIDA, K., KUBO, A., FUJITA, H., YOKOUCHI, M., ISHII, K., KAWASAKI, H., NOMURA, T., SHIMIZU, H., KOUYAMA, K. & EBIHARA, T. 2014. Distinct behavior of human Langerhans cells and inflammatory dendritic epidermal cells at tight junctions in patients with atopic dermatitis. *Journal of allergy and clinical immunology,* 134**,** 856-864.

YOUNGBLOOD, B., HALE, J. S. & AHMED, R. 2013. T-cell memory differentiation: insights from transcriptional signatures and epigenetics. *Immunology,* 139**,** 277-284.

ZABIHOLLAHI, R., MOTEVASELI, E., SADAT, S. M., AZIZI-SARAJI, A. R., ASAADI-DALAIE, S. & MODARRESSI, M. H. 2012. Inhibition of HIV and HSV infection by vaginal lactobacilli in vitro and in vivo. *DARU Journal of Pharmaceutical Sciences,* 20**,** 1-7.

ZAID, A., HOR, J. L., CHRISTO, S. N., GROOM, J. R., HEATH, W. R., MACKAY, L. K. & MUELLER, S. N. 2017. Chemokine Receptor-Dependent Control of Skin Tissue-Resident Memory T Cell Formation. *The Journal of immunology (1950),* 199**,** 2451-2459.

ZAITSEVA, M., BLAUVELT, A., LEE, S., LAPHAM, C. K., KLAUS-KOVTUN, V., MOSTOWSKI, H., MANISCHEWITZ, J. & GOLDING, H. 1997. Expression and function of CCR5 and CXCR4 on human Langerhans cells and macrophages: implications for HIV primary infection. *Nat Med,* 3**,** 1369-75.

ZARROUK, K., PIRET, J. & BOIVIN, G. J. V. R. 2017. Herpesvirus DNA polymerases: structures, functions and inhibitors. 234**,** 177-192.

ZHANG, Y. H., S, A. C. & KARTHIKEYAN, S. 2018. Finite element analysis of hollow out-of-plane HfO(2) microneedles for transdermal drug delivery applications. *Biomed Microdevices,* 20**,** 19.

ZHENG, M., CONRADY, C. D., WARD, J. M., BRYANT-HUDSON, K. M. & CARR, D. J. 2012. Comparison of the host immune response to herpes simplex virus 1 (HSV-1) and HSV-2 at two different mucosal sites. *Journal of virology,* 86**,** 7454-7458.

ZHU, J., HLADIK, F., WOODWARD, A., KLOCK, A., PENG, T., JOHNSTON, C., REMINGTON, M., MAGARET, A., KOELLE, D. M. & WALD, A. 2009. Persistence of HIV-1 receptor–positive cells after HSV-2 reactivation is a potential mechanism for increased HIV-1 acquisition. *Nature medicine,* 15**,** 886-892.

ZHU, J., KOELLE, D. M., CAO, J., VAZQUEZ, J., HUANG, M. L., HLADIK, F., WALD, A. & COREY, L. 2007. Virus-specific CD8+ T cells accumulate near sensory nerve endings in genital skin during subclinical HSV-2 reactivation. *The Journal of experimental medicine,* 204**,** 595-603.

ZHU, X., BORCHERS, C., BIENSTOCK, R. J. & TOMER, K. B. 2000. Mass spectrometric characterization of the glycosylation pattern of HIV-gp120 expressed in CHO cells. *Biochemistry,* 39**,** 11194-11204.

Appendices

A. Fiji script for alignment of two rounds of image based on registration

```
/*
 * This macro will perform registration of two rounds of images based on comparison of DAPI between rounds of staining.
 * Files should be in two folders "1" and "2". In each folder there should be another folder which contains individual channels of the image
 * Folders "1" and "2" should be alphabetically matched so that the lists are in correspondence.
 *
 */

setBatchMode(true);

roiManager("reset");
run("Clear Results");
run("Close All");


dir = getDirectory("select main directory");
dirFirst = getDirectory("Select folder with 1st round Tiffs in folders");
dirSecond = getDirectory("Select folder with 2nd round Tiffs in folders");

listOne = getFileList(dirFirst);
listTwo = getFileList(dirSecond);
//Array.show(listOne);

if(listOne.length != listTwo.length){
	print("Directories must have equal number of files");
	exit;
}
if(File.exists(dir + "/TransformationFiles") == 0){
			File.makeDirectory(dir + "/TransformationFiles");
}
if(File.exists(dir + "/alignedStacks") == 0){
			File.makeDirectory(dir + "/alignedStacks");
}

transformationFiles = dir + "/TransformationFiles";
alignedStacks = dir + "/alignedStacks";

//Naming for output files for each round in order of CH0, CH1... etc).
//Note: The CH0, and consequently the first entry in rd1 and rd2 must be DAPI for this program to work.
rd1 = newArray("DAPI1", "CD3", "CD11c", "CD4");
rd2 = newArray("DAPI2", "LANG", "HSV");

//resolutions to assign to images. x20 mag
var resolution = "0.32529";
//resolutions to assign to images. x40 mag
//resolution = "0.16278";

i=0;

for(i=0; i<listOne.length; i++){

	//names of images containing all imageInfo
	name1 = substring(listOne[i], 0,lengthOf(listOne[i])-1);
	name2 = substring(listTwo[i], 0,lengthOf(listTwo[i])-1);
```

```
	//Create subdirectory to output aligned channels
	savePath = alignedStacks + File.separator + name1;
	print(savePath);
	if(File.exists(savePath) == 0) File.makeDirectory(savePath);
	else continue;

	//Paths to access images from rd1 and rd2
	files1 = dirFirst + name1 + File.separator;// + "Layer0";
	files2 = dirSecond + name2 + File.separator;// + "Layer0";

	//open all images in rd1 and rd2. Convert names (e.g. round 1 CH0 = rd1[0])
	for(j=0;j<rd1.length;j++) fileFinderWithError("CH" + d2s(j,0), d2s(i,0), files1, rd1[j]);
	for(j=0;j<rd2.length;j++) fileFinderWithError("CH" + d2s(j,0), d2s(i,0), files2, rd2[j]);

	//Merge stacks and then split stacks to get image size same for all images
	run("Images to Stack", "method=[Copy (center)] name=Stack title=[] use");
	run("Stack to Images");

	//Save all rd1 images which are now of a new size equivaling rd2 image size. Keep only the DAPI
image open.
	for(j=0;j<rd1.length;j++) {
		selectWindow(rd1[j]);
		saveAs("Tiff", savePath + File.separator + rd1[j] + ".tif");
		if(j!=0) close();
	}

	//Inside the "[ ]" you can choose the transformation type. i.e. 'Rigid Body', 'Affine', 'Translation' etc.
	run("MultiStackReg", "stack_1=" + rd1[0] + ".tif action_1=[Use as Reference] file_1=[] stack_2=" +
rd2[0] + " action_2=[Align to First Stack] file_2=[" + transformationFiles + "/" + name1 + ".txt]
transformation=[Rigid Body] save");
	selectWindow(rd2[0]);
	saveAs("Tiff", savePath + File.separator + rd2[0] + ".tif");

	for(j=1; j<rd2.length; j++){
		selectWindow(rd2[j]);
		run("MultiStackReg", "stack_1=" + rd2[j] + " action_1=[Load Transformation File] file_1=[" +
transformationFiles + "/" + name1 + ".txt] stack_2=None action_2=Ignore file_2=[] transformation=[Rigid
Body]");
		saveAs("Tiff", savePath + File.separator + rd2[j] + ".tif");
		close();
	}
	print(savePath);
//Finds and opens a file within a specified directory. Inputs: name1 = part of file name, name2 = another part
of file name, directory
//of file, suffix of file name (i.e. the file type e.g. ".tiff", ".zip", ".roi").

//This file finder has been modified so that an exact match is required.
function fileFinder(name1, name2, directory){
	list = getFileList(directory);
	//n is used as a counter to determine if a file is found. n increases with each cycle through the loop
below. If n==0 at the end the function
	//returns 0, if n>0 then 1 is returned.
	n = 0;
	for(i=0;i<list.length;i++){
		if((indexOf(list[i], name1)>= 0) && (indexOf(list[i], name2) >=0)){
			fileName = list[i];
```

```
                        n++;

                        if((endsWith(fileName, ".roi") == 1) || (endsWith(fileName, ".zip") == 1)){
                                roiManager("open", directory + File.separator + fileName);
                        }
                        else
                                print(directory + File.separator + fileName);
                                //run("Bio-Formats", "open=" + directory + File.separator + fileName + "
autoscale color_mode=Default rois_import=[ROI manager] view=Hyperstack stack_order=XYCZT");
                                open(directory + File.separator + fileName);
                }
        }
        if(n==0){
                return 0;
        }
        else
                return 1;
}


function directoryFinder(name, directory){
        list = getFileList(directory);
        //n is used as a counter to determine if a file is found. n increases with each cycle through the loop
below. If n==0 at the end the function
        //returns 0, if n>0 then 1 is returned.
        n = 0;
        for(i=0;i<list.length;i++){
                if((indexOf(list[i], name)>= 0)) {
                        return list[i];
                        n++
                }
        }
        if(n==0) return "NA";
}

/* This function executes the fileFinder function, but will give an error message when files are not found and
continue to next image for registration.
 * name = unique substring of image, allowing filefinder to identify and open image.
 * imageNo = current loop cycle count input as string (allows error message to contain info on images that are
missing)
 * path = directory to search using fileFinder
 * Additionally, the images are renames to 'newName' and assigned a 'resolution' which is defined at the top of
the macro as a gloabl variable.
 */

function fileFinderWithError(name, imageNo, path, newName){
        if(fileFinder(name, name, path) == 0) {
                print("Missing file at " + imageNo);
                run("Close All");
                continue;
        }
        rename(newName);
        run("Set Scale...", "distance=1 known=" + resolution + " unit=um");
}
```